Inhibiting Disease-Associated Anaerobic Choline Metabolism by Human Gut Bacteria

Inhibiting disease-associated anaerobic choline metabolism by human gut bacteria

A dissertation presented

by

Marina Orman

to

the Committee on Higher Degrees in Chemical Biology

in partial fulfillment of the requirements for the degree of

Doctor of Philosophy

in the subject of

Chemical Biology

Harvard University

Cambridge, Massachusetts

April 2019

Dissertation advisor: Professor Emily P. Balskus Marina Orman

Inhibiting disease-associated anaerobic choline metabolism by human gut bacteria

Abstract

The consortium of microorganisms that inhabit the human gastrointestinal tract, the human gut microbiota, harbors an extensive set of metabolic capabilities. The complex biological and chemical interactions between humans and the human gut microbiota have a profound influence on host health. However, the molecular details of how gut bacterial metabolism impacts human health and disease are largely unknown. By developing small molecule inhibitors specifically targeting gut microbial pathways, we can elucidate the roles of bacterial metabolism in disease and create a new paradigm for therapeutics.

To illustrate this strategy's potential, we sought to develop small molecule inhibitors of the catabolism of the essential nutrient choline by anaerobic gut microbes. Within the human gastrointestinal tract, bacteria can cleave the C–N bond of choline to produce trimethylamine (TMA), which is subsequently oxidized to trimethylamine *N*-oxide (TMAO) by host hepatic enzymes. This microbial-human co-metabolic pathway has been linked to several diseases, including non-alcoholic fatty liver disease and atherosclerosis.

Here, we describe the discovery that betaine aldehyde inhibits TMA production from choline by human gut bacterial isolates and a complex gut community. *In vitro* assays and a crystal structure suggest betaine aldehyde targets the gut microbial enzyme choline TMA-lyase (CutC). In our system, we do not observe activity for the previously reported CutC inhibitor 3,3-dimethylbutanol (DMB). The workflow we establish for identifying and characterizing betaine

aldehyde provides a framework for developing additional inhibitors of gut microbial choline metabolism, including therapeutic candidates.

Chapter 3 describes further efforts towards discovering small molecule inhibitors of CutC-mediated choline cleavage. Overall, our results show that small molecules can interfere with choline metabolism by anaerobic gut microbes and sets the stage for more extensive efforts to discover novel potent inhibitors of this pathway.

Table of Contents

List of Figures

List of Tables

Chapter 1: Introduction to host-gut microbiota metabolic interactions, the glycyl radical enzyme family, and anaerobic choline metabolism

1.1. General introduction to the human gut microbiota

The complex interactions between humans and the bacteria that comprise the human gut microbiota have a profound influence on host health and the development and progression of disease. The gut's microbial inhabitants are capable of digesting food components inaccessible to the host, synthesizing essential vitamins and nutrients, shaping and maintaining the host's immune system, and modifying pharmaceuticals.[1-3] The breadth of functional genes encoded by the human gut microbial population outnumbers the human genome by approximately 150-fold.[4] As a result, these communities posses a diverse repertoire of enzymes that are capable of mediating important chemical transformations and producing bioactive metabolites that complement, and occasionally interfere with, human biology. Indeed, small molecules from the human gut microbiota have been associated with several pathologies of the host, including metabolic disease, cancer, inflammatory bowel disease, and neurological disorders.[5,6]

Despite the increasing number of connections drawn between gut microbial-derived molecules and human physiology, our understanding of the functional roles of these metabolites in the context of the human body has proven challenging. Antibiotics, probiotics, prebiotics, and fecal transplants have been used, with varying degrees of success, to eradicate or alter gut bacterial populations, allowing associations to be drawn between the presence of a microbial community as a whole and particular host phenotypes.[7] However, uncovering the functional roles of microbial-derived metabolites in human health and disease has proven challenging. To

elucidate the mechanisms by which gut microbial functions affect host biology, the capability of modulating specific chemical reactions within this community is required.

1.2. Importance and metabolism of choline in mammalian cells

Choline is an essential nutrient and lies at the intersection of critical human biological functions (Figure 1.1).[8] In nucleated cells, choline is converted via the Kennedy pathway to generate phosphatidylcholine (PC) and sphingomyelin, the predominant phospholipids in mammalian membranes. Upon crossing the blood-brain barrier, choline is processed in the brain to form the neurotransmitter acetylcholine. Choline is irreversibly oxidized in the mitochondria of liver and kidney cells to form glycine betaine, a source of methyl groups for the synthesis of *S*-adenosylmethionine (SAM), which serves as the primary methyl donor throughout all kingdoms of life. Glycine betaine also functions as an osmolyte in renal glomerular cells, aiding in the reabsorption of water from the kidney tubule.

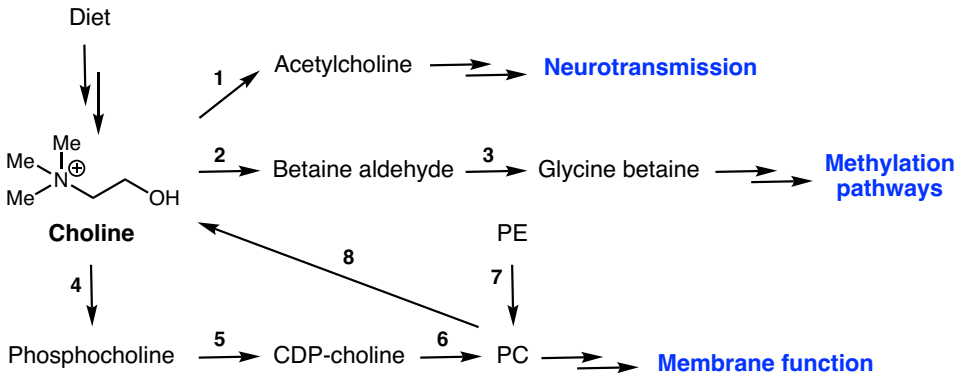

Figure 1.1. Mammalian metabolic pathways involving choline. CTP, cytidine 5′-triphosphate; CDP, cytidine 5′-diphosphate; PE, phosphatidylethanolamine; PC, phosphatidylcholine. Enzyme names are indicated by numbers: 1, choline acetyltransferase; 2, choline oxidase; 3, betaine aldehyde dehydrogenase; 4, choline kinase; 5, CTP:phosphocholine cytidylyltransferase; 6, CDP-choline:1,2-diacylglycerol choline phosphotransferase; 7, phosphatidylethanolamine *N*-methyltransferase; 8, phospholipases (type A, C or D).

Choline is required for brain and memory development in the fetus and is shown to regulate stem cell proliferation, affect neural tube formation, and influence lifelong memory function.[8-10] Choline, folate, and methionine metabolism intersect via a common intermediate, SAM, the universal donor of methyl groups in biological reactions. Thus, perturbing the availability of one nutrient results in compensatory changes in the others.[11] Folate affects embryogenesis of the brain, and folate supplementation is recommended for pregnant women in order to reduce the risk of defects in fetal brain development.[12] The involvement of choline and folate in one-carbon metabolism is a common mechanism by which these molecules likely impact neurogenesis and exert metabolic and epigenetic effects.[13,14]

The importance of choline extends into adulthood and old age. Several studies showed that healthy adults fed a choline-deficient diet developed fatty liver disease and muscle damage, which, in some instances, could be resolved when choline was reintroduced to the diet.[15,16] Choline is incorporated into PC, a phospholipid essential for the assembly and secretion of very-low-density lipoproteins that transport triglycerides out of the liver.[8] Deficiency of choline therefore results in the accumulation of triglycerides in the liver and contributes to hepatosis. These observations led the US Institute of Medicine to set estimated adequate intake (AI) values for the consumption of this nutrient.

While choline can be endogenously produced in hepatic cells by the sequential methylation of phosphatidylethanolamine (PE), its *de novo* biosynthesis only accounts for ~15% of choline in the human bloodstream.[8] Thus, most people need to consume choline in order to meet the daily AI requirements. The most concentrated choline dietary sources are animal products such as eggs, beef, chicken, fish, and milk. Choline is predominantly ingested as PC, which can be hydrolyzed by mammalian and human gut bacterial phospholipase enzymes,[17]

releasing the free headgroup. Dietary choline is absorbed by the intestine and its uptake is mediated by choline transporters.[8] Upon entering the cell, the major fate of choline is conversion to PC, ensuring the maintenance of cell membrane function.

1.3. Bacterial metabolism of choline

While PC is ubiquitous in eukaryotic membranes, its concentration in different bacterial species varies widely, ranging from a few percent of the total membrane lipid content (e.g. 0-4% in *Pseudomonas aeruginosa*) to ~70% in *Acetobacter aceti*.[18] Moreover, it is estimated that only 15% of bacteria (primarily *Actinomycetales*, *Alphaproteobacteria*, and *Deltaproteobacteria*) can biosynthesize PC.[19] Thus, the major fate of choline in bacterial cells under aerobic conditions is conversion to glycine betaine, an osmoprotectant that can enhance bacterial survival in high-salinity environments.[20]

The metabolites from aerobic choline catabolism are conserved among bacterial species (Figure 1.2A). In *Alcaligenes* spp., a soluble flavin-dependant choline oxidase carries out the concerted two-step oxidation of choline to form glycine betaine.[21] In *Escherichia coli* and other bacteria, a membrane-bound choline dehydrogenase is primarily responsible for choline oxidation to betaine aldehyde, which is further oxidized by a soluble betaine aldehyde dehydrogenase, generating glycine betaine.[22] Demethylation of glycine betaine to dimethylglycine proceeds either through a zinc-dependent betaine-homocysteine methyltransferase (in *Cyanobacteria*) or a Rieske-type dioxygenase (in *Proteobacteria*).[23] Further demethylation to sarcosine and glycine is catalyzed by flavin-dependent oxidases that exist either as single-subunit (*Arthrobacter*, *Bacillus*) or multi-subunit (*Pseudomonads*) enzymes.[23,24]

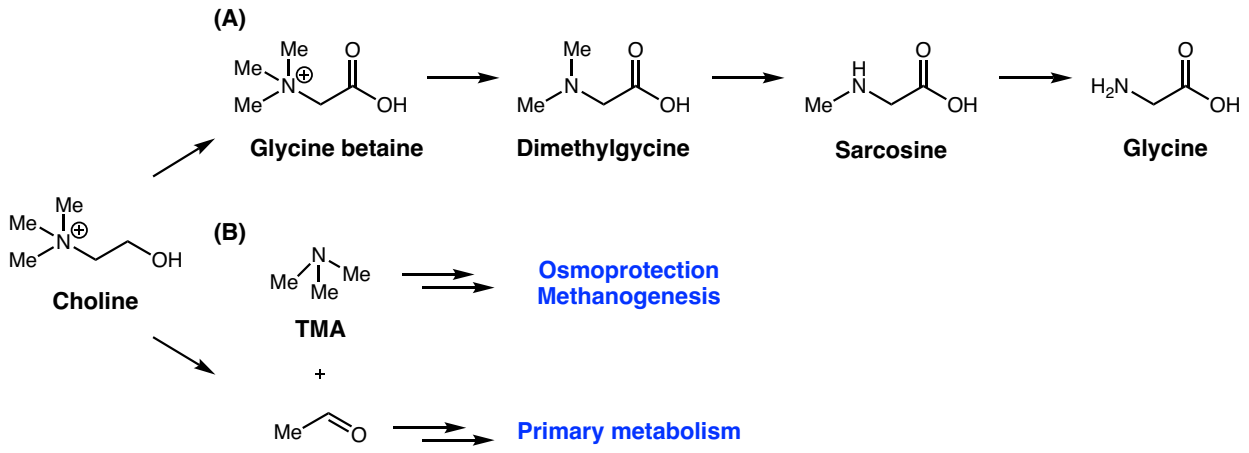

Figure 1.2. Choline catabolic pathways in bacteria under (A) aerobic and (B) anaerobic conditions.

Under anaerobic conditions, certain gut bacteria cleave the C–N bond of choline to generate trimethylamine (TMA) and acetaldehyde (Figure 1.2B). This metabolic pathway was first reported in 1910 and subsequently found to exist in both facultative and obligate anaerobes associated with a range of habitats, including the environment and human gastrointestinal (GI) tracts.[25-31] The acetaldehyde produced from this reaction can be further converted by bacteria into ethanol and acetate for utilization as a carbon and energy source. Archaea found in the GI tracts of ruminants[32] and marine sediments[29] consume TMA for methanogenesis.

In humans, most of the TMA produced in the gut is transported via portal circulation to the liver, where it is rapidly metabolized to trimethylamine-*N*-oxide (TMAO) by hepatic flavin monooxygenase (FMO) enzymes such as FMO3 (Figure 1.3).[33,34] TMAO, a water-soluble metabolite, is then excreted from the body into urine. In addition to regulation by bile acids, FMO3 may also be influenced by hormonal levels, as evidenced in mouse models demonstrating that testosterone suppresses and estrogen induces FMO3 expression.[35] In fact, FMO3 activity has been shown to be 100 times higher in female than in male mice. However, more modest gender-related differences are observed in humans, and a genome-wide association analysis failed to

find any significant human genetic influences on circulating TMAO concentrations.[35,36] Thus, there is still a need to understand the factors limiting TMAO production in humans, as well as the contributions of various isoforms of FMO and their differential regulation.

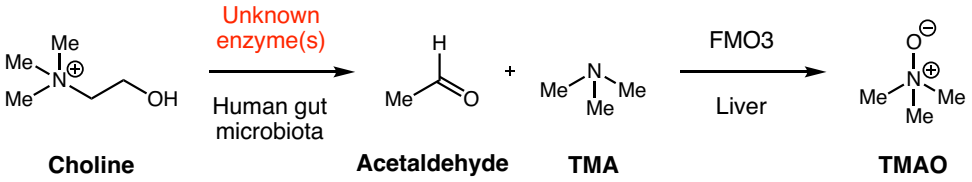

Figure 1.3. Choline metabolism to TMAO within the human body.

Several studies showed that the conversion of choline to TMA is an exclusively microbial capability.6 Gnotobiotic mice do not produce TMA, and treatment of conventional mice with antibiotics depletes plasma levels of this metabolite.[37,38] Furthermore, colonization of gnotobiotic mice with choline-converting bacteria not only increases cecal TMA production but also lowers serum concentrations of choline. These findings have been verified in humans.[39,40] However, despite mounting evidence that anaerobic choline metabolism is directly implicated in the generation of TMA in the human gut, its genetics and biochemical mechanism remained a mystery. Finally, in 2012, work in the Balskus lab successfully traced this transformation to the action of a glycyl radical enzyme (GRE) and a GRE-activating enzyme.[41] The GRE family is described in detail in Section 1.5, and Section 1.6 expands upon the discovery and characterization of the particular GRE responsible for the cleavage of choline into TMA.

1.4. Link of gut microbial choline metabolism to human health and disease

Multiple human diseases are associated with microbial metabolism of choline in the gut. Elevated levels of plasma TMAO in humans have been linked to a wide range of disorders, including nonalcoholic fatty liver disease,[42,43] cardiovascular disease,[39,44-46] chronic kidney

disease,[47,48] and type 2 diabetes mellitus.[49] Additionally, patients with the inherited metabolic disorder trimethylaminuria exhibit decreased FMO activity and accumulate the malodorous compound TMA in bodily fluids.[50-52] Despite the many connections between anaerobic choline metabolism and human health, the mechanisms by which choline-degrading gut microbes affect host physiology and interact with other members of the microbiota remain largely uncharacterized. Targeting TMA formation by gut microbes with a small molecule inhibitor may be an effective strategy for studying the role of the choline-to-TMAO pathway in complex microbial communities and for understanding the impact of this pathway on human health.

1.5. Glycyl radical enzymes play key roles in anaerobic microbial metabolism

GREs use protein-based radicals to accomplish a variety of chemically challenging transformations. Members of the this family play prominent roles in anaerobic microbial metabolic pathways, including carbohydrate utilization, mixed acid fermentation, and deoxyribonucleotide synthesis.[53,54] Based on the type of biochemical reaction catalyzed, this enzyme group can be divided into five categories: formate-lyases, class III ribonucleotide reductases, 1,2-eliminases, decarboxylases, and X-succinate synthases (where X denotes an aryl or alkyl substituent) (Figure 1.4).

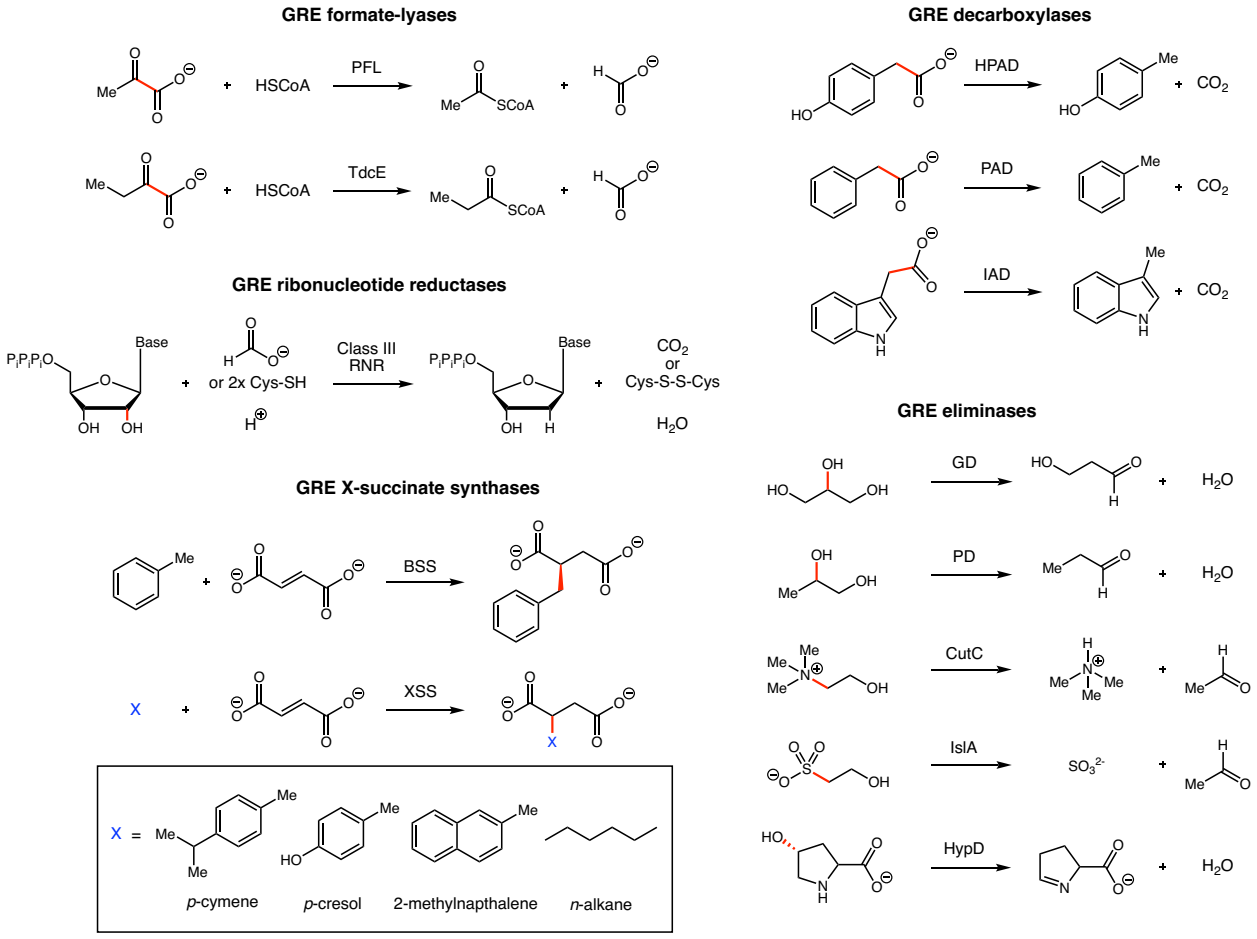

Figure 1.4. Classification of characterized GREs. The five classes of GREs include: (1) GRE formate-lyases (pyruvate formate-lyases, PFL, and ketobutyrate formate-lyases, TdcE); (2) GRE 1,2-eliminases (glycerol dehydratase, GD, propane-1,2-diol dehydratase, PD, choline trimethylamine-lyase, CutC, and *trans*-4-hydroxy-L-proline dehydratase, HypD); (3) GRE ribonucleotide reductases (class III RNRs); (4) GRE decarboxylases (4-hydroxyphenylacetate decarboxylase, HPAD, phenylacetate decarboxylase, PAD, and indole-3-acetate decarboxylase, IAD); and (5) GRE X-succinate synthases (XSSs, where X = toluene in the case of benzylsuccinate synthase, BSS).

1.5.1. GREs share common structural and mechanistic features

Protein-based radicals can be transient or stable and typically involve tyrosine, tryptophan, cysteine, or glycine residues. For all members of the GRE family, the key glycine-centered radical is post-translationally installed by the action of a separate enzyme, referred to as an activating enzyme (AE) or activase (Figure 1.5). Upon formation of the glycyl radical, the

GRE is effectively activated and can initiate a series of radical-based reactions within its active site. Each GRE has a specific AE, and the genes for this pair of enzymes are typically encoded adjacent to one another in microbial genomes. A single AE can only activate a GRE possessing the same activity as its native GRE partner, i.e. AEs do not promiscuously activate unrelated GREs. AEs are members of the radical SAM enzyme family, the largest known superfamily of enzymes, which utilize a reduced $[4Fe\text{-}4S]^{+}$ cluster to homolytically cleave SAM into the 5′-deoxyadenosyl radical (5′-dA•) and L-methionine (Figure 1.5).[53,54]

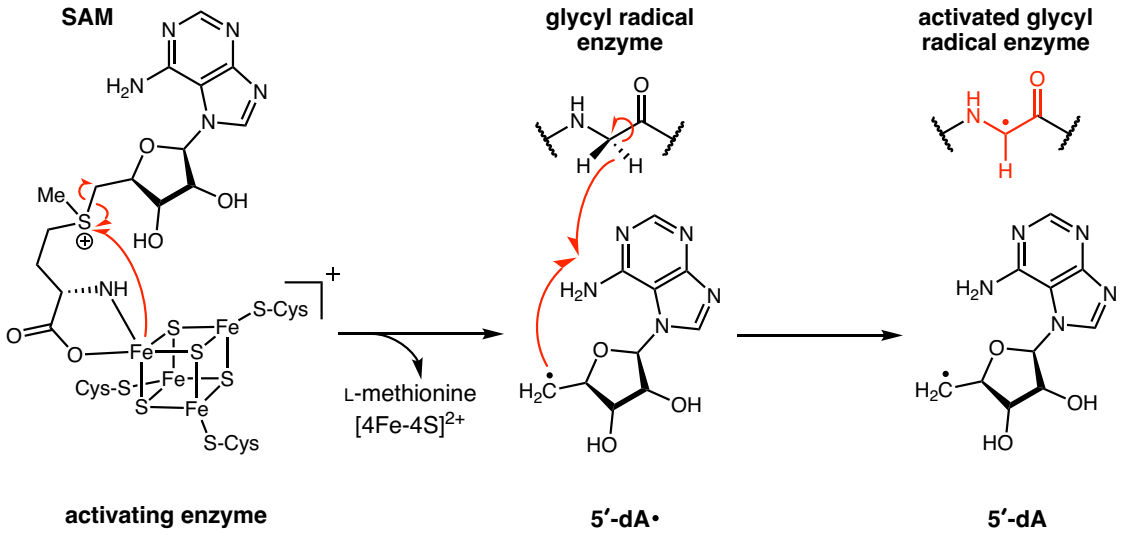

Figure 1.5. General scheme for the activation of a GRE by a GRE-AE. A $[4Fe\text{-}4S]^{+}$ cluster bound to the activating enzyme reductively cleaves SAM to generate L-methionine and a 5′-dA• species. The 5′-dA• abstracts the *pro-S* hydrogen atom from the GRE glycine. SAM = *S*-adenosylmethionine, 5′-dA = 5′-deoxyadenosine, 5′-dA• = 5′-deoxyadenosyl radical.

The extreme oxygen sensitivity of the [4Fe-4S] cluster makes it difficult to express AEs in heterologous hosts and recapitulate their activities *in vitro*. Thus far, the only available AE crystal structures belong to that of pyruvate formate-lyase-AE (PFL-AE).[55] Similar to other radical SAM enzymes, the active site of PFL-AE contains three Cys residues, located in a conserved CX_3CX_2C motif, each of which coordinates an Fe atom of a [4Fe-4S] cluster (Figure

1.5).[56,57] Mössbauer and ENDOR spectroscopy experiments,[58-60] along with structural data, revealed that the fourth Fe is coordinated to the amino nitrogen and carboxyl oxygen of SAM in a square-pyramidal geometry that allows the bottom of the pyramid to be occupied by the SAM sulfonium group. This arrangement enables the transfer of an electron between the reduced [4Fe-4S] cluster (in the +1 oxidation state) to the 5′ C–S antibonding σ* orbital of SAM.[61] The electron transfer lowers the bond dissociation energy (BDE) of the 5′ C–S bond in SAM such that homolytic bond cleavage can occur, generating 5′-dA• and L-methionine (in most instances, although cleavage of the S-Cγ bond and S-C_{methyl} bond have been reported).[61-64] The 5′-dA• is extremely reactive and, either directly (as depicted in Figure 1.5) or via the formation of an organometallic intermediate (termed Ω, in which the 5′ C of 5′-dA• is bound to the unique Fe of the iron-sulfur cluster),[65] stereospecfically abstracts the *pro-S* H atom from the active site glycine of a GRE.[66] For PFL-AE, *in vivo* reduction of the [4Fe-4S] cluster, from the +2 to the +1 state, is believed to occur via the action of flavodoxin, which is first reduced by either NADP:flavodoxin oxidoreductase or pyruvate:flavodoxin oxidoreductase.[67]

Electron paramagnetic resonance (EPR) spectroscopy studies of PFL performed by the Knappe group determined that the radical in activated PFL is present on an sp^2-hybridized α-carbon atom of a specific glycine residue.[68,69] Positioned between an electron-donating nitrogen and an electron-accepting carbonyl, α-carbon radicals are thus stabilized by the captodative effect (Figure 1.5). Moreover, as the least substituted of the peptide radicals, glycyl radicals exhibit the smallest repulsive steric effects between their α-carbon substituent and adjacent protein residues, thereby rendering them remarkably thermodynamically stable for a radical species.[70] Under anaerobic conditions, GREs display a similar EPR signal, composed of a doublet with hyperfine coupling of 1.4–1.5 mT (due to the interaction of the glycyl radical with

the nucleus of the α-hydrogen), centered at g = 2.003. This specific EPR signal allows the quantification of the extent of activation *in vitro*, as well as the detection of activated GREs in whole cells.[71]

After glycyl radical formation, hydrogen atom transfer is thought to occur between the glycyl radical and a neighboring Cys to form a transient thiyl radical (Figure 1.6). Although formation of the GRE thiyl radical has never been directly detected, evidence of its formation is available for the closely related class II ribonucleotide reductase (RNR) from *Lactobacillus leichmannii* and is indirectly inferred from H/D exchange experiments, demonstrated in various GRES, including *E. coli* class III RNR and PFL.[72-74] Moreover, both the Gly and Cys residues are conserved and catalytically essential in all known GREs and are found in close proximity to one another in all elucidated GRE structures. This supports a mechanism in which the thiyl radical initiates catalysis by abstracting a hydrogen atom from the substrate (Figure 1.6). Following a series of reactions and/or rearrangements, a product-based radical re-abstracts a hydrogen atom from the Cys residue, regenerating the thiyl radical, which in turn regenerates the glycyl radical. The stability of the glycyl radical allows it to serve as a radical "storage device" until the next round of GRE catalysis. The consumption of one molecule of SAM and one electron by an activating enzyme, which can then activate multiple copies of its partner GRE, each of which will subsequently contain a glycyl radical that is reformed after every catalytic cycle, makes this set of enzymes particularly useful in central metabolic processes requiring high turnover numbers and flux, especially under conditions where energy conservation is critical.

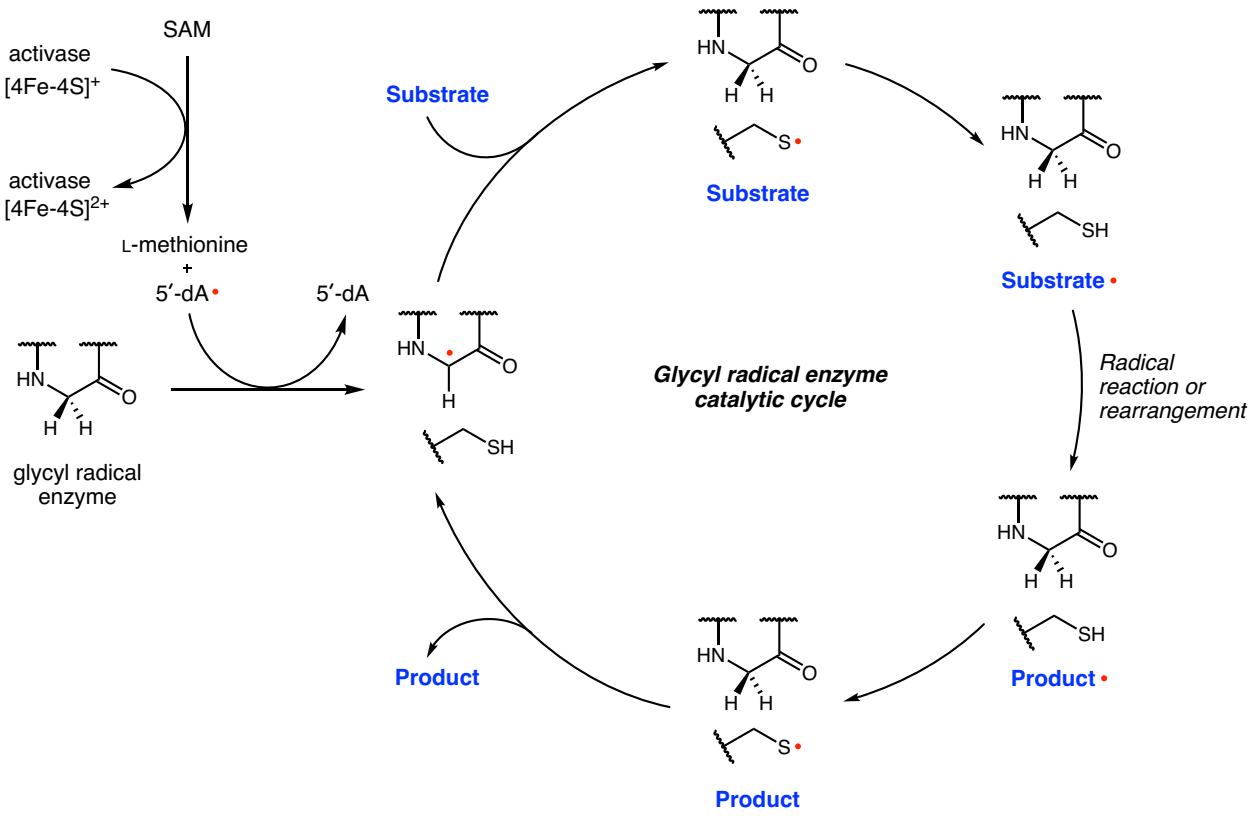

Figure 1.6. Shared mechanistic hypothesis for GRE function. Once the glycyl radical is generated on the GRE, hydrogen atom transfer is thought to occur from a neighboring Cys in the active site, forming a thiyl radical. This thiyl radical initiates catalysis by abstracting a hydrogen atom from the substrate, yielding a substrate radical, which undergoes reactions and rearrangements to yield a product radical. Finally, hydrogen atom-abstraction from Cys regenerates the thiyl radical, which in turn regenerates the glycyl radical.

Crystallographic studies on PFL, benzylsuccinate synthase (BSS), 4-hydroxyphenylacetate decarboxylase (HPAD), and class III RNR have revealed that GREs employ a conserved barrel-like architecture to facilitate radical catalysis. The so-called "GRE fold" consists of two, five-stranded half barrels arranged antiparallel to each other with α-helices on the outside.[53,54] The active site is buried in the center of the barrel, presumably to shield radicals from solvent, and contains the essential glycine residue, which is part of a loop (termed the Gly loop), containing a highly conserved stretch of amino acids (RVXG).[53] The conserved cysteine residue is located on a second loop (termed the Cys loop) and is in close proximity to

the Gly such that the two residues can interact with each other and participate in radical relay. GREs are typically homodimeric proteins with a subunit size of 80-100 kDa, although BSS and HPAD contain additional subunits. EPR studies with recombinant enzymes indicate the presence of only one glycyl radical per GRE dimer, suggesting that, at least *in vitro*, the activation of one monomer somehow precludes activation of the other.[75,76] The molecular mechanism for this observed half-site reactivity is unknown.

Since a crystal structure of a GRE in complex with its AE has yet to be elucidated, it remains unclear how exactly the two enzymes interact to initiate catalysis. In 2008, Vey and coworkers crystallized PFL-AE from *E. coli* bound to a seven-residue (RVSGYAV) peptide, which corresponds to the Gly loop of PFL and was demonstrated to act as a substrate for PFL-AE.[55] This amino acid motif is completely conserved in PFL but only the residues corresponding to R731 and G734 (numbered according to PFL from *E. coli*) are conserved among all GREs. The peptide was bound such that the Gly residue was adjacent (4.1 Å) to a molecule of SAM. In this conformation, the 5′-dA• resulting from SAM cleavage would be poised to abstract the *pro-S* hydrogen of Gly, supporting previous experiments (in which the Gly residue of a PFL-based peptide was replaced with L- or D-Ala)[77] that demonstrated the stereospecificity of glycyl radical formation via the 5′-dA• radical.

The crystal structures of GREs determined thus far indicate that the conserved Gly residue is buried 8-20 Å from the surface of the protein, a configuration that would prohibit direct H-atom abstraction by the 5′-dA• radical bound to the GRE-AE.[53] Studies on PFL and PFL-AE using circular dichroism (CD) and EPR spectroscopy revealed that the GRE is conformationally flexible, at times adopting a more open conformation that exposes the Gly residue and allows the AE to perform the initial H-atom abstraction.[78] The region of the GRE

that opens up to expose the Gly residue for activation has been coined the "Gly radical domain." It was proposed that the open and closed states of PFL are in equilibrium and, in the presence of PFL-AE, this equilibrium is shifted towards the open state, enabling PFL activation.

1.5.2. GRE formate-lyases

1.5.2.1. Pyruvate formate-lyase (PFL)

As the anaerobic counterpart to pyruvate dehydrogenase, PFL is central to anaerobic primary metabolism, catalyzing the conversion of pyruvate and CoA to formate and acetyl-CoA (Figure 1.7), two central metabolites that can be used for biosynthesis or the generation of ATP.[54] Recent chemically guided functional profiling efforts by the Balskus lab found that PFL is the most abundant family member in all GRE-containing metagenomes, consistent with its critical role in anaerobic glucose metabolism.[79] As one of the best-characterized members of the GRE family, PFL from *E. coli* was the first GRE to be overexpressed and purified *in vitro* and shown to be post-translationally modified by its activating enzyme, PFL-AE, under strict anaerobic conditions.[69,80] Based on extensive biochemical and computational studies, along with crystallographic snapshots of PFL, an enzyme mechanism has been proposed (Figure 1.8).[81-83]

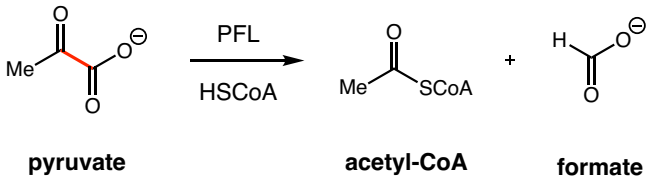

Figure 1.7. The activity of PFL.

The first step in the mechanism is H-atom abstraction by the glycyl radical (on Gly734 in *E. coli*) to form the catalytically essential thiyl radical on Cys418. X-ray crystal structures indicate that Gly734 is positioned adjacent to two conserved Cys residues (418 and 419), both of

which participate in the reaction. H-atom abstraction from Cys419 could be followed by H-atom abstraction from Cys418 to yield a Cys418 thiyl radical. Nucleophilic attack by the Cys418 thiyl radical on C2 of pyruvate would create a tetrahedral oxyradical intermediate, which, upon collapse, would generate a Cys418 acylated thioester and a formyl radical. The formyl radical could abstract a H-atom from Cys419, releasing formate and regenerating the Cys419 thiyl radical. A CoA-radical species, formed via the Cys419 thiyl radical, is proposed to interact with the acylated Cys418, resulting in the release of acetyl-CoA.

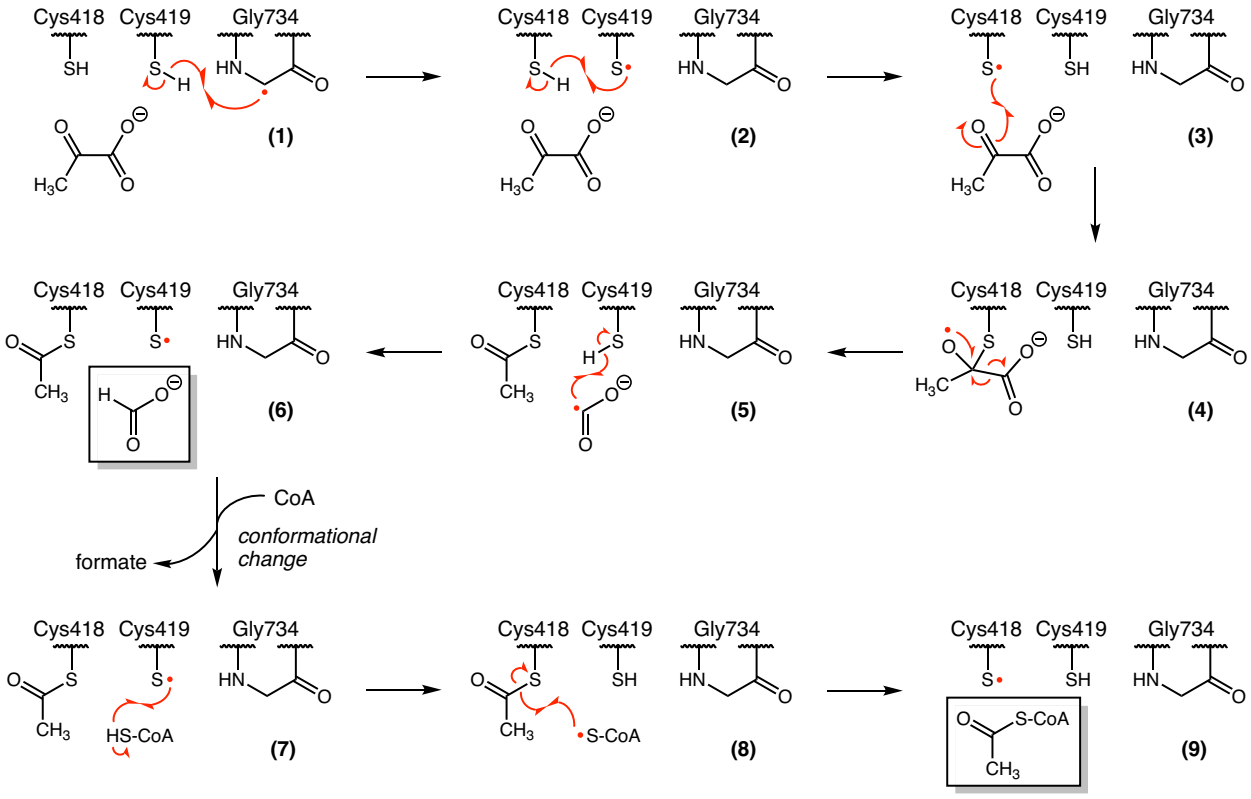

Figure 1.8. Proposed mechanism for the radical reaction of PFL. Amino acids are numbered corresponding to PFL from *E. coli*.

Upon exposure to O_2, activated PFL is irreversibly cleaved at the site of the glycyl radical (Gly734 in *E. coli*) to form two fragments, of 82 kDa (residues 1-733) and 3 kDa, thereby inactivating the enzyme.[84] In this circumstance, some organisms produce a short protein with

high homology to the last 59 residues of PFL (including G734), referred to as YfiD in *E. coli*.[85] After activation by PFL-AE, YfiD can associate with cleaved PFL, replacing its lost radical-containing domain and yielding a functional heteroenzyme complex. By restoring the activity of oxygen-cleaved PFL once anaerobic conditions return, YfiD essentially acts as a ‘‘spare part,’’ enabling these enzymes to cope with changing redox environments and potentially explaining the wide distribution of PFL in both anaerobic and aerobic environments. It remains to be seen if similar oxygen-damage repair mechanisms exist for other GREs.

1.5.2.2. 2-Ketobutyrate formate-lyase (TdcE)

A second member of the GRE formate-lyases, 2-ketobutyrate formate-lyase (TdcE), shares 82% sequence identity with PFL and can be activated by PFL-AE.[86] Complementation assays in *E. coli* showed that TdcE can replace PFL during glucose fermentation, but its main role is likely the anaerobic degradation of L-Thr, as TdcE is able to convert CoA and 2-ketobutyrate, the deamination product of L-Thr, into propionyl-CoA and formate (Figure 1.9).[86] Propionyl-CoA can be further processed to propionate in a reaction that generates ATP.

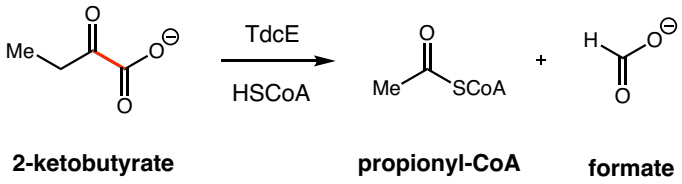

Figure 1.9. The activity of TdcE.

1.5.3. GRE eliminases

1.5.3.1. Glycerol dehydratase (GD)

A number of microorganisms are able to grow anaerobically on glycerol as the sole carbon and energy source. Two metabolic pathways are responsible for the dissimilation of

glycerol into glycolytic intermediates and the synthesis of 1,3-propanediol.[53] An oxidative pathway dehydrogenates glycerol to produce dihydroxyacetone, which, upon phosphorylation, can enter glycolysis, enabling the formation of essential metabolic intermediates and fermentation products. A parallel reductive pathway involves the action of a coenzyme B_{12}-dependent glycerol dehydratase, which converts glycerol to 3-hydroxypropionaldehyde. Reduction of this intermediate generates 1,3-propanediol. This reductive branch consumes NADH, thus providing a means for the cell to achieve a redox balance.[53]

Recently, the anaerobic bacteria *Clostridium glycolicum* and *C. butyricum* were shown to ferment glycerol in a coenzyme B_{12}-independent manner.[87] Further studies confirmed that a GRE, glycerol dehydratase (GD), catalyzes the first step in glycerol dehydration to 3-hydroxypropionaldehyde (Figure 1.10), which is then reduced by an NADH-dependent alcohol dehydrogenase to generate 1,3-propanediol.[88] GD can also dehydrate 1,2-propanediol to propionaldehyde (and thus act as a 1,2-propanediol dehydratase (PD)), but it is unclear if this reaction is important *in vivo*.

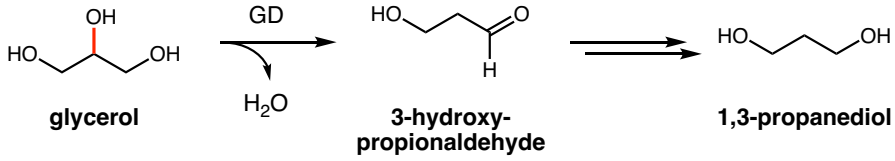

Figure 1.10. The activity of GD and its proposed role in glycerol fermentation.

A computational study proposed that, in contrast to B_{12}-dependent GD, glycerol dehydration by the GRE from *C. butyricum* does not need to involve migration of the middle hydroxyl group to one of the two terminal positions of the molecule.[89] Instead, upon H-atom abstraction from the C1 position of glycerol, the C2 hydroxyl group is eliminated and subsequently protonated by the neighboring His164, generating water (Figure 1.11).

Deprotonation of the C1 hydroxyl group by the active site residue Glu435 and H-atom abstraction from the catalytically essential Cys433 by the resulting product-based radical would reform the thiyl radical and release 3-hydroxypropionaldehyde. Direct elimination of water from an initial α-hydroxyalkyl radical (referred to as a "spin-center shift") appears to be a common theme among GREs.

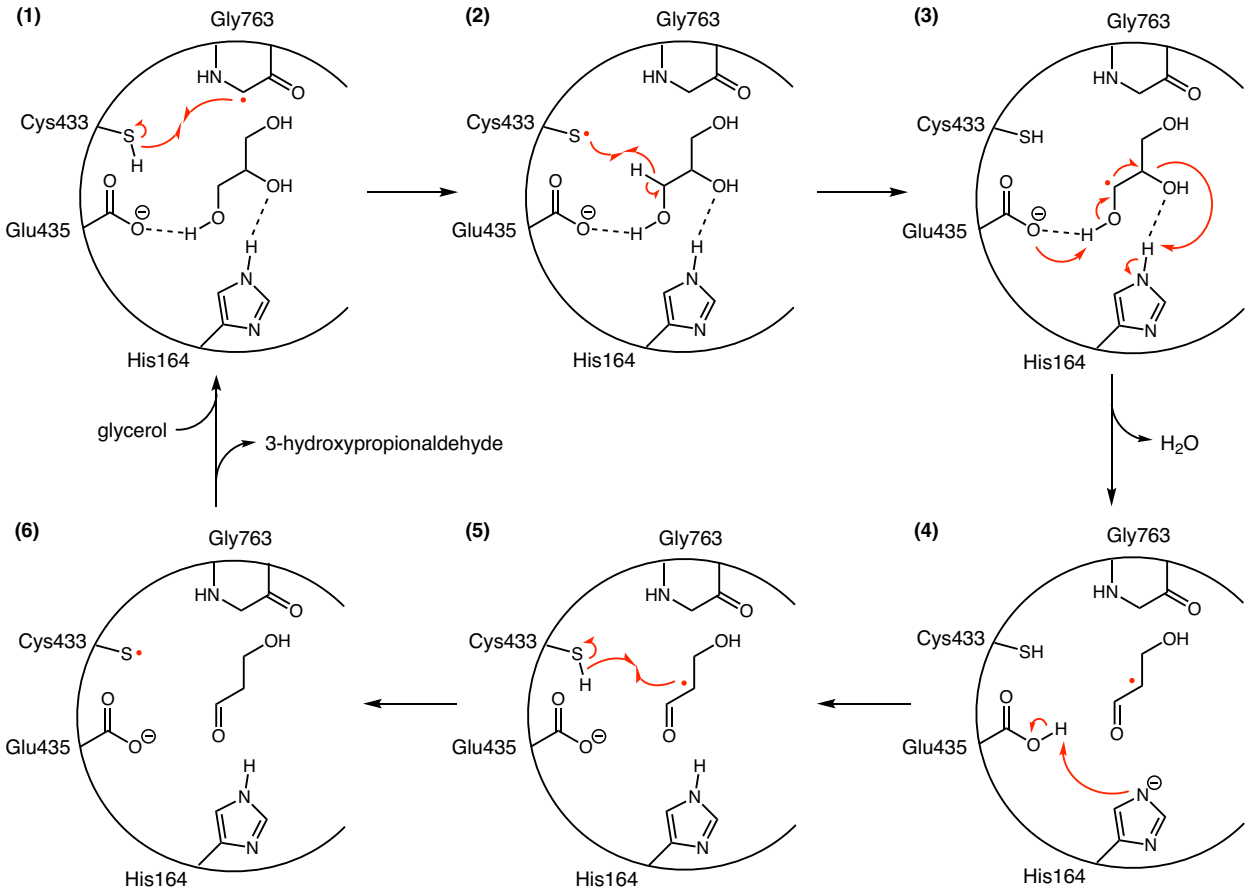

Figure 1.11. Proposed mechanism for the radical reaction of GDH. Amino acids are numbered corresponding to PFL from *C. butyricum*.

1.5.3.2. 1,2-Propanediol dehydratase (PD)

Gut bacterial fermentation of dietary polysaccharides that are indigestible by the host (for instance, L-fucose) results in the production of short chain fatty acids (SCFAs), including

propionate, acetate, and butyrate, which play critical roles in host physiology.[90-92] Cleavage of glycans lining the surfaces of colonic epithelial cells by microbial α-fucosidases liberates L-fucose. Gut bacteria possessing the L-fucose utilization (*fuc*) pathway can process this deoxysugar to yield dihydroxyacetone phosphate, which can be redirected to glycolysis for further catalysis, and (*S*)-lactaldehyde, which is used as an electron acceptor and reduced to (*S*)-1,2-propanediol.[93] Certain microbial organisms are capable of further converting (*S*)-1,2-propanediol to propionaldehyde via the action of a B_{12}-dependent 1,2-propanediol dehydratase (B_{12}-PD). Propionaldehyde can either be used as an electron acceptor in a reaction that generates 1-propanol or it can be oxidized to propionate, yielding ATP.[94] In this manner, certain gut microbes can utilize host-derived L-fucose as a source of carbon and energy.

Transcriptional profiling of genes upregulated during growth on L-fucose by the human gut bacterium *Roseburia inulinivorans,* which lacks an encoded B_{12}-PD, identified a B_{12}-independent 1,2-propanediol dehydratase (PD),[95] later confirmed to be a GRE.[79,96,97] PD shares 48% sequence identity with GD but catalyzes the conversion of 1,2-propanediol to propionaldehyde (Figure 1.12), with a preference for the (*S*)- over the (*R*)-enantiomer of the starting material.[79,97] Chemically guided functional profiling of metagenomes from healthy participants revealed that PD is present in 96% of stool samples, is the third-most abundant GRE in stool metagenomes, and is enriched in this habitat relative to other body locations.[79] Labeling experiments with ^{18}O suggested that PD and B_{12}-PD employ distinct mechanisms, with PD catalyzing the direct elimination of a hydroxyl group from an initially formed substrate-based radical,[97] avoiding the migration of the hydroxyl group and the generation of a 1,1-*gem* diol intermediate that occurs during B_{12}-PD catalysis.[98-100]

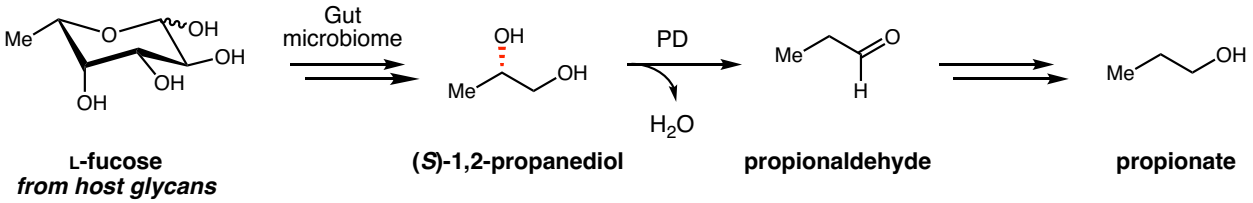

Figure 1.12. Hypothesized role of PD in L-fucose metabolism. The *fuc* pathway converts L-fucose to (*S*)-1,2-propanediol. PD, along with other microbial enzymes, further processes (*S*)-1,2-propanediol to propionate.

1.5.3.3. *trans*-4-L-Hydroxyproline dehydratase (HypD)

By applying a functional profiling pipeline to assess the distribution of GREs in Human Microbiome Project (HMP) metagenomes, the Balskus lab identified *trans*-4-L-hydroxyproline dehydratase (HypD), encoded in >850 sequenced prokaryotic genomes deposited in the NCBI database, including the human pathogens *Clostridium difficile*, C. *botulinum*, and *Treponema maltophilum*.[79] HypD is the most abundant previously uncharacterized GRE found in the human gut and is the second most abundant GRE. In the genomes of Clostridiales, the gene encoding this GRE is often clustered with genes encoding a GRE-AE and a predicted Δ^1-pyrroline-5-carboxylate (P5C) reductase, which reduces P5C to L-proline as the final step in L-proline biosynthesis (Figure 1.13).[101] This observation informed the hypothesis that HypD might catalyze the removal of water from the non-proteinogenic amino acid *trans*-4-hydroxy-L-proline (Hyp) to generate P5C, which could then be reduced to L-proline by P5C reductase. The Balskus lab demonstrated that HypD indeed catalyzes the dehydration of Hyp *in vitro*, and culture-based studies with Clostridia support the role of Hyp as an electron acceptor in Stickland fermentation (Figure 1.13), a pathway in which pairs of amino acids are used as electron donors and acceptors in energy metabolism.[79,102] It is possible that the conversion of Hyp to P5C and L-proline also serves to supply the microbiome with sources of carbon and nitrogen. Furthermore, Hyp metabolism might affect L-proline availability for the host. Due to its presence in collagen, the

most abundant protein in the diet, Hyp is available in large quantities in the human microbiome.[103] Gut microbes may liberate Hyp from collagen or collagen-derived peptides, affecting collagen homeostasis and potentially contributing to colonization resistance or pathogenicity in the host gut.

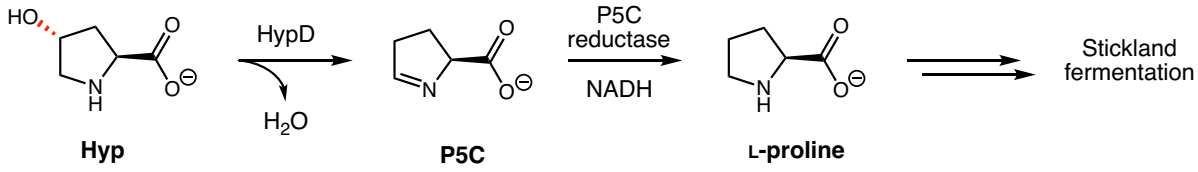

Figure 1.13. Hypothesized role of HypD in amino acid fermentation. HypD catalyzes the removal of water from Hyp to generate P5C. P5C reductase subsequently reduces P5C to L-proline, which is used as an electron acceptor in Stickland fermentation.

1.5.3.4. Isethionate sulfite-lyase (IslA)

Anaerobic microbial metabolism of organosulfonate compounds generates sulfite (SO_3^{2-}), which is used as a terminal electron acceptor by bacteria in a process that generates hydrogen sulfide (H_2S). In the gut, the production of H_2S has been implicated in host health and disease.[104,105] H_2S has been shown to act as a potent genotoxin, potentially contributing to the onset of colorectal cancer,[106] to reduce disulfide bonds in the mucus layer of the gut epithelium, disrupting its barrier function and possibly leading to inflammatory bowel disease (IBD),[107] and to induce antibiotic resistance, possibly triggering blooms of opportunistic bacteria during antibiotic treatment.[108] However, by functioning as a signaling molecule in the host, H_2S produced by gut microbes may also lead to beneficial effects, such as cardioprotection.[105,109]

Several human gut bacterium and opportunistic pathogens, including *Bilophila wadsworthia*, produce H_2S when respiring sulfite, which is released upon microbial degradation of organosulfonate substrates such as the abundant dietary and host-derived molecule taurine (2-aminoethanesulfonate) (Figure 1.14).[110] *B. wadsworthia*, which is typically present in low

abundance in the colonic microbiota of healthy humans,[111] has been associated with appendicitis and bone, brain, liver, and ear abscesses,[112] as well as with colorectal cancer.[113] In mice, *B. wadsworthia* can cause systemic inflammation[114] and proliferates with the onset of ulcerative colitis when taurine-conjugated bile acids are abundant in the GI tract.[115]

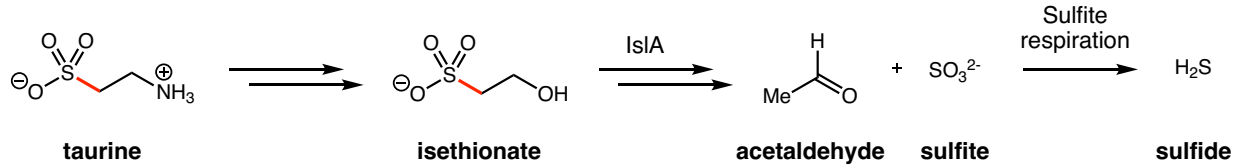

Figure 1.14. The activity of IslA and its role in sulfite respiration.

In *B. wadsworthia*, the metabolism of taurine involves its conversion to isethionate (2-hydroxyethanesulfonate). Desulfonation of isethionate generates free sulfite, which is then reduced to H_2S via the action of dissimilatory sulfite reductase.[110,116] Until recently, the enzymes that allow intestinal bacteria to access sulfite from isethionate (and from its precursor, taurine) under anaerobic conditions were unknown. A collaborative effort between the Schleheck and Balskus labs led to the identification of enzymes upregulated in *B. wadsworthia* and two *Desulfovibrio* strains during growth on taurine and isethionate.[117] This analysis revealed a GRE that was shown to cleave the C–S bond of isethionate (derived from taurine in *B. wadsworthia*) to produce sulfite and acetaldehyde *in vitro* (Figure 1.14). The GRE, referred to as isethionate sulfite-lyase (IslA or, as published in a later study, IseG[118]) differs from other 1,2-eliminases in its use of a sulfur-based leaving group.

1.5.3.5. Choline trimethylamine-lyase (CutC)

Choline trimethylamine-lyase (CutC) cleaves choline to TMA and acetaldehyde as the first step in anaerobic choline degradation (Figure 1.15). The discovery of CutC and its

biochemical and structural elucidation, along with studies on its distribution in metagenomes, are elaborated upon in Section 1.6.

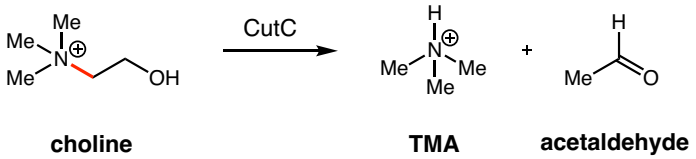

Figure 1.15. The activity of CutC.

1.5.4. GRE class III or anaerobic ribonucleotide reductase (class III RNR)

RNRs are essential enzymes in the *de novo* synthesis of deoxynucleotides from ribonucleotides (Figure 1.16), a process that occurs in all living organisms and provides the building blocks for DNA replication and repair. Ribonucleotide reduction is accomplished by three different classes of RNRs, hypothesized to have evolved from the same common ancestor and diversified depending on the presence of oxygen in the surrounding environment.[119] Although not all RNRs are GREs, they all exhibit the 10-stranded α/β barrel GRE fold and, despite relying on different cofactors, generate an active site thiyl radical that initiates radical-based catalysis.[120] The class I RNRs, which form a tyrosyl radical, use cofactors resulting from the reaction of reduced metals (Fe, Mn, and Fe/Mn) with O_2 and are present only in aerobic organisms.[54] Class II RNRs are coenzyme B_{12}-dependent and can be active under both aerobic and anaerobic conditions.[54] Only the O_2-sensitive class III RNRs, also known as NrdDs (where "Nrd" stands for nucleotide reductase and "D" specifies class III RNR), employ a glycyl radical.[54] Sequence similarity analysis of the GRE family shows that class III RNRs do not cluster close to other GREs, even though elements of their mechanism are similar to GRE eliminases. Despite being oxygen sensitive, class III RNRs are found in both strict and facultative anaerobes, including *E. coli*, *Lactococcus lactis*, *Thermotoga maritima*, and T4

bacteriophage. Several pathogens encode multiple RNRs of different classes and upregulate class III RNR to cope with oxygen limitation within biofilms.[121,122]

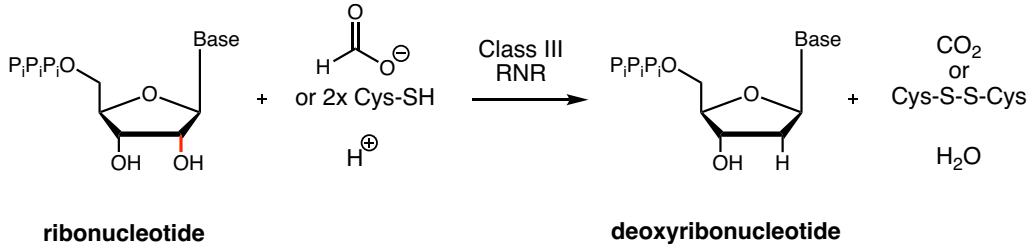

Figure 1.16. The activity of class III RNR.

Recent phylogenetic and metabolic pathway analyses on class III RNRs suggested that this group of enzymes can be further divided into at least three subclasses, which are distinguished by the presence or absence of 3-4 catalytic residues and the requirement for formate as the reductant.[54] The general mechanism of NrdDs consists of two distinct stages (Figure 1.17). In all RNRs studied thus far (classes I, II, and III), the first stage involves the generation of a 3′-nucleotide radical by the active site thiyl radical (formed on Cys1 in Figure 1.17). This is followed by dehydration of the ribonucleotide 2′ carbon and deprotonation of the 3′ hydroxyl group, which is facilitated by a general base catalyst (formate in the case of NrdD1 or an active site Glu residue in Nrd2). These steps resemble the dehydration mechanism proposed for the GRE eliminases.

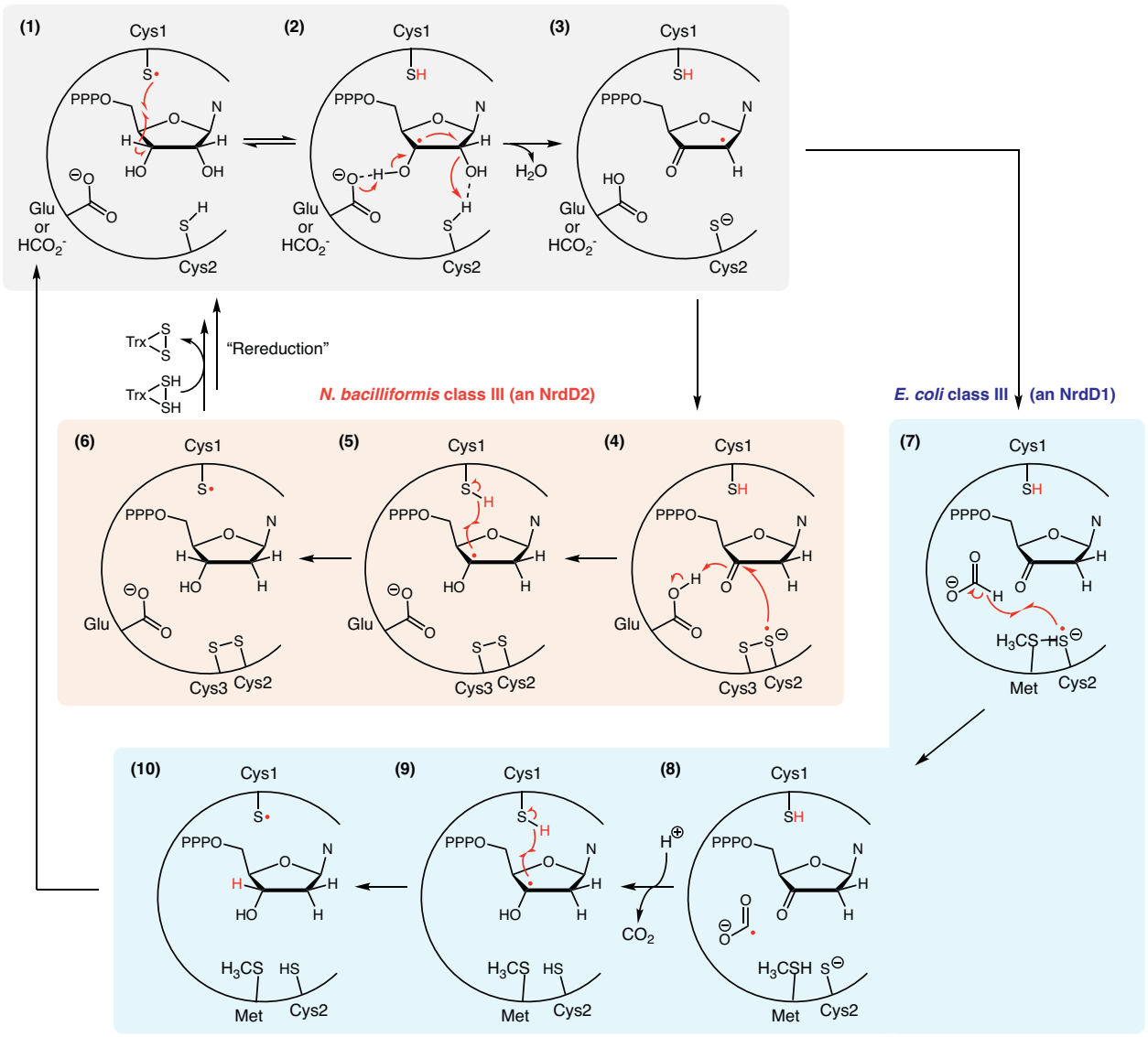

Figure 1.17. Proposed mechanism for the radical reaction of class III RNR (or NrdD).

In the second stage of the reaction, reduction of the resulting 2′-deoxy-3′-ketonucleotide generates a 2′-deoxy-3′-nucleotide radical that subsequently re-abstracts the thiol hydrogen from Cys1, resulting in deoxynucleotide formation. Experiments with the NrdDs from *E. coli* and *Neisseria bacilliformis* have revealed that stage 2 involves at least two mechanisms and two kinds of reducing agents. Oxidation of formate to CO_2 serves as the source of reducing equivalents in *E. coli* NrdD, a member of the NrdD1 subclass. Two key residues are thought to

be involved in formate oxidation: a Cys residue (labeled as Cys2 in Figure 1.17) and Met. Following dehydration at the 2′ position, Cys2 is oxidized by H-atom abstraction and forms a stable thiosulfuranyl radical with the adjacent Met. H-atom abstraction from formate restores Cys2 and Met and provides the putative reductant for the ketonucleotide, a formyl radical. Reabstraction of the H-atom from Cys1 completes the nucleotide reduction.

NrdD2 enzymes, exemplified by the *N. bacilliformis* class III RNR, do not require formate, instead obtaining reducing equivalents from a thioredoxin/thioredoxin reductase system, analogous to class I and II RNRs.[123] Wei and coworkers proposed that a pair of Cys residues, Cys2 and Cys3 in Figure 1.17, are reduced in a thioredoxin-dependent reaction prior to turnover and act as the immediate source of reducing equivalents during turnover.[124] Following elimination of water, Cys2 and Cys3 are oxidized by the 2′ radical, creating a disulfide anion radical. This species is expected to reduce the ketonucleotide as Glu re-protonates the 2′ hydroxyl group. H-atom abstraction produces the deoxyribonucleotide and leaves behind a disulfide that must be re-reduced prior to another round of turnover.

A third NrdD subclass (NrdD3), found in *Methanosarcina barkeri*, lacks the conserved Glu residue thought to be the catalytic acid/base in NrdD2 enzymes but contains Cys2 and Cys3 residues and does not oxidize formate.[125] Instead of thioredoxin, it uses the glutaredoxin-like protein NrdH to acquire electrons from reduced ferredoxin through a ferredoxin:disulfide reductase. No structure of a member of this subclass is currently available.

1.5.5. GRE decarboxylases

The GRE 4-hydroxyphenylacetate decarboxylase (HPAD) is primarily present in commensal and pathogenic Clostridia and catalyzes the decarboxylation of 4-

hydroxyphenylacetate, which is derived from tyrosine, into the bacteriostatic metabolite *p*-cresol (4-methylphenol) and CO_2 (Figure 1.18).[126] *p*-Cresol production by *Clostridium difficile* (and related pathogens) is postulated to promote virulence, since these bacteria can withstand 35-fold greater concentrations of *p*-cresol than other strains. HPAD is a functional heterotetramer $(\beta\gamma)_4$ composed of 100 kDa catalytic subunits, termed β, which harbor the Gly and Cys loops, and small 9.5 kDa subunits, termed γ, that bind two [4Fe-4S] clusters located approximately 40 Å away from the active site.[127,128] The γ-subunits are structurally homologous to high potential iron-sulfur proteins (HiPIP) and are believed to be involved in regulating the oligomeric state and activity of the heterotetrameric complex, for instance, by mediating electron transfer, such as quenching of the glycyl radical in the absence of substrate. The structural architecture of HPAD introduces a new subclass of [4Fe-4S] cluster-containing GREs that also includes BSS.

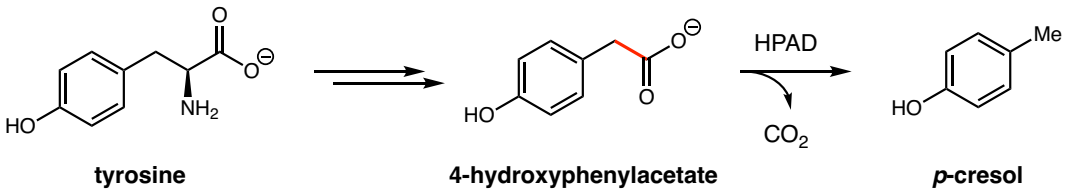

Figure 1.18. The activity of HPAD and its proposed role in the fermentation of tyrosine.

Structural and computational studies[129] of the HPAD mechanism suggested that the reaction proceeds through a biologically unprecedented Kolbe decarboxylation mechanism (Figure 1.19), defined as the one-electron oxidation of carboxylate ions. In the case of HPAD, the orientation of the carboxyl group of the substrate towards Cys503 (numbered according to *Clostridium scatalogenes*) suggests that the Cys503 thiyl radical could oxidize the carboxylate group, generating a carboxyl radical. This step is proposed to be coupled to phenol deprotonation by a conserved Glu residue in the active site. The thiol anion likely accepts a proton from another

conserved Glu residue. Decarboxylation of the carboxyl radical is proposed to be coupled to phenol protonation, generating a 4-hydroxybenzyl radical. H-atom abstraction from Cys503 would then generate *p*-cresol.

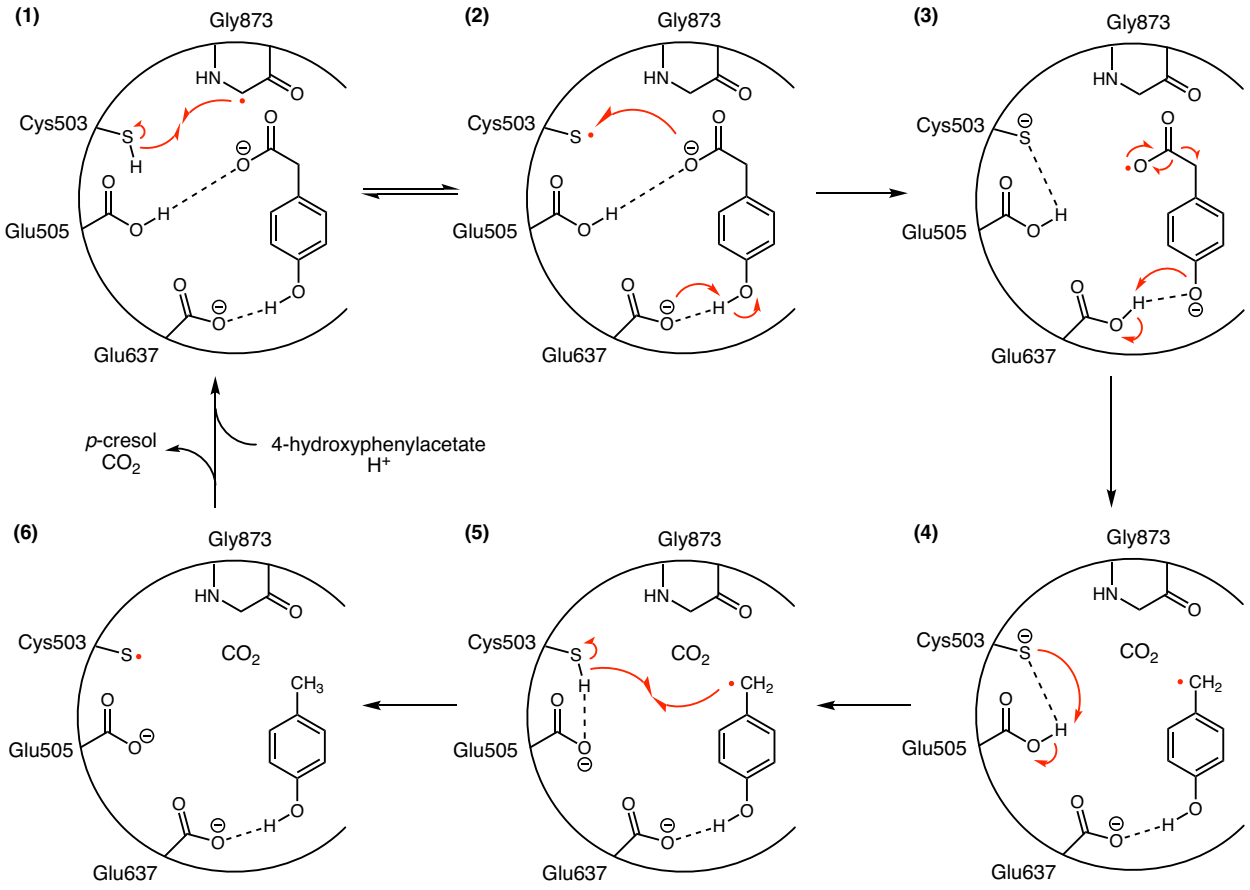

Figure 1.19. Proposed mechanism for the radical reaction of HPAD. Amino acids are numbered corresponding to HPAD from *Clostridium scatologenes*.

Recently, the GRE phenylacetate decarboxylase (PAD) was identified from an anaerobic, sewage-derived enrichment culture.[130,131] This enzyme was shown to catalyze the decarboxylation of phenylacetate (derived from phenylalanine) *in vitro* and in cell-free extracts, producing toluene and CO_2 (Figure 1.20), though the slow rate of this reaction *in vitro* raises questions about its physiological relevance. PAD also appears to lack a small subunit. Given that

phenylacetate is missing the hydroxyl group required for a Kolbe decarboxylation mechanism, catalysis by PAD is likely to proceed through a mechanism different from that of HPAD. Indeed, PAD does not contain the conserved Glu from HPAD that is proposed to deprotonate the phenol of 4-hydroxyphenylacetate.

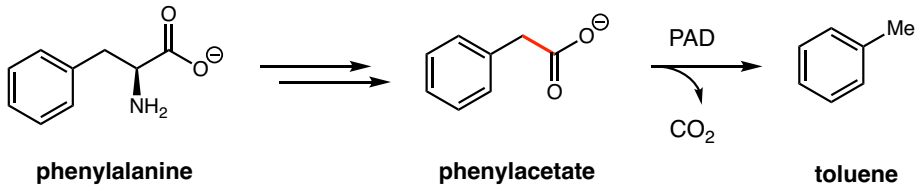

Figure 1.20. The activity of PAD and its proposed role in the fermentation of phenylalanine.

The GRE indoleacetate decarboxylase (IAD) from *Olsenella scatoligenes*, isolated from pig manure, was recently demonstrated to anaerobically catalyze the decarboxylation of indoleacetate, forming skatole as the terminal step of tryptophan fermentation (Figure 1.21).[132] Skatole production is linked to diseases of livestock, including boar taint in pigs and fog fever in cattle. In humans, skatole is a pulmonary and hepatic toxin.

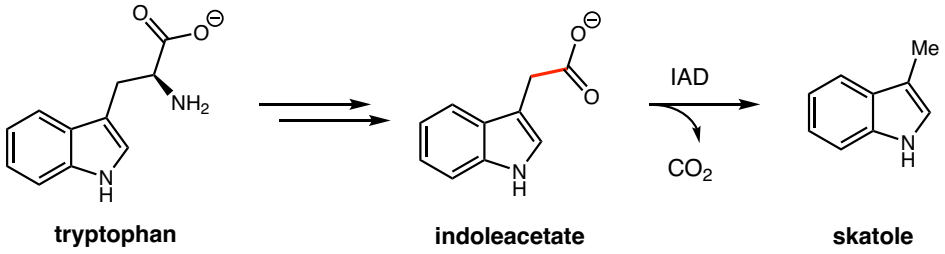

Figure 1.21. The activity of IAD and its proposed role in the fermentation of indoleacetate.

1.5.5. GRE X-succinate synthases

X-succinate synthases (XSSs) are a class of GREs that perform a remarkable C-C bond forming reaction on inert hydrocarbon substrates, thus initiating the decontamination of

hydrocarbon-polluted environments.[54,133] This class of enzymes, referred to as XSS (where X is the resulting hydrocarbon adduct), is proposed to act on both aryl and alkyl substrates. XSS enzymes are active under anoxic conditions and are important contributors to the bioremediation of habitats such as the deep ocean and underground aquifers.[131,134]

The most well studied member of the XSS enzymes is benzylsuccinate synthase (BSS), first isolated from *Thauera aromatica*, which catalyzes the addition of toluene to fumarate, generating (*R*)-benzylsuccinate (Figure 1.22), a potential source of carbon and energy.[135] Biochemical and structural studies revealed that BSS forms a stable $(\alpha\beta\gamma)_2$ heterohexamer *in vitro*.[136] The α-subunit, which contains the catalytically essential Gly residue, displays the 10-stranded α/β barrel fold characteristic of GREs and is responsible for binding to toluene and fumarate. The additional subunits, termed β and γ, which are essential for the growth of *T. aromatica* on toluene,[137] display homology to high potential iron–sulfur proteins (in fact, they are similar in structure to the small subunits of HPAD)[128,138] and appear to play redox and structural roles. BSSγ binds distally to the active site, occluding a hydrophobic region of BSSα from solvent,[138] while BSSβ binds near the active site and contacts the top of the putative substrate channel, potentially acting as a plug to prevent the escape of toluene and possibly regulating the formation of the glycyl radical.[139] Despite the successful purification and crystallization of the BSS complex and the reconstitution of BSS activity in crude cell extracts,[136,140-143] BSS-AE has resisted purification and its activity has not yet been reconstituted *in vitro*.

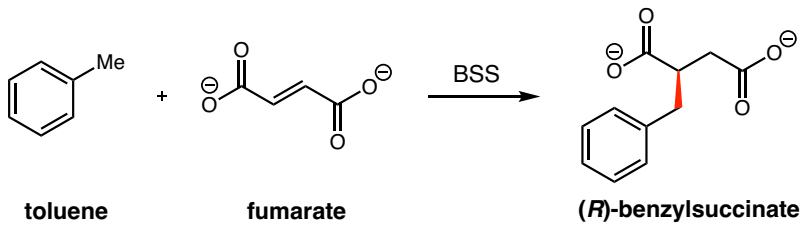

Figure 1.22. The activity of BSS.

In the active site of BSS, fumarate is held in place by hydrogen bonds formed with the Cys loop backbone and an Arg residue (Figure 1.23).[139,141-144] Toluene is sandwiched against fumarate and a "hydrophobic wall," comprised of Leu, Val, Ile, and Phe residues near the Cys loop, and thus, despite lacking any active functional handles, is held in the correct orientation within the active site. Insights from structural data and biochemical experiments inspired a mechanistic proposal for (*R*)-benzylsuccinate synthesis (Figure 1.23).[139,141-144] After formation of the thiyl radical, an H-atom is abstracted from the toluene methyl group, followed by the immediate formation of a product-like benzylsuccinyl radical. A slight rearrangement of this radical is necessary for H-atom abstraction from the active site Cys to generate product and re-generate the thiyl radical. Quantum mechanical modeling supports this proposed mechanism and suggests that H-atom abstraction is the rate-limiting step.[145]

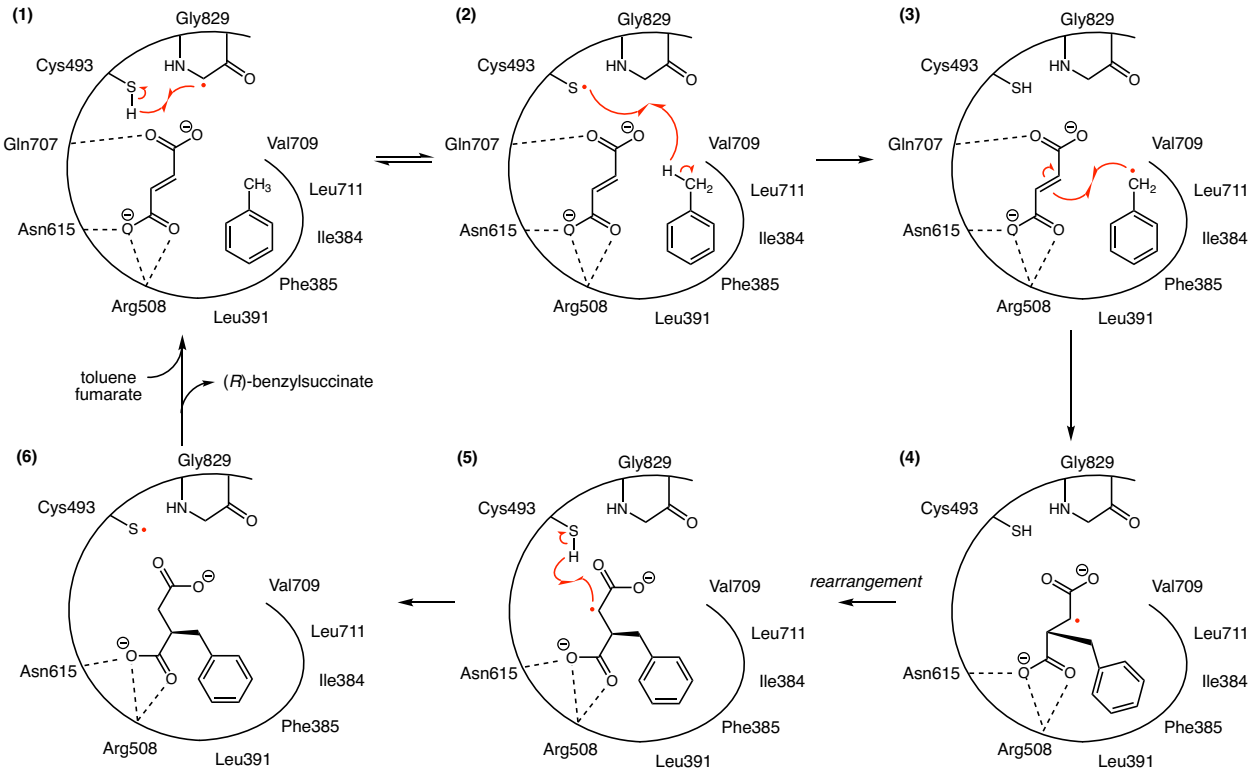

Figure 1.23. Proposed mechanism for the radical reaction of BSS. Amino acids are numbered corresponding to BSS from *Thauera aromatic.*

Several homologs with known aryl and alkyl hydrocarbon substrates have been identified in anaerobic phototrophic bacteria and in syntrophic communities of methanogenic archaea and sulfate-reducing bacteria. These XSS enzymes include 4-isopropylbenzylsuccinate synthase (IBSS),[146,147] hydroxybenzylsuccinate synthase (HBSS),[148,149] 2-methylnaphthylsuccinate synthase (NMSS),[150] and 1-methylalkylsuccinate synthase (MASS) (Figure 1.24).[151-153] While residues in the Cys loop that play a role in fumarate binding appear to be conserved within the XSS family (but not in other GREs), residues predicted to make up the "hydrophobic wall" show little sequence conservation in other XSS enzymes, suggesting the coevolution of active site residues with changing substrate specificity.[139,154] The substrate scope and distribution of XSSs underscores the importance of this metabolic pathway for bacterial survival in hydrocarbon-rich environments.

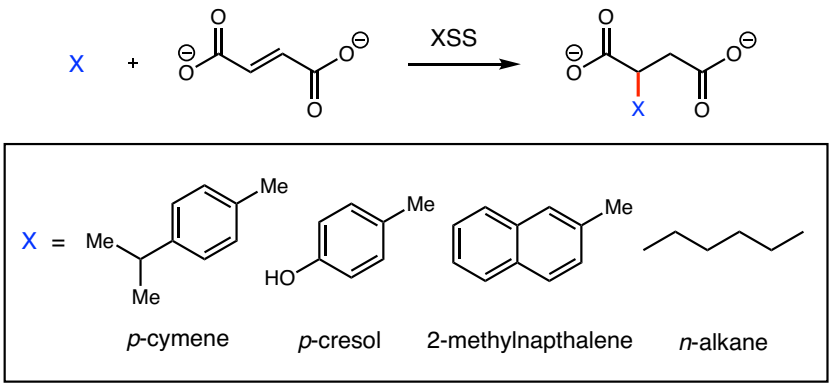

Figure 1.24. The activity of XSS enzymes.

1.6. Discovery of an anaerobic microbial choline utilization gene cluster

Given the significance of anaerobic choline metabolism in human health and disease (see Section 1.4), there was an obvious and urgent need to identify the underlying genetics and biochemical mechanism effecting this transformation. In 2012, the Balskus lab employed a chemically guided genome-mining approach to uncover the choline utilization (*cut*) gene cluster.[41] Their discovery was premised on the hypothesis that conversion of choline to TMA and acetaldehyde might share similarities with the well-studied catabolism of ethanolamine (a choline analog containing a primary amine in place of the trimethylammonium group), which forms ammonia and acetaldehyde (Figure 1.25) and is catalyzed by bacterial enzymes encoded in the ethanolamine utilization (*eut*) gene cluster.[155]

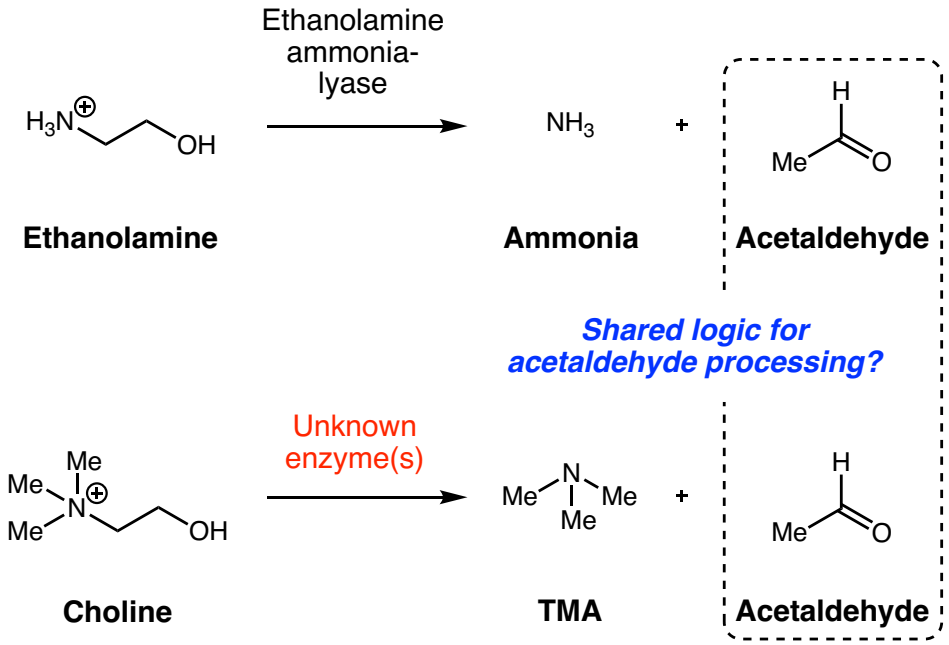

Figure 1.25. Potential parallel logic between anaerobic choline utilization and bacterial ethanolamine utilization pathways.

Within the *eut* gene cluster of *Salmonella enterica*, *eutB* and *eutC* genes encode the subunits of the vitamin B_{12}-dependent enzyme ethanolamine ammonia-lyase (EAL), which catalyzes the C-N bond cleavage of ethanolamine.[155] The acetaldehyde generated from this reaction can be converted to ethanol and acetyl-CoA by alcohol dehydrogenase (EutG) and aldehyde oxidoreductase (EutE), respectively, both of which are encoded by the *eut* operon. Acetyl-CoA is subsequently used in a range of metabolic processes, such as the TCA (tricarboxylic acid) cycle, the glyoxylate cycle, or lipid biosynthesis. Alternatively, it can be phosphorylated by EutD to form acetyl phosphate, which is further processed by housekeeping acetate kinase (AckA) to generate ATP and acetate. In this manner, ethanolamine functions as a source of carbon and energy for the bacterial cell, perhaps explaining why this reaction is sequestered inside a protein-based organelle known as a microcompartment.

1.7. Validation of the microbial *cut* gene cluster via genetic knockout and heterologous expression

Similar to other B_{12}-dependent enzyme-catalyzed eliminations, the mechanism of ethanolamine cleavage relies on the formation of crucial hydrogen bonding interactions between the substrate's N-H bonds and the active site of EAL. It therefore seems unlikely that this family of enzymes would be responsible for the cleavage of choline, whose *N*-methyl-groups cannot make key contacts with active site residues.[156,157] Nevertheless, the Balskus lab recognized that the degradation of choline and ethanolamine converged on a common intermediate, acetaldehyde, and that the bacterial machinery for processing, and even sequestering, this volatile molecule might be similar (Figure 1.25). This rationale prompted them to search the genomes of *Desulfovibrio desulfuricans* and *Desulfovibrio alaskensis*, anaerobic sulfate-reading organisms that metabolize choline to TMA, for homologs of EutG (alcohol dehydrogenase), EutE (aldehyde oxidoreductase), and the microcompartment protein EutM from *S. enterica*. Thus, they identified the *cut* gene cluster (Figure 1.26), a ~16-kb genomic region that displays similar organization to the *eut* gene cluster but, noticeably, is missing *eutBC*, the subunits of EAL.[41] In fact, homologs of this B_{12}-dependent enzyme were absent from both the newly discovered 19-gene cluster and the rest of the *D. desulfuricans* genome. Instead, the *cut* operon contained genes that were predicted to encode a GRE, CutC, and a GRE-AE, CutD.

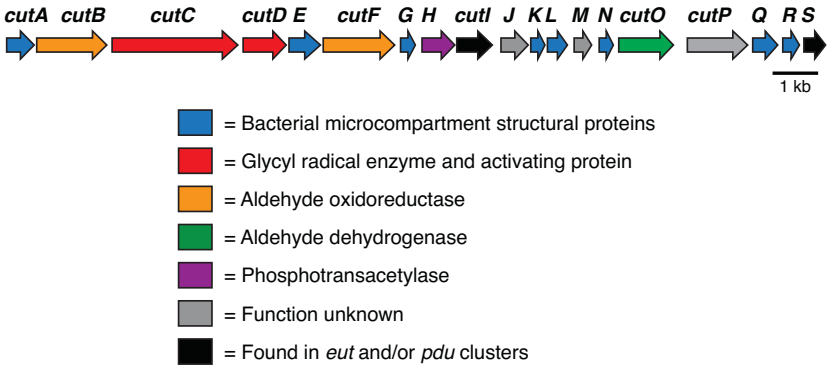

Figure 1.26. Genetic organization of the *Desulfovibrio desulfuricans* ATCC 27774 *cut* gene cluster.

Multiple sequence alignment of CutC from *D. desulfuricans* with other characterized GREs revealed the presence of the key active site residues, glycine and cysteine, which are involved in radical-mediated catalysis and are essential for GRE function. Moreover, putative choline TMA-lyases from different bacterial genera also showed conservation of these two active site residues. Genetic knockout of *cutC* in the anaerobic choline user *D. alaskensis* G20 and heterologous co-expression of both *cutC* and *cutD* from this organism in *E. coli* BL21(DE3) confirmed that these genes are necessary and sufficient for the cleavage of choline into TMA (Figure 1.27).[41] Expression of either gene alone in *E. coli* or mutation of Gly821 or Cys489 of CutC to Ala prevented TMA formation, providing further support for the annotation of *cutC* and *cutD* as a GRE and a GRE-activating protein, respectively.[41] In addition, whole-cell EPR studies showed that *D. desulfuricans* cells grown on choline-containing medium possess a paramagnetic species whose spectroscopic properties (g value of 2.003 and strong hyperfine coupling of 1.3 mT to a single proton) indicate the presence of an organic radical located at the α-carbon of an amino acid, presumably from activated CutC.[41] Bioinformatic analyses demonstrated that CutC homologs form a distinct clade within the GRE family of enzymes, which, prior to this work, had not been reported to perform C-N bond cleavage.

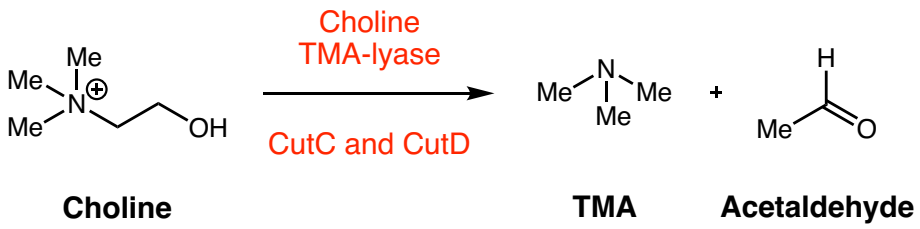

Figure 1.27. Anaerobic conversion of choline to TMA and acetaldehyde is catalyzed by a GRE, CutC, and a GRE-AE, CutD.

1.8. Further biochemical characterization of the *cut* gene cluster

In addition to TMA-generating enzymes, the *cut* gene cluster of *D. desulfuricans* ATCC 27774 encodes other functions likely involved in choline metabolism. Many of the *cut* genes are closely related to components of the B_{12}-dependent *eut* and 1,2-propanediol utilization (*pdu*) pathways,[158,159] including 8 genes encoding putative BMC shell proteins (*cutA*, *cutE*, *cutG*, *cutK*, *cutL*, *cutN*, *cutQ*, and *cutR*), two predicted coenzyme A (CoA)-acylating aldehyde oxidoreductases (*cutB* and *cutF*), a phosphotransacetylase (*cutH*), a putative chaperonin (*cutI*), an alcohol dehydrogenase (*cutO*), and a Ras-like GTPase (*cutS*). Analogous to the induction of ethanolamine and propanediol metabolic pathways in response to their respective substrates, transcription of all 19 *cut* genes increased during growth of *D. desulfuricans* on choline relative to growth on lactate, suggesting that several, if not all, of the proteins encoded by the cluster are involved in anaerobic choline metabolism.[160] The genes with the highest induction levels (*cutA*, *cutE*, *cutG*, and *cutL*) corresponded to the shell proteins of the BMC. In line with the proposed role of BMCs in ethanolamine metabolism, the choline utilization-associated BMC may encapsulate the acetaldehyde generated by CutC/D in order to protect the cell from the compound's toxic effects or to prevent the escape of this useful carbon and energy source.

Inside the microcompartment of *S. enterica*, vitamin B_{12}-dependent EAL cleaves ethanolamine to generate ammonia and acetaldehyde.[155] Ammonia can serve as a supply of

reduced nitrogen for the bacterial cell, while acetaldehyde is further processed within the BMC by aldehyde oxidoreductase EutE, which uses coenzyme A (CoA) and NAD^+ as cofactors, to form acetyl-CoA. The phosphotransacetylase EutD subsequently catalyzes the reversible conversion of acetyl-CoA to acetyl phosphate. Upon transport out of the microcompartment, acetyl-CoA is converted to acetate by the constitutively expressed acetate kinase AckA, a process that concomitantly generates ATP. Alternatively, acetyl-CoA can be used in various metabolic pathways such as the TCA or glyoxlate cycles or in lipid biosynthesis. Reduction of acetaldehyde within the microcompartment by the alcohol dehydrogenase EutG, an NADH-dependent enzyme, helps maintain redox balance.

Following this logic, choline enters the bacterial cell through diffusion or with the help of certain transporters (for instance, the gene directly upstream of cutA in *D. alaskensis* G20, Ddes_1354, is a predicted transporter whose expression was induced in the presence of choline) (Figure 1.28).[160] Within the choline-utilization microcompartment of *D. alaskensis* G20, which is composed of the structural proteins CutAEGKLNQR, acetaldehyde produced from the cleavage of choline could be further processed by CutF and CutO, the putative aldehyde oxidoreductase and alcohol dehydrogenase enzymes encoded by the *cut* gene cluster. Indeed, recombinant CutF from *D. alaskensis* G20 converted acetaldehyde to acetyl-CoA in the presence of NAD^+ and CoA, while recombinant CutO, which was expressed and purified under anaerobic conditions, reduced acetaldehyde to ethanol *in vitro*.[160] These data confirmed that CutF and CutO possess activities consistent with their proposed roles in choline fermentation. Phosphotransacetylase CutH could act on acetyl-CoA to produce acetyl phosphate, which can subsequently be converted to ATP by an acetate kinase homolog (Ddes_0296) encoded elsewhere in the genome of *D. alaskensis* G20. Flux through this pathway would generate the fermentation products

ethanol and acetyl-CoA and thus produce one molecule of ATP for every two molecules of choline.

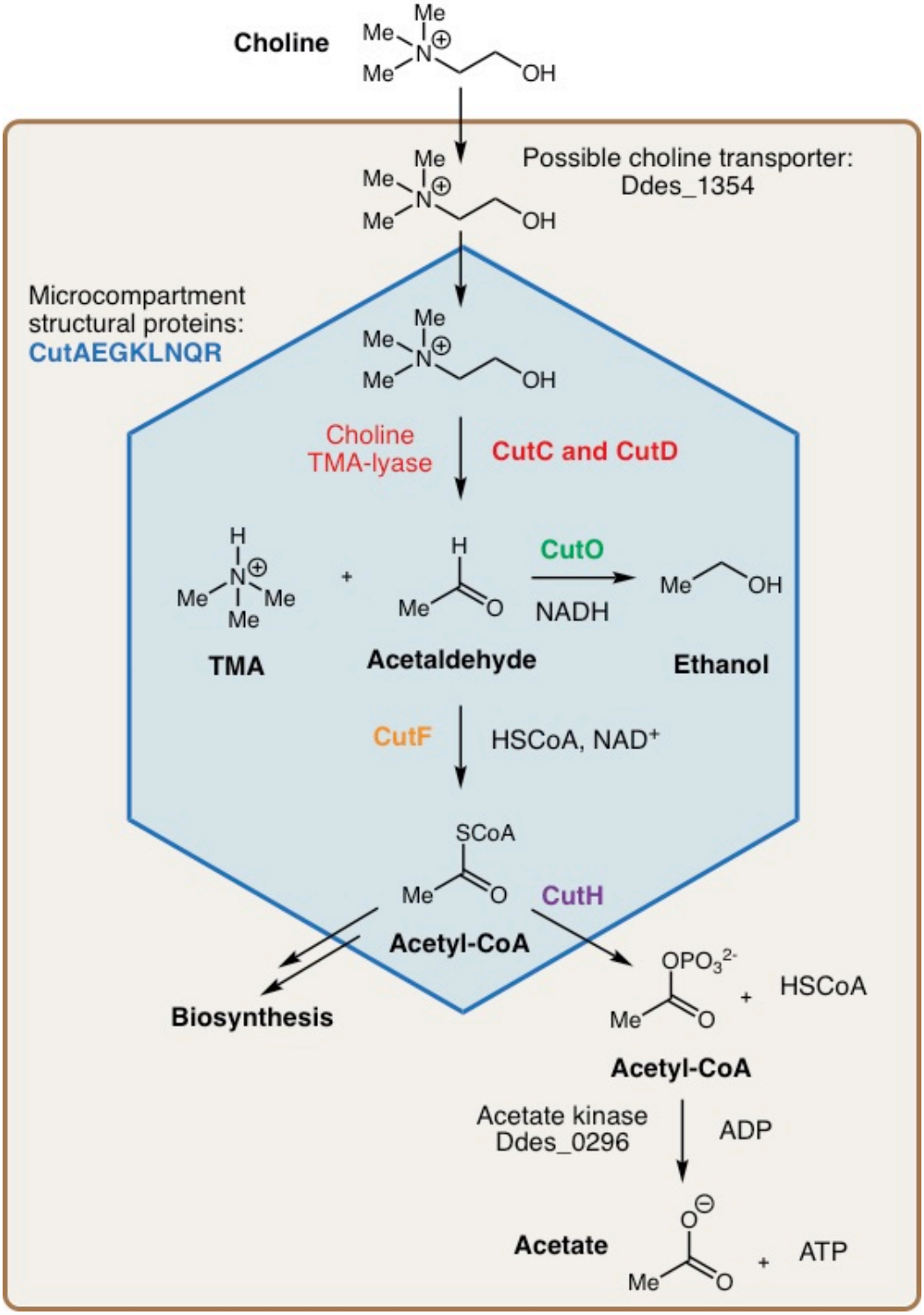

Figure 1.28. Proposed model for anaerobic choline catabolism in *D. alaskensis* G20.

1.9. Distribution of the *cut* gene cluster in bacterial genomes

To assess the distribution and diversity of *cut* gene clusters in sequenced bacterial genomes, Dr. Ana Martínez-del Campo from the Balskus lab used the CutC protein sequence from *D. desulfuricans* ATCC 27774 as a query for BLASTP searches against the nonredundant protein sequences database from NCBI.[160] All hits were evaluated for the presence of essential CutC active site amino acids (Asp216, Phe395, Cys489, Glu491, and Gly821), as established from biochemical experiments described in Section 1.10, to distinguish them from other GREs. This analysis uncovered over 800 CutC homologs (88% to 61% amino acid identity) distributed across three bacterial phyla, *Proteobacteria*, *Firmicutes*, and *Actinobacteria,* indicating that anaerobic choline utilization is a widely distributed microbial metabolic pathway (Figure 1.29). The majority of the sequences were found in *Proteobacteria* (*Gammaproteobacteria* and *Deltaproteobacteria*) and *Firmicutes* (*Clostridia* and *Bacilli*), with ~1% from *Actinobacteria* (*Coriobacteridae*). A small portion of hits (<1%) was identified in *Fusobacteria* (*Fusobacteriia*). CutC was conspicuously absent from *Bacteroidetes*, the dominant phyla in healthy adult intestinal microbiotas.[4] Culture-based experiments with bacterial isolates across the three *cutC*-encoding phyla demonstrated that all organisms containing this gene were able to generate TMA from isotopically labeled choline, with the exception of strains lacking the GRE activase, *cutD*.[160] Thus, the presence of the *cut* gene cluster likely serves as a functional marker for anaerobic choline metabolism.

The sequence search also revealed that the human body, including the gut, urogenital tract, oral cavity, and airways, is a major site of *cutC*-containing strains.[160] This gene was also identified in bacteria isolated from other mammals, insects, fish, and from the environment, suggesting that anaerobic choline utilization may be important for survival in many microbial

habitats. A discontinuous distribution of the gene cluster was observed across most microbial species; for instance, only ~4% of *E. coli* genes contained a CutC homolog, indicating that the conversion of choline to TMA is a strain-specific metabolic trait likely acquired via lateral gene transfer.[160] Of the 164 *E. coli* strains that harbor *cutC*, ~96% originated from the human urogenital tract, gastrointestinal tract, or bloodstream.[14]

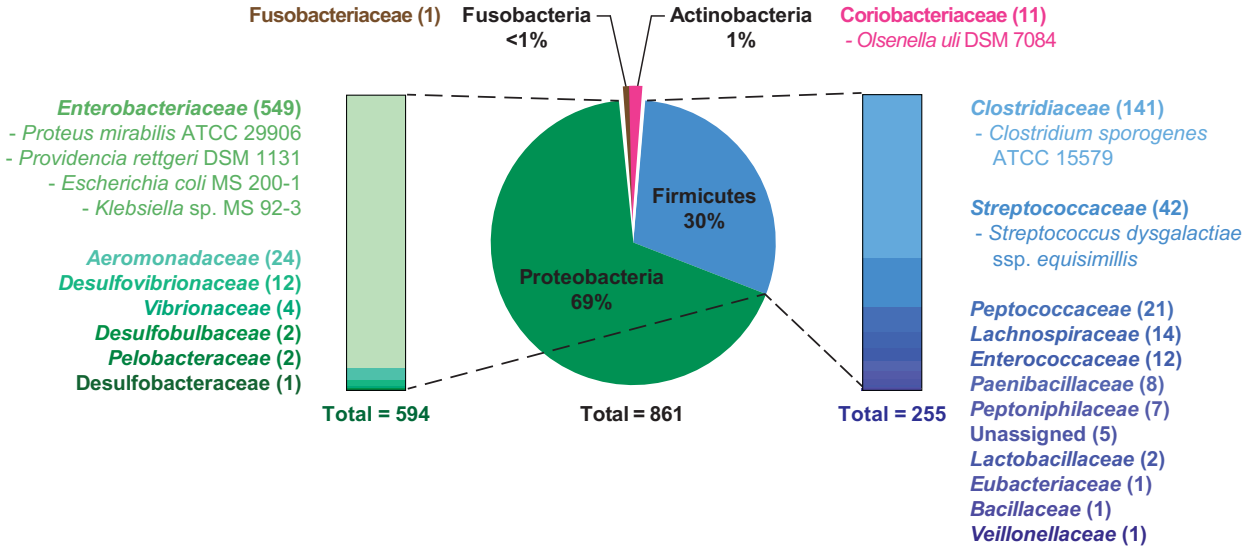

Figure 1.29. Analyses of the *cut* gene cluster in sequenced genomes reveals that it is widely distributed among bacteria.

Comparison of the gene content and arrangement of the ~800 *cut* clusters revealed two distinct subtypes, named types I and II, which differ in the number of BMC structural genes and the length of the N-terminal domain on CutC.[160] Type I clusters, found in *Firmicutes*, *Actinobacteria*, and *Deltaproteobacteria*, contained ~20 genes, including homologs of BMC-encoding genes (*cutAEGKLNQR*) and the central enzymes involved in choline fermentation (*cutC*, *cutD*, *cutF*, *cutO*, and *cutH*), along with *cutB*, *cutI, cutJ*, *cutS*, and, in some cases, *cutP*. Although gene content was consistent for these clusters, their order and transcriptional orientation varied. Nevertheless, all type I *cutC* genes contained a short N-terminal extension

that is predicted to function as a microcompartment targeting sequence, promoting attachment of the GRE to the luminal face of the BMC shell.[161] In contrast, type II cut clusters, found in *Gammaproteobacteria*, typically contained only 10 genes: the central enzymes involved in choline fermentation and four BMC structural proteins. The overall arrangement of the type II *cut* clusters was identical in all species. Rather than a short N-terminal localization sequence, type II *cutC* genes harbored a large (~350-amino-acid) N-terminal extension that shares some sequence similarity with the N-terminus of *cutC* sequences from type I clusters and therefore may also play a role in encapsulation or organization within the BMC. While type I *cut* clusters were distributed among both facultative and obligate anaerobes, type II clusters were found exclusively in facultative anaerobes, highlighting the oxygen sensitivity of GREs and suggesting that differences in *cut* gene content among microbes may have emerged as a result of their exposure to different levels of molecular oxygen.

Phylogenetic reconstruction of CutC protein sequences was incongruous with the phylogeny based on 16S rRNA sequencing, suggesting that horizontal gene transfer events mediated acquisition of these clusters in multiple organisms.[160] This proposal is also supported by the discontinuous distribution of this metabolic pathway across the majority of bacterial species possessing *cut* clusters and the presence of mobile genetic elements near many of these gene clusters. Microbial acquisition of *cut* genes in habitats where choline is an abundant growth substrate (such as in the human gut, where levels of choline are estimated to reach 1 mM)[162] may confer a competitive advantage. In addition, recent work has suggested that horizontal gene transfer occurs relatively frequently in the human gut.[163]

To assess whether the *cut* gene cluster was functional in human gut microbes, new choline-metabolizing organisms were isolated from human fecal samples that had been

continuously passaged on choline-containing media.[160] The identity of the organisms in enrichment cultures possessing the ability to convert (trimethyl-d_9)-choline chloride (d_9-choline) to d_9-TMA was determined by 16S rRNA gene sequencing, revealing the presence of nine distinct choline-utilizing strains from four genera (*Clostridia*, *Klebsiella*, *Escherichia*, and *Enterococcus*). Degenerate PCR established that anaerobic choline metabolism in these gut isolates was correlated with the presence of *cutC*, once again supporting that this gene can function as a molecular marker for choline utilization in complex microbial communities. Analysis of assembled stool metagenomes enabled the identification of functional CutC homologs (i.e. those containing the conserved active site residues Phe395, Cys489, and Glu491) in 143 different samples (97% of the total samples).[160] Altogether, these data suggest that the pathway encoded by the *cut* cluster could be a predominant mechanism for choline degradation and TMA production within the human gut.

1.10. Biochemical characterization of CutC and CutD enzymes and potential mechanism(s) of choline cleavage

In order to reproduce the choline-cleavage activity of CutC/CutD *in vitro*, Dr. Smaranda Bodea from the Balskus lab cloned the two enzymes from *D. alaskensis* G20 and overexpressed them in *E. coli*.[74] CutC was expressed and purified aerobically, and analytical gel filtration revealed the enzyme to exist in solution in a predominately dimeric oligomerization state, which is consistent with results for GD,[164] PFL,[68] and class III RNR.[165] It is possible that the interactions that mediate dimerization could be important for the assembly and packaging of GREs within the BMC. Expression, purification, and reconstitution (of iron-sulfur cluster(s)) of the putative GRE activase CutD were performed under strictly anaerobic conditions with co-

expression of the *E. coli isc* operon, which encodes a pathway for iron-sulfur cluster assembly.[166] CutD exists as a monomer in solution.

Multiple sequence alignment of CutD with characterized GRE activases revealed the conserved [4Fe−4S]-binding motif (CX_3CX_2C), putative SAM and GRE binding sites, and two "Clostridial"-type motifs ($CX_{2-5}CX_{2-4}CX_3C$), indicating the possibility of auxiliary [4Fe−4S] clusters.[55,167] Analyses of CutD-bound iron and sulfide content suggested the presence of two [4Fe−4S] clusters (~8.4 mol of Fe and 7.6 mol of S per mole of protein).[74] The UV−vis spectrum of reconstituted CutD displayed a broad peak at 380−420 nm, indicative of $[4Fe{-}4S]^{2+}$ clusters, that decreased in intensity upon reduction (to the $[4Fe{-}4S]^{+}$ state) with sodium dithionite (NaDT).[168] The EPR spectrum of NaDT-reduced CutD taken at 9 K contained an axial signal with $g_{\parallel}$ of 2.045 and $g_{\perp}$ of 1.94, which broadened at 40 K.[74] The g-values and temperature dependence of this signal confirmed the presence of $[4Fe{-}4S]^{+}$ centers in this enzyme. Using high performance liquid chromatography (HPLC), chemically reduced CutD was shown to cleave SAM into 5′-deoxyadenosine and L-methionine.[74] Together, these analyses support the assignment of CutD as a radical SAM enzyme.

EPR experiments of anaerobic reaction mixtures containing CutD, CutC, SAM, and NaDT at 77 K revealed a signal, centered at g = 2.0037, that exhibited a 2-fold splitting of ~1.46 mT, which is consistent with the glycine-centered radicals from activated PFL and class III RNR.[69,74,165] Under these conditions, 18-20% of CutC dimers were activated. Although efforts to optimize activation (for instance, by employing catalytic amounts of CutD, including choline in the reaction mixture, or using the NADPH:flavodoxin reductase−flavodoxin system from *E. coli*) were not promising, the activity of CutC appears to be consistent between preparations.[74,169] Furthermore, anaerobic endpoint assays with activated CutC showed complete conversion of

choline to TMA (detected by LC-MS/MS) and acetaldehyde (detected by GC-MS/MS). Mutation of C489 and G821 of CutC, residues that are conserved among all known GREs and critical to their function, completely inhibited the production of TMA.[74] These results confirmed that CutC is a C−N bond-cleaving GRE.

To investigate the substrate scope of CutC and demonstrate that the reaction it catalyzes is distinct from diol dehydratation, several choline analogs, as well as 1,2-propanediol and glycerol, were tested in endpoint assays.[74] None of the corresponding C-N bond cleavage or dehydration products were detected (Figure 1.30). Thus, the selectivity of CutC provides further evidence that this enzyme is likely a specific molecular marker for anaerobic choline metabolism. Finally, kinetic parameters for this novel GRE were obtained using a continuous spectrophotometric assay in which CutC activity (i.e. the generation of acetaldehyde) was coupled to the reduction of acetaldehyde by NADH-dependent yeast alcohol dehydrogenase (YADH),[82] resulting in a K_M of 0.13 ± 0.01 mM and a turnover number of 747 ± 27 s^{-1} for CutC dimer.[74] The latter value is equivalent to the normalized k_{cat}, calculated by dividing the experimentally obtained k_{cat} by the proportion of activated enzyme (as estimated from EPR measurements and the assumption that activated CutC, like PFL[170] and class III RNR,[75] possesses 0.5 glycyl radicals per polypeptide).

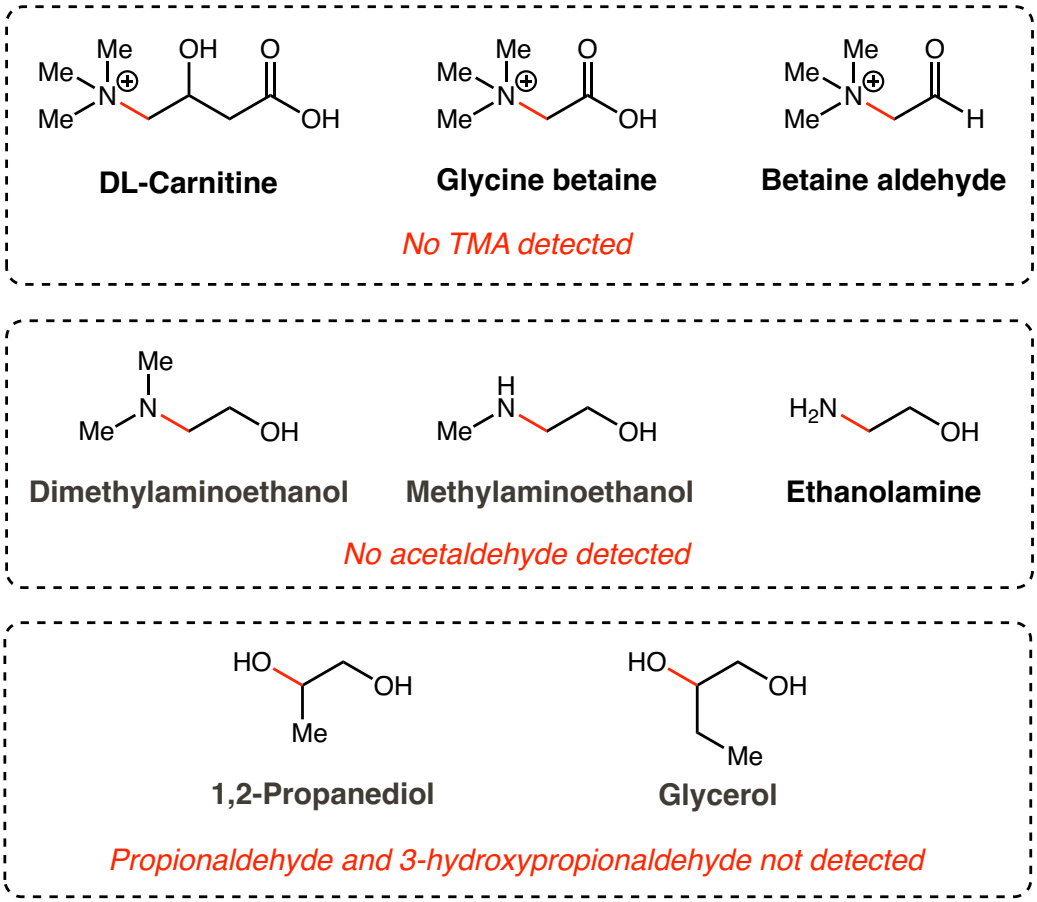

Figure 1.30. Substrates examined in an endpoint assay for cleavage by activated CutC.

1.11. Crystallization of CutC provides insight into the mechanism of choline cleavage

Collaborative work between the Balskus and Drennan labs led to the elucidation of the structure of choline-bound CutC from *Desulfovibrio alaskensis* G20.[169] Similar to the GREs GD,[164] PFL2,[171] and HPAD,[128] CutC crystallized as a dimer of dimers (Figure 1.31). Each monomer adopted the canonical GRE fold: a ten-stranded β/α barrel with two loops, containing the catalytic residues, located in the center of the barrel. The Gly loop, which contains the universally conserved glycine (Gly821 in CutC), is believed to undergo conformational changes that closes or exposes the active site during installation of the glycyl radical by the activating enzyme.[55] Next to the Gly loop in the enzyme interior is the Cys loop, which harbors a

universally conserved cysteine residue (Cys489 in CutC). The active site cavity is found directly above the Cys loop and rests below a hydrophobic tunnel extending from β3.[169] Rotation of residues located at the top of this hydrophobic barrel, particularly the side chains of Phe389 and Trp379, may block access to the active site from the exterior of the protein. Surprisingly, CutC crystallized with choline bound in its active site, despite the fact that adventitious choline had not been added to the media during expression, purification, and dialysis of the protein.

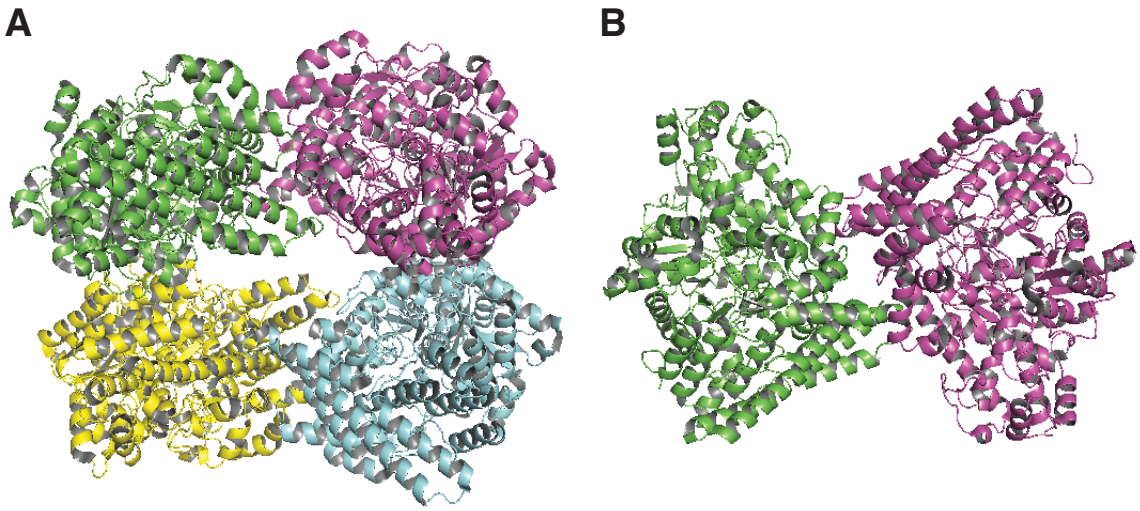

Figure 1.31. Crystal structure of wild-type CutC from *D. alaskensis* G20. (A) CutC crystallizes as a dimer of dimers. (B) The dimeric unit from (A) is shown after a rotation of 90°. PDB accession number 5FAU.[169]

Within the polar active site of CutC, choline is oriented such that its hydroxyl engages in hydrogen bonding with Glu491 and the backbone amide nitrogen of Gly488/Cys489 (Figure 1.32).[169] This positions the C1 of choline 3.6 Å from the Cys489 thiol, a distance suitable for *pro-S* hydrogen atom abstraction by the putative thiyl radical. C2 of choline is also in proximity (4.3 Å) to Cys489, potentially facilitating reformation of the thiyl radical following choline cleavage. In addition, C2 of choline bears a partial positive charge and thus may participate in a cation-π-like interaction with Phe395 (whose ring center is 3.8 Å away). Indeed, mutation of

F395 to leucine completely abolished CutC activity in an endpoint assay.[74] The carboxylate of Asp216 could form electrostatic interactions with the positively charged trimethylammonium moiety of choline. Moreover, the polarized methyl groups of this moiety make several CH—O hydrogen bonds with the side-chain oxygen atoms of Tyr208, Tyr506, Asp216, and a water molecule held in the active site. CH—O bonds play critical roles in substrate recognition for various quaternary amine-binding enzymes and, in some cases, are similar in strength to weak hydrogen bonds. For CutC, these interactions are believed to be the protein's primary choline-specific contacts.[172-176]

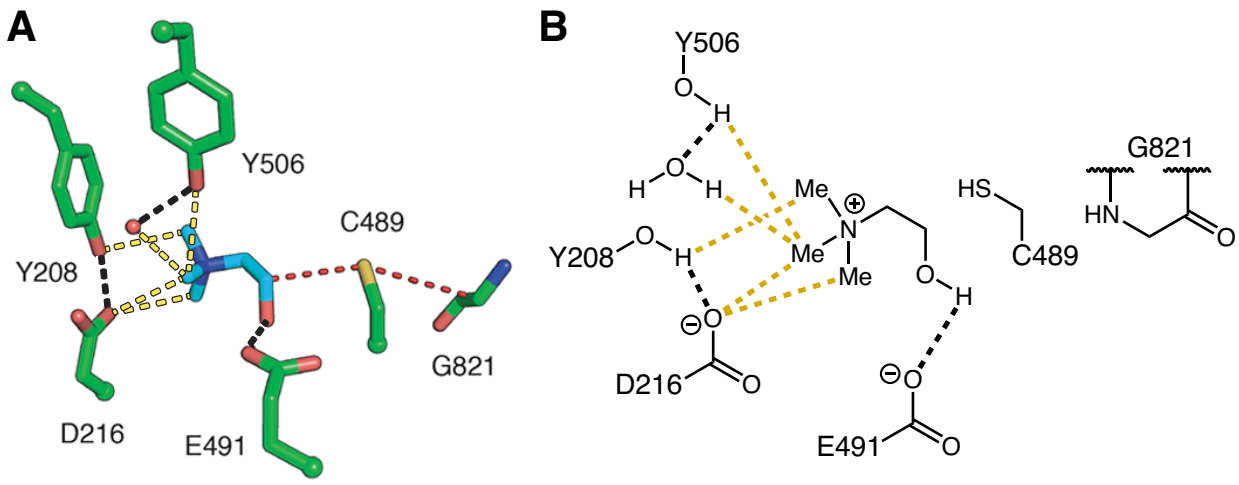

Figure 1.32. CutC orients choline through hydrogen bonding with a putative general base and CH—O hydrogen bonds with a water molecule and residues in the active site. (A) Crystal structure of CutC from *D. alaskensis* G20 bound to choline (PBD = 5FAU). (B) Diagram of hydrogen bonds between a putative general base, Glu491, and choline and of close interactions between phenolic and carboxylate oxygen atoms of the protein (and a water molecule in the active site) and the polarized methyl groups of the trimethylammonium moiety. CH—O hydrogen bonds are indicated in yellow and hydrogen bonds are in black.

The insights from these structural and biochemical data informed a preliminary model for the mechanism of choline cleavage (Figure 1.33). After the glycyl radical of CutC is installed, it can abstract a hydrogen atom from an adjacent cysteine (Cys489), generating a thiyl radical intermediate that initiates the reaction with choline. The thiyl radical could abstract the *pro-S*

hydrogen atom from C1 of choline (which is oriented toward Cys489 in the crystal structure), generating an α-hydroxylalkyl radical. From here, two potential mechanistic routes for C-N bond cleavage are conceivable. Either a base-catalyzed 1,2-elimination of TMA (Figure 1.33A) or a 1,2-migration followed by elimination (Figure 1.33B) could yield the final products. The first scenario resembles the mechanisms proposed for SAM-dependent radical C–N lyase DesII[177] and a related GRE, glycerol dehydratase (GD),[164] which performs an analogous C–O bond scission. The alternative hypothesis, involving heteroatom migration, is based on the widely accepted mechanisms for B_{12}-dependent eliminating enzymes,[157] including ethanolamine ammonia lyase (EAL), which, as mentioned in Sections 1.6-1.8, catalyzes the C-N bond cleavage of ethanolamine.

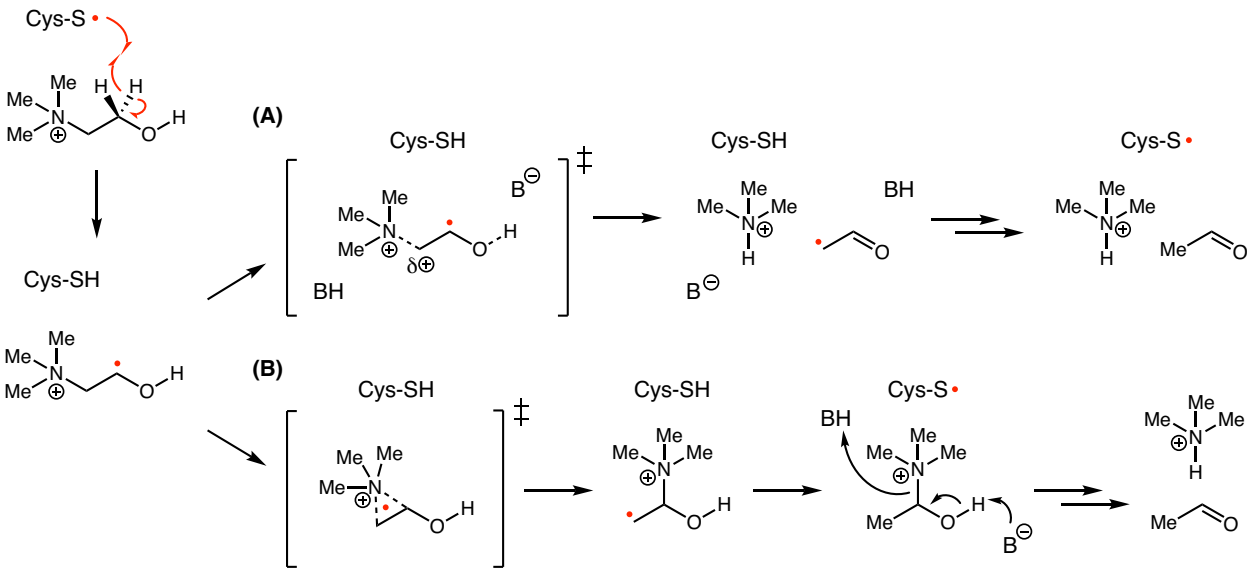

Figure 1.33. Two possible mechanisms for the CutC-catalyzed elimination of TMA from choline. A thiyl radical generated in the active site is proposed to serve as the active oxidant in all GREs. (A) Following initial hydrogen atom abstraction to form an α-hydroxy radical, CutC may perform base-catalyzed direct elimination of TMA. (B) Alternately, choline cleavage could involve a 1,2-migration of the trimethylammonium moiety followed by decomposition of the resulting carbinolamine.

Both mechanistic hypotheses in Figure 1.33 require an acceptor for the choline hydroxyl proton, and, based on the crystal structure, Glu491 appears well positioned to perform this function. This residue is found on the Cys loop, in a GCVEP motif that is conserved between CutC and GD,[74] and was proposed to function as a hydrogen bond acceptor to the choline C1 hydroxyl. An equivalent Glu in the *E. coli* class Ia ribonucleotide reductase (RNR) enzyme was shown to play a modest role in substrate binding and a critical role as an acid/base catalyst.[178,179] Moreover, Glu491 occupies a position in the GRE active site that is often associated with acid/base chemistry.[123,180] In the case of the GRE GD, computational studies found that proton transfer between the C1 OH group of glycerol and the analogous active site Glu triggers dehydration by direct elimination.[164]

CutC-E491A and CutC-E491Q mutants proved to be completely inactive in overnight endpoint assays, indicating that this Glu affects substrate binding and/or catalysis.[74,169] The crystal structures of CutC-E491A and CutC-E491Q were virtually identical in their amino acid arrangements from the wild-type enzyme, confirming that inactivity of the mutants is not due to a disruption in protein folding.[169] Nevertheless, substrate binding was impaired. Despite inclusion of 10 mM choline in the protein solution prior to crystallization, no clear density was observed for choline within either active site. This result, along with the complete absence of activity even at high choline concentrations, support the hypothesis that Glu491, like the structurally similar Glu441 in class Ia RNR, is a catalytic base that also contributes to substrate binding affinity.

In order to complete the catalytic cycle, the active site base that removed the choline proton, i.e. Glu491, must be deprotonated. Since the structure of CutC does not contain any obvious proton pathway leading from the active site to the protein exterior, TMA could serve as

the ultimate acceptor for the C1 hydroxyl proton. However, the distance between the nitrogen of TMA and the side chain of Glu491 is too large (4.6 Å) to allow for direct protonation.[169] Moreover, the movement of Glu491 appears to be sterically blocked by both the C1 of choline and Thr502. Although Asp216 is positioned close to the trimethylammonium moiety and could theoretically serve as the general acid, it is too far from Glu491 for direct proton transfer (5.8 Å) and its movement (towards TMA) would likely be impeded by Thr502. Thus, Thr502 was suggested to relay the proton between Glu491 and Asp216. Located 2.5 Å from Glu491, Thr502 is already perfectly positioned in the wild-type CutC structure to hydrogen bond with the putative base and, upon rotation, could form a new hydrogen bond with Asp216. Both Asp216 and Thr502 are absolutely conserved in CutC enzymes.

Reexamining the mechanism for choline cleavage, the extensive structural and biochemical data that was gathered by the Balskus and Drennan labs favored the direct elimination of TMA (Figure 1.33A).[169] After *pro-S* hydrogen atom abstraction from C1 of choline by the Cys489 thiyl radical, a general base, likely Glu491, could deprotonate the C1 hydroxyl (Figure 1.34). Not only is the pKa of the choline hydroxyl (~13.9)[181] lower than that of a typical alcohol, the pKa values of α-hydroxy radicals are often further depressed by an additional 4–8 pH units,[182] indicating that deprotonation of the C1 OH by Glu491 is a reasonable proposal.

Next, rapid heterolytic C–N bond cleavage via a "spin-center shift" would eliminate TMA (Figure 1.16), a fragmentation process that has been shown to naturally and quickly occur under neutral conditions.[183] The observed CH—O hydrogen bonds between the trimethylammonium group and the polar residues lining the back of the active site (Asp216, Tyr208, Tyr506) would be expected to weaken the C–N bond of choline. Furthermore, in B_{12}-

dependent enzymes such as EAL, the active site environment plays a critical role in controlling heteroatom migration in the substrate-based radical species. The EAL residues that facilitate this migration engage in direct contacts with the amine moiety and are catalytically essential.[184] In contrast, CutC-D216N, Y208F, and Y506F mutants and the Y208F/Y506F double mutant were all active in overnight endpoint assays (although they did exhibit reduced catalytic efficiency in kinetics experiments).[169] Moreover, migration of the bulky trimethylammonium moiety is physically restricted by Thr502, which packs against the substrate.

Finally, the product-based radical species formed in the CutC active site could re-abstract a hydrogen atom from Cys489, reforming the thiyl radical and generating acetaldehyde. A series of proton transfers from Glu491 to Thr502 to Asp216 could effectively deprotonate Glu491 and reset the CutC active site for the next round of catalysis. Asp216, positioned close to the trimethylammonium moiety, may serve as the general acid, donating a proton to TMA. A recent computational study of CutC, performed by the Kulik lab at MIT, has provided further support for the direct elimination mechanism, with quantum mechanical-molecular mechanical (QM/MM) simulations revealing spontaneous departure of TMA upon deprotonation of an initial α-hydroxyalkyl substrate-centered radical intermediate.

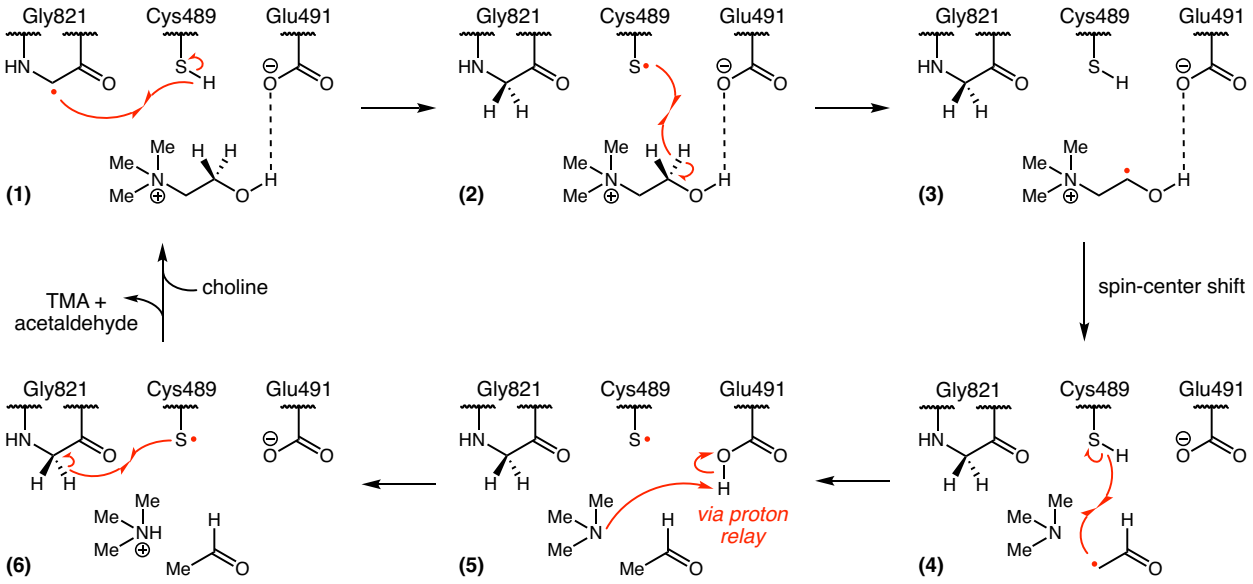

Figure 1.34. Proposed mechanism for choline cleavage by CutC. (1) The glycyl radical of CutC abstracts a hydrogen atom from Cys489, generating a thiyl radical. (2) Catalysis begins with *pro-S* hydrogen atom abstraction from C1 of choline. (3) Trimethylamine is eliminated from the resulting α-hydroxyalkyl radical species via a "spin-center shift." (4) The subsequent product-based radical species re-abstracts a hydrogen atom from Cys489, reforming the thiyl radical and generating acetaldehyde. (5) A series of proton transfers may take place, ultimately deprotonating the putative general base, Glu491. (6) The thiyl radical re-abstracts a hydrogen atom from Gly821, regenerating the glycyl radical and resetting the active site for the next round of catalysis.

1.12. References

(1) Sonnenburg, J. L.; Bäckhed, F. Diet–Microbiota Interactions as Moderators of Human Metabolism. *Nature* **2016**, *535* (7610), 56–64.

(2) Schroeder, B. O.; Bäckhed, F. Signals From the Gut Microbiota to Distant Organs in Physiology and Disease. *Nat. Med.* **2016**, *22* (10), 1079–1089.

(3) Koppel, N.; Balskus, E. P. Exploring and Understanding the Biochemical Diversity of the Human Microbiota. *Cell Chem. Biol.* **2016**, *23* (1), 18–30.

(4) Qin, J.; Li, R.; Raes, J.; Arumugam, M.; Burgdorf, K. S.; Manichanh, C.; Nielsen, T.; Pons, N.; Levenez, F.; Yamada, T.; Mende, D. R.; Li, J.; Xu, J.; Li, S.; Li, D.; Wang, B.; Liang, H.; Zheng, H.; Xie, Y.; Tap, J.; Lepage, P.; Bertalan, M.; Batto, J.-M.; Hansen, T.; Le Paslier, D.; Linneberg, A.; Nielsen, H. B.; Pelletier, E.; Renault, P.; Sicheritz-Ponten, T.; Turner, K.; Zhu, H.; Yu, C.; Li, S.; Jian, M.; Zhou, Y.; Li, Y.; Zhang, X.; Li, S.; Qin, N.; Yang, H.; Wang, J.; Brunak, S.; Dore, J.; Guarner, F.; Kristiansen, K.; Pedersen, O.; Parkhill, J.; Weissenbach, J.; (null), M. C.; Bork, P.; Ehrlich, S. D.; Wang, J. A Human Gut Microbial Gene Catalogue Established by

Metagenomic Sequencing. *Nature* **2010**, *464* (7285), 59–65.

(5) Sharon, G.; Garg, N.; Debelius, J.; Knight, R.; Dorrestein, P. C.; Mazmanian, S. K. Specialized Metabolites From the Microbiome in Health and Disease. *Cell Metab.* **2014**, *20* (5), 719–730.

(6) Postler, T. S.; Ghosh, S. Understanding the Holobiont: How Microbial Metabolites Affect Human Health and Shape the Immune System. *Cell Metab.* **2017**, *26* (1), 110–130.

(7) Schmidt, T. S. B.; Raes, J.; Bork, P. The Human Gut Microbiome: From Association to Modulation. *Cell* **2018**, *172* (6), 1198–1215.

(8) Zeisel, S. H.; da Costa, K.-A. Choline: an Essential Nutrient for Public Health. *Nutr. Rev.* **2009**, *67* (11), 615–623.

(9) Craciunescu, C. N.; Albright, C. D.; Mar, M.-H.; Song, J.; Zeisel, S. H. Choline Availability During Embryonic Development Alters Progenitor Cell Mitosis in Developing Mouse Hippocampus. *J. Nutr.* **2003**, *133* (11), 3614–3618.

(10) Zeisel, S. H. Choline: Critical Role During Fetal Development and Dietary Requirements in Adults. *Annu. Rev. Nutr.* **2006**, *26* (1), 229–250.

(11) da Costa, K.-A.; Badea, M.; Fischer, L. M.; Zeisel, S. H. Elevated Serum Creatine Phosphokinase in Choline-Deficient Humans: Mechanistic Studies in C2C12 Mouse Myoblasts. *Am. J. Clin. Nutr.* **2004**, *80* (1), 163–170.

(12) Craciunescu, C. N.; Brown, E. C.; Mar, M.-H.; Albright, C. D.; Nadeau, M. R.; Zeisel, S. H. Folic Acid Deficiency During Late Gestation Decreases Progenitor Cell Proliferation and Increases Apoptosis in Fetal Mouse Brain. *J. Nutr.* **2004**, *134* (1), 162–166.

(13) Zeisel, S. H. Metabolic Crosstalk Between Choline/1-Carbon Metabolism and Energy Homeostasis. *Clin. Chem. Lab. Med.* **2013**, *51* (3), 1–9.

(14) Romano, K. A.; Martínez-del Campo, A.; Kasahara, K.; Chittim, C. L.; Vivas, E. I.; Amador-Noguez, D.; Balskus, E. P.; Rey, F. E. Metabolic, Epigenetic, and Transgenerational Effects of Gut Bacterial Choline Consumption. *Cell Host Microbe* **2017**, *22* (3), 279–290.

(15) Fischer, L. M.; daCosta, K. A.; Kwock, L.; Stewart, P. W.; Lu, T.-S.; Stabler, S. P.; Allen, R. H.; Zeisel, S. H. Sex and Menopausal Status Influence Human Dietary Requirements for the Nutrient Choline. *Am. J. Clin. Nutr.* **2007**, *85* (5), 1275–1285.

(16) Spencer, M. D.; Hamp, T. J.; Reid, R. W.; Fischer, L. M.; Zeisel, S. H.; Fodor, A. A. Association Between Composition of the Human Gastrointestinal Microbiome and

Development of Fatty Liver with Choline Deficiency. *Gastroenterology* **2011**, *140* (3), 976–986.

(17) Chittim, C. L.; del Campo, A. M.; Balskus, E. P. Gut Bacterial Phospholipase Ds Support Disease-Associated Metabolism by Generating Choline. *Nature Microbiology* **2018**, 1–11.

(18) Aktas, M.; Wessel, M.; Hacker, S.; Klüsener, S.; Gleichenhagen, J.; Narberhaus, F. Phosphatidylcholine Biosynthesis and Its Significance in Bacteria Interacting with Eukaryotic Cells. *Eur. J. Cell Biol.* **2010**, *89* (12), 888–894.

(19) Geiger, O.; López-Lara, I. M.; Sohlenkamp, C. Phosphatidylcholine Biosynthesis and Function in Bacteria. *Biochim. Biophys. Acta* **2013**, *1831* (3), 503–513.

(20) Boch, J.; Kempf, B.; Bremer, E. Osmoregulation in *Bacillus subtilis*: Synthesis of the Osmoprotectant Glycine Betaine From Exogenously Provided Choline. *J. Bacteriol.* **1994**, *176* (17), 5364–5371.

(21) Ohta-Fukuyama, M.; Miyake, Y.; Emi, S.; Yamano, T. Identification and Properties of the Prosthetic Group of Choline Oxidase From *Alcaligenes* Sp. *J. Biochem.* **1980**, *88* (1), 197–203.

(22) Landfald, B.; Strom, A. R. Choline-Glycine Betaine Pathway Confers a High Level of Osmotic Tolerance in *Escherichia coli*. *J. Bacteriol.* **1986**.

(23) Wargo, M. J. Homeostasis and Catabolism of Choline and Glycine Betaine: Lessons From *Pseudomonas Aeruginosa*. *Appl. Environ. Microbiol.* **2013**, *79* (7), 2112–2120.

(24) Wagner, M. A.; Khanna, P.; Jorns, M. S. Structure of the Flavocoenzyme of Two Homologous Amine Oxidases: Monomeric Sarcosine Oxidase and *N*-Methyltryptophan Oxidase. *Biochemistry* **1999**, *38* (17), 5588–5595.

(25) Hayward, H. R.; Stadtman, T. C. Anaerobic Degradation of Choline. I. Fermentation of Choline by an Anaerobic, Cytochrome-Producing Bacterium, *Vibrio cholinicus* N. Sp. *J. Bacteriol.* **1959**, *78*, 557–561.

(26) Hayward, H. R.; Stadtman, T. C. Anaerobic Degradation of Choline. II. Preparation and Properties of Cell-Free Extracts of *Vibrio cholinicus*. *J. Biol. Chem.* **1960**, *235* (2), 538–543.

(27) Hayward, H. R. Anaerobic Degradation of Choline. III. Acetaldehyde as an Intermediate in the Fermentation of Choline by Extracts of *Vibrio cholinicus*. *J. Biol. Chem.* **1960**, *235* (12), 3592–3596.

(28) Bradbeer, C. Clostridial Fermentations of Choline and Ethanolamine. I. Preparation and Properties of Cell-Free Extracts. *J. Biol. Chem.* **1965**, *240* (12), 4669–4674.

(29) King, G. M. Metabolism of Trimethylamine, Choline, and Glycine Betaine by Sulfate-Reducing and Methanogenic Bacteria in Marine Sediments. *Appl. Environ. Microbiol.* **1984**, *48* (4), 719–725.

(30) Sanhdu, S. S.; Chase, T., Jr. Anaerobic Degradation of Choline by *Proteus mirabilis*: Enzymatic Requirements and Pathways. *Can. J. Microbiol.* **1986**, *32* (9), 743–750.

(31) Chao, C.-K.; Zeisel, S. H. Formation of Trimethylamine From Dietary Choline by S*treptococcus Sanguis* I, Which Colonizes the Mouth. *J. Nutr. Biochem.* **1990**, *1* (2), 89–97.

(32) Neill, A. R.; Grime, D. W.; Dawson, R. M. C. Conversion of Choline Methyl Groups Through Trimethylamine Into Methane in the Rumen. *Biochem. J.* **1978**, *170* (3), 529–535.

(33) Krueger, S. K.; Williams, D. E. Mammalian Flavin-Containing Monooxygenases: Structure/Function, Genetic Polymorphisms and Role in Drug Metabolism. *Pharmacol. Ther.* **2005**, *106* (3), 357–387.

(34) Zeisel, S. H.; Warrier, M. Trimethylamine *N*-Oxide, the Microbiome, and Heart and Kidney Disease. *Annu. Rev. Nutr.* **2017**, *37* (1), 135–136.

(35) Bennett, B. J.; de Aguiar Vallim, T. Q.; Wang, Z.; Shih, D. M.; Meng, Y.; Gregory, J.; Allayee, H.; Lee, R.; Graham, M.; Crooke, R.; Edwards, P. A.; Hazen, S. L.; Lusis, A. J. Trimethylamine-*N*-Oxide, a Metabolite Associated with Atherosclerosis, Exhibits Complex Genetic and Dietary Regulation. *Cell Metab.* **2013**, *17* (1), 49–60.

(36) Hartiala, J.; Bennett, B. J.; Tang, W. H. W.; Wang, Z.; Stewart, A. F. R.; Roberts, R.; McPherson, R.; Lusis, A. J.; Hazen, S. L.; Allayee, H. Comparative Genome-Wide Association Studies in Mice and Humans for Trimethylamine *N*-Oxide, a Proatherogenic Metabolite of Choline and L-Carnitine. *Arterioscler. Thromb. Vasc. Biol.* **2014**, *34* (6), 1307–1313.

(37) Al-Waiz, M.; Mikov, M.; Mitchell, S. C.; Smith, R. L. The Exogenous Origin of Trimethylamine in the Mouse. *Metab.* **1992**, *41* (2), 135–136.

(38) Romano, K. A.; Vivas, E. I.; Amador-Noguez, D.; Rey, F. E. Intestinal Microbiota Composition Modulates Choline Bioavailability From Diet and Accumulation of the Proatherogenic Metabolite Trimethylamine-*N*-Oxide. *mBio* **2015**, *6* (2), e02481–14–8.

(39) Wang, Z.; Klipfell, E.; Bennett, B. J.; Koeth, R.; Levison, B. S.; DuGar, B.; Feldstein, A. E.; Britt, E. B.; Fu, X.; Chung, Y.-M.; Wu, Y.; Schauer, P.; Smith, J. D.; Allayee, H.; Tang, W. H. W.; DiDonato, J. A.; Lusis, A. J.; Hazen, S. L. Gut Flora Metabolism of Phosphatidylcholine Promotes Cardiovascular Disease. *Nature* **2011**, *472* (7341), 57–63.

(40) Tang, W. H. W.; Wang, Z.; Levison, B. S.; Koeth, R. A.; Britt, E. B.; Fu, X.; Wu, Y.; Hazen, S. L. Intestinal Microbial Metabolism of Phosphatidylcholine and Cardiovascular Risk. *N. Engl. J. Med.* **2013**, *368* (17), 1575–1584.

(41) Craciun, S.; Balskus, E. P. Microbial Conversion of Choline to Trimethylamine Requires a Glycyl Radical Enzyme. *Proc. Natl. Acad. Sci. U.S.A.* **2012**, *109* (52), 21307–21312.

(42) Dumas, M. E.; Barton, R. H.; Toye, A.; Cloarec, O.; Blancher, C.; Rothwell, A.; Fearnside, J.; Tatoud, R.; Blanc, V.; Lindon, J. C.; Mitchell, S. C.; Holmes, E.; McCarthy, M. I.; Scott, J.; Gauguier, D.; Nicholson, J. K. Metabolic Profiling Reveals a Contribution of Gut Microbiota to Fatty Liver Phenotype in Insulin-Resistant Mice. *Proc. Natl. Acad. Sci. U.S.A.* **2006**, *103* (33), 12511–12516.

(43) Spencer, M. D.; Hamp, T. J.; Reid, R. W.; Fischer, L. M.; Zeisel, S. H.; Fodor, A. A. Association Between Composition of the Human Gastrointestinal Microbiome and Development of Fatty Liver with Choline Deficiency. *Gastroenterology* **2011**, *140* (3), 976–986.

(44) Koeth, R. A.; Wang, Z.; Levison, B. S.; Buffa, J. A.; Org, E.; Sheehy, B. T.; Britt, E. B.; Fu, X.; Wu, Y.; Li, L.; Smith, J. D.; DiDonato, J. A.; Chen, J.; Li, H.; Wu, G. D.; Lewis, J. D.; Warrier, M.; Brown, J. M.; Krauss, R. M.; Tang, W. H. W.; Bushman, F. D.; Lusis, A. J.; Hazen, S. L. Intestinal Microbiota Metabolism of L-Carnitine, a Nutrient in Red Meat, Promotes Atherosclerosis. *Nat. Med.* **2013**, *19* (5), 576–585.

(45) Tang, W. H. W.; Wang, Z.; Levison, B. S.; Koeth, R. A.; Britt, E. B.; Fu, X.; Wu, Y.; Hazen, S. L. Intestinal Microbial Metabolism of Phosphatidylcholine and Cardiovascular Risk. *N. Engl. J. Med.* **2013**, *368* (17), 1575–1584.

(46) Gregory, J. C.; Buffa, J. A.; Org, E.; Wang, Z.; Levison, B. S.; Zhu, W.; Wagner, M. A.; Bennett, B. J.; Li, L.; DiDonato, J. A.; Lusis, A. J.; Hazen, S. L. Transmission of Atherosclerosis Susceptibility with Gut Microbial Transplantation. *J. Biol. Chem.* **2015**, *290* (9), 5647–5660.

(47) Tang, W. H. W.; Wang, Z.; Kennedy, D. J.; Wu, Y.; Buffa, J. A.; Agatisa-Boyle, B.; Li, X. S.; Levison, B. S.; Hazen, S. L. Gut Microbiota-Dependent Trimethylamine *N*-Oxide (TMAO) Pathway Contributes to Both Development of Renal Insufficiency and Mortality Risk in Chronic Kidney Disease. *Circ. Res.* **2015**, *116*, 448–455.

(48) Missailidis, C.; Hällqvist, J.; Qureshi, A. R.; Barany, P.; Heimbürger, O.; Lindholm, B.; Stenvinkel, P.; Bergman, P. Serum Trimethylamine-*N*-Oxide Is Strongly Related to Renal Function and Predicts Outcome in Chronic Kidney Disease. *PLoS One* **2016**, *11* (1), e0141738.

(49) Miao, J.; Ling, A. V.; Manthena, P. V.; Gearing, M. E.; Graham, M. J.; Crooke, R. M.;

Croce, K. J.; Esquejo, R. M.; Clish, C. B.; Vicent, D.; Biddinger, S. B. Flavin-Containing Monooxygenase 3 as a Potential Player in Diabetes-Associated Atherosclerosis. *Nat. Commun.* **2014**, 1–10.

(50) Mitchell, S. C.; Smith, R. L. Trimethylaminuria: the Fish Malodor Syndrome. *Drug Metab. Dispos.* **2001**, *29* (4), 517–521.

(51) Dolphin, C. T.; Janmohamed, A.; Smith, R. L.; Shephard, E. A.; Phillips, I. R. Missense Mutation in Flavin-Containing Mono-Oxygenase 3 Gene, *Fmo3*, Underlies Fish-Odour Syndrome. *Nat. Genet.* **1997**, *17* (4), 491–494.

(52) Christodoulou, J. Trimethylaminuria: an Under-Recognised and Socially Debilitating Metabolic Disorder. *J. Paediatr. Child Health* **2012**, *48* (3), E153–E155.

(53) Selmer, T.; Pierik, A. J.; Heider, J. New Glycyl Radical Enzymes Catalysing Key Metabolic Steps in Anaerobic Bacteria. *Biol. Chem.* **2005**, *386* (10), 981–988.

(54) Backman, L. R. F.; Funk, M. A.; Dawson, C. D.; Drennan, C. L. New Tricks for the Glycyl Radical Enzyme Family. *Crit. Rev. Biochem. Mol. Biol.* **2017**, *52* (6), 674–695.

(55) Vey, J. L.; Yang, J.; Li, M.; Broderick, W. E.; Broderick, J. B.; Drennan, C. L. Structural Basis for Glycyl Radical Formation by Pyruvate Formate-Lyase Activating Enzyme. *Proc. Natl. Acad. Sci. U.S.A.* **2008**, *105* (42), 16137–16141.

(56) Wang, S. C.; Frey, P. A. *S*-Adenosylmethionine as an Oxidant: the Radical SAM Superfamily. *Trends. Biochem. Sci.* **2007**, *32* (3), 101–110.

(57) Vey, J. L.; Drennan, C. L. Structural Insights Into Radical Generation by the Radical SAM Superfamily. *Chem. Rev.* **2011**, *111* (4), 2487–2506.

(58) Krebs, C.; Broderick, W. E.; Henshaw, T. F.; Broderick, J. B.; Huynh, B. H. Coordination of Adenosylmethionine to a Unique Iron Site of the [4Fe-4S] of Pyruvate Formate-Lyase Activating Enzyme: a Mössbauer Spectroscopic Study. *J. Am. Chem. Soc.* **2002**, *124* (6), 912–913.

(59) Walsby, C. J.; Ortillo, D.; Broderick, W. E.; Broderick, J. B.; Hoffman, B. M. An Anchoring Role for FeS Clusters: Chelation of the Amino Acid Moiety of *S*-Adenosylmethionine to the Unique Iron Site of the [4Fe−4S] Cluster of Pyruvate Formate-Lyase Activating Enzyme. *J. Am. Chem. Soc.* **2002**, *124* (38), 11270–11271.

(60) Walsby, C. J.; Hong, W.; Broderick, W. E.; Cheek, J.; Ortillo, D.; Broderick, J. B.; Hoffman, B. M. Electron-Nuclear Double Resonance Spectroscopic Evidence That *S*-Adenosylmethionine Binds in Contact with the Catalytically Active $[4Fe{-}4S]^{+}$ Cluster of Pyruvate Formate-Lyase Activating Enzyme. *J. Am. Chem. Soc.* **2002**, *124* (12), 3143–3151.

(61) Dey, A.; Peng, Y.; Broderick, W. E.; Hedman, B.; Hodgson, K. O.; Broderick, J. B.; Solomon, E. I. S K-Edge XAS and DFT Calculations on SAM Dependent Pyruvate Formate-Lyase Activating Enzyme: Nature of Interaction Between the Fe_4S_4 Cluster and SAM and Its Role in Reactivity. *J. Am. Chem. Soc.* **2011**, *133* (46), 18656–18662.

(62) Zhang, Y.; Zhu, X.; Torelli, A. T.; Lee, M.; Dzikovski, B.; Koralewski, R. M.; Wang, E.; Freed, J.; Krebs, C.; Ealick, S. E.; Lin, H. Diphthamide Biosynthesis Requires an Organic Radical Generated by an Iron-Sulphur Enzyme. *Nature* **2010**, *465* (7300), 891–896.

(63) Demick, J. M.; Lanzilotta, W. N. Radical SAM Activation of the B 12-Independent Glycerol Dehydratase Results in Formation of 5′-Deoxy-5′-(Methylthio)Adenosine and Not 5′-Deoxyadenosine. *Biochemistry* **2011**, *50* (4), 440–442.

(64) Pierre, S.; Guillot, A.; Benjdia, A.; Sandstrom, C.; Langella, P.; Berteau, O. Thiostrepton Tryptophan Methyltransferase Expands the Chemistry of Radical SAM Enzymes. *Nat. Chem. Biol.* **2012**, *8* (12), 957–959.

(65) Horitani, M.; Shisler, K.; Broderick, W. E.; Hutcheson, R. U.; Duschene, K. S.; Marts, A. R.; Hoffman, B. M.; Broderick, J. B. Radical SAM Catalysis via an Organometallic Intermediate with an Fe-[5'-C]-Deoxyadenosyl Bond. *Science* **2016**, *352* (6287), 822–825.

(66) Fontecave, M.; Atta, M.; Mulliez, E. *S*-Adenosylmethionine: Nothing Goes to Waste. *Trends. Biochem. Sci.* **2004**, *29* (5), 243–249.

(67) Crain, A. V.; Broderick, J. B. Pyruvate Formate-Lyase and Its Activation by Pyruvate Formate-Lyase Activating Enzyme. *J. Biol. Chem.* **2014**, *289* (9), 5723–5729.

(68) Unkrig, V.; Neugebauer, F. A.; Knappe, J. The Free Radical of Pyruvate Formate-Lyase. Characterization by EPR Spectroscopy and Involvement in Catalysis as Studied with the Substrate-Analogue Hypopthosphite. *Eur. J. Biochem.* **1989**, *184* (3), 723–728.

(69) Wagner, A. F.; Frey, M.; Neugebauer, F. A.; Schafer, W.; Knappe, J. The Free Radical in Pyruvate Formate-Lyase Is Located on Glycine-734. *Proc. Natl. Acad. Sci. U.S.A.* **1992**, *89* (3), 996–1000.

(70) Hioe, J.; Savasci, G.; Brand, H.; Zipse, H. The Stability of Cα Peptide Radicals: Why Glycyl Radical Enzymes? *Chem. Eur. J.* **2011**, *17* (13), 3781–3789.

(71) Rabus, R.; Wilkes, H.; Behrends, A.; Armstroff, A.; Fischer, T.; Pierik, A. J.; Widdel, F. Anaerobic Initial Reaction of *N*-Alkanes in a Denitrifying Bacterium: Evidence for (1-Methylpentyl)Succinate as Initial Product and for Involvement of an Organic Radical in *N*-Hexane Metabolism. *J. Bacteriol.* **2001**, *183* (5), 1707–1715.

(72) Licht, S.; Gerfen, G. J.; Stubbe, J. Thiyl Radicals in Ribonucleotide Reductases. *Science* **1996**, *271* (5248), 477–481.

(73) Aurelius, O.; Johansson, R.; Bågenholm, V.; Lundin, D.; Tholander, F.; Balhuizen, A.; Beck, T.; Sahlin, M.; Sjöberg, B.-M.; Mulliez, E.; Logan, D. T. The Crystal Structure of *Thermotoga maritima* Class III Ribonucleotide Reductase Lacks a Radical Cysteine Pre-Positioned in the Active Site. *PLoS One* **2015**, *10* (7), e0128199–20.

(74) Craciun, S.; Marks, J. A.; Balskus, E. P. Characterization of Choline Trimethylamine-Lyase Expands the Chemistry of Glycyl Radical Enzymes. *ACS Chem. Biol.* **2014**, *9* (7), 1408–1413.

(75) Mulliez, E.; Padovani, D.; Atta, M.; Alcouffe, C.; Fontecave, M. Activation of Class III Ribonucleotide Reductase by Flavodoxin: a Protein Radical-Driven Electron Transfer to the Iron−Sulfur Center. *Biochemistry* **2001**, *40* (12), 3730–3736.

(76) Crain, A. V.; Broderick, J. B. Flavodoxin Cofactor Binding Induces Structural Changes That Are Required for Protein–Protein Interactions with NADP(+) Oxidoreductase and Pyruvate Formate-Lyase Activating Enzyme. *Biochim. Biophys. Acta.* **2013**, *1834* (12), 2512–2519.

(77) Frey, M.; Rothe, M.; Wagner, A. F.; Knappe, J. Adenosylmethionine-Dependent Synthesis of the Glycyl Radical in Pyruvate Formate-Lyase by Abstraction of the Glycine C-2 Pro-*S* Hydrogen Atom. Studies of [2H]Glycine-Substituted Enzyme and Peptides Homologous to the Glycine 734 Site. *J. Biol. Chem.* **1994**, *269* (17), 12432–12437.

(78) Peng, Y.; Veneziano, S. E.; Gillispie, G. D.; Broderick, J. B. Pyruvate Formate-Lyase, Evidence for an Open Conformation Favored in the Presence of Its Activating Enzyme. *J. Biol. Chem.* **2010**, *285* (35), 27224–27231.

(79) Levin, B. J.; Huang, Y. Y.; Peck, S. C.; Wei, Y.; Martínez-del Campo, A.; Marks, J. A.; Franzosa, E. A.; Huttenhower, C.; Balskus, E. P. A Prominent Glycyl Radical Enzyme in Human Gut Microbiomes Metabolizes *Trans*-4-Hydroxy-L-Proline. *Science* **2017**, *355* (6325), eaai8386–11.

(80) Unkrig, V.; Neugebauer, F. A.; Knappe, J. The Free Radical of Pyruvate Formate-Lyase. Characterization by EPR Spectroscopy and Involvement in Catalysis as Studied with the Substrate-Analogue Hypopthosphite. *Eur. J. Biochem.* **1989**, *184* (3), 723–728.

(81) Becker, A.; Fritz-Wolf, K.; Kabsch, W.; Knappe, J.; Schultz, S.; Volker Wagner, A. F. Structure and Mechanism of the Glycyl Radical Enzyme Pyruvate Formate-Lyase. *Nat. Struct Biol.* **1999**, *6* (10), 969–975.

(82) Leppänen, V.-M.; Merckel, M. C.; Ollis, D. L.; Wong, K. K.; Kozarich, J. W.;

Goldman, A. Pyruvate Formate Lyase Is Structurally Homologous to Type I Ribonucleotide Reductase. *Structure* **1999**, *7* (7), 733–744.

(83) Becker, A.; Kabsch, W. X-Ray Structure of Pyruvate Formate-Lyase in Complex with Pyruvate and CoA. *J. Biol. Chem.* **2002**, *277* (42), 40036–40042.

(84) Reddy, S. G.; Wong, K. K.; Parast, C. V.; Peisach, J.; Magliozzo, R. S.; Kozarich, J. W. Dioxygen Inactivation of Pyruvate Formate-Lyase: EPR Evidence for the Formation of Protein-Based Sulfinyl and Peroxyl Radicals. *Biochemistry* **1998**, *37* (2), 558–563.

(85) Wagner, A. F. V.; Schultz, S.; Bomke, J.; Pils, T.; Lehmann, W. D.; Knappe, J. YfiD of Escherichia Coli and Y06I of Bacteriophage T4 as Autonomous Glycyl Radical Cofactors Reconstituting the Catalytic Center of Oxygen-Fragmented Pyruvate Formate-Lyase. *Biochemical and Biophysical Research Communications* **2001**, *285* (2), 456–462.

(86) Sawers, G.; Hesslinger, C.; Muller, N.; Kaiser, M. The Glycyl Radical Enzyme TdcE Can Replace Pyruvate Formate-Lyase in Glucose Fermentation. *J. Bacteriol.* **1998**, *180* (14), 3509–3516.

(87) Saint-Amans, S.; Girbal, L.; Andrade, J.; Ahrens, K.; Soucaille, P. Regulation of Carbon and Electron Flow in *Clostridium butyricum* VPI 3266 Grown on Glucose-Glycerol Mixtures. *J. Bacteriol.* **2001**, *183* (5), 1748–1754.

(88) Raynaud, C.; Sarcabal, P.; Meynial-Salles, I.; Croux, C.; Soucaille, P. Molecular Characterization of the 1,3-Propanediol (1,3-PD) Operon of *Clostridium butyricum*. *Proc. Natl. Acad. Sci. U.S.A.* **2003**, *100* (9), 5010–5015.

(89) Feliks, M.; Ullmann, G. M. Glycerol Dehydratation by the B12-Independent Enzyme May Not Involve the Migration of a Hydroxyl Group: a Computational Study. *J. Phys. Chem. B* **2012**, *116* (24), 7076–7087.

(90) Hosseini, E.; Grootaert, C.; Verstraete, W.; Van de Wiele, T. Propionate as a Health-Promoting Microbial Metabolite in the Human Gut. *Nutr. Rev.* **2011**, *69* (5), 245–258.

(91) Besten, den, G.; van Eunen, K.; Groen, A. K.; Venema, K.; Reijngoud, D.-J.; Bakker, B. M. The Role of Short-Chain Fatty Acids in the Interplay Between Diet, Gut Microbiota, and Host Energy Metabolism. *J. Lipid Res.* **2013**, *54* (9), 2325–2340.

(92) Louis, P.; Flint, H. J. Formation of Propionate and Butyrate by the Human Colonic Microbiota. *Environ. Microbiol.* **2016**, *19* (1), 29–41.

(93) Chen, Y. M.; Zhu, Y.; Lin, E. C. C. The Organization of the *Fuc* Regulon Specifying L-Fucose Dissimilation in *Escherichia coli* K12 as Determined by Gene Cloning. *Molec Gen Genet* **1987**, *210* (2), 331–337.

(94) Bobik, T. A.; Havemann, G. D.; Busch, R. J.; Williams, D. S.; Aldrich, H. C. The Propanediol Utilization (*Pdu*) Operon of *Salmonella enterica* Serovar Typhimurium LT2 Includes Genes Necessary for Formation of Polyhedral Organelles Involved in Coenzyme B(12)-Dependent 1,2-Propanediol Degradation. *J. Bacteriol.* **1999**, *181* (19), 5967–5975.

(95) Scott, K. P.; Martin, J. C.; Campbell, G.; Mayer, C. D.; Flint, H. J. Whole-Genome Transcription Profiling Reveals Genes Up-Regulated by Growth on Fucose in the Human Gut Bacterium *Roseburia inulinivorans*. *J. Bacteriol.* **2006**, *188* (12), 4340–4349.

(96) LaMattina, J. W.; Keul, N. D.; Reitzer, P.; Kapoor, S.; Galzerani, F.; Koch, D. J.; Gouvea, I. E.; Lanzilotta, W. N. 1,2-Propanediol Dehydration in *Roseburia inulinivorans*. *J. Biol. Chem.* **2016**, *291* (30), 15515–15526.

(97) Levin, B. J.; Balskus, E. P. Characterization of 1,2-Propanediol Dehydratases Reveals Distinct Mechanisms for B12-Dependent and Glycyl Radical Enzymes. *Biochemistry* **2018**, *57* (23), 3222–3226.

(98) Zagalak, B.; Frey, P. A.; Karabatsos, G. L.; Abeles, R. H. The Stereochemistry of the Conversion of D and L 1,2-Propanediols to Propionaldehyde. *J. Biol. Chem.* **1966**, *241* (13), 3028–3035.

(99) Retey, J.; Umani-Ronchi, A.; Seibl, J.; Arigoni, D. Zum Mechanismus Der Propandioldehydrase-Reaktion. [On the Mechanism of the Propanediol Dehydrase Reaction]. *Experientia* **1966**, *22* (8), 502–503.

(100) Toraya, T. Cobalamin-Dependent Dehydratases and a Deaminase: Radical Catalysis and Reactivating Chaperones. *Arch. Biochem. Biophys.* **2014**, *544* (C), 40–57.

(101) Deutch, A. H.; Smith, C. J.; Rushlow, K. E.; Krelschmer, P. J. *Escherichia Coli* Δ^1-Pyrroline-5-Carboxylate Reductase: Gene Sequence, Protein Overproduction and Purification. *Nucleic Acids Research* **1982**, *10* (23), 7701–7714.

(102) Huang, Y. Y.; Martínez-del Campo, A.; Balskus, E. P. Anaerobic 4-Hydroxyproline Utilization: Discovery of a New Glycyl Radical Enzyme in the Human Gut Microbiome Uncovers a Widespread Microbial Metabolic Activity. *Gut Microbes* **2018**, *9* (5), 437–451.

(103) Gorres, K. L.; Raines, R. T. Prolyl 4-Hydroxylase. *Crit. Rev. Biochem. Mol. Biol.* **2010**, *45* (2), 106–124.

(104) Carbonero, F.; Benefiel, A. C.; Alizadeh-Ghamsari, A. H.; Gaskins, H. R. Microbial Pathways in Colonic Sulfur Metabolism and Links with Health and Disease. *Front. Physiol.* **2012**, *3*, 1–11.

(105) Singh, S.; Lin, H. Hydrogen Sulfide in Physiology and Diseases of the Digestive Tract. *Microorganisms* **2015**, *3* (4), 866–889.

(106) Attene-Ramos, M. S.; Nava, G. M.; Muellner, M. G.; Wagner, E. D.; Plewa, M. J.; Gaskins, H. R. DNA Damage and Toxicogenomic Analyses of Hydrogen Sulfide in Human Intestinal Epithelial FHs 74 Int Cells. *Environ. Mol. Mutagen.* **2010**, *51* (4), 304–314.

(107) Ijssennagger, N.; van der Meer, R.; van Mil, S. W. C. Sulfide as a Mucus Barrier-Breaker in Inflammatory Bowel Disease? *Trends. Mol. Med.* **2016**, *22* (3), 190–199.

(108) Shatalin, K.; Shatalina, E.; Mironov, A.; Nudler, E. H_2S: a Universal Defense Against Antibiotics in Bacteria. *Science* **2011**, *334* (6058), 982–986.

(109) Tomasova, L.; Konopelski, P.; Ufnal, M. Gut Bacteria and Hydrogen Sulfide: the New Old Players in Circulatory System Homeostasis. *Molecules* **2016**, *21* (11), 1558–18.

(110) Laue, H.; Denger, K.; Cook, A. M. Taurine Reduction in Anaerobic Respiration of *Bilophila wadsworthia* Rzatau. *Appl. Environ. Microbiol.* **1997**, *63* (5), 2016–2021.

(111) Nava, G. M.; Carbonero, F.; Croix, J. A.; Greenberg, E.; Gaskins, H. R. Abundance and Diversity of Mucosa-Associated Hydrogenotrophic Microbes in the Healthy Human Colon. *The ISME Journal* **2011**, *6* (1), 57–70.

(112) Baron, E. J.; Curren, M.; Henderson, G.; Jousimies-Somer, H.; Lee, K.; Lechowitz, K.; Strong, C. A.; Summanen, P.; Tunér, K.; Finegold, S. M. *Bilophila wadsworthia* Isolates From Clinial Specimens. *J. Clin. Microbiol.* **1992**, *30* (7), 1882–1884.

(113) Yazici, C.; Wolf, P. G.; Kim, H.; Cross, T.-W. L.; Vermillion, K.; Carroll, T.; Augustus, G. J.; Mutlu, E.; Tussing-Humphreys, L.; Braunschweig, C.; Xicola, R. M.; Jung, B.; Llor, X.; Ellis, N. A.; Gaskins, H. R. Race-Dependent Association of Sulfidogenic Bacteria with Colorectal Cancer. *Gut* **2017**, *66* (11), 1983–1994.

(114) Feng, Z.; Long, W.; Hao, B.; Ding, D.; Ma, X.; Zhao, L.; Pang, X. A Human Stool-Derived *Bilophila wadsworthia* Strain Caused Systemic Inflammation in Specific-Pathogen-Free Mice. *Gut Pathogens* **2017**, *9* (59).

(115) Devkota, S.; Wang, Y.; Musch, M. W.; Leone, V.; Fehlner-Peach, H.; Nadimpalli, A.; Antonopoulos, D. A.; Jabri, B.; Chang, E. B. Dietary-Fat-Induced Taurocholic Acid Promotes Pathobiont Expansion and Colitis in Il10 −/− Mice. *Nature* **2012**, *487* (7405), 104–108.

(116) Lie, T. J.; Pitta, T.; Leadbetter, E. R.; Godchaux, W., III; Leadbetter, J. R. Sulfonates: Novel Electron Acceptors in Anaerobic Respiration. *Archives of Microbiology* **1996**, *166* (3), 204–210.

(117) Peck, S. C.; Denger, K.; Burrichter, A.; Irwin, S. M.; Balskus, E. P.; Schleheck, D. A Glycyl Radical Enzyme Enables Hydrogen Sulfide Production by the Human Intestinal Bacterium *Bilophila wadsworthia*. *Proc. Natl. Acad. Sci. U.S.A.* **2019**, *116* (8), 3171–3176.

(118) Xing, M.; Wei, Y.; Zhou, Y.; Zhang, J.; Lin, L.; Hu, Y.; Hua, G.; Urs, A. N. N.; Liu, D.; Wang, F.; Guo, C.; Tong, Y.; Li, M.; Liu, Y.; Ang, E. L.; Zhao, H.; Yuchi, Z.; Zhang, Y. Radical-Mediated C-S Bond Cleavage in C2 Sulfonate Degradation by Anaerobic Bacteria. *Nat. Commun.* **2019**, 1–11.

(119) Stubbe, J.; Ge, J.; Yee, C. S. The Evolution of Ribonucleotide Reduction Revisited. *Trends. Biochem. Sci.* **2001**, *26* (2), 93–99.

(120) Lenz, R.; Giese, B. Studies on the Mechanism of Ribonucleotide Reductases. *J. Am. Chem. Soc.* **1997**, *119* (12), 2784–2794.

(121) Cendra, M. D. M.; Juárez, A.; Torrents, E. Biofilm Modifies Expression of Ribonucleotide Reductase Genes in *Escherichia coli*. *PLoS One* **2012**, *7* (9), e46350–e46359.

(122) Crespo, A.; Pedraz, L.; Astola, J.; Torrents, E. *Pseudomonas aeruginosa* Exhibits Deficient Biofilm Formation in the Absence of Class II and III Ribonucleotide Reductases Due to Hindered Anaerobic Growth. *Front. Microbiol.* **2016**, *7* (103), 153–14.

(123) Wei, Y.; Funk, M. A.; Rosado, L. A.; Baek, J.; Drennan, C. L.; Stubbe, J. The Class III Ribonucleotide Reductase From *Neisseria bacilliformis* Can Utilize Thioredoxin as a Reductant. *Proc. Natl. Acad. Sci. U.S.A.* **2014**, *111* (36), E3756–E3765.

(124) Wei, Y.; Mathies, G.; Yokoyama, K.; Chen, J.; Griffin, R. G.; Stubbe, J. A Chemically Competent Thiosulfuranyl Radical on the *Escherichia coli* Class III Ribonucleotide Reductase. *J. Am. Chem. Soc.* **2014**, *136* (25), 9001–9013.

(125) Wei, Y.; Li, B.; Prakash, D.; Ferry, J. G.; Elliott, S. J.; Stubbe, J. A Ferredoxin Disulfide Reductase Delivers Electrons to the *Methanosarcina barkeri* Class III Ribonucleotide Reductase. *Biochemistry* **2015**, *54* (47), 7019–7028.

(126) Yu, L.; Blaser, M.; Andrei, P. I.; Pierik, A. J.; Selmer, T. 4-Hydroxyphenylacetate Decarboxylases: Properties of a Novel Subclass of Glycyl Radical Enzyme Systems. *Biochemistry* **2006**, *45* (31), 9584–9592.

(127) Andrei, P. I.; Pierik, A. J.; Zauner, S.; Andrei-Selmer, L. C.; Selmer, T. Subunit Composition of the Glycyl Radical Enzyme *p*-Hydroxyphenylacetate Decarboxylase. *Eur. J. Biochem.* **2004**, *271* (11), 2225–2230.

(128) Martins, B. M.; Blaser, M.; Feliks, M.; Ullmann, G. M.; Buckel, W.; Selmer, T.

Structural Basis for a Kolbe-Type Decarboxylation Catalyzed by a Glycyl Radical Enzyme. *J. Am. Chem. Soc.* **2011**, *133* (37), 14666–14674.

(129) Feliks, M.; Martins, B. M.; Ullmann, G. M. Catalytic Mechanism of the Glycyl Radical Enzyme 4-Hydroxyphenylacetate Decarboxylase From Continuum Electrostatic and QC/MM Calculations. *J. Am. Chem. Soc.* **2013**, *135* (39), 14574–14585.

(130) Zargar, K.; Saville, R.; Phelan, R. M.; Tringe, S. G.; Petzold, C. J.; Keasling, J. D.; Beller, H. R. *In vitro* Characterization of Phenylacetate Decarboxylase, a Novel Enzyme Catalyzing Toluene Biosynthesis in an Anaerobic Microbial Community. *Sci. Rep.* **2016**, *6*, 31362.

(131) Beller, H. R.; Edwards, E. A. Anaerobic Toluene Activation by Benzylsuccinate Synthase in a Highly Enriched Methanogenic Culture. *Appl. Environ. Microbiol.* **2000**, *66* (12), 5503–5505.

(132) Liu, D.; Wei, Y.; Liu, X.; Zhou, Y.; Jiang, L.; Yin, J.; Wang, F.; Hu, Y.; Urs, A. N. N.; Liu, Y.; Ang, E. L.; Zhao, S.; Zhao, H.; Zhang, Y. Indoleacetate Decarboxylase Is a Glycyl Radical Enzyme Catalysing the Formation of Malodorant Skatole. *Nat. Commun.* **2018**, *9*, 4224.

(133) Selmer, T.; Pierik, A. J.; Heider, J. New Glycyl Radical Enzymes Catalysing Key Metabolic Steps in Anaerobic Bacteria. *Biol. Chem.* **2005**, *386* (10), 1–8.

(134) Acosta-González, A.; Rosselló-Móra, R.; Marqués, S. Diversity of Benzylsuccinate Synthase-Like (*bssA*) Genes in Hydrocarbon-Polluted Marine Sediments Suggests Substrate-Dependent Clustering. *Appl. Environ. Microbiol.* **2013**, *79* (12), 3667–3676.

(135) Biegert, T.; Fuchs, G.; Heider, J. Evidence That Anaerobic Oxidation of Toluene in the Denitrifying Bacterium *Thauera aromatica* Is Initiated by Formation of Benzylsuccinate From Toluene and Fumarate. *Eur. J. Biochem.* **1996**, *238* (3), 661–668.

(136) Leuthner, B.; Leutwein, C.; Schulz, H.; Hörth, P.; Haehnel, W.; Schiltz, E.; Schägger, H.; Heider, J. Biochemical and Genetic Characterization of Benzylsuccinate Synthase From *Thauera aromatica*: A New Glycyl Radical Enzyme Catalysing the First Step in Anaerobic Toluene Metabolism. *Molecular Microbiology* **1998**, *28* (3), 615–628.

(137) Coschigano, P. W. Construction and Characterization of Insertion/Deletion Mutations of the *tutF*, *tutD*, And *tutG* Genes of *Thauera aromatica* Strain T1. *FEMS Microbiol. Lett.* **2002**, *217* (1), 37–42.

(138) Funk, M. A.; Judd, E. T.; Marsh, E. N. G.; Elliott, S. J.; Drennan, C. L. Structures of Benzylsuccinate Synthase Elucidate Roles of Accessory Subunits in Glycyl Radical Enzyme Activation and Activity. *Proc. Natl. Acad. Sci. U.S.A.* **2014**, *111* (28), 10161–

10166.

(139) Funk, M. A.; Marsh, E. N. G.; Drennan, C. L. Substrate-Bound Structures of Benzylsuccinate Synthase Reveal How Toluene Is Activated in Anaerobic Hydrocarbon Degradation. *J. Biol. Chem.* **2015**, *290* (37), 22398–22408.

(140) Beller, H. R.; Spormann, A. M. Substrate Range of Benzylsuccinate Synthase From *Azoarcussp*. Strain T. *FEMS Microbiol. Lett.* **1999**, *178* (1), 147–153.

(141) Qiao, C.; Marsh, E. N. G. Mechanism of Benzylsuccinate Synthase: Stereochemistry of Toluene Addition to Fumarate and Maleate. *J. Am. Chem. Soc.* **2005**, *127* (24), 8608–8609.

(142) Li, L.; Marsh, E. N. G. Deuterium Isotope Effects in the Unusual Addition of Toluene to Fumarate Catalyzed by Benzylsuccinate Synthase. *Biochemistry* **2006**, *45* (46), 13932–13938.

(143) Li, L.; Marsh, E. N. G. Mechanism of Benzylsuccinate Synthase Probed by Substrate and Isotope Exchange. *J. Am. Chem. Soc.* **2006**, *128* (50), 16056–16057.

(144) Seyhan, D.; Friedrich, P.; Szaleniec, M.; Hilberg, M.; Buckel, W.; Golding, B. T.; Heider, J. Stereochemischer Verlauf Der Enzymatischen Synthese Von Benzylsuccinat Mit Chiral Markiertem Toluol. *Angew. Chem.* **2016**, *128* (38), 11836–11839.

(145) Szaleniec, M.; Heider, J. Modeling of the Reaction Mechanism of Enzymatic Radical C–C Coupling by Benzylsuccinate Synthase. *IJMS* **2016**, *17* (4), 514–522.

(146) Harms, G.; Rabus, R.; Widdel, F. Anaerobic Oxidation of the Aromatic Plant Hydrocarbon *p*-Cymene by Newly Isolated Denitrifying Bacteria. *Archives of Microbiology* **1999**, *172* (5), 303–312.

(147) Strijkstra, A.; Trautwein, K.; Jarling, R.; Wöhlbrand, L.; Dörries, M.; Reinhardt, R.; Drozdowska, M.; Golding, B. T.; Wilkes, H.; Rabus, R. Anaerobic Activation of *p*-Cymene in Denitrifying Betaproteobacteria: Methyl Group Hydroxylation Versus Addition to Fumarate. *Appl. Environ. Microbiol.* **2014**, *80* (24), 7592–7603.

(148) Muller, J. A.; Galushko, A. S.; Kappler, A.; Schink, B. Initiation of Anaerobic Degradation of *p*-Cresol by Formation of 4-Hydroxybenzylsuccinate in *Desulfobacterium cetonicum*. *J. Bacteriol.* **2001**, *183* (2), 752–757.

(149) Wöhlbrand, L.; Jacob, J. H.; Kube, M.; Mussmann, M.; Jarling, R.; Beck, A.; Amann, R.; Wilkes, H.; Reinhardt, R.; Rabus, R. Complete Genome, Catabolic Sub-Proteomes and Key-Metabolites of *Desulfobacula toluolica* Tol2, a Marine, Aromatic Compound-Degrading, Sulfate-Reducing Bacterium. *Environ. Microbiol.* **2012**, *15* (5), 1334–1355.

(150) Selesi, D.; Jehmlich, N.; Bergen, von, M.; Schmidt, F.; Rattei, T.; Tischler, P.; Lueders, T.; Meckenstock, R. U. Combined Genomic and Proteomic Approaches Identify Gene Clusters Involved in Anaerobic 2-Methylnaphthalene Degradation in the Sulfate-Reducing Enrichment Culture N47. *J. Bacteriol.* **2010**, *192* (1), 295–306.

(151) Rabus, R.; Wilkes, H.; Behrends, A.; Armstroff, A.; Fischer, T.; Pierik, A. J.; Widdel, F. Anaerobic Initial Reaction of *N*-Alkanes in a Denitrifying Bacterium: Evidence for (1-Methylpentyl)Succinate as Initial Product and for Involvement of an Organic Radical in *N*-Hexane Metabolism. *J. Bacteriol.* **2001**, *183* (5), 1707–1715.

(152) Callaghan, A. V.; Wawrik, B.; Ní Chadhain, S. M.; Young, L. Y.; Zylstra, G. J. Anaerobic Alkane-Degrading Strain AK-01 Contains Two Alkylsuccinate Synthase Genes. *Biochemical and Biophysical Research Communications* **2008**, *366* (1), 142–148.

(153) Grundmann, O.; Behrends, A.; Rabus, R.; Amann, J.; Halder, T.; Heider, J.; Widdel, F. Genes Encoding the Candidate Enzyme for Anaerobic Activation of *N*-Alkanes in the Denitrifying Bacterium, Strain HxN1. *Environ. Microbiol.* **2008**, *10* (2), 376–385.

(154) Heider, J.; Szaleniec, M.; Martins, B. M.; Seyhan, D.; Buckel, W.; Golding, B. T. Structure and Function of Benzylsuccinate Synthase and Related Fumarate-Adding Glycyl Radical Enzymes. *J Mol Microbiol Biotechnol* **2016**, *26* (1-3), 29–44.

(155) Garsin, D. A. Ethanolamine Utilization in Bacterial Pathogens: Roles and Regulation. *Nat. Rev. Microbiol.* **2010**, *8* (4), 290–295.

(156) Shibata, N.; Tamagaki, H.; Hieda, N.; Akita, K.; Komori, H.; Shomura, Y.; Terawaki, S.-I.; Mori, K.; Yasuoka, N.; Higuchi, Y.; Toraya, T. Crystal Structures of Ethanolamine Ammonia-Lyase Complexed with Coenzyme B12 Analogs and Substrates. *J. Biol. Chem.* **2010**, *285* (34), 26484–26493.

(157) Toraya, T. Radical Catalysis in Coenzyme B_{12}-Dependent Isomerization (Eliminating) Reactions. *Chem. Rev.* **2003**, *103* (6), 2095–2128.

(158) Kofoid, E.; Rappleye, C.; Stojiljkovic, I.; Roth, J. The 17-Gene Ethanolamine (*eut*) Operon of *Salmonella typhimurium* Encodes Five Homologues of Carboxysome Shell Proteins. *J. Bacteriol.* **1999**, *181* (17), 5317–5329.

(159) Bobik, T. A.; Havemann, G. D.; Busch, R. J.; Williams, D. S.; Aldrich, H. C. The Propanediol Utilization (*Pdu*) Operon of *Salmonella enterica* Serovar Typhimurium LT2 Includes Genes Necessary for Formation of Polyhedral Organelles Involved in Coenzyme B(12)-Dependent 1,2-Propanediol Degradation. *J. Bacteriol.* **1999**, *181* (19), 5967–5975.

(160) Martínez-del Campo, A.; Bodea, S.; Hamer, H. A.; Marks, J. A.; Haiser, H. J.; Turnbaugh, P. J.; Balskus, E. P. Characterization and Detection of a Widely

Distributed Gene Cluster That Predicts Anaerobic Choline Utilization by Human Gut Bacteria. *mBio* **2015**, *6* (2), e00042–15–12.

(161) Ferlez, B.; Sutter, M.; Kerfeld, C. A. Glycyl Radical Enzyme-Associated Microcompartments: Redox-Replete Bacterial Organelles. *mBio* **2019**, *10* (1), 1372–13.

(162) Zeisel, S. H.; daCosta, K. A.; Youssef, M.; Hensey, S. Conversion of Dietary Choline to Trimethylamine and Dimethylamine in Rats: Dose-Response Relationship. *J. Nutr.* **1989**, *119* (5), 800–804.

(163) Smillie, C. S.; Smith, M. B.; Friedman, J.; Cordero, O. X.; David, L. A.; Alm, E. J. Ecology Drives a Global Network of Gene Exchange Connecting the Human Microbiome. *Nature* **2011**, *480* (7376), 241–244.

(164) O'Brien, J. R.; Raynaud, C.; Croux, C.; Girbal, L.; Soucaille, P.; Lanzilotta, W. N. Insight Into the Mechanism of the B_{12}-Independent Glycerol Dehydratase From *Clostridium butyricum*: Preliminary Biochemical and Structural Characterization. *Biochemistry* **2004**, *43* (16), 4635–4645.

(165) Sun, X.; Ollagnier, S.; Schmidt, P. P.; Atta, M.; Mulliez, E.; Lepape, L.; Eliasson, R.; Gräslund, A.; Fontecave, M.; Reichard, P.; Sjöberg, B.-M. The Free Radical of the Anaerobic Ribonucleotide Reductase From *Escherichia coli* Is at Glycine 681. *J. Biol. Chem.* **1996**, *271* (12), 6827–6831.

(166) Tokumoto, U.; Takahashi, Y. Genetic Analysis of the *isc* Operon in *Escherichia coli* Involved in the Biogenesis of Cellular Iron-Sulfur Proteins. *J. Biochem.* **2001**, *130* (1), 63–71.

(167) Selvaraj, B.; Pierik, A. J.; Bill, E.; Martins, B. M. 4-Hydroxyphenylacetate Decarboxylase Activating Enzyme Catalyses a Classical *S*-Adenosylmethionine Reductive Cleavage Reaction. *J Biol Inorg Chem* **2013**, *18* (6), 633–643.

(168) Wecksler, S. R.; Stoll, S.; Tran, H.; Magnusson, O. T.; Wu, S.-P.; King, D.; Britt, R. D.; Klinman, J. P. Pyrroloquinoline Quinone Biogenesis: Demonstration That PqqE From *Klebsiella pneumoniae* Is A Radical *S*-Adenosyl-L-Methionine Enzyme. *Biochemistry* **2009**, *48* (42), 10151–10161.

(169) Bodea, S.; Funk, M. A.; Balskus, E. P.; Drennan, C. L. Molecular Basis of C-N Bond Cleavage by the Glycyl Radical Enzyme Choline Trimethylamine-Lyase. *Cell Chem. Biol.* **2016**, *23* (10), 1206–1216.

(170) Crain, A. V.; Broderick, J. B. Pyruvate Formate-Lyase and Its Activation by Pyruvate Formate-Lyase Activating Enzyme. *J. Biol. Chem.* **2014**, *289* (9), 5723–5729.

(171) Lehtiö, L.; Günter Grossmann, J.; Kokona, B.; Fairman, R.; Goldman, A. Crystal

Structure of a Glycyl Radical Enzyme From *Archaeoglobus fulgidus*. *J. Mol. Biol.* **2006**, *357* (1), 221–235.

(172) Gu, Y.; Kar, T.; Scheiner, S. Fundamental Properties of the CH···O Interaction: Is It a True Hydrogen Bond? *J. Am. Chem. Soc.* **1999**, *121* (40), 9411–9422.

(173) Raymo, F. M.; Bartberger, M. D.; Houk, K. N.; Stoddart, J. F. The Magnitude of [C−H···O] Hydrogen Bonding in Molecular and Supramolecular Assemblies. *J. Am. Chem. Soc.* **2001**, *123* (38), 9264–9267.

(174) Horowitz, S.; Trievel, R. C. Carbon-Oxygen Hydrogen Bonding in Biological Structure and Function. *J. Biol. Chem.* **2012**, *287* (50), 41576–41582.

(175) Adhikari, U.; Scheiner, S. Magnitude and Mechanism of Charge Enhancement of CH··O Hydrogen Bonds. *J. Phys. Chem. A* **2013**, *117* (40), 10551–10562.

(176) Horowitz, S.; Dirk, L. M. A.; Yesselman, J. D.; Nimtz, J. S.; Adhikari, U.; Mehl, R. A.; Scheiner, S.; Houtz, R. L.; Al-Hashimi, H. M.; Trievel, R. C. Conservation and Functional Importance of Carbon–Oxygen Hydrogen Bonding in AdoMet-Dependent Methyltransferases. *J. Am. Chem. Soc.* **2013**, *135* (41), 15536–15548.

(177) Ruszczycky, M. W.; Liu, H.-W. Mechanistic Enzymology of the Radical SAM Enzyme DesII. *Isr. J. Chem.* **2015**, *55* (3-4), 315–324.

(178) Persson, A. L.; Eriksson, M.; Katterle, B.; Pötsch, S.; Sahlin, M.; Sjöberg, B.-M. A New Mechanism-Based Radical Intermediate in a Mutant R1 Protein Affecting the Catalytically Essential Glu 441in *Escherichia coli* Ribonucleotide Reductase. *J. Biol. Chem.* **1997**, *272* (50), 31533–31541.

(179) Lawrence, C. C.; Bennati, M.; Obias, H. V.; Bar, G.; Griffin, R. G.; Stubbe, J. High-Field EPR Detection of a Disulfide Radical Anion in the Reduction of Cytidine 5'-Diphosphate by the E441Q R1 Mutant of *Escherichia coli* Ribonucleotide Reductase. *Proc. Natl. Acad. Sci. U.S.A.* **1999**, *96* (16), 8979–8984.

(180) Lehtiö, L.; Goldman, A. The Pyruvate Formate Lyase Family: Sequences, Structures and Activation. *Protein Eng. Des. Sel.* **2004**, *17* (6), 545–552.

(181) Dawson, R. M. C. *Data for Biochemical Research*; London/New York: Oxford University Press (Clarendon), 1969.

(182) Laroff, G. P.; Fessenden, R. W. Equilibrium and Kinetics of the Acid Dissociation of Several Hydroxyalkyl Radicals. *J. Phys. Chem.* **1973**, *77* (10), 1283–1288.

(183) Foster, T.; West, P. R. Photolysis of Aqueous Solutions of Hydrogen Peroxide Containing B-Ammonio Alcohols. *Can. J. Chem.* **1974**, *52* (21), 3589–3598.

(184) Mori, K.; Oiwa, T.; Kawaguchi, S.; Kondo, K.; Takahashi, Y.; Toraya, T. Catalytic Roles of Substrate-Binding Residues in Coenzyme B_{12}-Dependent Ethanolamine Ammonia-Lyase. *Biochemistry* **2014**, *53* (16), 2661–2671.

Chapter 2: Structure-guided identification of a small molecule that inhibits anaerobic choline metabolism by human gut bacteria[1]

2.1. Introduction

One approach for studying the impact of microbial metabolic activities on human physiology is the use of small molecules that selectively target bacterial enzymes. While small molecule inhibitors that disrupt pathogen-host interactions have been discovered,[1] the use of tool compounds to selectively modulate biochemical transformations or metabolites from the human gut microbiota remains largely unexplored. Work from the Redinbo lab demonstrated the feasibility of inhibiting bacterial β-glucuronidases and remains one of the few successful examples of the chemical manipulation of a specific gut microbial reaction.[2] β-Glucuronidase enzymes are capable of hydrolyzing glucuronic acid-containing sugar moieties from a variety of compounds, including the chemotherapeutic agent CPT-11. Like other pharmaceuticals, this cancer drug is normally inactivated via glucuronidation by mammalian enzymes in the liver and subsequently excreted into the GI tract. Within the gut lumen, however, certain sugar-scavenging bacteria deconjugate the glucuronide group, liberating the active form of CPT-11, which contributes to the damage of intestinal epithelial cells and leads to severe diarrhea. By employing a high-throughput screening method and leveraging insights from biochemical and structural studies, Wallace et al. uncovered inhibitors that selectively target microbial β-glucuonidases, are not lethal to either bacteria or human cells, and prevent the toxicity of CPT-11 in mouse models.[2] This work demonstrated the feasibility of employing drug discovery strategies towards targeting gut bacterial enzymes to study and improve human health.

[1]This chapter is an unofficial adaptation of the following: Orman, M., Bodea, S., Funk, M. A., Martínez-del Campo, A., Bollenbach, M., Drennan, C. L., Balskus, E. P. *J. Am. Chem. Soc.* **2018**, 141 (1), 33–37.

The development of small molecules that modulate additional metabolic pathways in the gut microbiota would provide tremendous aid in understanding the complex biochemical dialogue that ensues between microorganisms and their hosts. The breadth of biosynthetic potential encoded in the gut microbiome suggests that it is a rich source of novel targets for chemical genetics. In addition, direct targeting of the gut microbiota with small molecule inhibitors may serve as a viable therapeutic approach for the treatment of human diseases. Potentially, these molecules may act in a non-microbicidal manner and be less likely to disrupt the beneficial activities of commensal gut organisms.

Gut microbial metabolism of the essential nutrient choline to produce TMA is a prominent, disease-associated pathway (Figure 2.1).[3] In humans, most of the TMA produced in the gut is transported via portal circulation to the liver, where it is oxidized by human flavin monooxygenases such as FMO3 to the water-soluble metabolite TMAO.[4,5] Elevated levels of plasma TMAO have been linked to a wide range of human disorders, including nonalcoholic fatty liver disease,[6,7] cardiovascular disease,[8-11] chronic kidney disease,[12,13] and type 2 diabetes mellitus.[14] Additionally, patients with the inherited metabolic disorder trimethylaminuria exhibit decreased FMO3 activity and, as a result, accumulate the malodorous compound TMA in bodily fluids.[15-17] Despite the many connections between anaerobic choline metabolism and human health, the mechanisms by which choline-degrading gut microbes affect host physiology and interact with other members of the gut microbiota remain largely uncharacterized.

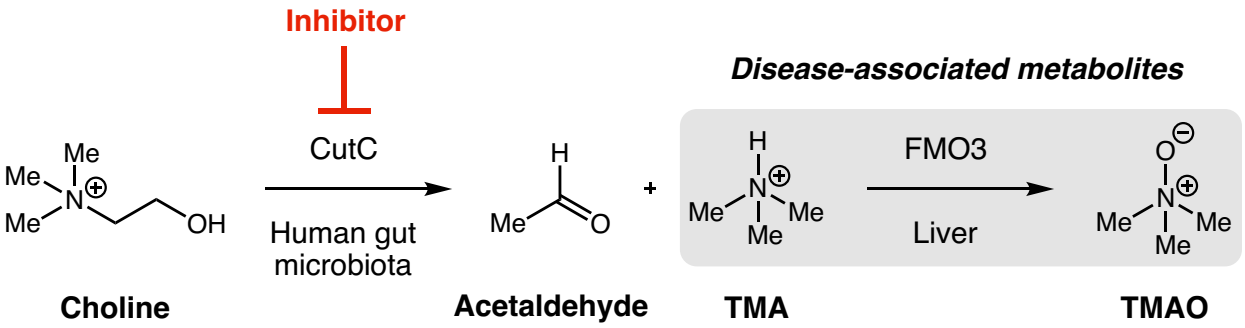

Figure 2.1. Anaerobic choline metabolism is a disease-linked gut microbial activity and a potential target for small-molecule inhibitors. Acetaldehyde and TMA are generated from choline by microbes found in the human gut. TMA is subsequently processed in the liver to TMAO. TMA and TMAO have been associated with human diseases such as nonalcoholic fatty liver disease, cardiovascular disease, chronic kidney disease, and type 2 diabetes mellitus.

As described in Chapter 1, the choline utilization (*cut*) gene cluster encodes the bacterial enzymes involved in anaerobic choline metabolism, including the glycyl radical enzyme (GRE) choline TMA-lyase (CutC) and its corresponding activating enzyme (AE), CutD.[18-20] Employing a mechanism common to all GRE-AEs (see Chapter 1, Section 1.5), CutD utilizes SAM and a [4Fe-4S] cluster to install a radical on a conserved glycine residue within CutC's active site. This post-translational modification activates CutC, enabling its catalysis of the C–N bond cleavage of choline, which generates TMA and acetaldehyde (Figure 2.1).

Previous work in the Balskus and Drennan labs elucidated the structure of choline-bound CutC, cloned from *Desulfovibrio alaskensis* G20, and provided insight into the mechanism of choline cleavage.[20] Within the polar active site of CutC, choline is oriented such that its C1 hydroxyl engages in hydrogen bonding with Glu491 (Figure 2.2). The primary substrate-specific contacts are an array of CH—O hydrogen bonds between the polarized methyl groups of the trimethylammonium moiety and the side-chain oxygen atoms of Tyr208, Tyr506, Asp216, and a bound water molecule (Figure 2.2). Once installed, the glycyl radical of CutC is proposed to abstract a hydrogen atom from an adjacent cysteine (Cys489), generating a thiyl radical

intermediate that initiates the reaction with choline (Figure 2.3). The thiyl radical could abstract the *pro-S* hydrogen atom from C1 of choline. Subsequent deprotonation of the C1-OH by Glu491, followed by C–N bond cleavage via a "spin-center shift" would eliminate trimethylamine. The resulting product-based radical could re-abstract the hydrogen atom from Cys489, reforming the thiyl radical and generating acetaldehyde.

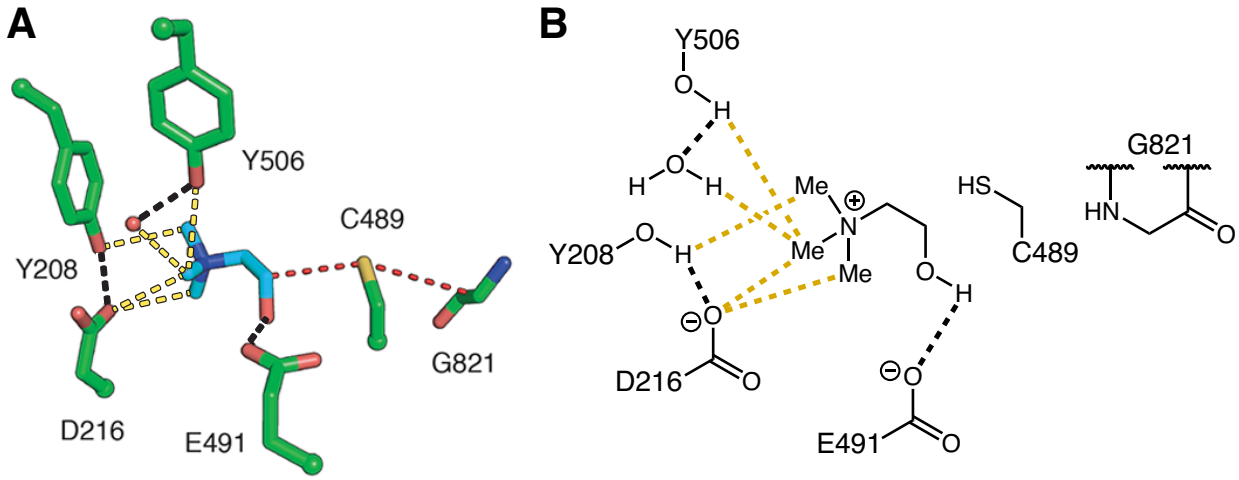

Figure 2.2. CutC orients choline through hydrogen bonding with a putative general base and CH—O hydrogen bonds with a water molecule and residues in the active site. (A) Crystal structure of CutC from *D. alaskensis* G20 bound to choline (PBD = 5FAU[20]). (B) Diagram of hydrogen bonds between a putative general base, Glu491, and choline and of close interactions between phenolic and carboxylate oxygen atoms of the protein (and a water molecule in the active site) and the polarized methyl groups of the trimethylammonium moiety. CH—O hydrogen bonds are indicated in yellow and hydrogen bonds are in black.

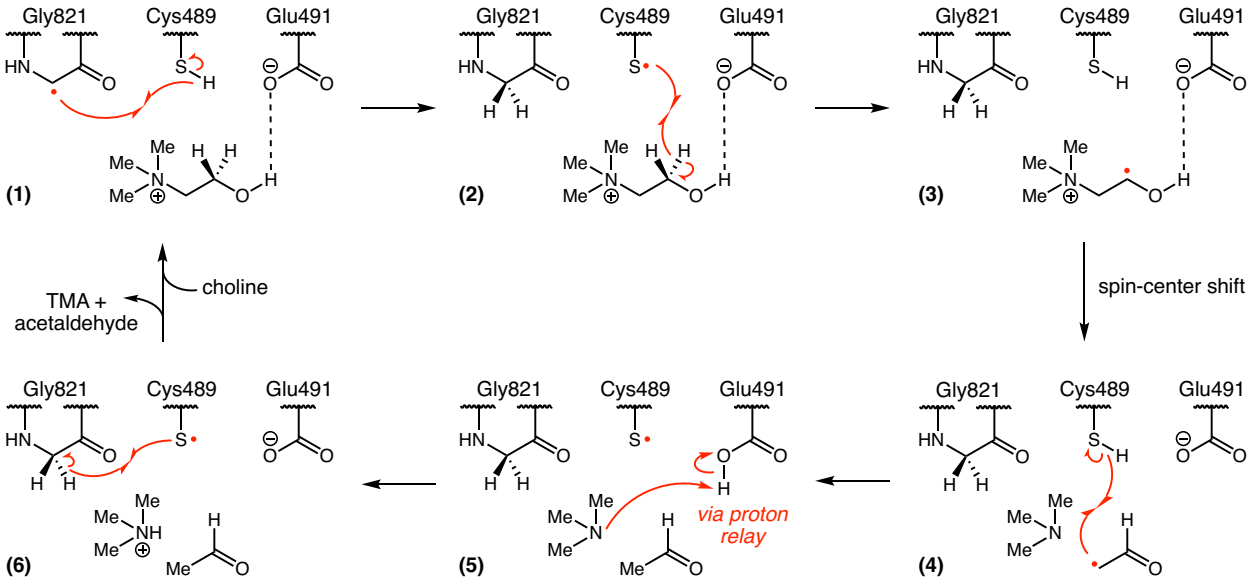

Figure 2.3. Proposed mechanism for choline cleavage by CutC. (1) The glycyl radical of CutC abstracts a hydrogen atom from Cys489, generating a thiyl radical. (2) Catalysis begins with *pro-S* hydrogen atom abstraction from C1 of choline. (3) TMA is eliminated from the resulting α-hydroxyalkyl radical species via a "spin-center shift." (4) The subsequent product-based radical species re-abstracts a hydrogen atom from Cys489, reforming the thiyl radical and generating acetaldehyde. (5) A series of proton transfers takes place, ultimately deprotonating the putative general base, Glu491. (6) The thiyl radical re-abstracts a hydrogen atom from Gly821, regenerating the glycyl radical and resetting the active site for the next round of catalysis.

By leveraging our mechanistic and molecular understanding of the enzymatic reaction performed by CutC, we were able to compile a set of putative small molecule inhibitors, which we tested for their ability to inhibit TMA production from choline in several assays. Our results are described in this chapter. We found that our most potent inhibitor, betaine aldehyde, covalently interacts with CutC *in vitro* and inhibits anaerobic choline utilization in gut bacterial cultures and a human fecal suspension. In addition, a previously reported inhibitor of gut microbial TMA formation, 3,3-dimethylbutanol (DMB),[21] was not active in our assays, suggesting that it does not directly block anaerobic CutC-mediated cleavage of choline but may instead act through alternative pathways. This study provides a framework for identifying small molecules that selectively target anaerobic gut microbial choline metabolism and represents a

critical step towards developing tools that will enable further exploration of the role of choline degradation in diverse microbial communities.

2.2. Results and Discussion

2.2.1. Rational design and testing of putative CutC inhibitors

The information gleaned from our crystallographic and biochemical studies informed our search for small molecule inhibitors of CutC. We sought to preserve many of the key interactions between choline and active site residues and therefore assembled a series of choline analogs that were commercially available or readily accessible by chemical synthesis. Dr. Smaranda Bodea performed the synthesis of non-commercially available analogs (**2**, **3**, **6** **7**, and **9**).[22,23] The 13 molecules shown in Figure 2.4A were tested for their ability to inhibit anaerobic choline metabolism in the *cut* gene cluster-containing organism *Escherichia coli* MS 200-1, originally isolated from the ileum of a healthy patient. For our initial screen, cultures were incubated anaerobically in a rich medium containing 1 mM of (trimethyl-d_9)-choline (d_9-choline) and three concentrations (1, 5, and 10 mM) of compound. Production of d_9-TMA was analyzed by LC-MS/MS. Compounds thiocholine (**2**) and betaine aldehyde (**9**) emerged as the most promising inhibitors. Notably, we did not observe inhibitory activity with DMB (**12**), a small molecule previously reported to inhibit gut microbial production of TMA from choline,[21] and only modest inhibition with the corresponding oxidized analog, 3,3-dimethylbutyric aldehyde (DMBA) (**13**). These two compounds are described in greater detail in Section 2.2.6. Betaine aldehyde, which contains a trimethylammonium moiety, can presumably maintain critical interactions, such as CH—O hydrogen bonds, within the CutC active site. We have also previously demonstrated that this molecule is not a substrate for C–N cleavage by CutC.[19] We therefore chose to explore

betaine aldehyde's range of activity in a variety of bacterial and *in vitro* assays and to examine its mechanism of inhibition.

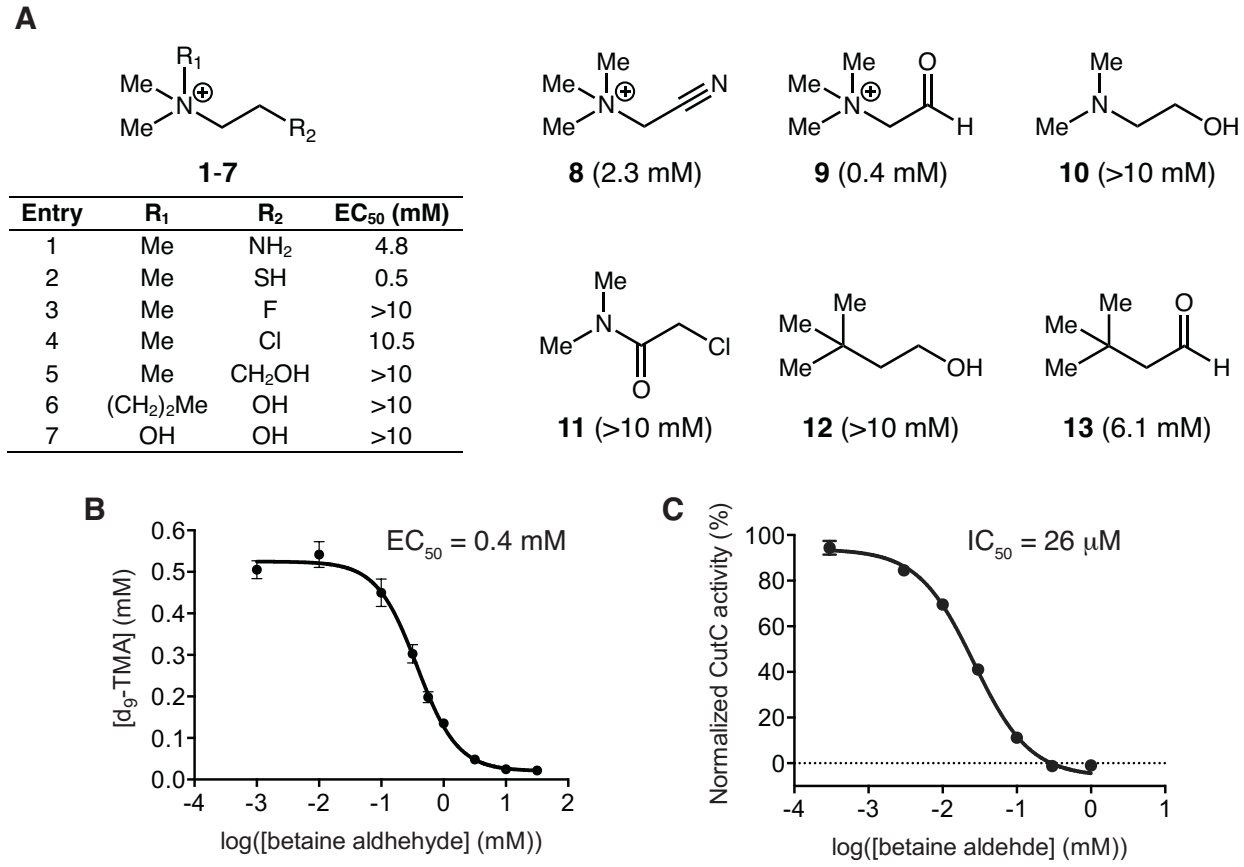

Entry	R_1	R_2	EC_{50} (mM)
1	Me	NH_2	4.8
2	Me	SH	0.5
3	Me	F	>10
4	Me	Cl	10.5
5	Me	CH_2OH	>10
6	$(CH_2)_2Me$	OH	>10
7	OH	OH	>10

Figure 2.4. Betaine aldehyde inhibits TMA formation in *E. coli* and *in vitro*. (A) Choline analogs were tested for inhibition of anaerobic choline metabolism in *E. coli* MS 200-1. Bacteria were incubated in BHI medium with 1 mM d_9-choline and 1, 5, or 10 mM of inhibitor at 37 °C. Production of d_9-TMA was measured by LC-MS/MS after 3.5 hours. Dose-response curves were fit using nonlinear regression to determine EC_{50} values, which are listed either in the table or below the corresponding chemical structure. (B) Betaine aldehyde inhibits anaerobic d_9-TMA formation in *E. coli* MS 200-1 in a dose-dependent manner. Bacteria were incubated in BHI medium with 1 mM d_9-choline and inhibitor (1 μM to 30 mM) at 37 °C. Production of d_9-TMA was measured by LC-MS/MS after 3.5 hours. Data were fit using nonlinear regression. Error bars represent the mean ± SD of three replicates. (C) Betaine aldehyde inhibits the activity of CutC *in vitro*. Betaine aldehyde (0.30 μM to 1 mM) was added immediately before the addition of choline. The activity of CutC was coupled to that of NADH-dependent yeast alcohol dehydrogenase and the absorbance of NADH at 340 nm was recorded over time. Data were fit using nonlinear regression. Error bars represent the mean ± SD of three replicates.

2.2.2. Betaine aldehyde is a CutC inhibitor

Betaine aldehyde was re-tested in the whole cell *E. coli* MS 200-1 assay at concentrations ranging from 1 µM to 30 mM and exhibited an EC_{50} value of 0.4 mM (Figure 2.4B). To assess whether reduction of TMA formation arose from inhibition of CutC, we investigated the effect of betaine aldehyde on CutC-mediated choline cleavage *in vitro* under an anaerobic atmosphere. Recombinant wild-type CutC and CutD from *D. alaskensis* G20 were expressed and purified as previously described.[19,20] Using a 7-point dilution series, the IC_{50} of betaine aldehyde for CutC was determined to be 26.4 ± 2 µM (Figure 2.4C). DMB did not inhibit CutC, even at the highest concentrations tested. Thus, betaine aldehyde's ability to reduce TMA levels in *E. coli* may arise from its direct targeting of CutC inside cells. In contrast, we find no evidence that DMB and DMBA are CutC inhibitors.

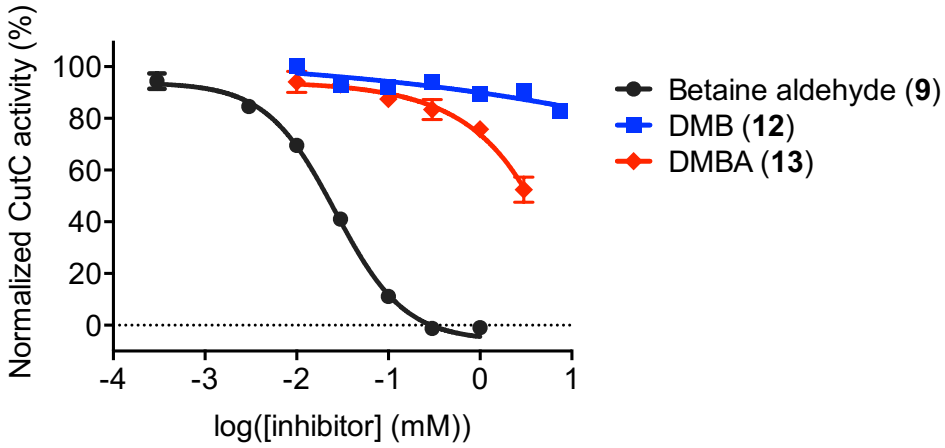

Figure 2.5. Betaine aldehyde, but not DMB, inhibits CutC-mediated TMA production *in vitro*. The activity of CutC was coupled to that of yeast alcohol dehydrogenase. Inhibitors (0.30 µM to 5 mM) were added prior to the addition of choline. The absorbance of NADH at 340 nm was recorded over time to calculate initial rates and kinetic parameters. Initial rates were normalized to a control assay without inhibitor, and data were fit using nonlinear regression in Graphpad Prism. Error bars represent the mean ± SD of three replicates.

2.2.3. Betaine aldehyde is a reversible covalent inhibitor

We hypothesized that the aldehyde moiety of betaine aldehyde could interfere with choline binding to CutC by forming a covalent adduct with the catalytically essential Cys489 thiol (Figure 2.6), thereby blocking access to the active site. To gain information about how betaine aldehyde interacts with CutC, we performed X-ray crystallographic studies on the unactivated enzyme-inhibitor complex. Dr. Smaranda Bodea expressed and purified CutC while Dr. Michael A. Funk from the Drennan lab at MIT performed the X-ray crystallography data collection and analysis.

After pre-incubating wild-type CutC with 10 mM of inhibitor, Dr. Funk obtained a homogenous solution that was crystalized using conditions similar to those for choline-bound CutC.[20] The resulting structure (see Table 2.1 in Section 2.4.6) was determined to 2.2-Å resolution and showed a large continuous patch of density around Cys489. Dr. Funk modeled a thiohemiacetal adduct of betaine aldehyde at Cys489 (Figure 2.7A, Table 2.2 in Section 2.4.6) and validated this assignment through composite omit electron density maps (Figure 2.7B). This structure supports the hypothesis that betaine aldehyde functions as a covalent, reversible inhibitor of CutC.

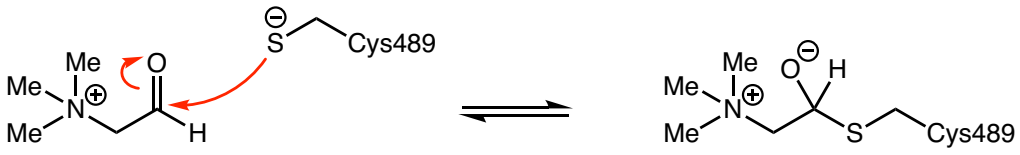

Figure 2.6. Proposed model for inhibition of CutC by betaine aldehyde. The catalytically essential Cys489 could react with the carbonyl group of betaine aldehyde, forming a covalent bond between protein and inhibitor that is expected to be reversible.

Betaine aldehyde establishes similar interactions with CutC active site residues as those observed in the choline-bound crystal structure (Figure 2.7C). The thiohemiacetal alcohol participates in hydrogen bonds with Glu491 (2.5 Å) and the backbone amide of Cys489 (2.7 Å). The trimethylammonium moiety is shifted slightly away from the rear of the active site, where residues Asp216, Tyr208, and Tyr506 and a water molecule make numerous CH–O hydrogen bonds to the polarized methyl groups, slightly altering the distances from what was observed in the choline-bound structure (Table 2.3 in in Section 2.4.6). In addition, the α-carbon of betaine aldehyde is shifted closer to the aromatic ring of Phe395 (3.5 Å vs. 3.8 Å), a residue thought to make a cation-π-like interaction with the substrate. Overall, betaine aldehyde appears to be well accommodated in this active site. The observed covalent interaction could explain betaine aldehyde's ability to inhibit CutC and the apparent decrease in IC_{50} upon pre-incubation of inhibitor with the enzyme (Figure 2.8). Alternatively, inhibition could result from a long dwell time of this molecule in the active site due to these favorable interactions.

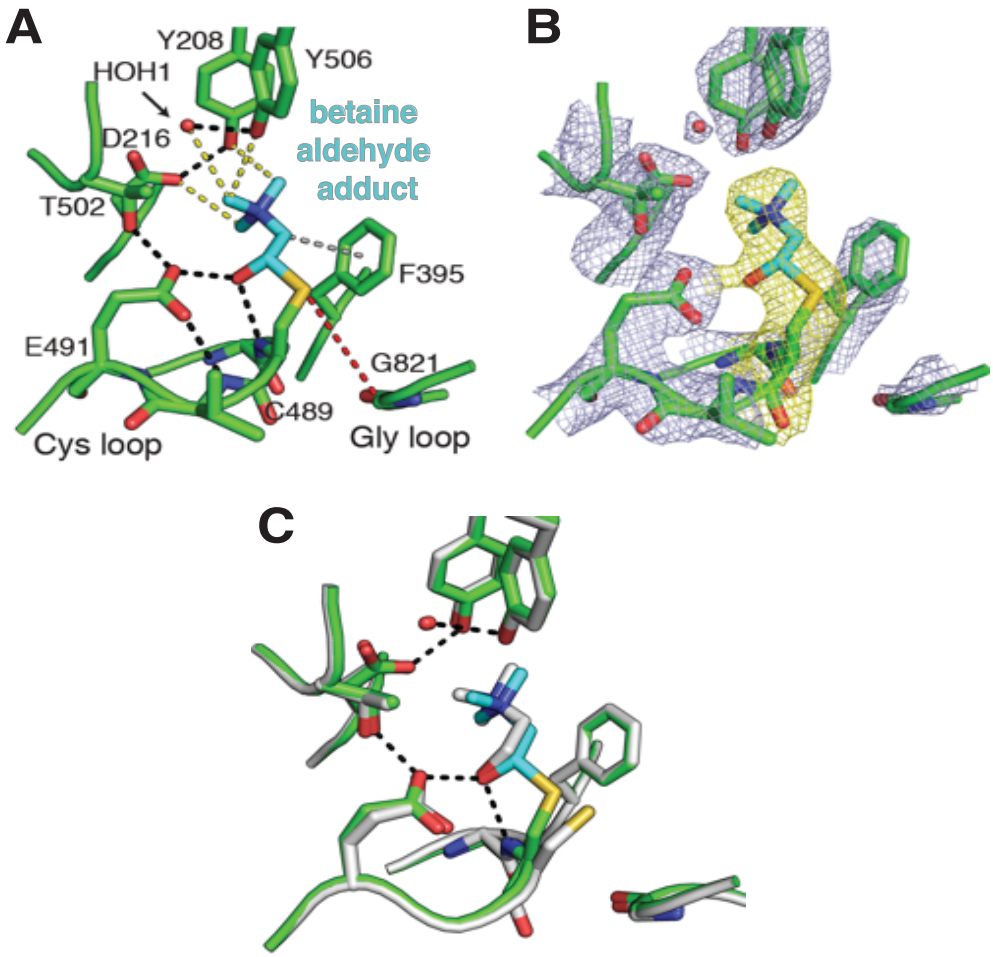

Figure 2.7. Betaine aldehyde binding to CutC appears to involve a covalent, thiohemiacetal linkage. (A) Crystal structure of unactivated CutC from *D. alaskensis* G20 soaked with betaine aldehyde (10 mM) reveals interactions between CutC active site residues and bound inhibitor (cyan). Shown are traditional hydrogen bonds (2.5-3.2 Å, black dashes), CH—O hydrogen bonds (3.2-3.7 Å, yellow dashes), and a cation-π-like interaction (gray dashes). (B) Composite omit $2F_o$-F_c density (light blue) contoured at 1.8σ. Density surrounding betaine aldehyde-modified Cys493 is highlighted (yellow). (C) Comparison of inhibitor-bound CutC (green) active site residues with those of the choline-bound CutC structure (grey). Hydrogen bonding interactions with the Cys loop (black dashes) are shown.

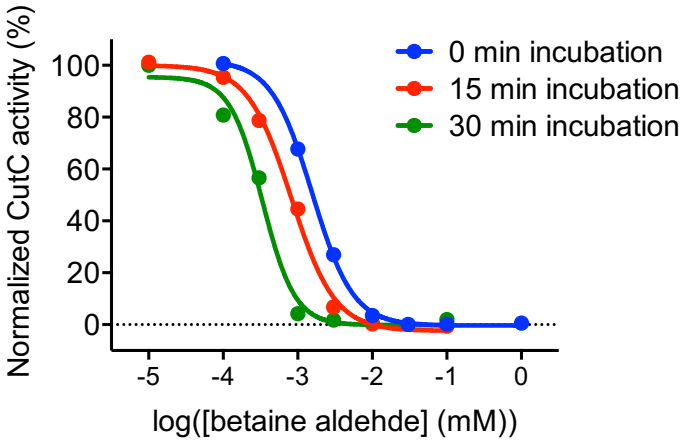

Figure 2.8. Betaine aldehyde inhibits CutC activity *in vitro* in a time-dependent manner. The activity of CutC was coupled to that of yeast alcohol dehydrogenase (YADH). Betaine aldehyde (0.01 μM to 1 mM) was incubated with activated CutC for various lengths of time (0, 15, and 30 minutes) prior to the addition of choline. The absorbance of NADH at 340 nm was recorded over time to calculate initial rates and kinetic parameters. Initial rates were normalized to a control assay without inhibitor, and the data were fit using nonlinear regression in Graphpad Prism to obtain IC_{50} values of 1.56, 0.82, and 0.34 μM for 0, 15, and 30 min of incubation, respectively. Error bars represent the mean ± SD of three replicates.

2.2.4. Betaine aldehyde inhibits anaerobic *E. coli* growth on choline and is not metabolized in minimal and rich media

We have previously shown that functional CutC is essential for the growth of *cut* gene cluster-containing *E. coli* under anaerobic conditions in which choline is provided as the sole carbon source and fumarate as a terminal electron acceptor.[24] To determine whether inhibition of CutC by betaine aldehyde would impact anaerobic growth on choline-containing minimal medium, the choline-metabolizing strain *E. coli* MS 69-1 was grown in medium containing 30 mM choline as the sole carbon source and increasing concentrations of betaine aldehyde. Under an N_2 atmosphere, 20 mM of betaine aldehyde effectively abolished growth on choline but had no impact on growth in minimal medium containing 30 mM glycerol as the sole carbon source (Figure 2.9A) or growth in BHI, a complex medium containing 2 g/L (~11 mM) of glucose (Figure 2.9B). This result, along with previous work in gnotobiotic animal models,[24] indicates

that choline metabolism is non-essential when alternative carbon sources are present. Interestingly, DMB and DMBA diminished growth on choline minimal medium but in a different manner from that of betaine aldehyde (Figure 2.10A), suggesting that these compounds do not share a mechanism(s) of action. DMB and DMBA also slightly delayed growth on glycerol minimal medium (Figure 2.10B), implying that they do not specifically target anaerobic choline metabolism.

The ability of betaine aldehyde to inhibit TMA production on a rich medium without any discernable growth defect suggests that this may be a promising strategy for inhibiting CutC-mediated choline cleavage in the context of the nutrient-rich environment of the gut. We speculate that a CutC inhibitor might not exert selective pressure on the gut microbial community, potentially reducing the likelihood of the development of resistance. Finally, the stability of betaine aldehyde, which is endogenously produced in bacteria as an intermediate in the oxidation of choline to glycine betaine, was monitored in cultures grown anaerobically on choline (Figure 2.11) and BHI media (Figure 2.12). The metabolism of the inhibitor was not observed in either of these conditions.

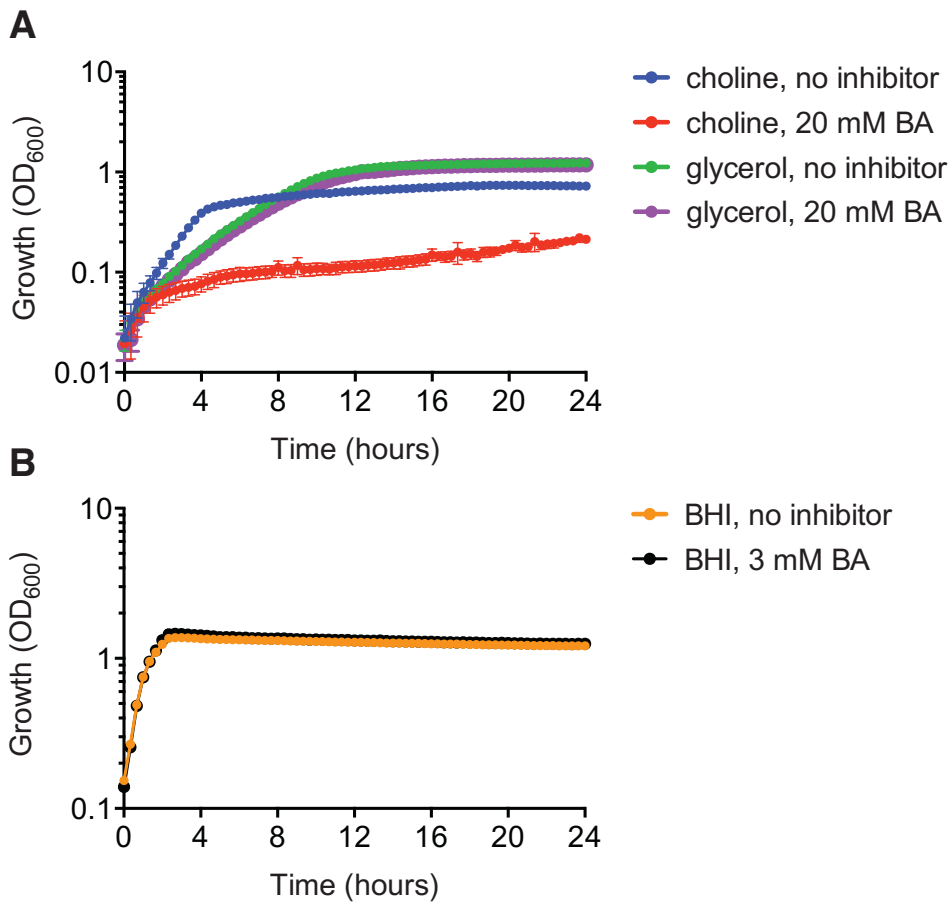

Figure 2.9. Betaine aldehyde inhibits anaerobic growth on choline in *E. coli* MS 69-1. Growth of *E. coli* MS 69-1 on minimal media containing (A) 30 mM choline or 30 mM glycerol and (B) on BHI, a rich medium containing 11 mM glucose. Cultures were supplemented with either phosphate buffer (no inhibitor) or betaine aldehyde (BA) and grown under an N_2 atmosphere in an MBraun chamber at 37 °C. Error bars represent the mean ± SD of three replicates.

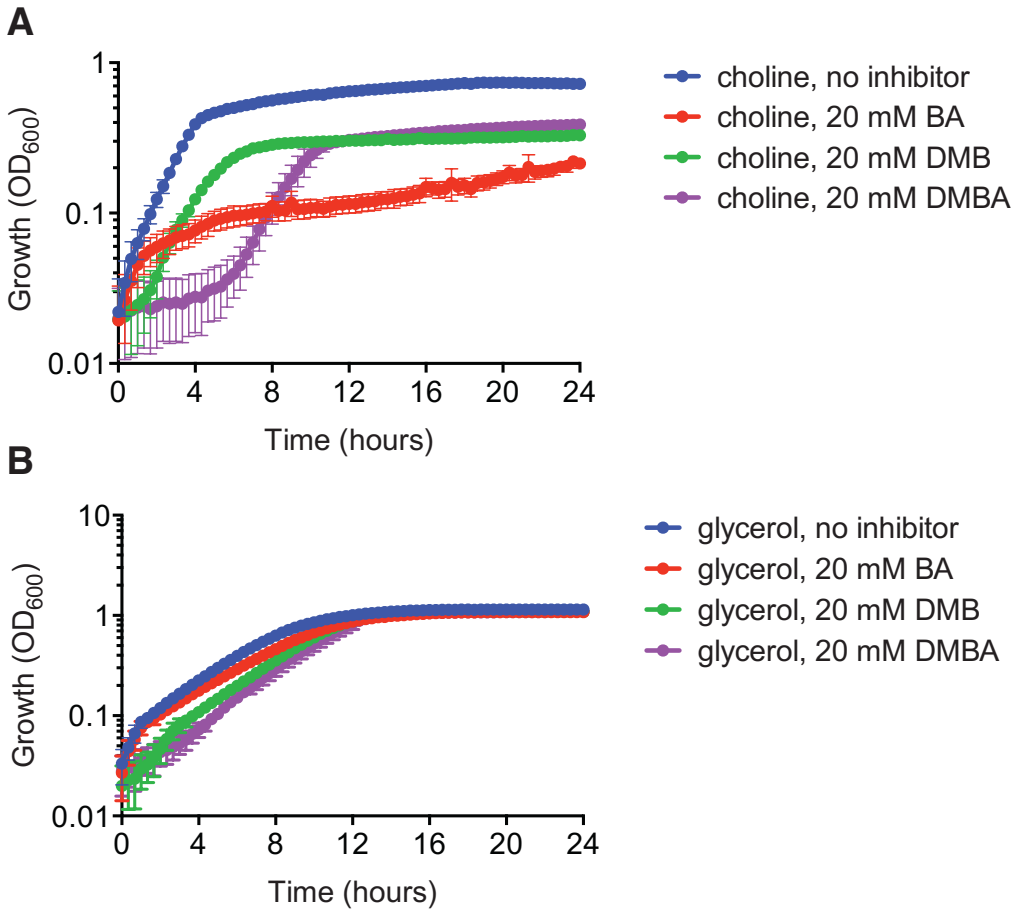

Figure 2.10. Betaine aldehyde, DMB, and DMBA exhibit different anaerobic growth phenotypes in *E. coli* MS 69-1 on minimal media. Growth of *E. coli* MS 69-1 on minimal media containing either (A) 30 mM choline or (B) 30 mM glycerol. Cultures were supplemented with phosphate buffer (no inhibitor), betaine aldehyde (BA), 3,3-dimethylbutanol (DMB), or 3,3-dimethylbutyl aldehyde (DMBA) and grown under an N_2 atmosphere in an MBraun chamber at 37 °C. Error bars represent the mean ± SD of three replicates.

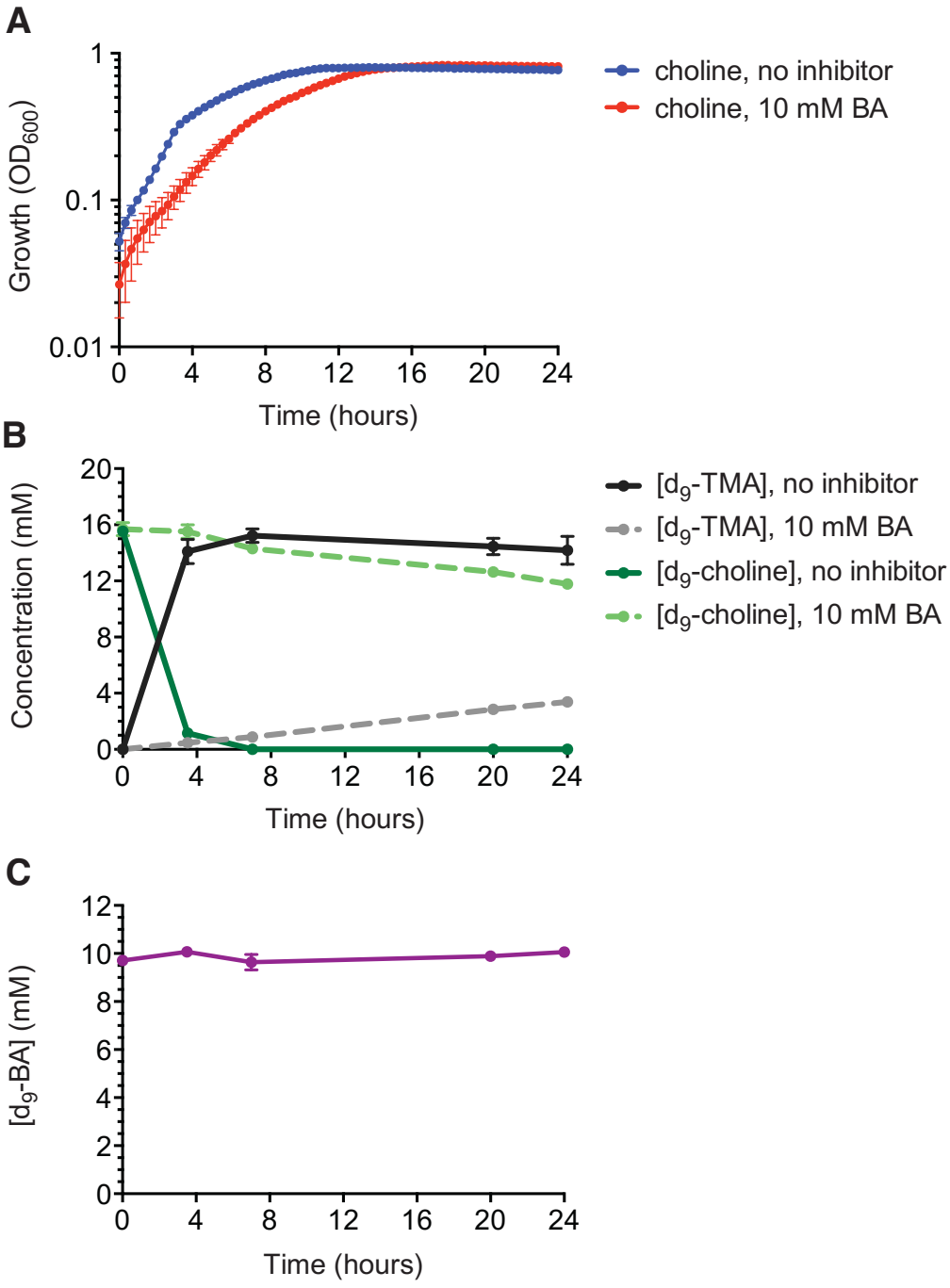

Figure 2.11. Betaine aldehyde can slow growth of choline-metabolizing *E. coli* on choline-containing minimal medium and is not metabolized. (A) Growth curves of *E. coli* MS 69-1 on minimal medium containing 15 mM choline. Cultures were supplemented with either phosphate buffer (no inhibitor) or 10 mM of betaine aldehyde (BA) and grown under an atmosphere of 98% N_2 and 2% H_2 in a vinyl chamber. (B) Anaerobic d_9-TMA and d_9-choline formation in *E. coli* MS 69-1 grown on minimal medium containing 15 mM d_9-choline. Cultures were supplemented with phosphate buffer (no inhibitor) or 10 mM of d_9-betaine aldehyde (BA) and incubated at 37 °C. Production of d_9-TMA and d_9-choline was measured by LC-MS/MS at 0, 3.5, 7, 20, and 24

hours. Error bars represent the mean ± SD of three replicates. (C) The concentration of d_9-betaine aldehyde is not altered during growth of *E. coli* MS 69-1 on choline. Bacteria were incubated in medium containing 15 mM d_9-choline at 37 °C and 10 mM d_9-betaine aldehyde. Concentrations of d_9-betaine aldehyde were measured by LC-MS/MS at 0, 3.5, 7, 20, and 24 hours. Error bars represent the mean ± SD of three replicates.

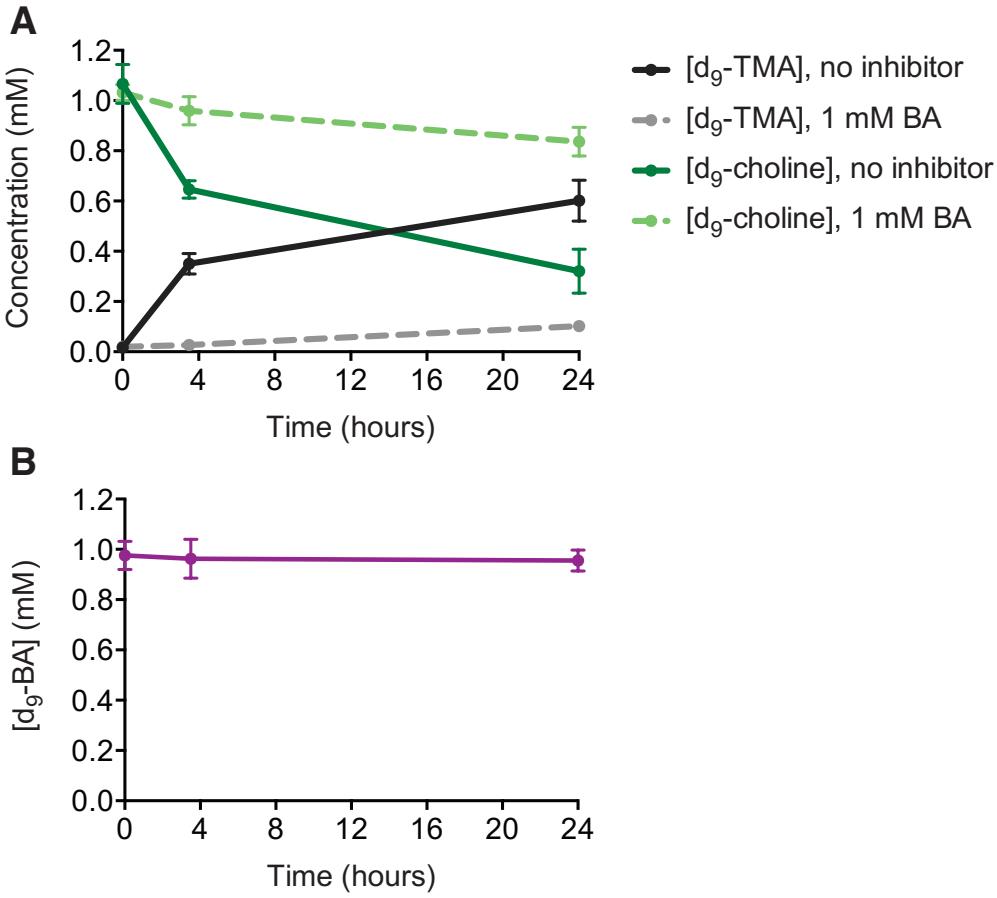

Figure 2.12. Betaine aldehyde is not metabolized by choline-metabolizing *E. coli* in rich growth medium. (A) Anaerobic d_9-TMA and d_9-choline formation in *E. coli* MS 200-1 grown on BHI rich medium containing 1 mM d_9-choline. Cultures were supplemented with phosphate buffer (no inhibitor) or 1 mM of d_9-betaine aldehyde (BA) and incubated at 37 °C. Production of d_9-TMA and d_9-choline was measured by LC-MS/MS at 0, 3.5, and 24 hours. Error bars represent the mean ± SD of three replicates. (B) The concentration of d_9-betaine aldehyde is not altered during growth of *E. coli* MS 200-1 on BHI. Bacteria were incubated in BHI medium containing 1 mM d_9-choline and 1 mM d_9-betaine aldehyde at 37 °C. Concentration of d_9-betaine aldehyde was measured by LC-MS/MS at 0, 3.5, and 24 hours. Error bars represent the mean ± SD of three replicates.

2.2.5. Betaine aldehyde inhibits choline utilization in gut bacterial cultures and a human fecal suspension

Culture-based studies and bioinformatics analysis of sequenced microbial genomes have revealed that *cut* genes are widely distributed among human gut bacteria, indicating that they likely encode a major pathway for choline utilization in the GI tract.[25] With the help of Dr. Smaranda Bodea, the ability of betaine aldehyde to inhibit TMA production was tested in additional Gram-positive (*Clostridium sporogenes* ATCC 15579) and Gram-negative (*Proteus mirabilis* BB2000, *Escherichia coli* MS 69-1, *Klebsiella* sp. MS 93-2) choline-metabolizing human gut isolates (Figure 2.13A). Betaine aldehyde was effective against all the strains assayed, including *C. sporogenes*, a member of the Firmicutes phylum. This group of microbes constitutes ~50% of gut bacteria in some individuals and may be the predominant group of choline metabolizing organisms in the healthy human gut. The observed EC_{50} values ranged from 1 to 5 mM, potentially due to differences in cell wall structure, microcompartment architecture and permeability, or the activity of efflux pumps in Gram-positive bacteria. Dr. Smaranda Bodea also established that betaine aldehyde effectively inhibited the conversion of choline to TMA by a human fecal suspension *ex vivo* (Figure 2.13B), confirming its efficacy in a complex setting more reminiscent of the gut microbiota. Overall, these findings demonstrate the feasibility of using a small molecule to inhibit anaerobic choline metabolism across a range of gut bacteria and in a microbial mixture.

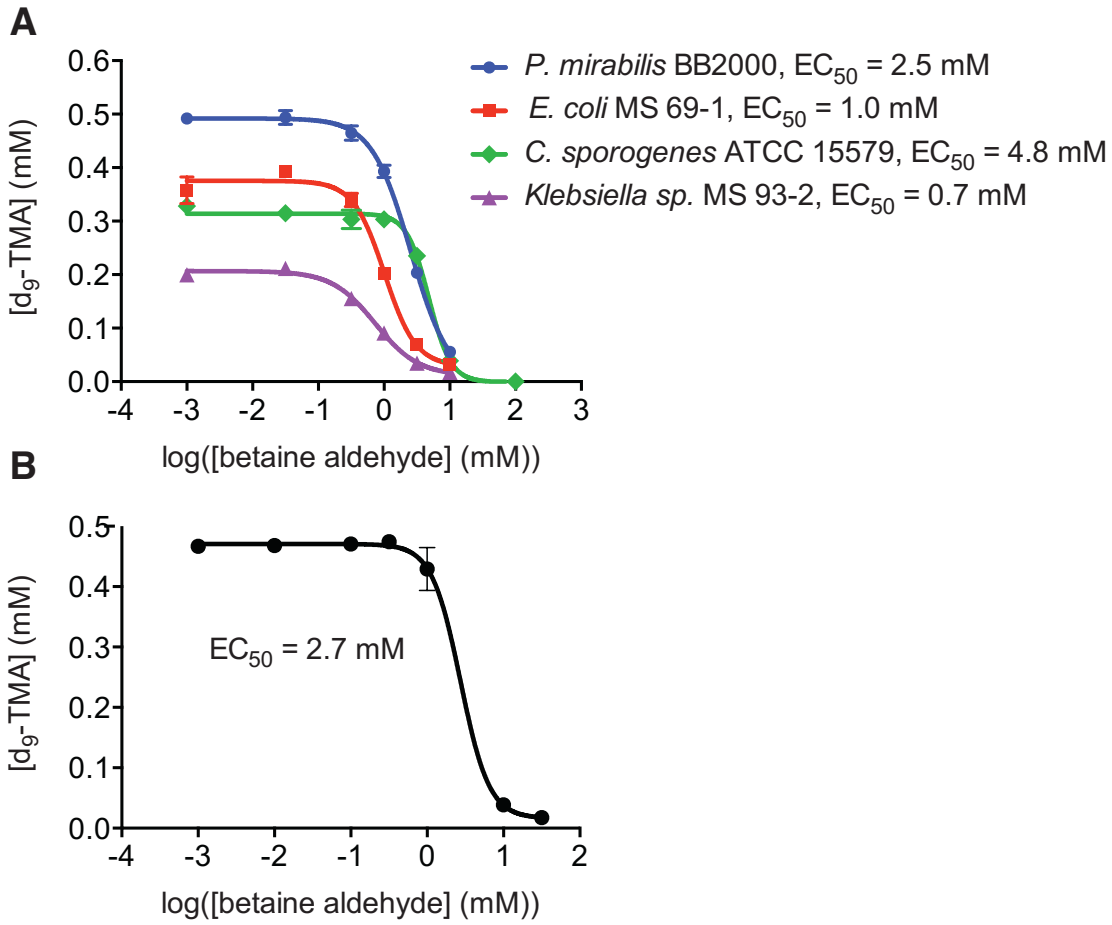

Figure 2.13. Betaine aldehyde inhibits choline utilization in gut bacterial cultures and a human fecal suspension. (A) Betaine aldehyde inhibits d_9-TMA formation from d_9-choline in *cut* gene cluster-harboring gut bacteria, including *Proteus mirabilis* BB2000, *Escherichia coli* MS 69-1, *Clostridium sporogenes* ATCC 15579, and *Klebsiella sp*. MS 93-2. Production of d9-TMA was measured by LC-MS/MS. Error bars represent the mean ± SD of three replicates. Data were fit using nonlinear regression. (B) Betaine aldehyde inhibits d_9-TMA formation from d_9-choline by a human fecal suspension. Production of d_9-TMA was measured by LC-MS/MS. Data were fit using nonlinear regression. Error bars represent the mean ± SD of two replicates.

2.2.6. Betaine aldehyde, but not DMB, inhibits choline utilization in *P. mirabilis* cells

Previous work has explored inhibiting microbial choline metabolism as a potential strategy for treating atherosclerosis.[21] The lead compound that emerged from this study, DMB (**12**), attenuated plasma TMAO levels and reduced the size of aortic lesions in mice fed a high-choline diet. Described as a specific inhibitor of TMA production, DMB has been used in additional animal studies.[26,27] Unexpectedly, we found that DMB did not reduce TMA production from choline by CutC *in vitro* (Figure 2.5) or in *E. coli* (Figure 2.4A). This result may be explained by the inability of DMB to engage in critical CH—O hydrogen bonding interactions within the active site of CutC, as well as lack of an electrophilic moiety for covalent bond formation with the enzyme. As DMB is rapidly metabolized *in vivo* by liver alcohol dehydrogenase,[21] we wondered whether an oxidized metabolite could be responsible for the phenotypes observed in mice. However, the corresponding aldehyde, DMBA (**13**), was a relatively poor inhibitor of TMA generation by *E. coli* (Figure 2.4A), despite its electrophilic functional group. Other aldehydes lacking a trimethylammonium moiety were also poor inhibitors of CutC activity *in vitro* (Figure 2.14).

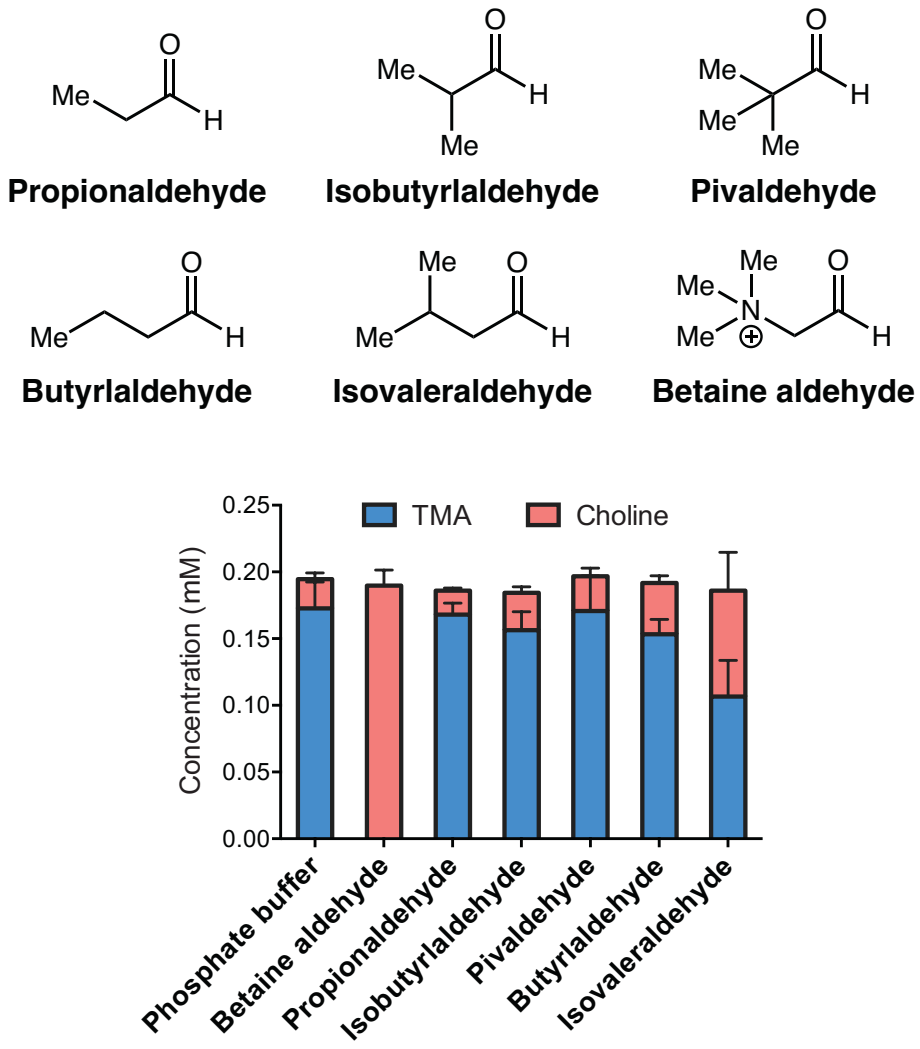

Figure 2.14. The trimethylammonium moiety of betaine aldehyde may be important for its inhibitory activity *in vitro*. Activated CutC was incubated with either phosphate buffer or various aldehydes (each at 0.1 mM) for 30 min prior to the addition of choline (0.2 mM). The mixture was incubated for an additional 15 min. Production of TMA was measured by LC-MS/MS. Error bars represent the mean ± SD of three replicates.

Using the same *P. mirabilis* strain employed by Wang et al.,[21] we observed minimal inhibition of TMA production by whole cells with DMB and DMBA (5 mM), whereas betaine aldehyde had an EC_{50} of 2.3−11.1 μM (Figure 2.15). DMB was also ineffective at inhibiting TMA generation by *P. mirabilis* cell lysates (Figure 2.16). We therefore conclude that DMB does not directly target anaerobic choline metabolism under these conditions and may not be an

appropriate tool compound for studying this microbial activity. These findings also suggest the TMAO-lowering activity of DMB *in vivo* may not originate from inhibiting CutC.

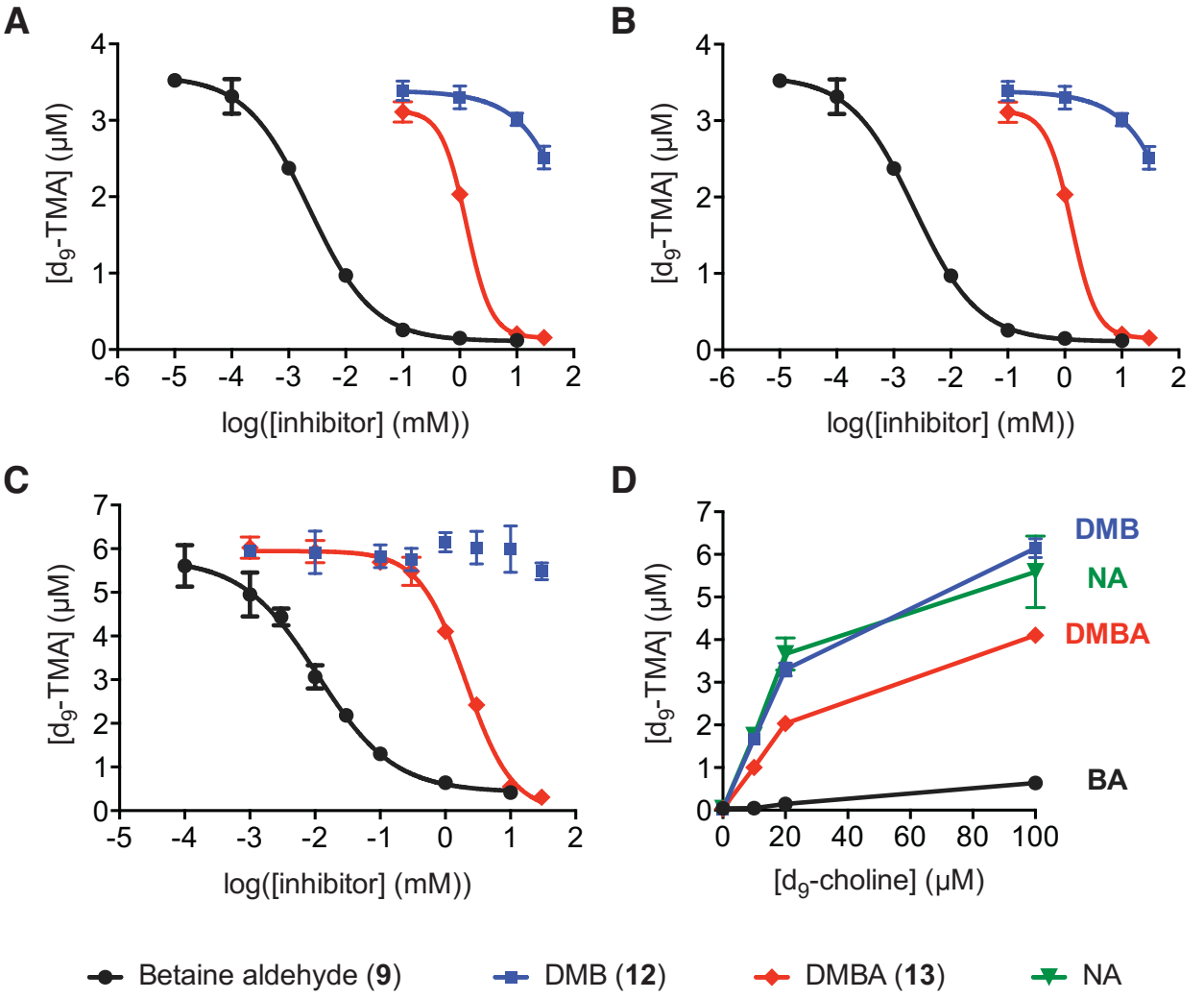

Figure 2.15. Betaine aldehyde inhibits CutC-mediated TMA production in whole-cell assays using *P. mirabilis* ATCC 29906 resting cells. Bacteria were re-suspended in PBS supplemented with either (A) 10, (B) 20, or (C) 100 μM d_9-choline and inhibitor (0.01 μM to 10 mM) at 37 °C. Production of d_9-TMA was measured by LC-MS/MS after 10 h. Betaine aldehyde inhibits anaerobic d_9-TMA formation in intact *P. mirabilis* ATCC 29906 cells in a dose-dependent manner, with an EC_{50} of (A) 4.1, (B) 2.3, and (C) 11.1 μM. DMBA is less potent than betaine aldehyde, inhibiting anaerobic d_9-TMA formation with an EC_{50} of (A) 1.2, (B) 1.3, and (C) 2.1 mM. DMB exhibits minimal inhibition of d_9-TMA formation. In (D), the d_9-TMA values from (A-C) are plotted against the concentration of d_9-choline added to intact *P. mirabilis* cells incubated with 1 mM of betaine aldehyde, DMB, or DMBA and without inhibitor (NA). Data were fit using nonlinear regression in Graphpad Prism. Error bars represent the mean ± SD of three replicates.

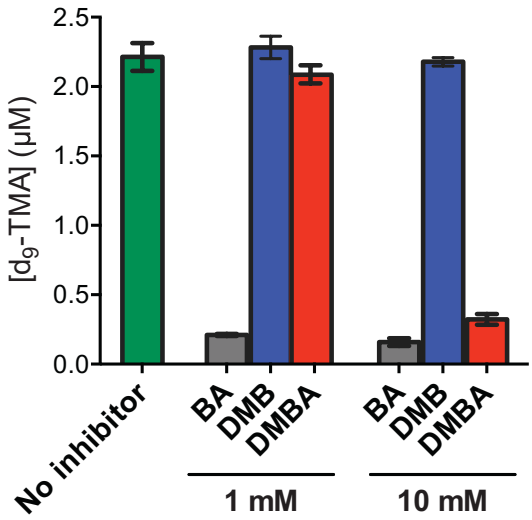

Figure 2.16. Betaine aldehyde inhibits CutC-mediated TMA production in *P. mirabilis* ATCC 29906 cell lysates. Betaine aldehyde inhibits anaerobic d_9-TMA formation in *P. mirabilis* ATCC 29906 protein lysates. Lysates were re-suspended in PBS supplemented with 100 μM d_9-choline and inhibitor (0, 1, or 10 mM) at 37 °C. Production of d_9-TMA was measured by LC-MS/MS after 10 h. Error bars represent the mean ± SD of three replicates.

2.3. Conclusions

In this work, we report the first well-characterized inhibitor of the gut bacterial choline-metabolizing GRE, CutC. Our comprehensive analysis includes *in vitro* data, a crystal structure (more specifically, the first crystal structure of an inhibitor bound to CutC), and inhibitory activity against multiple choline metabolizing organisms. We also demonstrate the efficacy of our small molecule inhibitor in a complex community of gut microorganisms. Betaine aldehyde is thus one the few examples of a non-antibiotic inhibitor that targets a pathway in commensal gut microbiota.

Inhibition of anaerobic choline metabolism has been the focus of several research efforts. In 2015, Wang et al. published their work on DMB, a small molecule that they described as a tool compound for studying the role of the microbiota in atherosclerosis.[21] However, our efforts to reproduce their results with *P. mirabilis* have been unsuccessful, and, in every side-by-

side comparison with DMB, our inhibitor was more effective at inhibiting anaerobic TMA production from choline. In fact, many of the experiments we performed, including crystallization studies and inhibition assays with purified CutC, are simply not reported or are inaccurately implemented in their paper. For instance, the authors tested DMB *in vitro* using an enzyme preparation that, at most, exhibited 0.2% of the turnover expected for CutC. Furthermore, there were no attempts at validating the enzyme preparations for proper reconstitution, either with EPR data to quantify the amount of active glycyl radical in a CutC/D mixture or kinetics or enzyme activity data to verify that CutC was functioning similarly to previously reported results. Therefore, while we recognize that betaine aldehyde lacks the potency to be a useful tool compound, the workflow we establish to characterize its activity as a true CutC inhibitor using rigorous anaerobic biochemical techniques will greatly aid the design and optimization of more potent compounds.

2.4. Material and methods

2.4.1. General materials and methods

Unless stated otherwise, all chemicals were purchased from Sigma-Aldrich. Trimethylamine-d_9 hydrochloride was purchased from CDN Isotopes, choline chloride-(trimethyl-d_9) was purchased from Cambridge Isotope Laboratories, and β-nicotinamide adenine dinucleotide reduced disodium salt hydrate (NADH) was purchased from EMD Millipore. Lennox Luria-Bertani (LB) medium and Lennox LB agar were purchased from EMD Millipore, BBL Brain Heart Infusion (BHI) broth and BBL BHI agar were purchased from BD Biosciences, Reinforced Clostridial Medium (RCM) was purchased from BD Biosciences, and Dulbecco's Phosphate Buffered Saline (PBS) was purchased from ThermoFisher Scientific. Acetonitrile used for liquid chromatography-mass spectrometry (LC-MS) was a B&J Brand high-purity solvent (Honeywell Burdick & Jackson). NMR solvents were purchased from Cambridge Isotope Laboratories.

LC-MS/MS was performed on an Agilent 6410 Triple Quadrupole LC-MS instrument (Agilent Technologies) using electrospray ionization. The mass spectrometer was operated in multiple reaction monitoring (MRM) mode with positive ionization monitoring. The precursor-product ion pairs used in MRM mode were: m/z 69.1 → 49.1 (d_9-TMA), m/z 113.2 → 69.1 (d_9-choline), m/z 111.1 → 66.1 (d_9-betaine aldehyde), m/z 60.1 → 40.1 (TMA), and m/z 109.1 → 60.1 (choline). The capillary voltage was set to 4.0 kV and the fragmentor voltage to 110 V. The drying gas temperature was maintained at 200 °C, with a flow rate of 10 L/min and a nebulizer pressure of 25 psi. The collision energy for the precursor-product ion pairs was set to 21 V. MS^1 resolution was set to wide and MS^2 resolution to unit. The time filter width used was 0.07 min, and the ΔEMV (Electron Multiplier Voltage) was 400 V. The injection volume of all samples

was 5 μL. Samples were injected onto a Kinetex (Phenomenex) HILIC column (2.6 μm, 30×2.1 mm, 100 Å). The LC conditions were: 0% B for 1 min, a gradient increasing to 100% B over 2 min, 100% B for 1.5 min, a gradient decreasing to 0% B over 1.5 min, and, finally, 0% B for 2 min (solvent A = 95% acetonitrile / 5% of 100 mM ammonium formate in water, with 0.02% formic acid; solvent B = 50% acetonitrile / 45% water / 5% of 100 mM ammonium formate in water, with 0.02% formic acid). The flow rate was maintained at 0.6 mL/min for each run. Data analysis was performed with Mass Hunter Workstation Data Acquisition software (Agilent Technologies).

Optical densities of bacterial cultures (for plasmid overexpression) were determined with a DU 730 Life Sciences UV/Vis spectrophotometer (Beckman Coulter) by measuring absorbance at 600 nm. *E. coli* BL21 (DE3) cells overexpressing CutC were lysed with a cell disruptor (Avestin EmulsiFlex-C3). Sonication for disrupting *E. coli* BL21 (DE3) cells overexpressing CutD was performed with a Branson Sonifier S-450D equipped with a 1⁄2 inch horn in a glove box (Coy Laboratory Products) under an atmosphere of 98% N_2 and 2% H_2 at 4 °C. Sonication for disrupting *Proteus mirabilis* cells was performed with a Branson Sonifier S-450D equipped with a 1⁄4 inch horn in the same glove box at 4 °C. Nickel-nitrilotriacetic acid agarose (Ni-NTA) resin was purchased from Qiagen. SDS-PAGE gels were purchased from BioRad.

All *in vitro* experiments with CutC-52aa and CutD were conducted anaerobically in an MBraun glovebox (MBraun) under an N_2 atmosphere with less than 5 ppm of O_2. Activity assays were set up in 96-well plates (Corning) and performed at 20 °C. The absorbance at 340 nm was monitored using a PowerWave HT Microplate Spectrophotometer (BioTek).

Other than cultures for protein overexpression, all bacteria were grown anaerobically, either in a vinyl glovebox (Coy Laboratory Products) under an atmosphere of 95% N_2 and 5% H_2

or an MBraun glovebox (described above). For measuring optical densities of bacteria grown on 96-well plates, plates were brought into an anaerobic glovebox and the absorbance of each well was monitored at 600 nm using a PowerWave HT Microplate Spectrophotometer (BioTek). Absorbance values were corrected for a path length of 1 cm. A Genesys^{TM} 20 Visible spectrophotometer was used for measuring optical densities of bacteria grown in Hungate tubes (16×125 mm, Chemglass Life Sciences).

Samples were made anaerobic as follows. Solids were brought into anaerobic chambers (MBraun and Coy Laboratory) in perforated 1.5 mL microcentrifuge tubes. CutC protein solutions were made anaerobic by flushing the headspace of the solution with argon for 30 min. Buffers and other solutions were made anaerobic by bubbling argon through the liquid for 30 min. Media solutions of 200 to 500 mL in volume were first autoclaved and then sparged with argon for 30 min.

Proton nuclear magnetic resonance (^{1}H NMR) spectra and carbon nuclear magnetic resonance (^{13}C NMR) spectra were recorded in the Magnetic Resonance Laboratory in the Harvard University Department of Chemistry and Chemical Biology on a Varian Inova-500 (500 MHz, 125 MHz) or Varian Mercury-400 (400 MHz, 100 MHz) NMR spectrometer. Chemical shifts are reported in parts per million downfield from tetramethylsilane using the solvent resonance as an internal standard for ^{1}H (CD_3OD, δ_H = 3.31, 4.87 ppm or D_2O, δ_H = 4.79 ppm) and ^{13}C (CD_3OD, δ_C = 49.00 ppm). Data are reported as follows: chemical shift, integration multiplicity (s = singlet, d = doublet, t = triplet, m = multiplet), coupling constant, integration, and assignment. NMR spectra were visualized using MestReNova Version 11.0.2-18153 (Mestrelab Research).

High-resolution mass spectral (HRMS) data for the synthetic compounds were obtained in the Magnetic Resonance Laboratory in the Harvard University Department of Chemistry and Chemical Biology on a Bruker Micro QTOF-QII fitted with a dual-spray electrospray ionization (ESI) source. The capillary voltage was set to 4.5 kV and the end plate offset to -500 V, the drying gas temperature was maintained at 190 °C with a flow rate of 8 L/min and a nebulizer pressure of 21.8 psi. The liquid chromatography (LC) was performed using an Agilent Technologies 1100 series LC with 50% H_2O and 50% acetonitrile as solvent.

2.4.2. LC-MS/MS assay for determining choline TMA-lyase activity in *E. coli* MS 200-1

A frozen stock of *E. coli* MS 200-1 was streaked out onto a BHI agar plate inside an anaerobic chamber (Coy Laboratory) and incubated at 37 °C overnight. A single colony was inoculated into 5 mL of BHI supplemented with 1 mM choline chloride (to induce expression of the *cut* genes) and grown anaerobically at 37 °C. The starter culture was inoculated (2%) into fresh BHI containing 1 mM of choline chloride-(trimethyl-d_9). The bacterial culture was distributed among the wells of a 96-well plate (Corning). Inhibitors were dissolved in 50 mM potassium phosphate buffer, pH 7.4, and aliquoted to the wells so that the final volume of each well was 200 µL. Plates were covered with aluminum seals (VWR) and incubated at 37 °C for 3.5 hours inside an anaerobic chamber (Coy Laboratory). An aliquot of each culture was diluted (up to 3750-fold) in a mixture composed of 95% acetonitrile and 5% of 100 mM ammonium formate buffer (final formic acid concentration of 0.02%) and analyzed by LC-MS/MS for d_9-TMA and d_9-choline.

Concentrations of d_9-TMA and d_9-choline in each sample were determined by comparing the peak integrations to that of a standard curve of d_9-TMA and d_9-choline (0.1 to 2.0 mM). The

calculated [d_9-TMA] values were plotted against the logarithm of inhibitor concentration in each sample and fit to a nonlinear regression model in Graphpad Prism to obtain EC_{50} values.

2.4.3. Overexpression and purification of CutC and CutD

Plasmids containing the wild-type *D. desulfuricans* G20 *cutC* gene with an 18- or 52-residue, N-terminal truncation of the resulting protein sequence were constructed previously.[19,20] The N-terminal truncations remove a putative microcompartment localization sequence. Both truncation constructs incorporate an N-terminal hexahistidine tag and thrombin cleavage site. Truncated constructs were found to have similar activity to wild-type protein, but the truncated variants are more soluble and less prone to aggregation.[19,20]

CutC was purified in 50 mM potassium phosphate, pH 8.0, 50 mM KCl, and 10% glycerol according to the protocol previously described,[19,20] but was not concentrated after dialysis since the process of concentration contributed to aggregation. The 18-residue truncated construct was used for crystallization. The 52-residue construct was rendered anoxic by sparging with argon prior to its use in EPR and kinetics assays. A NanoDrop 2000 UV-Vis Spectrophotometer (Thermo Scientific) was used to measure the absorbance at 280 nm of CutC variants (ε = 128 870 $M^{-1}cm^{-1}$). The extinction coefficients were obtained using the ExPASy protparam tool (http://www.expasy.org/tools/protparam.html).

CutD was also purified as previously described except for two modifications to the protocol. Upon induction with 500 μM IPTG (Teknova), cells expressing CutD were brought inside the MBraun anaerobic chamber and incubated at 15 °C for 16 to 18 hours without shaking. As previously described, cells were subsequently harvested by centrifugation, brought inside a Coy anaerobic chamber (containing an atmosphere of 98% N_2/2% H_2 and kept at 4 °C), and re-

suspended in 45-50 mL of anoxic lysis buffer. However, instead of removing the re-suspension from the anaerobic chamber and lysing cells with a cell disruptor, the cells were disrupted using a sonicator inside the oxygen-free Coy chamber. Purification with Ni-NTA resin, reconstitution of iron-sulfur clusters, and dialysis were performed as previously described.[19,20] CutD was used for *in vitro* EPR and kinetics assays. The concentration of CutD was determined according to the method of Bradford,[28] using bovine serum albumin (New England Biolabs) as a standard and dye reagent concentrate from BioRad. All proteins were judged to be of high purity by denaturing polyacrylamide gel electrophoresis.

2.4.4. Glycyl radical quantification by EPR spectroscopy

CutC-52aa was prepared for EPR spectroscopy as follows. Assays were set up in an anaerobic chamber (MBraun) kept at 20 °C in 1.5 mL polypropylene Eppendorf tubes. All assay concentrations are final concentrations. CutD (40 μM) and sodium dithionite (150 μM) were incubated together in buffer (50 mM potassium phosphate, pH 8.0, 50 mM KCl) for 20 min. CutC was rendered anoxic by sparging the headspace of the solution with argon for 30 min. Anoxic CutC (20 μM total monomer concentration) and SAM (200 μM) were added to the activating enzyme mixture and incubated for 1 h. The entire volume of 220 μL for each sample was used for analysis. EPR assays were performed in triplicate.

Perpendicular mode X-band EPR spectra were recorded on a Bruker ElexSysE500 EPR instrument fitted with a quartz dewar (Wilmad Lab-Glass) for measurements at 77 K. All samples were loaded into EPR tubes with 4 mm outer diameter and 8” length (Wilmad Lab-Glass, 734-LPV-7), sealed, and frozen in liquid N_2. Data acquisition was performed with Xepr software (Bruker). The magnetic field was calibrated with a standard sample of α,γ-

bisdiphenylene-β-phenylallyl (BDPA), g = 2.0026 (Bruker). The experimental spectra for the glycyl radical were modeled with EasySpin (Version 5.0.22)[29] or Matlab (MathWorks) to obtain g values, hyperfine coupling constants, and line widths. Spin concentration measurements were performed by numerically calculating the double integral of the simulated spectra and comparing the area with that of a $K_2(SO_3)_2NO$ standard. This standard was freshly prepared before each set of EPR measurements by dissolving solid $K_2(SO_3)_2NO$ under anaerobic conditions in anoxic 0.5 M $KHCO_3$ and diluting to a final concentration of 0.3–0.5 mM. To account for any decomposition during dissolution, the concentration was measured at 248 nm (ε = 1690 $M^{-1}cm^{-1}$) using a NanoDrop 2000 UV-Vis Spectrophotometer. For glycyl radical-containing samples and the $K_2(SO_3)_2NO$ standard, EPR spectra represent the average of 3 scans and were recorded under the following conditions: temperature, 77 K; center field, 3370 Gauss; sweep width, 200 Gauss; microwave power, 20 μW; microwave frequency, 9.45 MHz; modulation amplitude, 0.4 mT; modulation frequency, 100 kHz; time constant, 20.48 ms; conversion time, 20.48 ms; scan time, 20.97 s; receiver gain, 60 dB (for enzymatic assays) or 30 dB (for standards). Normalization for the difference in receiver gain was performed by the spectrometer. EPR experiments showed that CutD activated 18 ± 1% of CutC monomers, consistent with the results of previous studies.[19]

2.4.5. *In vitro* assay for measuring CutC activity in the presence of inhibitors

The activity of CutC was coupled to the reduction of acetaldehyde by NADH-dependent yeast alcohol dehydrogenase (YADH). Assays were conducted in a buffer of 50 mM potassium phosphate, pH 8.0, 50 mM KCl and were set up in an anaerobic chamber (MBraun) kept at 20 °C in 1.5 mL polypropylene Eppendorf tubes. CutD (40 μM) and sodium dithionite (150 μM) were incubated for 20 min prior to the addition of 200 μM of *S*-(5'-adenosyl)-L-methionine (SAM,

purchased from Sigma-Aldrich as a *p*-toluenesulfonate salt) and 20 μM of CutC monomer in a total reaction mixture of 50 μL. Glycyl radical formation was carried out for 1 hour, after which the activated CutC mixture was immediately diluted 20-fold into phosphate buffer. An aliquot of the diluted mixture was added to a master mix containing NADH (200 μM) and YADH (0.4 μM) such that the final concentration of CutC monomer was 5 nM (after addition of inhibitor/buffer and choline). The master mix was distributed to the wells of a 96-well plate (180 μL per well), to which was added either inhibitor or buffer (10 μL per well), followed by choline (10 μL per well). The final concentration of choline was 200 μM (~K_M value).

Following the addition of choline, the absorbance of NADH at 340 nm was immediately recorded, with measurements taken every 20 s for 10 min. Initial rates were calculated from absorbance measurements that decreased linearly. Path lengths were corrected to 1 cm and absorbance values were converted to concentrations assuming ε_{340} = 6,220 $M^{-1}cm^{-1}$ for NADH. The rate from assays containing no substrate was subtracted from assays containing substrate to account for background activity. Assays were performed in triplicate. All of the data were fit to the Michaelis–Menten equation simultaneously using nonlinear regression in Graphpad Prism. Initial rates at each inhibitor concentration were normalized to control samples without inhibitor. Normalized activity values were plotted against the logarithm of inhibitor concentration and fit to a nonlinear regression model in Graphpad Prism to obtain IC_{50} values.

2.4.6. Crystallization and structure determination of CutC bound to betaine aldehyde

Crystallization conditions for CutC with an 18-amino acid N-terminal truncation and His_6-tag were previously identified.[20] Crystals of CutC-18aa were obtained in 16-19% PEG 8000, 0.2-0.4 M LiCl, and 0.1 M Tris pH 8.0 by hanging drop vapor diffusion at 21 °C. CutC

protein in 50 mM potassium phosphate, pH 8.0, 50 mM KCl, and 10% (v/v) glycerol was pre-incubated at 80 μM with 10 mM betaine aldehyde. Protein and precipitant were mixed in a 1:1 ratio and incubated for 3-5 days. Crystals were cryoprotected in a stabilization solution containing 20% (v/v) glycerol, 25% (w/v) PEG 8000, 0.5 M lithium chloride, and 0.1 M Tris pH 8.0 and subsequently supplemented with 50 mM betaine aldehyde. Crystals were flash-frozen by plunging in liquid nitrogen.

Diffraction images were collected at the Advanced Photon Source beamline 24ID-C at a wavelength of 0.9795 Å on a Pilatus 6M detector (Dectris). The diffraction patterns were indexed, integrated, and scaled in HKL20002.[30] Crystals diffracted to 2.20-Å resolution in space group $P2_1$ with cell edges a = 105.2 Å, b = 234.7 Å, c = 159.0 Å, β = 109.0°. The structure was solved by molecular replacement in the Phenix implementation of Phaser[31] using the wild type monomer (PDB ID 5FAU[20]) with all ligands removed as the search model. The asymmetric unit contains two tetrameric assemblies resembling that observed in the wild-type CutC structure.[20] Refinement was performed in phenix.refine[32] with manual rebuilding in Coot.[33]

The final model contains residues 51-846 (chains D and H), 52-846 (chains A, C, E, and G) or residues 53-846 (chains B and F) according to the native protein numbering. Apart from residues 18-51, there are no missing residues within the protein or at the C terminus. Non-crystallographic symmetry constraints were used early in refinement but were removed as structure approached convergence. Water molecules were placed automatically by phenix.refine and were edited manually in Coot. The final model contains all residues found in the wild-type structure. Betaine aldehyde covalently attached to cysteine as the thiohemiacetal was modeled into difference density generated after removal of Cys493. Parameter files were made in Phenix eLBOW.[32] The *S* configuration is favored based on the expected binding mode prior to

nucleophilic attack; however, the stereochemistry cannot be unambiguously assigned by the electron density alone. The position of the betaine aldehyde adduct was verified with composite omit maps generated by Phenix.

Table 2.1. Data collection statistics for CutC-18aa bound to betaine aldehyde

	Wild type CutC, betaine aldehyde
Space Group	$P2_1$
Cell Dimensions	a = 105.2 Å, b = 234.7 Å, c = 159.0 Å, β = 109.0°
Resolution (Å)[a,b]	50-2.35 (2.39-2.35)
Completeness (%)[b]	99.7 (99.7)
$\langle I/\sigma I \rangle$[b]	10.4 (2.1)
R_{sym}[b,c]	0.12 (1.0)
R_{pim}[c]	0.05 (0.42)
Unique reflections	293583
Redundancy[b]	6.8 (6.5)
CC1/2	0.79

[a] Data were trimmed based on CC1/2 value rather than R_{sym} or $\langle I/\sigma I \rangle$. Inclusion of highest resolution data improved the quality of the electron density maps.
[b] Values in parenthesis are for the highest resolution shell.
[c] R_{pim} is reported due to the high redundancy of these datasets.

Table 2.2. Model refinement statistics for CutC-18aa bound to betaine aldehyde

	Wild type CutC, betaine aldehyde
PDB accession code	6ND3
Resolution (Å)[a]	50-2.35 (2.37-2.35)
Reflections	
R_{work}, R_{free}	0.19, 0.22
R_{free} set size	8879
No. molecules in asymmetric unit	8
No. of atoms	
Protein	50248
Betaine aldehyde adduct	56
Water molecules	1813
RMSD[b] Bond length (Å)	0.002
RMSD Bond angle (°)	0.544
Coordinate error (Å)	0.27
Rotamer outliers (%)	0.86
Ramachandran plot (%)	
Most favored	97.06
Additionally allowed	2.78
Disfavored	0.16
Average B factors (Å^2)	
Monomer A	46.4
Monomer B	63.9
Monomer C	47.8
Monomer D	50.6
Monomer E	51.4
Monomer F	77.6
Monomer G	56.2
Monomer H	57.1
Betaine aldehyde adduct	44.7
Water	48.0

[a] Values in parenthesis are for the highest resolution shell.
[b] RMSD, root-mean-square deviation

Table 2.3. Changes in CH–O bond lengths between choline and betaine aldehyde bound CutC.

atom 1[a]	atom 2	Choline avg	Choline stdev	Betaine aldehyde avg	Betaine aldehyde stdev
Y508	Me1[b]	3.56[c]	0.05	3.38	0.07
D216	Me3	3.52	0.05	3.42	0.08
HOH1	Me1	3.34	0.07	3.55	0.11
D216	Me1	3.30	0.09	3.88	0.08
Y208	Me2	3.30	0.05	3.48	0.11

[a]Atom 1 and atom 2 are the start and end points for distance determination.
[b]Me1, Me2, and Me3 are shown in Fig. 2.3A.
[c]Distances were calculated with a script in PyMOL and averaged over 4 (choline) or 8 (betaine aldehyde) non-crystallographic protomers.

2.4.7. *In vitro* assay for measuring CutC activity upon preincubation with betaine aldehyde

The activity of CutC was coupled to the reduction of acetaldehyde by NADH-dependent yeast alcohol dehydrogenase (YADH). Assays were conducted in a buffer of 50 mM potassium phosphate, pH 8.0, 50 mM KCl and were set up in an anaerobic chamber (MBraun) kept at 20 °C in 1.5 mL polypropylene Eppendorf tubes. CutD (40 μM) and sodium dithionite (150 μM) were incubated for 20 min prior to the addition of 200 μM of SAM and 20 μM of CutC monomer in a total reaction mixture of 50 μL. Glycyl radical formation was carried out for 1 h, after which the activated CutC mixture was immediately diluted 20-fold into phosphate buffer and incubated with various concentrations of betaine aldehyde (0.01 μM to 1 mM) for 0, 15, and 30 min. A mixture containing NADH (200 μM) and YADH (0.4 μM) was distributed to the wells of a 96-well plate (179 μL per well), to which was added choline (10 μL per well) and, lastly, the preincubated CutC-inhibitor solution (11 μL per well). The final concentration of choline in each well was 200 μM (~K_M value) and that of CutC was 5 nM.

Following the addition of choline, the absorbance of NADH at 340 nm was immediately recorded, with measurements taken every 20 s for 10 min. Initial rates were calculated from absorbance measurements that decreased linearly. Path lengths were corrected to 1 cm and absorbance values were converted to concentrations assuming ε_{340} = 6,220 $M^{-1}cm^{-1}$ for NADH. The rate from assays containing no substrate was subtracted from assays containing substrate to account for background activity. Assays were performed in triplicate. All of the data were fit to the Michaelis–Menten equation simultaneously using nonlinear regression in Graphpad Prism. Initial rates at each inhibitor concentration were normalized to control samples without inhibitor. Normalized activity values were plotted against the logarithm of inhibitor concentration and fit to a nonlinear regression model in Graphpad Prism to obtain IC_{50} values.

2.4.8. Growth studies of *E. coli* strains in minimal and rich media

A frozen stock of *E. coli* MS 200-1 was streaked out onto a BHI agar plate inside an anaerobic chamber (Coy Laboratory) and incubated at 37 °C overnight. A single colony was inoculated into 5 mL of BHI supplemented with 1 mM choline chloride, which was grown anaerobically at 37 °C. The starter culture was inoculated (2%) into fresh BHI containing 1 mM of choline chloride. Aliquots of the culture were transferred to a 96-well plate (Corning). Inhibitors, dissolved in 50 mM potassium phosphate buffer, pH 7.4, or phosphate buffer alone were added to the samples so that the final volume in each well was 200 µL. Plates were incubated at 37 °C for 16-24 hours either in an Mbraun glove box or a Coy vinyl glovebox and OD_{600} values were measured using a BioTek spectrophotometer.

A minimal medium for *E. coli* MS 69-1 was developed based on the “no carbon E” medium utilized for ethanolamine-dependent growth of *Salmonella enterica*.[24,34] The optimized

media for *E. coli* MS 69-1 contained 29 mM potassium phosphate monobasic, 29 mM potassium phosphate dibasic, 17 mM ammonium sodium phosphate dibasic, 40 mM sodium fumarate dibasic, 0.4% (wt/v) casamino acids (Becton Dickinson), and either 30 mM choline chloride or 30 mM glycerol. This mixture was supplemented with 1 mM magnesium sulfate, 1% ATCC vitamin supplement, and 1% ATCC trace mineral supplement.

A frozen stock of *E. coli* MS 69-1 was streaked out onto a BHI agar plate inside an anaerobic chamber (Coy Laboratory) and incubated at 37 °C overnight. A single colony was inoculated into 5 mL of BHI supplemented with 1 mM choline chloride (to induce expression of the *cut* genes), which was grown anaerobically at 37 °C. Minimal media were inoculated with 1% of the saturated *E. coli* MS 69-1 starter culture. Aliquots of the minimal media culture were transferred to a 96-well plate (Corning). Inhibitors, dissolved in 50 mM potassium phosphate buffer, pH 7.4, or phosphate buffer alone were added to the samples so that the final volume in each well was 200 μL. Plates were incubated at 37 °C for 16-24 hours either in an Mbraun glove box or a Coy vinyl glovebox under a nitrogen atmosphere and OD_{600} values were measured using a BioTek spectrophotometer.

2.4.9. LC-MS/MS assay for monitoring the stability of betaine aldehyde in *E. coli* strains

To monitor the stability of betaine aldehyde in *E. coli* MS 200-1 growing in a rich medium, a frozen stock of this strain was streaked out onto a BHI agar plate inside an anaerobic chamber (Coy Laboratory) and incubated at 37 °C overnight. A single colony was inoculated into 5 mL of BHI supplemented with 1 mM choline chloride, which was grown anaerobically at 37 °C. The starter culture was inoculated (2%) into fresh BHI and the diluted bacterial culture was distributed among the wells of a 96-well plate (190 μL per well). Either 5 μL of 50 mM

potassium phosphate buffer, pH 7.4, or 5 µL of synthesized d_9-betaine aldehyde (final concentration = 1 mM) in phosphate buffer were added to each well. Finally, 5 µL of H_2O or choline chloride-(trimethyl-d_9) (final concentration = 1 mM) dissolved in H_2O were added to each well. Plates were covered with aluminum seals (VWR) and incubated at 37 °C for 0, 3.5, and 24 hours inside an anaerobic chamber (Coy Laboratory).

An aliquot of each well was diluted (up to 3750-fold) in a mixture composed of 95% acetonitrile and 5% of 100 mM ammonium formate buffer (final formic acid concentration of 0.02%) and analyzed by LC-MS/MS for d_9-TMA, d_9-choline, and d_9-betaine aldehyde. Concentrations of these compounds in each sample were determined by comparing the peak integrations to that of a standard curve of d_9-TMA, d_9-choline, and d_9-betaine aldehyde (1 to 10 mM).

For monitoring the stability of betaine aldehyde in *E. coli* MS 69-1 in minimal media, a frozen stock of this strain was streaked out onto a BHI agar plate inside an anaerobic chamber (Coy Laboratory) and incubated at 37 °C overnight. A single colony was inoculated into 5 mL of BHI supplemented with 1 mM choline chloride, which was grown anaerobically at 37 °C. The starter culture was inoculated (1%) into minimal medium containing no choline or glycerol. This bacterial culture was distributed among the wells of a 96-well plate (190 µL per well). Either 5 µL of 50 mM potassium phosphate buffer, pH 7.4, or 5 µL of synthesized d_9-betaine aldehyde (final concentration = 10 mM) in phosphate buffer were added to each well. Dr. Maud Bollenbach performed the chemical synthesis of d_9-betaine aldehyde, which is described in Section 2.4.15. Finally, 5 µL of H_2O or choline chloride-(trimethyl-d_9) (final concentration = 15 mM) dissolved in H_2O were added to each well. Plates were covered with aluminum seals

(VWR) and incubated at 37 °C for 0, 3.5, 7, 20, and 24 hours inside an anaerobic chamber (Coy Laboratory).

An aliquot of each well was diluted (up to 3750-fold) in a mixture composed of 95% acetonitrile and 5% of 100 mM ammonium formate buffer (final formic acid concentration of 0.02%) and analyzed by LC-MS/MS for d_9-TMA, d_9-choline, and d_9-betaine aldehyde. Concentrations of these compounds in each sample were determined by comparing the peak integrations to that of a standard curve of d_9-TMA, d_9-choline, and/or d_9-betaine aldehyde (2 to 30 mM).

2.4.10. Determining choline TMA-lyase activity in cut gene cluster-harboring bacteria

Frozen stocks of *Escherichia coli* MS 69-1, *Proteus mirabilis* BB2000, and *Klebsiella* sp. MS 93-2 were streaked out onto BHI agar plates inside an anaerobic chamber (Coy Laboratory) and incubated at 37 °C overnight. A single colony of each strain was inoculated into 5 mL of BHI supplemented with 1 mM choline chloride (to induce expression of the *cut* genes), which was grown anaerobically at 37 °C. The same conditions were used for culturing *Clostridium sporogenes* ATCC 15579 except, instead of BHI, an RCM agar plate and RCM liquid broth were used. For each strain, BHI (or RCM) containing 1 mM of choline chloride-(trimethyl- d_9) was inoculated with 2% of the saturated bacterial starter culture. Cultures were distributed among the wells of a 96-well plate (Corning) and betaine aldehyde, dissolved in 50 mM potassium phosphate buffer, pH 7.4, was added to the samples in the wells. The final volume of each well was 200 μL. Plates were covered with aluminum seals (VWR) and incubated at 37 °C inside a vinyl anaerobic chamber (Coy Laboratory) for 4 hours (except for *C. sporogenes* ATCC 15579, which was incubated for 8 hours). An aliquot of each culture was diluted (up to 3750-fold) in a

mixture composed of 95% acetonitrile and 5% of 100 mM ammonium formate buffer (with a final formic acid concentration of 0.02%) and analyzed by LC-MS/MS for d_9-TMA and d_9-choline.

Concentrations of d_9-TMA and d_9-choline in each sample were determined by comparing the peak integrations to that of a standard curve of d_9-TMA and d_9-choline (0.5 to 100 μM). The calculated [d_9-TMA] values were plotted against the logarithm of betaine aldehyde concentration in each sample and fit to a nonlinear regression model in Graphpad Prism to obtain EC_{50} values.

2.4.11. Determining choline TMA-lyase activity in a fecal suspension *ex vivo*

A frozen fecal sample from a healthy individual was diluted 1:10 (wt/v) in sterile anaerobic PBS containing 1 mM of choline chloride-(trimethyl-d_9). This sample was collected by Peter Turnbaugh under the guidance of the Harvard Committee on the Use of Human Subjects in Research, protocol F18510. The dilution was vortexed for 1 min and allowed to settle for 15 min at room temperature inside an anaerobic chamber (Coy Laboratory). A 95 μL aliquot of the resulting supernatant was transferred to a 96-well plate containing 5 μL of different concentrations of betaine aldehyde (10 μM–31 mM), and the mixtures were incubated for 16 hours at 37 °C. An aliquot of each culture was diluted 2500-fold in a mixture composed of 95% acetonitrile and 5% of 100 mM ammonium formate buffer (with a final formic acid concentration of 0.02%) and analyzed by LC-MS/MS for d_9-TMA and d_9-choline.

Concentrations of d_9-TMA and d_9-choline in each sample were determined by comparing the peak integrations to that of a standard curve of d_9-TMA and d_9-choline (0.1 to 2.0 mM). The calculated [d_9-TMA] values were plotted against the logarithm of betaine aldehyde concentration in each sample and fit to a nonlinear regression model in Graphpad Prism to obtain EC_{50} values.

2.4.12. Endpoint assay for measuring CutC activity *in vitro*

Assays were conducted in a buffer of 50 mM potassium phosphate, pH 8.0, 50 mM KCl and were set up in an anaerobic chamber (MBraun) kept at 20 °C in 1.5 mL polypropylene Eppendorf tubes. CutD (40 μM) and sodium dithionite (150 μM) were incubated for 20 min prior to the addition of 200 μM of *S*-(5'-adenosyl)-L-methionine (SAM) and 20 μM of CutC monomer in a total reaction mixture of 50 μL. Glycyl radical formation was carried out for 1 h, after which the activated CutC mixture was immediately diluted 20-fold into phosphate buffer. Glycyl radical formation was carried out for 1 h, after which the activated CutC mixture was immediately diluted 20-fold into phosphate buffer. An aliquot of the diluted mixture was added to a master mix containing NADH (200 μM) and YADH (0.4 μM) such that the final concentration of CutC monomer was 5 nM (after addition of aldehyde/buffer and choline). The master mix was distributed to the wells of a 96-well plate (180 μL per well), to which was added buffer or various aldehydes at 0.1 mM (10 μL per well). The mixture was incubated for 30 minutes. Choline (10 μL per well) was subsequently added and the resulting mixture was incubated for another 15 minutes. The final concentration of choline was 200 μM (~K_M value).

An aliquot of each sample was diluted (up to 750-fold) in a mixture composed of 95% acetonitrile and 5% of 100 mM ammonium formate buffer (final formic acid concentration of 0.02%) and analyzed by LC-MS/MS for TMA and choline. Concentrations of TMA and choline in each sample were determined by comparing the peak integrations to that of a standard curve of TMA and choline (0.05 to 0.4 mM).

2.4.13. Determining choline TMA-lyase activity in *P. mirabilis* ATCC 29906 resting cells

Conditions for this assay were obtained from the procedure described by Wang et al.[21] This experiment attempted to replicate the previously described procedure as close as possible. A frozen stock of *Proteus mirabilis* ATCC 29906 was streaked out onto a BHI agar plate inside an anaerobic chamber (Coy Laboratory) and incubated at 37 °C overnight. A single colony was inoculated into 20 mL of nutrient broth supplemented with 1 mM choline chloride (to induce expression of the *cut* genes), which was grown anaerobically at 37 °C. The culture was centrifuged at 4,000 rpm for 20 min and brought back inside the anaerobic chamber (Coy Laboratory). Nutrient broth was discarded and the remaining bacterial pellet was dissolved in PBS containing 100 μM of choline chloride-(trimethyl-d_9) to an OD_{600} of ~1.0 The bacterial culture was distributed among the wells of a 96-well plate (Corning). Inhibitors were dissolved in PBS and aliquoted to the wells (10 μL). Choline chloride-(trimethyl-d_9) dissolved in H_2O was distributed to the wells (10 μL) so that the final concentrations of d_9-choline were 10, 20, and 100 μM and the final volume of each well was 200 μL. Plates were covered with aluminum seals (VWR) and incubated at 37 °C for 10 h inside the anaerobic chamber. An aliquot of each culture was diluted (up to 50-fold) in a mixture composed of 95% acetonitrile and 5% of 100 mM ammonium formate buffer (final formic acid concentration of 0.02%) and analyzed by LC-MS/MS for d_9-TMA and d_9-choline.

Concentrations of d_9-TMA and d_9-choline in each sample were determined by comparing the peak integrations to that of a standard curve of d_9-TMA and d_9-choline (0.02 to 140.0 μM). The calculated [d_9-TMA] values were plotted against the logarithm of inhibitor concentration in each sample and fit to a nonlinear regression model in Graphpad Prism to obtain EC_{50} values.

2.4.14. Determining choline TMA-lyase activity in *P. mirabilis* ATCC 29906 lysates

Conditions for this assay were obtained from the procedure described by Wang et al.[21] This experiment attempted to replicate the previously described procedure as close as possible. A frozen stock of *Proteus mirabilis* ATCC 29906 was streaked out onto a BHI agar plate inside an anaerobic chamber (Coy Laboratory) and incubated at 37 °C overnight. A single colony was inoculated into 20 mL of nutrient broth supplemented with 1 mM choline chloride (to induce expression of the *cut* genes), which was grown anaerobically at 37 °C overnight. The culture was diluted 1:100 into 10 L of fresh nutrient broth supplemented with 1 mM choline chloride, which was grown anaerobically at 37 °C overnight. Cells were harvested by centrifugation in 1 L centrifuge tubes (6,000 rpm x 30 min), brought inside the anaerobic chamber (Coy Laboratory) at 4 °C, and resuspended in 20 mL of anoxic lysis buffer (50 mM HEPES, 200 mM NaCl, 10 mM MgCl2, pH 8) supplemented with half of a SIGMAFAST™ protease inhibitor cocktail tablet (Sigma-Aldrich), 8 mg of chicken egg lysozyme, and 5 mM DL-dithiothreitol (DTT). Cells were lysed by sonication using the following parameters: 25% amplitude, 10 s on, 30 s off, for a total time of 12 min. The lysate was clarified by centrifugation (10,000 rpm x 30 min) and the protein content of the lysate was determined according to the method of Bradford,[28] using bovine serum albumin (New England Biolabs) as a standard and dye reagent concentrate from BioRad.

Inside the Coy anaerobic chamber, the protein lysate was distributed among the wells of a 96-well plate (Corning) such that the final amount of protein per well was 3 mg. Inhibitors were dissolved in PBS and aliquoted to the wells (10 µL). Choline chloride-(trimethyl-d_9) dissolved in H_2O was distributed to the wells (10 µL) so that the final concentration of d_9-choline was 100 µM. The wells were filled with PBS so that the final volume was 200 µL. Plates were covered with aluminum seals (VWR) and incubated at 37 °C for 10 h inside the anaerobic chamber. An

aliquot of each culture was diluted (up to 50-fold) in a mixture composed of 95% acetonitrile and 5% of 100 mM ammonium formate buffer (final formic acid concentration of 0.02%) and analyzed by LC-MS/MS for d_9-TMA and d_9-choline. Concentrations of d_9-TMA and d_9-choline in each sample were determined by comparing the peak integrations to that of a standard curve of d_9-TMA and d_9-choline (0.02 to 140.0 μM).

2.4.15. Chemical synthesis procedures and characterization data

Synthesis of 2,2-dihydroxy-*N,N,N*-tri(methyl-d_3)ethan-1-aminium chloride (d_9-betaine aldehyde)

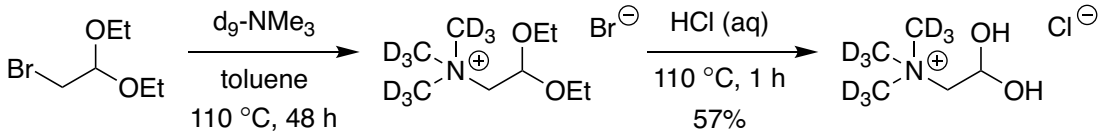

D_9-betaine aldehyde was synthesized by Dr. Maud Bollenbach. The compound was synthesized as the diol according to the previously described procedure[19] with slight modifications. In a high-pressure resistant screw-cap flask, bromoacetaldehyde diethyl acetal (1.0 equiv) was dissolved in anhydrous toluene. Trimethyl-d_9-amine (2.0 equiv) was condensed by cooling to -78°C and transferred via cannula to the acetaldehyde solution. The resulting mixture was heated at 110 °C for 24 h. After cooling to room temperature, the precipitate was collected by vacuum filtration, washed with hexanes, and dried under vacuum. The solid was dissolved in water, and 2.5 mL of concentrated aqueous HCl was subsequently added. The mixture was refluxed for 1 h at 110 °C. Upon cooling, the solvent was evaporated under vacuum and the resulting solid was triturated twice with diethyl ether to obtain the desired product as a white solid (0.522 g, 57%). ^{1}H NMR: (400 MHz, D_2O) 5.59 (t, J = 5.5 Hz, 1H, C**H**$(OH)_2$,), 3.44 (d, J = 5.5 Hz, 2H, NC**H**$_2$). ^{13}C NMR (100 MHz, D_2O): 85.0, 67.7, 53.1. HRMS (ESI) calculated for $C_5H_3D_9NO^+$ $[M]^+$: 129.1584; found: 129.1586.

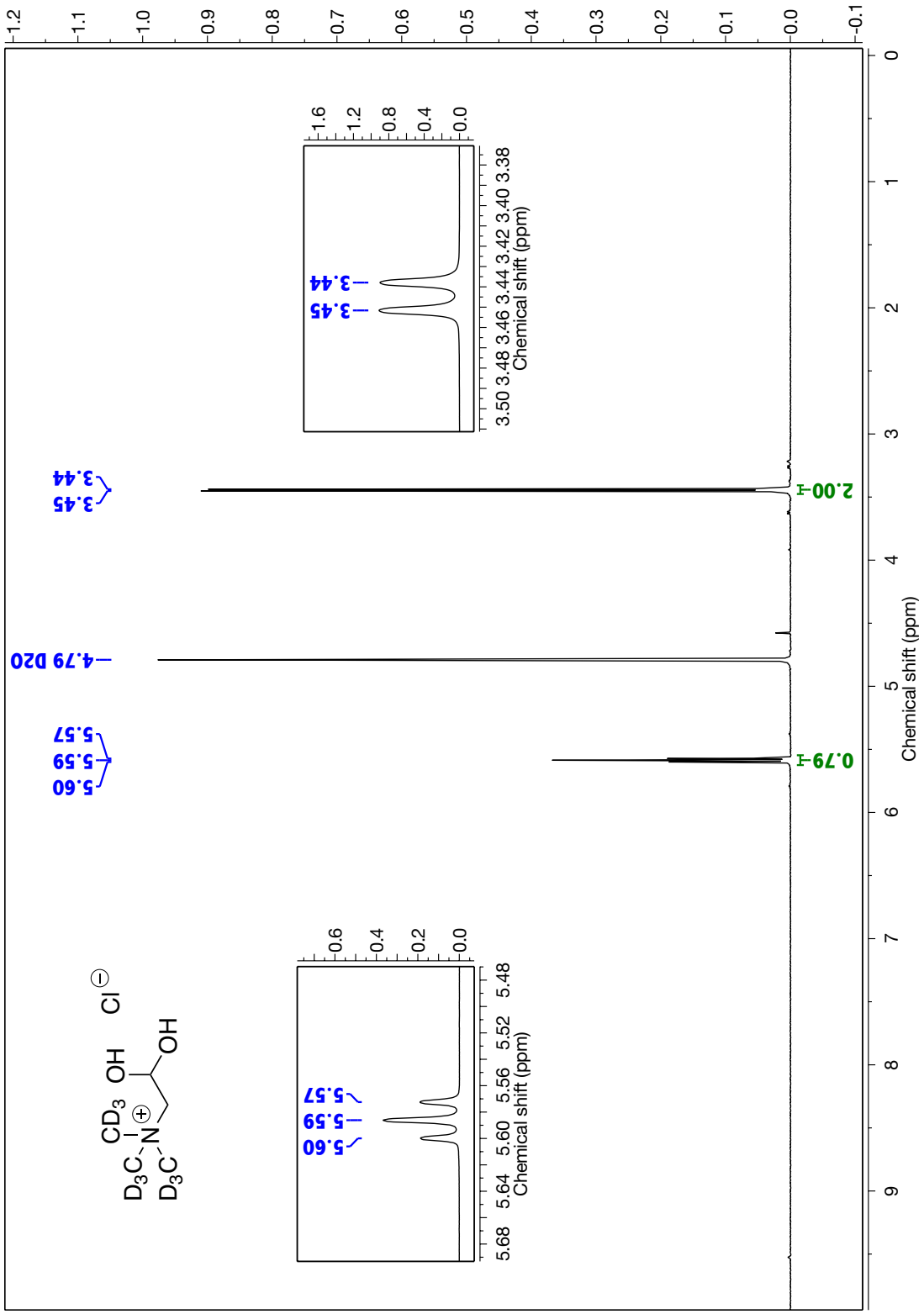

Figure 2.17. [1]H-NMR spectrum of d9-betaine aldehyde (D2O at 400 MHz).

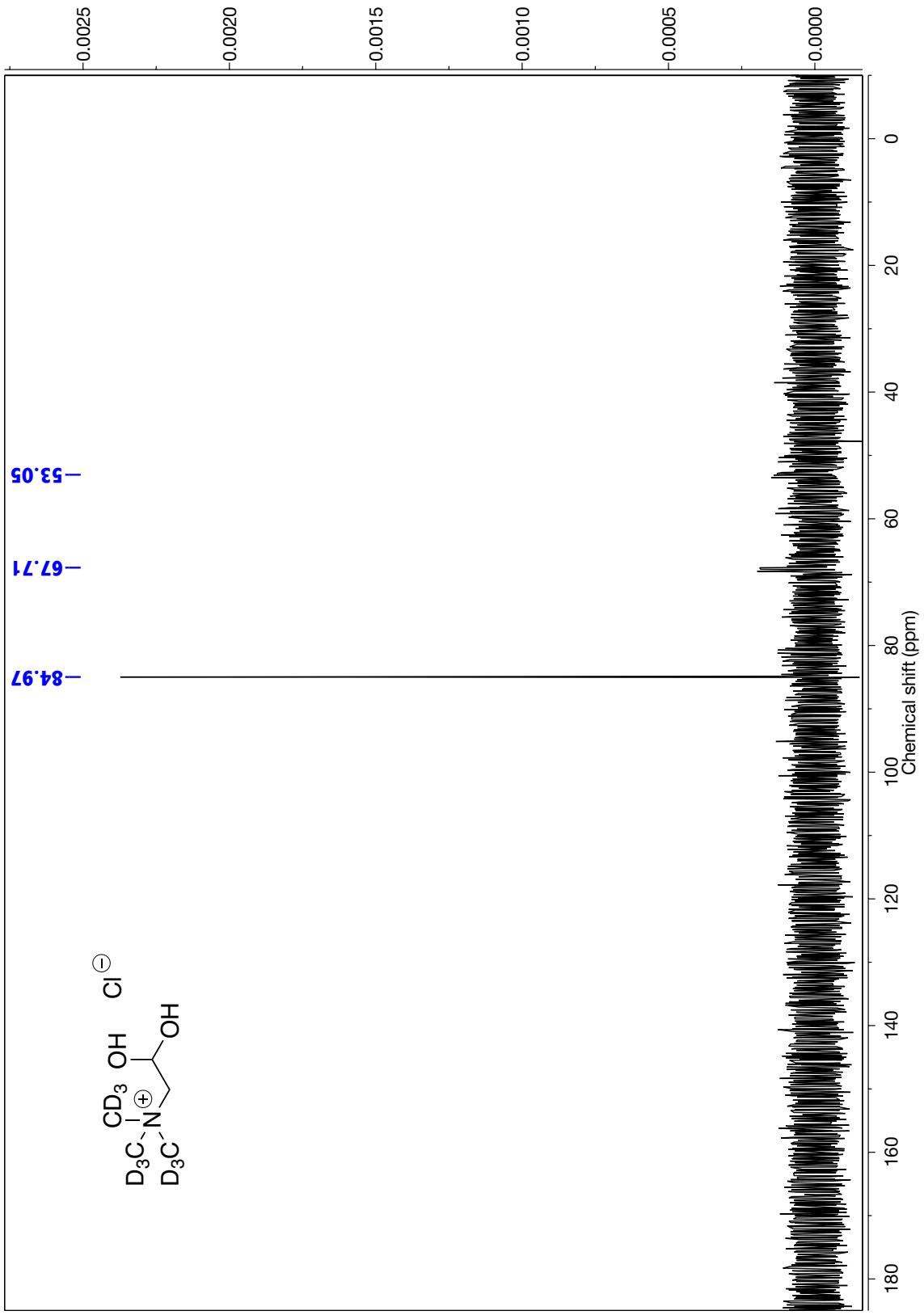

Figure 2.18. ^{13}C-NMR spectrum of d_9-betaine aldehyde (D_2O at 100 MHz).

2.5. References

(1) Sonnenburg, J. L.; Bäckhed, F. Diet–Microbiota Interactions as Moderators of Human Metabolism. *Nature* **2016**, *535* (7610), 56–64.

(2) Schroeder, B. O.; Bäckhed, F. Signals From the Gut Microbiota to Distant Organs in Physiology and Disease. *Nat. Med.* **2016**, *22* (10), 1079–1089.

(3) Koppel, N.; Balskus, E. P. Exploring and Understanding the Biochemical Diversity of the Human Microbiota. *Cell Chem. Biol.* **2016**, *23* (1), 18–30.

(4) Qin, J.; Li, R.; Raes, J.; Arumugam, M.; Burgdorf, K. S.; Manichanh, C.; Nielsen, T.; Pons, N.; Levenez, F.; Yamada, T.; Mende, D. R.; Li, J.; Xu, J.; Li, S.; Li, D.; Wang, B.; Liang, H.; Zheng, H.; Xie, Y.; Tap, J.; Lepage, P.; Bertalan, M.; Batto, J.-M.; Hansen, T.; Le Paslier, D.; Linneberg, A.; Nielsen, H. B.; Pelletier, E.; Renault, P.; Sicheritz-Ponten, T.; Turner, K.; Zhu, H.; Yu, C.; Li, S.; Jian, M.; Zhou, Y.; Li, Y.; Zhang, X.; Li, S.; Qin, N.; Yang, H.; Wang, J.; Brunak, S.; Dore, J.; Guarner, F.; Kristiansen, K.; Pedersen, O.; Parkhill, J.; Weissenbach, J.; (null), M. C.; Bork, P.; Ehrlich, S. D.; Wang, J. A Human Gut Microbial Gene Catalogue Established by Metagenomic Sequencing. *Nature* **2010**, *464* (7285), 59–65.

(5) Sharon, G.; Garg, N.; Debelius, J.; Knight, R.; Dorrestein, P. C.; Mazmanian, S. K. Specialized Metabolites From the Microbiome in Health and Disease. *Cell Metab.* **2014**, *20* (5), 719–730.

(6) Postler, T. S.; Ghosh, S. Understanding the Holobiont: How Microbial Metabolites Affect Human Health and Shape the Immune System. *Cell Metab.* **2017**, *26* (1), 110–130.

(7) Schmidt, T. S. B.; Raes, J.; Bork, P. The Human Gut Microbiome: From Association to Modulation. *Cell* **2018**, *172* (6), 1198–1215.

(8) Anthouard, R.; DiRita, V. J. Chemical Biology Applied to the Study of Bacterial Pathogens. *Infect. Immun.* **2015**, *83* (2), 456–469.

(9) Wallace, B. D.; Wang, H.; Lane, K. T.; Scott, J. E.; Orans, J.; Koo, J. S.; Venkatesh, M.; Jobin, C.; Yeh, L.-A.; Mani, S.; Redinbo, M. R. Alleviating Cancer Drug Toxicity by Inhibiting a Bacterial Enzyme. *Science* **2010**, *330* (6005), 831–835.

(10) Zeisel, S. H.; Warrier, M. Trimethylamine *N*-Oxide, the Microbiome, and Heart and Kidney Disease. *Annu. Rev. Nutr.* **2017**, *37* (1), 135–136.

(11) Krueger, S. K.; Williams, D. E. Mammalian Flavin-Containing Monooxygenases: Structure/Function, Genetic Polymorphisms and Role in Drug Metabolism. *Pharmacol. Ther.* **2005**, *106* (3), 357–387.

(12) Bennett, B. J.; de Aguiar Vallim, T. Q.; Wang, Z.; Shih, D. M.; Meng, Y.; Gregory, J.; Allayee, H.; Lee, R.; Graham, M.; Crooke, R.; Edwards, P. A.; Hazen, S. L.; Lusis, A. J. Trimethylamine-*N*-Oxide, a Metabolite Associated with Atherosclerosis, Exhibits Complex Genetic and Dietary Regulation. *Cell Metab.* **2013**, *17* (1), 49–60.

(13) Dumas, M. E.; Barton, R. H.; Toye, A.; Cloarec, O.; Blancher, C.; Rothwell, A.; Fearnside, J.; Tatoud, R.; Blanc, V.; Lindon, J. C.; Mitchell, S. C.; Holmes, E.; McCarthy, M. I.; Scott, J.; Gauguier, D.; Nicholson, J. K. Metabolic Profiling Reveals a Contribution of Gut Microbiota to Fatty Liver Phenotype in Insulin-Resistant Mice. *Proc. Natl. Acad. Sci. U.S.A.* **2006**, *103* (33), 12511–12516.

(14) Spencer, M. D.; Hamp, T. J.; Reid, R. W.; Fischer, L. M.; Zeisel, S. H.; Fodor, A. A. Association Between Composition of the Human Gastrointestinal Microbiome and Development of Fatty Liver with Choline Deficiency. *Gastroenterology* **2011**, *140* (3), 976–986.

(15) Wang, Z.; Klipfell, E.; Bennett, B. J.; Koeth, R.; Levison, B. S.; DuGar, B.; Feldstein, A. E.; Britt, E. B.; Fu, X.; Chung, Y.-M.; Wu, Y.; Schauer, P.; Smith, J. D.; Allayee, H.; Tang, W. H. W.; DiDonato, J. A.; Lusis, A. J.; Hazen, S. L. Gut Flora Metabolism of Phosphatidylcholine Promotes Cardiovascular Disease. *Nature* **2011**, *472* (7341), 57–63.

(16) Koeth, R. A.; Wang, Z.; Levison, B. S.; Buffa, J. A.; Org, E.; Sheehy, B. T.; Britt, E. B.; Fu, X.; Wu, Y.; Li, L.; Smith, J. D.; DiDonato, J. A.; Chen, J.; Li, H.; Wu, G. D.; Lewis, J. D.; Warrier, M.; Brown, J. M.; Krauss, R. M.; Tang, W. H. W.; Bushman, F. D.; Lusis, A. J.; Hazen, S. L. Intestinal Microbiota Metabolism of L-Carnitine, a Nutrient in Red Meat, Promotes Atherosclerosis. *Nat. Med.* **2013**, *19* (5), 576–585.

(17) Tang, W. H. W.; Wang, Z.; Levison, B. S.; Koeth, R. A.; Britt, E. B.; Fu, X.; Wu, Y.; Hazen, S. L. Intestinal Microbial Metabolism of Phosphatidylcholine and Cardiovascular Risk. *N. Engl. J. Med.* **2013**, *368* (17), 1575–1584.

(18) Gregory, J. C.; Buffa, J. A.; Org, E.; Wang, Z.; Levison, B. S.; Zhu, W.; Wagner, M. A.; Bennett, B. J.; Li, L.; DiDonato, J. A.; Lusis, A. J.; Hazen, S. L. Transmission of Atherosclerosis Susceptibility with Gut Microbial Transplantation. *J. Biol. Chem.* **2015**, *290* (9), 5647–5660.

(19) Tang, W. H. W.; Wang, Z.; Kennedy, D. J.; Wu, Y.; Buffa, J. A.; Agatisa-Boyle, B.; Li, X. S.; Levison, B. S.; Hazen, S. L. Gut Microbiota-Dependent Trimethylamine *N*-Oxide (TMAO) Pathway Contributes to Both Development of Renal Insufficiency and Mortality Risk in Chronic Kidney Disease. *Circ. Res.* **2015**, *116*, 448–455.

(20) Missailidis, C.; Hällqvist, J.; Qureshi, A. R.; Barany, P.; Heimbürger, O.; Lindholm, B.; Stenvinkel, P.; Bergman, P. Serum Trimethylamine-*N*-Oxide Is Strongly Related to Renal Function and Predicts Outcome in Chronic Kidney Disease. *PLoS One* **2016**, *11* (1), e0141738.

(21) Miao, J.; Ling, A. V.; Manthena, P. V.; Gearing, M. E.; Graham, M. J.; Crooke, R. M.; Croce, K. J.; Esquejo, R. M.; Clish, C. B.; Vicent, D.; Biddinger, S. B. Flavin-Containing Monooxygenase 3 as a Potential Player in Diabetes-Associated Atherosclerosis. *Nat. Commun.* **2014**, 1–10.

(22) Mitchell, S. C.; Smith, R. L. Trimethylaminuria: the Fish Malodor Syndrome. *Drug Metab. Dispos.* **2001**, *29* (4), 517–521.

(23) Dolphin, C. T.; Janmohamed, A.; Smith, R. L.; Shephard, E. A.; Phillips, I. R. Missense Mutation in Flavin-Containing Mono-Oxygenase 3 Gene, *Fmo3*, Underlies Fish-Odour Syndrome. *Nat. Genet.* **1997**, *17* (4), 491–494.

(24) Christodoulou, J. Trimethylaminuria: an Under-Recognised and Socially Debilitating Metabolic Disorder. *J. Paediatr. Child Health* **2012**, *48* (3), E153–E155.

(25) Craciun, S.; Balskus, E. P. Microbial Conversion of Choline to Trimethylamine Requires a Glycyl Radical Enzyme. *Proc. Natl. Acad. Sci. U.S.A.* **2012**, *109* (52), 21307–21312.

(26) Craciun, S.; Marks, J. A.; Balskus, E. P. Characterization of Choline Trimethylamine-Lyase Expands the Chemistry of Glycyl Radical Enzymes. *ACS Chem. Biol.* **2014**, *9* (7), 1408–1413.

(27) Bodea, S.; Funk, M. A.; Balskus, E. P.; Drennan, C. L. Molecular Basis of C-N Bond Cleavage by the Glycyl Radical Enzyme Choline Trimethylamine-Lyase. *Cell Chem. Biol.* **2016**, *23* (10), 1206–1216.

(28) Wang, Z.; Roberts, A. B.; Buffa, J. A.; Levison, B. S.; Zhu, W.; Org, E.; Gu, X.; Huang, Y.; Zamanian-Daryoush, M.; Culley, M. K.; DiDonato, A. J.; Fu, X.; Hazen, J. E.; Krajcik, D.; DiDonato, J. A.; Lusis, A. J.; Hazen, S. L. Non-Lethal Inhibition of Gut Microbial Trimethylamine Production for the Treatment of Atherosclerosis. *Cell* **2015**, *163* (7), 1585–1595.

(29) Bodea, S. **Understanding and Preventing Disease-Associated Anaerobic Choline Metabolism by the Human Gut Microbiota**, 2016, pp 1–224.

(30) Orman, M.; Bodea, S.; Funk, M. A.; Martínez-del Campo, A.; Bollenbach, M.; Drennan, C. L.; Balskus, E. P. Structure-Guided Identification of a Small Molecule That Inhibits Anaerobic Choline Metabolism by Human Gut Bacteria. *J. Am. Chem. Soc.* **2018**, *141* (1), 33–37.

(31) Romano, K. A.; Martínez-del Campo, A.; Kasahara, K.; Chittim, C. L.; Vivas, E. I.; Amador-Noguez, D.; Balskus, E. P.; Rey, F. E. Metabolic, Epigenetic, and Transgenerational Effects of Gut Bacterial Choline Consumption. *Cell Host Microbe* **2017**, *22* (3), 279–290.

(32) Martínez-del Campo, A.; Bodea, S.; Hamer, H. A.; Marks, J. A.; Haiser, H. J.;

Turnbaugh, P. J.; Balskus, E. P. Characterization and Detection of a Widely Distributed Gene Cluster That Predicts Anaerobic Choline Utilization by Human Gut Bacteria. *mBio* **2015**, *6* (2), e00042–15–12.

(33) Chen, K.; Zheng, X.; Feng, M.; Li, D.; Zhang, H. Gut Microbiota-Dependent Metabolite Trimethylamine *N*-Oxide Contributes to Cardiac Dysfunction in Western Diet-Induced Obese Mice. *Front. Physiol.* **2017**, *8*, 15718–15719.

(34) Chilloux, J.; Brial, F.; Everard, A.; Smyth, D.; Zhang, L.; Plovier, H.; Myridakis, A.; Hoyles, L.; Fuchs, J. E.; Blancher, C.; Gencer, S.; Martinez-Gili, L.; Fearnside, J. F.; Barton, R. H.; Neves, A. L.; Rothwell, A. R.; Gerard, C.; Calderari, S.; Boulangé, C. L.; Patel, S.; Scott, J.; Glen, R. C.; Gooderham, N. J.; Nicholson, J. K.; Gauguier, D.; Liu, P. P.; Cani, P. D.; Dumas, M.-E. E. Microbiome Inhibition of IRAK-4 by Trimethylamine Mediates Metabolic and Immune Benefits in High-Fat-Diet-Induced Insulin Resistance. *bioRxiv* **2018**, 1–40.

(35) Stoscheck, C. M. Quantitation of Protein. *Methods Enzymol.* **1990**, *182*, 50–68.

(36) Stoll, S.; Schweiger, A. EasySpin, a Comprehensive Software Package for Spectral Simulation and Analysis in EPR. *J. Magn. Reson.* **2006**, *178* (1), 42–55.

(37) Otwinowski, Z.; Minor, W. Processing of X-Ray Diffraction Data Collected in Oscillation Mode. *Methods Enzymol.* **1997**, *276*, 307–326.

(38) McCoy, A. J.; Grosse-Kunstleve, R. W.; Adams, P. D.; Winn, M. D.; Storoni, L. C.; Read, R. J. Phaser Crystallographic Software. *J. Appl. Cryst.* **2007**, *40*, 658–674.

(39) Adams, P. D.; Afonine, P. V.; Bunkoczi, G.; Chen, V. B.; Davis, I. W.; Echols, N.; Headd, J. J.; Hung, L. W.; Kapral, G. J.; Grosse-Kunstleve, R. W.; McCoy, A. J.; Moriarty, N. W.; Oeffner, R.; Read, R. J.; Richardson, D. C.; Richardson, J. S.; Terwilliger, T. C.; Zwart, P. H. PHENIX: a Comprehensive Python-Based System for Macromolecular Structure Solution. *Acta Crystallogr. D Biol. Crystallogr.* **2010**, *66*, 213–221.

(40) Emsley, P.; Lohkamp, B.; Scott, W. G.; Cowtan, K. Features and Development of Coot. *Acta Crystallogr. D Biol. Crystallogr.* **2010**, *66*, 486–501.

(41) Price-Carter, M.; Tingey, J.; Bobik, T. A.; Roth, J. R. The Alternative Electron Acceptor Tetrathionate Supports B12-Dependent Anaerobic Growth of Salmonella Enterica Serovar Typhimurium on Ethanolamine or 1,2-Propanediol. *J. Bacteriol.* **2001**, *183* (8), 2463–2475.

Chapter 3: Rational design of small molecules that inhibit anaerobic choline metabolism by human gut bacteria

3.1. Introduction

In Chapter 2, we described the development and optimization of a comprehensive set of experiments for validating inhibitors of anaerobic choline metabolism and, in turn, demonstrated the feasibility of designing low molecular weight compounds that target CutC. Our detailed workflow relied on the use of betaine aldehyde as a tool compound for modulating gut microbial choline metabolism in biochemical and bacterial cell-based assays. However, we recognize that the modest potency of betaine aldehyde precludes its application in more complex microbial communities, such as those found in living hosts.[1] Thus, there is still a demand for the identification of additional small molecule inhibitors of gut microbial choline metabolism that are improved candidates for animal studies and, potentially, for pre-clinical development. We planned to access these inhibitors by leveraging the information gleaned from our prior X-ray crystallography analyses of CutC and the investigations described in Chapter 2.

While a detailed description of the choline-bound structure of wild type CutC, along with relevant mutants, from *Desulfovibrio alaskensis* G20 can be found elsewhere (see Section 1.11), several findings were particularly relevant for our goal of developing inhibitors. Compared with other choline- and acetylcholine-binding proteins,[2] CutC contains a surprisingly polar active site. Within this pocket, choline is oriented such that its hydroxyl group engages in hydrogen bonding with Glu491 and the backbone amide nitrogen of Gly488/Cys489 (Section 2.1, Figure 2.2). C2 of choline, which bears a partial positive charge, may participate in a cation-π-like interaction with Phe395. The polarized methyl groups of choline's trimethylammonium moiety make several

CH—O hydrogen bonds with the side-chain oxygen atoms of Tyr208, Tyr506, Asp216, and a water molecule held in the active site. CH—O bonds play critical roles in substrate recognition for various quaternary amine-binding enzymes and, in some cases, are similar in strength to weak hydrogen bonds.[3-6] For CutC, these interactions are believed to be the protein's primary choline-specific contacts.

The insights from these structural and biochemical data informed our model for the mechanism of CutC (Figure 3.1).[7,8] As described in Section 1.11, catalysis likely begins with *pro-S* hydrogen atom abstraction from C1 of choline by the Cys489 thiyl radical. Deprotonation of the hydroxyl by a general base, likely Glu491, followed by rapid heterolytic C–N bond cleavage via a "spin-center shift" would eliminate TMA. A series of proton transfers from Glu491 to Thr502 to Asp216 could deprotonate Glu491 and reset the CutC active site for the next round of catalysis. Asp216 may serve as the general acid in this reaction, donating a proton to TMA.

As evidenced by the betaine-aldehyde bound structure of wild-type CutC from *D. alaskensis* G20 (Section 2.2.3, Figure 2.7), the presence of a trimethylammonium group appears to facilitate inhibition of TMA formation, suggesting the importance of preserving the CH—O hydrogen bonds. This is highlighted in the *in vitro* experiment with recombinant CutC and a panel of aldehyde-containing choline analogs in which the quaternary amine is replaced with various alkyl groups (Section 2.2.6). When tested in an endpoint assay, none of these aldehydes were effective inhibitors of CutC (Section 2.14). In addition to CH—O hydrogen bonds, betaine aldehyde establishes other similar interactions with CutC active site residues as those observed in the choline-bound crystal structure (Figure 2.7). The thiohemiacetal alcohol participates in hydrogen bonds with Glu491 and the backbone amide of C489, while the methylene carbon

forms a close cation-π-like interaction (3.5 Å) with the aromatic ring of Phe395. This suggests that a chemical scaffold capable of engaging these critical active site residues and perhaps forming additional interactions with the enzyme could lead to selective and more potent CutC inhibitors.

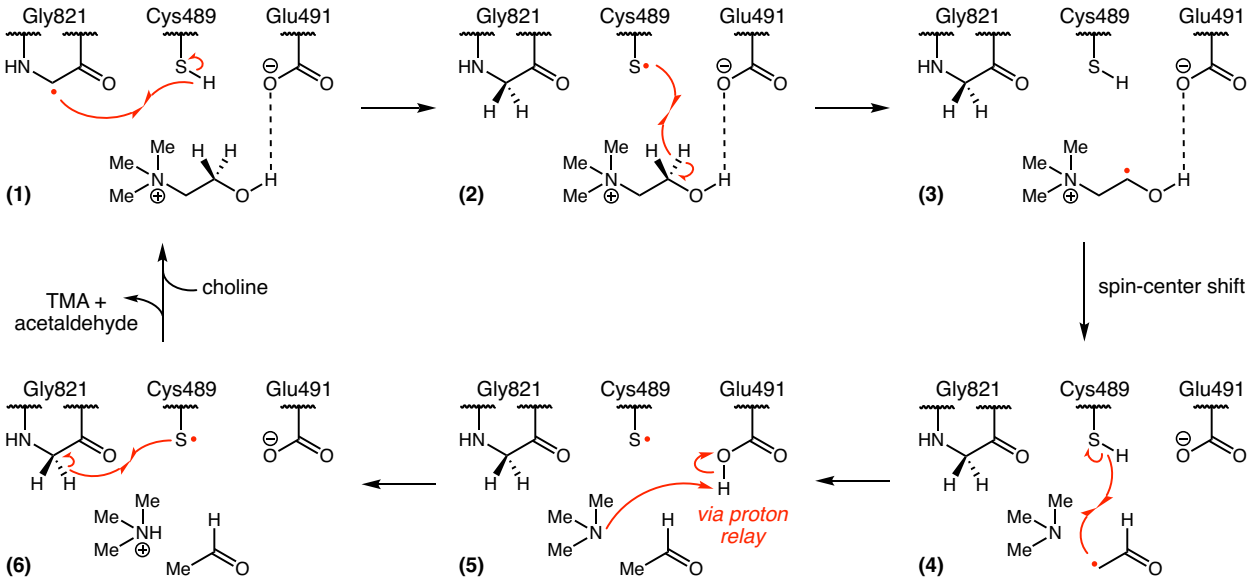

Figure 3.1. Proposed mechanism for choline cleavage by CutC. (1) The glycyl radical of CutC abstracts a hydrogen atom from Cys489, generating a thiyl radical. (2) Catalysis begins with *pro-S* hydrogen atom abstraction from C1 of choline. (3) Trimethylamine is eliminated from the resulting α-hydroxyalkyl radical species via a "spin-center shift." (4) The subsequent product-based radical species re-abstracts a hydrogen atom from Cys489, reforming the thiyl radical and generating acetaldehyde. (5) A series of proton transfers may take place, ultimately deprotonating the putative general base, Glu491. (6) The thiyl radical re-abstracts a hydrogen atom from Gly821, regenerating the glycyl radical and resetting the active site for the next round of catalysis.

In this chapter, we rely on two general approaches for identifying additional small molecules that inhibit bacterial TMA production. First, we expand on the initial set of choline analogs tested in the *E. coli* whole cell assay in Chapter 2, optimizing these compounds in order to increase productive interactions with CutC and generate a ligand that binds with higher efficiency and could serve as a potent inhibitor (Figure 3.2A). One possible design strategy is to

add substituents to the choline scaffold that extend into and make contacts with the hydrophobic tunnel adjacent to the active site. From the crystal structures, it appears that rotation of residues located at the top of this hydrophobic barrel, particularly the side chains of Phe389 and Trp379, may block access to the active site from the exterior of the protein.

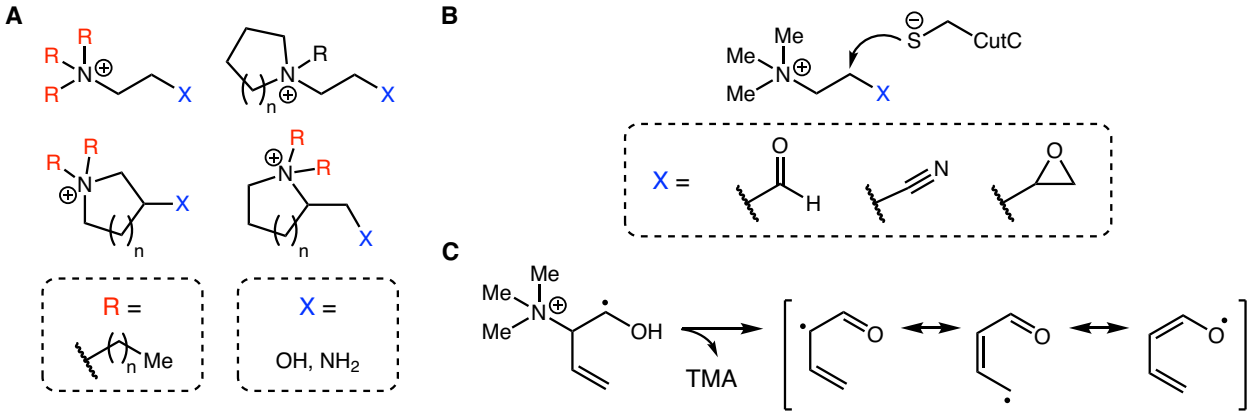

Figure 3.2. Strategies for the rational design of CutC inhibitors A) Functional groups that maximize interactions with active site residues can be added onto the choline scaffold to increase inhibitor binding and potency. B) Electrophilic moieties, such as aldehydes, nitriles, and epoxides, can promote covalent binding between the inhibitor and the catalytically essential cysteine in the active site. C) Radical traps, such as alkenes, can generate resonance-stabilized radical intermediates that occupy the active site.

Our second design strategy is to develop inhibitors that can interfere with the mechanism of CutC, either by covalently binding to the catalytic cysteine (Figure 3.2B) or by generating a stable radical species that occupies the active site and prevents reformation of the thiyl radical species (Figure 3.2C). For the former, a weak electrophile can be installed on the framework of a CutC-targeting compound. Ideally, the manner in which this inhibitor binds in the active site would position its electrophilic functionality in close proximity to the nucleophilic cysteine of CutC. Some common functional groups for covalent inhibition include acrylamides, aldehydes, nitriles, epoxides, and isothiocyanates.[9] Alternatively, installation of a "radical trap" on a ligand

with high efficiency towards CutC could abort the catalytic cycle once the Cys489 radical reacts with the trap. Such mechanism-based inhibition can arise from the generation of an inhibitor-based radical intermediate that subsequently interacts with the protein, abolishing enzymatic activity, or a radical that is stabilized by an adjacent moiety on the ligand, thereby precluding its abstraction of the H-atom on Cys489 (which is necessary in order to regenerate the thiyl radical and continue the catalytic cycle). A wide range of substituents have been employed for the development of "suicide substrates," including both electron withdrawing groups (EWGs), such as carbonyls and nitriles, and electron donating groups (EDGs), such as methoxy groups, as well as cyclopropyl rings and alkenes.

3.2. Results and Discussion

All non-commercially available compounds (listed in Section 3.4) used in the experiments described below were synthesized by Dr. Maud Bollenbach. In addition, the synthesis of compounds **2**, **3**, and **6** was performed by Dr. Smaranda Bodea.

3.2.1. Optimization of the choline scaffold to identify potent CutC inhibitors

We first conducted a simple structure-activity relationship (SAR) study on the choline hydroxyl group (Table 3.1). This moiety was replaced with F (**3**), Cl (**4**), Br (**14**), a thiol (**2**), a primary amine (**1**), an aldehyde (**9**), a nitrile (**8**), and a terminal alkyne (**15**). This latter compound was inspired from a patent, filed by Dr. Stanley Hazen of The Cleveland Clinic, in conjunction with The Proctor & Gamble Company, that described compounds and methods for inhibiting the production of TMA.[10] Extending the carbon chain of choline by one carbon yielded compound **5**. Adding a methyl group onto C1 of choline resulted in the racemic mixture

16. We tested these molecules for their ability to inhibit anaerobic choline metabolism in the *cut* gene cluster-containing organism *Escherichia coli* MS 200-1. Cultures were incubated anaerobically in a rich medium containing 1 mM of (trimethyl-d_9)-choline (d_9-choline) and at least three concentrations of inhibitor. Production of d_9-TMA was analyzed by LC-MS/MS after 3.5 hours. Although compounds **1**-**13** were briefly mentioned in Section 2.2.1, they are described below in greater detail.

We wondered if halogen-containing choline analogs, potentially **4** or **14**, could be a good starting point for the development of irreversible covalent inhibitors. Bond formation between C1 of the inhibitor and CutC's catalytic cysteine would result in loss of the halide. Although electrophilic alkyl halides have been employed as DNA alkylating agents, they are associated with significant toxicities and are therefore rarely used in current drug design strategies.[11] In our whole cell assay, compounds **3**, **4**, and **14** were completely inactive (Table 3.1). Only bromocholine (**14**) was tested on minimal medium containing choline as the sole carbon source. It had no discernible impact on growth (Figure 3.3A). Previously, we have shown that functional CutC is essential for the anaerobic growth of *cut* gene cluster-containing *E. coli* when choline is provided as the sole carbon source and fumarate as a terminal electron acceptor.[12] Thus, inhibition of CutC with a small molecule would impair the anaerobic metabolism of choline and likely cause growth defects on choline-containing minimal medium.

Table 3.1. EC_{50} values and minimal media growth results for compounds 1-5, 8, 9, 14-16

Compound	Structure	EC_{50} (mM)	Max OD_{600} / Time of ½ max(OD_{600})	
			Choline	Glycerol
—	No inhibitor	—	1.0 / 3.7 h	1.1 / 6.0 h
3	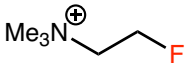	>10	—	—
4	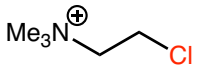	>10	—	—
14	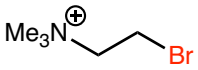	No inhibition	0.9 / 4.7 h	—
2	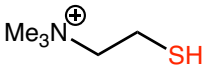	0.48	—	—
1	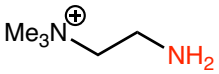	4.8	—	—
5	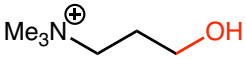	>10	—	—
9	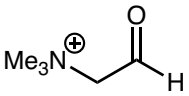	0.40	0.2 / 11 h	1.0 / 6.3 h
8	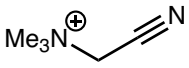	2.3	—	—
15	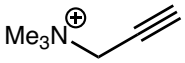	8.0×10^{-5}	0.3 / 17.7 h	1.1 / 7.3 h
16	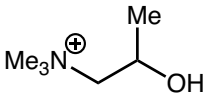	>10	0.8 / 4.0 h	—

E. coli MS 200-1 was incubated in BHI medium containing 1 mM d_9-choline and phosphate buffer or inhibitor (tested at ≥3 concentrations) at 37 °C in an anaerobic chamber. [d_9-TMA] was measured by LC-MS/MS after 3.5 hours. Dose-response curves were fit using nonlinear regression to determine the EC_{50}. OD_{600} values were obtained by incubating *E. coli* MS 69-1 with phosphate buffer or 20 mM of inhibitor in either 30 mM choline or 30 mM glycerol minimal media. Cultures were grown anaerobically for 24 hours at 37 °C.

Thiocholine (**2**, EC_{50} = 0.48 mM), which could potentially generate a thioalkyl radical and thus act as a mechanism-based inhibitor of CutC, and betaine aldehyde (**9**, EC_{50} = 0.40 mM), which, as described in Section 2.2.3, formed a thiohemiacetal with Cys489, both emerged as promising scaffolds. When incubated with *E. coli* on choline minimal medium for 24 hours in an anaerobic MBraun chamber, betaine aldehyde decreased the maximum OD_{600} from 1.0 to 0.2 (Figure 3.3A). It had no apparent effect on *E. coli* grown on glycerol minimal medium (Figure 3.3B), suggesting that betaine aldehyde might selectively inhibit the anaerobic metabolism of choline. It also had no effect on growth on a rich medium containing 2 g/L (~11 mM) of glucose (along with calf brain and beef heart infusions) (Figure 3.4A), providing further support that betaine aldehyde (**9**) is specifically impairing choline metabolism and is not eliciting an off-target effect that reduces bacterial viability and thereby non-selectively lowers TMA levels.

To assess whether reduction of TMA formation by betaine aldehyde (**9**) arose from inhibition of CutC, we performed *in vitro* experiments under an anaerobic atmosphere using recombinant wild-type CutC and CutD from *D. alaskensis* G20 (as described in Section 2.2.2). Using a 7-point dilution series, the IC_{50} of betaine aldehyde for CutC was determined to be 26.4 ± 2 μM (Figure 3.5). This suggests that betaine aldehyde's ability to reduce TMA levels in *E. coli* may indeed arise from its direct targeting of CutC inside cells.

Nitrile-based compounds that covalently interact with catalytically essential cysteines have been developed, albeit with limited clinical success, as protease inhibitors (e.g. odanacatib and saxagliptin).[11] Nevertheless, cyanocholine (**8**, EC_{50} = 2.3 mM) showed only modest inhibitory activity. Cyanocholine **8** no longer retains the C1 H-atom of choline that is abstracted by Cys489. However, positioning a nitrile group on the choline framework such that CutC could

abstract a hydrogen atom, thereby generating a nitrile-stabilized radical species, could be another potential strategy for the future development of mechanism-based inhibitors.

Radical-mediated reactions between thiols and alkynes have been explored as tools for polymerizations, materials synthesis, and bioconjugation.[13] The terminal alkyne **15**, which was inspired by compounds from a recent patent for TMA inhibitors, showed high potency in the LC-MS-based whole cell assay (EC_{50} = 80 nM) and inhibited growth on choline minimal medium without affecting growth on glycerol (Figure 3.3C,D) or on BHI medium (Figure 3.4B). Thus, compound **15** may be selective for CutC and potentially act as a covalent inhibitor, with bond formation between the thiyl radical of the enzyme and the carbon of the alkyne resulting in a vinyl thioether adduct.

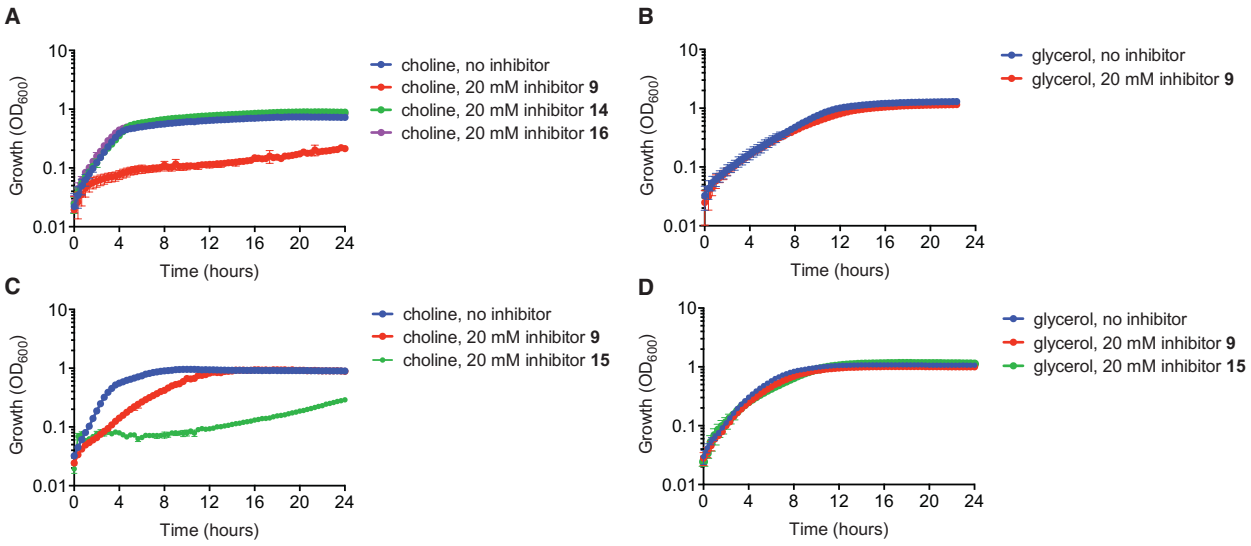

Figure 3.3. Effects of compounds 9, 14, 15, and 16 on anaerobic growth of *E. coli* on minimal media. *E. coli* MS 69-1 was grown in an MBraun glovebox, under an N_2 atmosphere, on minimal media with either (A) 30 mM choline or 30 mM glycerol or in a vinyl chamber, under 95% N_2 / 5% H_2, on (C) 30 mM choline or (D) 30 mM glycerol minimal media. Cultures were supplemented with phosphate buffer or inhibitor and incubated for 24 hours at 37 °C. Error bars represent the mean ± SD of three replicates.

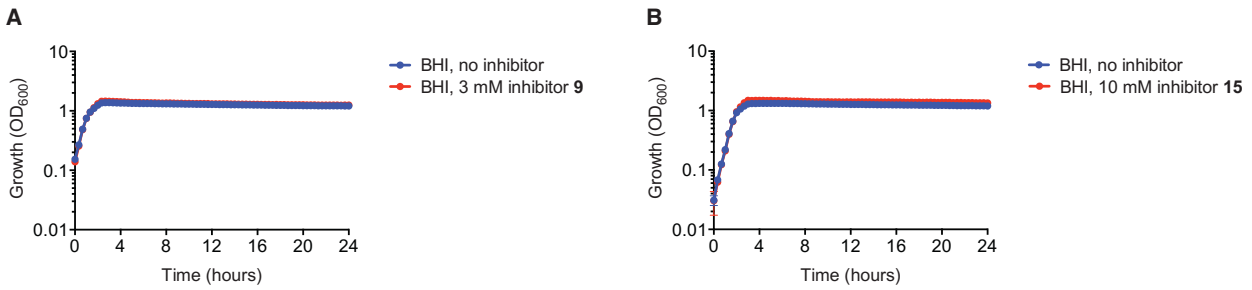

Figure 3.4. Effects of compounds 9 and 15 on anaerobic growth of *E. coli* on rich medium. *E. coli* MS 200-1 was grown on BHI medium containing 11 mM glucose in (A) an MBraun glovebox, under an N_2 atmosphere, or (B) a vinyl chamber, under 95% N_2 / 5% H_2. Cultures were supplemented with phosphate buffer or inhibitor and incubated for 24 hours at 37 °C. Error bars represent the mean ± SD of three replicates.

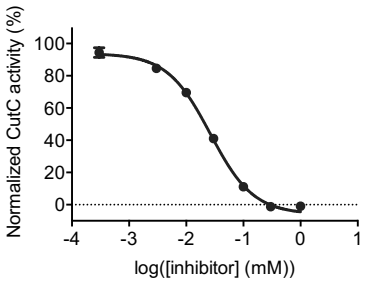

Figure 3.5. Betaine aldehyde (9) inhibits CutC-mediated TMA production *in vitro*. The activity of CutC was coupled to that of yeast alcohol dehydrogenase (YADH). Inhibitors (0.30 µM to 1 mM) were added prior to the addition of choline. The absorbance of NADH at 340 nm was recorded over time to calculate initial rates and kinetic parameters. Initial rates were normalized to a control assay without inhibitor, and data were fit using nonlinear regression in Graphpad Prism to obtain an IC_{50} value of 26.4 ± 2 µM. Error bars represent the mean ± SD of three replicates.

Next, we assessed the scope of the terminal alkyne scaffold (Table 3.2). The *N*-dimethylammonium variant (**17**) showed only a slight decrease in potency (~3-fold) compared to the parent compound **15**, as did an analog containing an *N*-methylchloride substituent (**19**). Although **17** was not tested for its impact on growth in minimal media, **19** slowed the rate of exponential phase growth of *E. coli* on choline (Figure 3.6A). However, compound **19** also resulted in a growth delay on glycerol minimal medium (Figure 3.6B), suggesting that it may not act as a specific inhibitor of anaerobic choline metabolism.

Exchange of the amine for a hydroxyl (**18**) resulted in a reduction of potency by ~10^5, highlighting an important role for the trimethylammonium moiety, as has been previously established in our studies of betaine aldehyde (see Chapter 2). Substitution of the alkyne of **15** for an alkene (**20**) did not affect potency, perhaps because the two molecules inhibit CutC via similar mechanisms. Indeed, the formation of thioethers via photochemically- or thermally-induced radical reactions of thiols and alkenes (known as thiol-ene coupling) has been well-studied and employed in the context of bioorganic click chemistry.[14] Although it was not tested on minimal medium, alkene **20** did not affect growth on a rich medium (Figure 3.7). Finally, replacement of the trimethylammonium group of **20** with a dimethylamine (**21**) resulted in a complete loss of potency.

Table 3.2. EC_{50} values and minimal media growth results for compounds 15-21

Compound	Structure	EC_{50} (mM)	Max OD_{600} / Time of ½ max(OD_{600})	
			Choline	Glycerol
—	No inhibitor	—	1.0 / 3.7 h	1.1 / 6.0 h
15	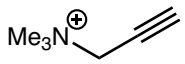	8.0×10^{-5}	0.3 / 17.3 h	1.1 / 7.3 h
17	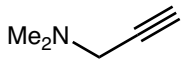	2.6×10^{-4}	—	—
18	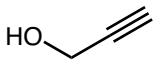	2.8	—	—
19	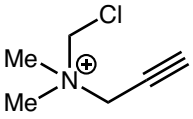	3.0×10^{-4}	0.6 / 13.0 h	1.1 / 10.0 h
20	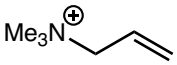	5.3×10^{-5}	—	—
21	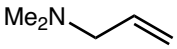	No inhibition	—	—

E. coli MS 200-1 was incubated in BHI medium containing 1 mM d_9-choline and either phosphate buffer or inhibitor (tested at ≥3 concentrations) at 37 °C in an anaerobic chamber. [d_9-TMA] was measured by LC-MS/MS after 3.5 hours. Dose-response curves were fit using nonlinear regression to determine the EC_{50}. OD_{600} values were obtained by incubating *E. coli* MS 69-1 with phosphate buffer or 20 mM of inhibitor on 30 mM choline or 30 mM glycerol minimal media. Cultures were grown anaerobically for 24 hours at 37 °C.

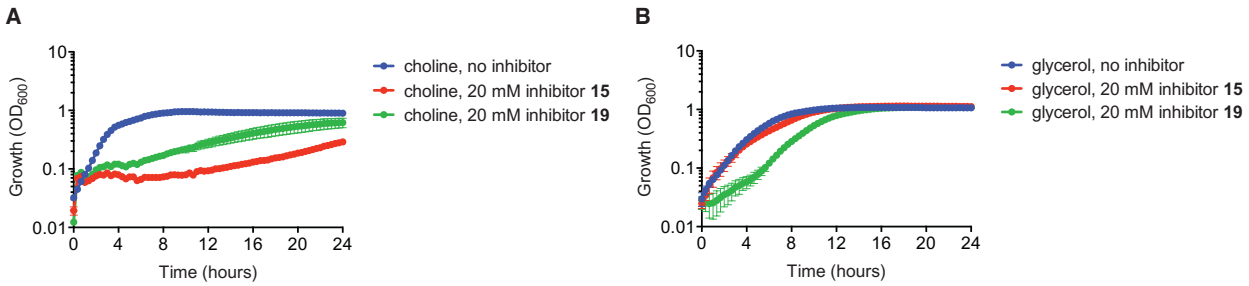

Figure 3.6. Effects of compounds 15 and 19 on anaerobic growth of *E. coli* on minimal media. *E. coli* MS 69-1 was grown in a vinyl chamber, under 95% N_2 / 5% H_2, on (A) 30 mM choline or (B) 30 mM glycerol minimal media. Cultures were incubated with phosphate buffer or inhibitor for 24 hours at 37 °C. Error bars represent the mean ± SD of three replicates.

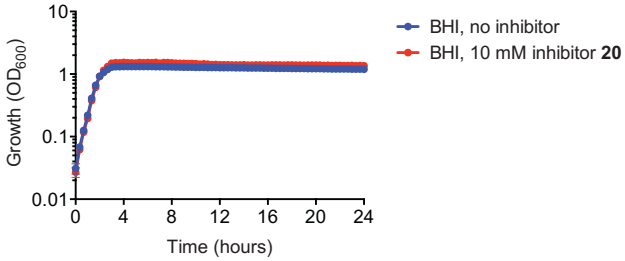

Figure 3.7. Effects of compound 20 on anaerobic growth of *E. coli* on rich medium. *E. coli* MS 200-1 was grown on BHI medium containing 11 mM glucose in a vinyl chamber, under 95% N_2 / 5% H_2. Cultures were supplemented with phosphate buffer or inhibitor and incubated for 24 hours at 37 °C. Error bars represent the mean ± SD of three replicates.

Addition of a methyl group onto C1 of choline resulted in the racemic mixture **16**, which did not inhibit TMA production from choline in whole cells (Table 3.1). We attempted to optimize the potency of **16**, first by replacing the trimethylammonium moiety with an *N*-dimethyl group (**22**), then by further modifying this compound with a dimethyl group at the C1 position (**23**) (Table 3.3). Neither molecule was active, which is perhaps unsurprising given they did not affect the growth of *E. coli* on choline (and on glycerol) minimal medium (Figure 3.8). To screen compounds quickly, we decided that testing and comparing their effects on growth in choline- and glycerol-containing minimal media could be a useful high-throughput approach,

particularly for filtering out bacteriostatic compounds (which inhibit growth on glycerol) from those that selectively target CutC (which would likely not inhibit growth on glycerol).

Table 3.3. EC_{50} values and minimal media growth results for compounds 16, 22, 23

Compound	Structure	EC_{50} (mM)	Max OD_{600} / Time of ½ max(OD_{600})	
			Choline	Glycerol
—	No inhibitor	—	0.7 / 4.0 h	1.3 / 9.3 h
16	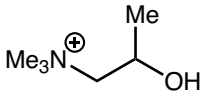	>10	0.8 / 4.0 h	1.1 / 10.7 h
22	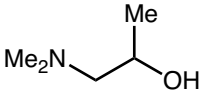	No inhibition	0.9 / 4.0 h	1.2 / 9.3 h
23	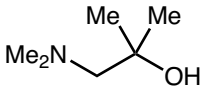	>10	0.8 / 4.3 h	1.1 / 9.3 h

E. coli MS 200-1 was incubated in BHI medium containing 1 mM d_9-choline with either phosphate buffer or inhibitor (tested at ≥3 concentrations) at 37 °C in an anaerobic chamber. [d_9-TMA] was measured by LC-MS/MS after 3.5 hours. Dose-response curves were fit using nonlinear regression to determine the EC_{50}. OD_{600} values were obtained by incubating *E. coli* MS 69-1 with either phosphate buffer or 20 mM of inhibitor in 30 mM choline or 30 mM glycerol minimal media. Cultures were grown anaerobically for 24 hours at 37 °C.

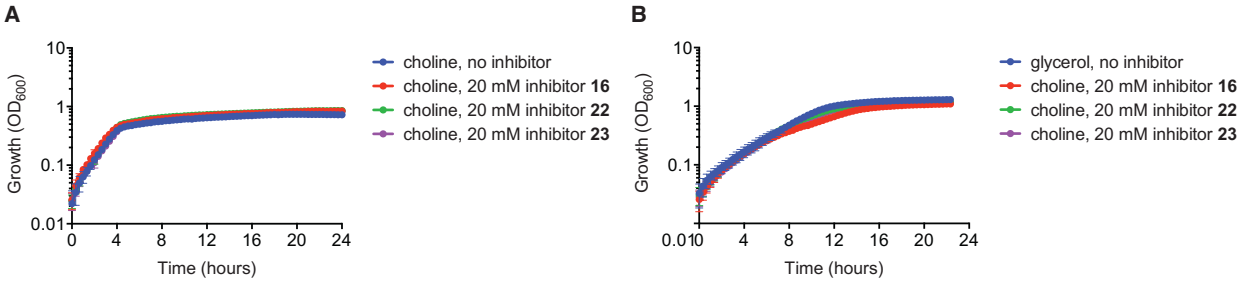

Figure 3.8. Effects of compounds 16, 22, and 23 on anaerobic growth of *E. coli* on minimal media. *E. coli* MS 69-1 was grown in an MBraun glovebox, under an N_2 atmosphere, in (A) 30 mM choline or (B) 30 mM glycerol minimal media. Cultures were supplemented with phosphate buffer or inhibitor and incubated for 24 hours at 37 °C. Error bars represent the mean ± SD of three replicates.

We had observed that extension of the carbon chain of choline by an extra carbon yielded compound **5**, a poor inhibitor of anaerobic choline metabolism (Table 3.1). Exchanging the trimethylammonium moiety of compound **5** for a secondary (**24**) or a primary amine (**25**) had no impact on growth on either choline or glycerol minimal media (Table 3.4, Figure 3.9). Adding steric bulk in the form of a cyclopropyl group at various positions on the carbon chain yielded compounds **26** and **27**, while extending the carbon chain of compound **24** resulted in 4-(methylamino)butan-1-ol (**28**). None of these molecules impacted growth on choline minimal media (Table 3.4, Figure 3.9).

Table 3.4. EC_{50} values and minimal media growth results for inhibitors 5, 24-28

Compound	Structure	EC_{50} (mM)	Max OD_{600} / Time of ½ max(OD_{600})	
			Choline	Glycerol
—	No inhibitor	—	0.7 / 4.0 h	1.3 / 9.3 h
5	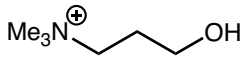	>10	—	—
24	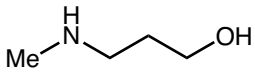	—	0.8 / 4.0 h	1.2 / 9.3 h
25	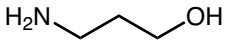	—	0.8 / 4.0 h	1.2 / 9.3 h
26	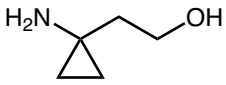	—	0.8 / 5.0 h	1.0 / 11.0 h
27		—	0.7 / 4.3 h	1.1 / 11.3 h
28	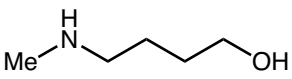	—	0.7 / 4.0 h	1.2 / 9.7 h

Table 3.4 (continued) *E. coli* MS 200-1 was incubated in BHI medium containing 1 mM d_9-choline with either phosphate buffer or inhibitor (tested at ≥3 concentrations) at 37 °C in an anaerobic chamber. [d_9-TMA] was measured by LC-MS/MS after 3.5 hours. Dose-response curves were fit using nonlinear regression to determine the EC_{50}. OD_{600} values were obtained by incubating *E. coli* MS 69-1 with either phosphate buffer or 20 mM of inhibitor in 30 mM choline or 30 mM glycerol minimal media. Cultures were grown anaerobically for 24 hours at 37 °C.

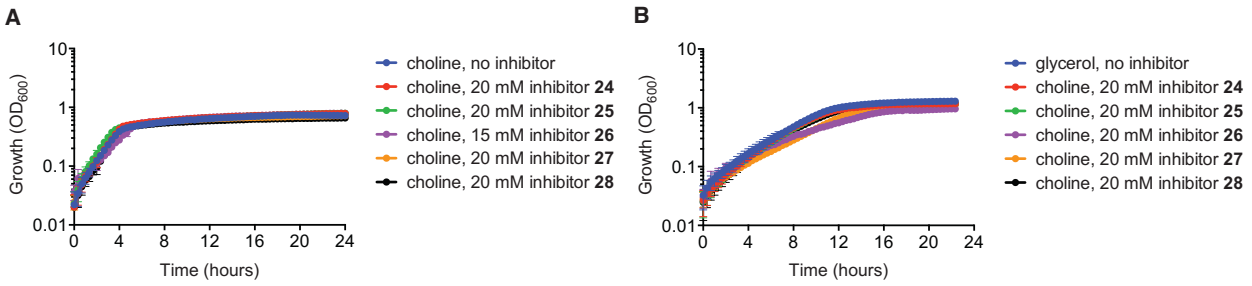

Figure 3.9. Effects of compounds 24-28 on anaerobic growth of *E. coli* on minimal media. *E. coli* MS 69-1 was grown in an MBraun glovebox, under N_2, in (A) 30 mM choline or (B) 30 mM glycerol minimal media. Cultures were supplemented with phosphate buffer or inhibitor and incubated for 24 hours at 37 °C. Error bars represent the mean ± SD of three replicates.

We also performed an SAR analysis on the amine group of choline (Table 3.5). As was previously seen for analogs **15** and **17**, as well as **20** and **21**, replacement of the trimethylammonium group with a dimethylamine resulted in a loss of potency. Following this pattern, 2-(dimethylamino)ethan-1-ol (**10**) did not show any inhibitory activity in the *E. coli* whole cell assay. Replacement of an *N*-methyl group of choline with a hydroxyl (*N*-oxide analog **7**), or with a propyl chain (**6**) did not yield any promising activity either. Adding a methyliodide substitutent, however, resulted in a highly potent compound (**29**) with an EC_{50} of 0.3 μM in *E. coli* whole cells and an IC_{50} value of 37 pM in the *in vitro* assay with recombinent CutC (Figure 3.10). Betaine aldehyde (**9**) displayed an IC_{50} of 46 μM (Figure 3.10) in the same *in vitro* assay. The hydrazine analog (**30**) inhibited growth on both choline and glycerol minimal media (Figure 3.11A,B).

Table 3.5. EC_{50} values and minimal media growth results for compounds 6, 7, 10, 29-35

Compound	Structure	EC_{50} (mM)	Max OD_{600} / Time of ½ max(OD_{600})	
			Choline	Glycerol
—	No inhibitor	—	0.9 / 4.3 h	1.0 / 6.0 h
10	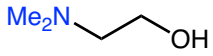	No inhibition	—	—
7	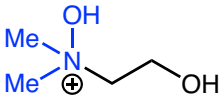	>10	—	—
6	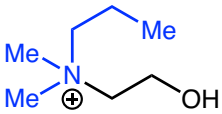	>10	—	—
29	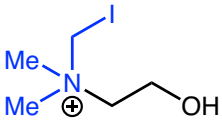	3.0×10^{-4}	—	—
30	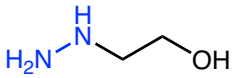	—	0.05 / 7.3 h	0.03 / 0.3 h
31	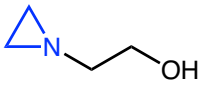	>10	0.4 / 4.3 h	0.5 / 18.3 h
32	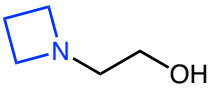	1.0	0.4 / 4.0 h	0.1 / 3.0 h
33	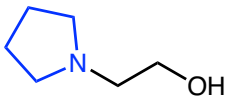	0.79	1.0 / 4.3 h	1.0 / 5.3 h
34	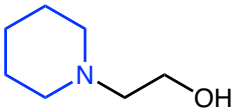	0.14	1.0 / 5.3 h	1.0 / 5.3 h
35	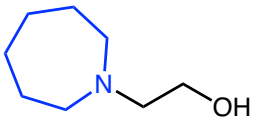	9.3×10^{-2}	1.0 / 6.0 h	1.0 / 5.7 h

Table 3.5 (continued) *E. coli* MS 200-1 was incubated in BHI medium containing 1 mM d_9-choline with either phosphate buffer or inhibitor (tested at ≥3 concentrations) at 37 °C in an anaerobic chamber. [d_9-TMA] was measured by LC-MS/MS after 3.5 hours. Dose-response curves were fit using nonlinear regression to determine the EC_{50}. OD_{600} values were obtained by incubating *E. coli* MS 69-1 with either phosphate buffer or 20 mM of inhibitor in 30 mM choline or 30 mM glycerol minimal media. Cultures were grown anaerobically for 24 hours at 37 °C.

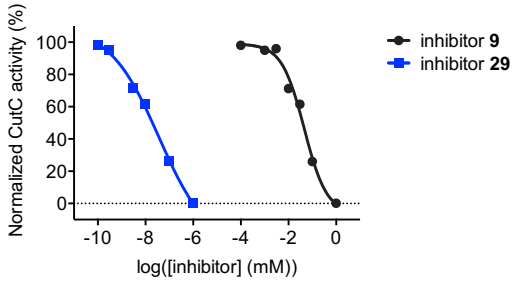

Figure 3.10. Effects of compounds 9 and 29 on CutC-mediated TMA production *in vitro*. The activity of CutC was coupled to that of YADH. Inhibitors (0.10 pM to 1 mM) were added prior to the addition of choline. The absorbance of NADH at 340 nm was recorded over time to calculate initial rates and kinetic parameters. Initial rates were normalized to a control without inhibitor, and data were fit using nonlinear regression in Graphpad Prism to obtain IC_{50} values of 46 μM and 37 pM for inhibitors **9** and **29**, respectively. Error bars represent the mean ± SD of three replicates.

Given that nitrogen heterocycles are frequently found in various natural products, biologically active structures, and medicinally relevant compounds,[15] we attempted to determine if the amine moiety of choline could be exchanged for a heterocyclic ring (Table 3.5). The aziridine analog (**31**) showed poor potency in bacteria and inhibited growth on both choline and glycerol minimal media (Figure 3.11A,B). Azirdine groups are known to serve as alkylating agents,[16] which may explain compound **31**'s effect in glycerol minimal medium. Interestingly, it did not seem to impact anaerobic growth on a rich medium (Figure 3.12).

We noticed that potency in the *E. coli* whole cell assay increased with increased heterocycle ring size. Among the aziridine (**31**), azetidine (**32**), pyrrolidine (**33**), piperidine (**34**), and azepane (**35**) analogs tested, compound **35** performed the best, with an EC_{50} of 94 μM. While compounds **33**, **34**, and **35** did not affect growth on glycerol minimal medium or on BHI

medium, they also did not appreciably impact growth on choline (Figures 3.11C,D and 3.12). Whether the magnitude of the effect on choline-dependent growth is not indicative of a molecule's potency towards CutC or compounds **33-35** do not actually target CutC remains unknown. It would be interesting to see how these compounds perform *in vitro*.

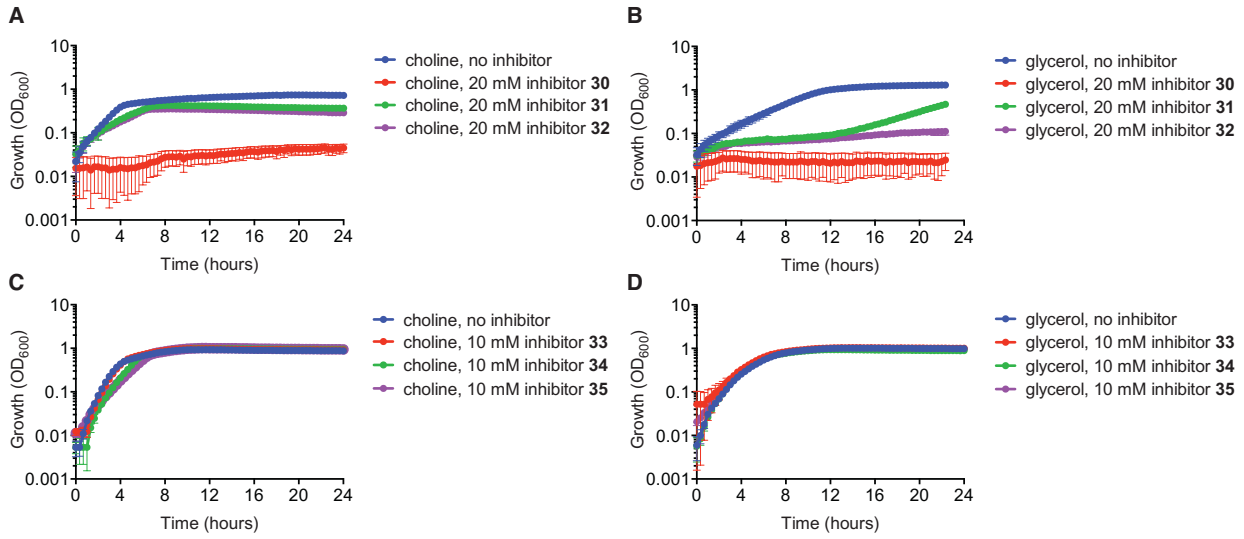

Figure 3.11. Effects of compounds 30-35 on anaerobic growth of *E. coli* on minimal media. *E. coli* MS 69-1 was grown in an MBraun glovebox, under N_2, in minimal media with (A) 30 mM choline or 30 mM or in a vinyl chamber, under 95% N_2 and 5% H_2, in 30 mM (C) choline or (D) glycerol minimal media. Cultures were incubated with buffer or inhibitor for 24 hours at 37 °C. Error bars represent the mean ± SD of three replicates.

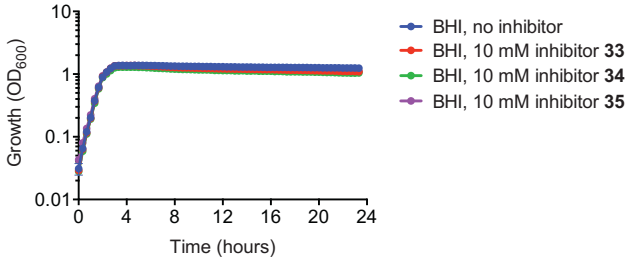

Figure 3.12. Effects of compounds 33-35 on anaerobic growth of *E. coli* on rich medium. *E. coli* MS 200-1 was grown in BHI medium containing 11 mM glucose in a vinyl chamber, under 95% N_2 / 5% H_2. Cultures were supplemented with phosphate buffer or inhibitor and incubated for 24 hours at 37 °C. Error bars represent the mean ± SD of three replicates.

The next modifications were made to the hydroxyl group of the pyrrolidine analog (**33**). Replacing this substituent with a primary amine (**36**) resulted in a 4-fold loss of potency, while analogs containing either a chlorine (**37**) or bromine atom (**38**) were both ~2 times more potent than the parent compound (Table 3.6). Although analogs **37** and **38** did not affect growth on rich medium (Figure 3.14), they decreased the rate of exponential growth on glycerol without noticeably impacting growth on choline (Figure 3.13). They were therefore not chosen for further development.

Table 3.6. EC_{50} values and minimal media growth results for compounds 33-38

Compound	Structure	EC_{50} (mM)	Max OD_{600} / Time of ½ max(OD_{600})	
			Choline	Glycerol
—	No inhibitor	—	0.9 / 4.3 h	1.0 / 6.0 h
33	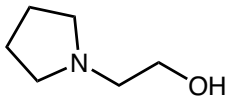	0.79	1.0 / 4.3 h	1.0 / 5.3 h
36	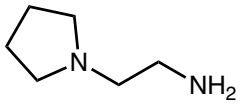	2.9	—	—
37	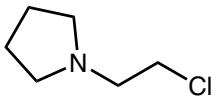	0.26	0.8 / 4.7 h	0.9 / 10.0 h
38	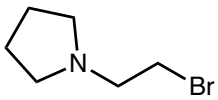	0.30	0.8 / 4.7 h	0.5 / 19.0 h

E. coli MS 200-1 was incubated in BHI medium containing 1 mM d_9-choline with either phosphate buffer or inhibitor (tested at ≥3 concentrations) at 37 °C in an anaerobic chamber. [d_9-TMA] was measured by LC-MS/MS after 3.5 hours. Dose-response curves were fit using nonlinear regression to determine the EC_{50}. OD_{600} values were obtained by incubating *E. coli* MS 69-1 with either phosphate buffer or 20 mM of inhibitor in 30 mM choline or 30 mM glycerol minimal media. Cultures were grown anaerobically for 24 hours at 37 °C.

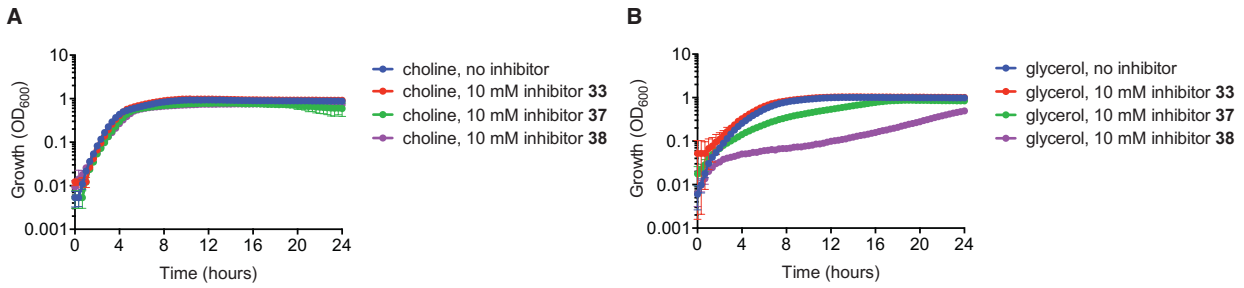

Figure 3.13. Effects of compounds 33, 37, and 38 on anaerobic growth of *E. coli* on minimal media. *E. coli* MS 69-1 was grown in a vinyl chamber, under an atmosphere of 95% N_2 and 5% H_2, in minimal media containing either (A) 30 mM choline or (B) 30 mM glycerol. Cultures were supplemented with either phosphate buffer or inhibitor and incubated for 24 hours at 37 °C. Error bars represent the mean ± SD of three replicates.

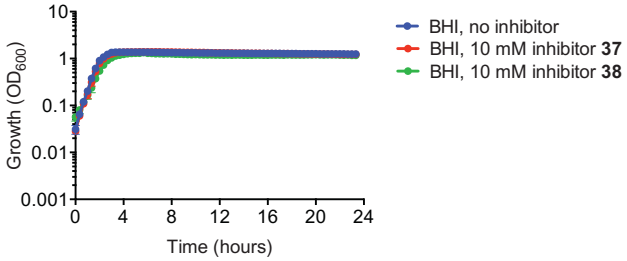

Figure 3.14. Effect of compounds 37-38 on anaerobic growth of *E. coli* on rich medium. *E. coli* MS 200-1 was grown in BHI medium containing 11 mM glucose in a vinyl chamber, under 95% N_2 / 5% H_2. Cultures were supplemented with phosphate buffer or inhibitor and incubated for 24 hours at 37 °C. Error bars represent the mean ± SD of three replicates.

In Chapter 2, we observed that the compound 3,3-dimethylbutanol (DMB, **12**), which contains a *tert*-butyl group in place of the trimethylammonium group of choline, was ineffective at inhibiting TMA production from choline in any of the assays we conducted despite previous studies by the Hazen lab claiming DMB to be a CutC inhibitor[17] (see Chapter 2 and Table 3.7). We hypothesized that loss of the polarized *N*-methyl groups prevented compound **12** from making the CH—O interactions that choline typically forms with CutC active site residues, thereby reducing its ability to compete with choline for binding to the enzyme. This lack of efficiency may also explain why compound **13**, the aldehyde analog of **12**, was a poor inhibitor

of CutC (see Chapter 2 and Table 3.7), despite having a functional group that could covalently react with the catalytic cysteine in the active site. In addition, although compound **13** increased the length of the lag phase of *E. coli* growing on choline minimal medium, it also slightly delayed exponential growth on glycerol (Figure 3.15A,B).

We also found that analogs of **12** were poor inhibitors of TMA production (Table 3.7). Substitution of one of the methyl groups of the *tert*-butyl moiety for a hydroxyl (**39**), a primary amine (**40**), and an *N*-methyl (**41**) group resulted in modest to poor inhibition. Surprisingly, despite their relatively poor potencies, 3-amino-3-methylbutan-1-ol (**40**, EC_{50} = 9.7 mM) and 3-methyl-3-(methylamino)butan-1-ol (**41**, EC_{50} = 2.7 mM) both delayed growth on choline minimal medium without affecting growth on glycerol (Figure 3.15A-D). As mentioned above in the discussion of compounds **33**, **34**, and **35**, it is possible that the effect on choline-dependent growth is not necessarily indicative of a molecule's potency towards CutC. Removal of a methyl group from C3 of compound **41** resulted in the racemic mixture **42**, which was also tested as pure (*R*)- (**43**) and (*S*)- (**44**) enantiomers. None of these three molecules showed inhibitory activity in the *E. coli* whole cell assay.

Table 3.7. EC_{50} values and minimal media growth results for compounds 12, 13, 39-44

Compound	Structure	EC_{50} (mM)	Max OD_{600} / Time of ½ max(OD_{600})	
			Choline	Glycerol
—	No inhibitor	—	0.7 / 4.0 h	1.2 / 8.3 h
12	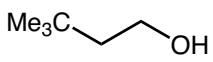	>10	0.3 / 4.7 h	1.1 / 9.7 h
13	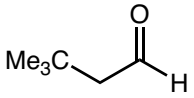	6.1	0.4 / 9.3 h	1.1 / 10.3 h
39	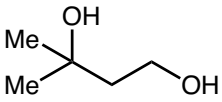	—	0.7 / 3.7 h	1.1 / 9.3 h
40	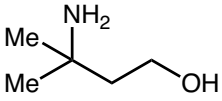	9.7	0.7 / 6.0 h	1.2 / 8.7 h
41	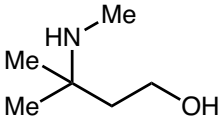	2.7	0.7 / 7.3 h	1.2 / 8.3 h
42	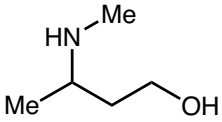	>10	0.7 / 4.0 h	1.1 / 9.3 h
43	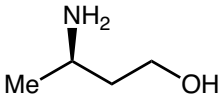	>10	0.7 / 4.7 h	1.2 / 8.7 h
44	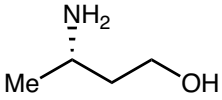	No inhibition	0.7 / 4.0 h	1.2 / 8.7 h

E. coli MS 200-1 was incubated in BHI medium containing 1 mM d_9-choline and either phosphate buffer or inhibitor (tested at ≥3 concentrations) at 37 °C in an anaerobic chamber. [d_9-TMA] was measured by LC-MS/MS after 3.5 hours. Dose-response curves were fit using nonlinear regression to determine the EC_{50}. OD_{600} values were obtained by incubating *E. coli* MS 69-1 with either phosphate buffer or 20 mM of inhibitor in 30 mM choline or 30 mM glycerol minimal media. Cultures were grown anaerobically for 24 hours at 37 °C.

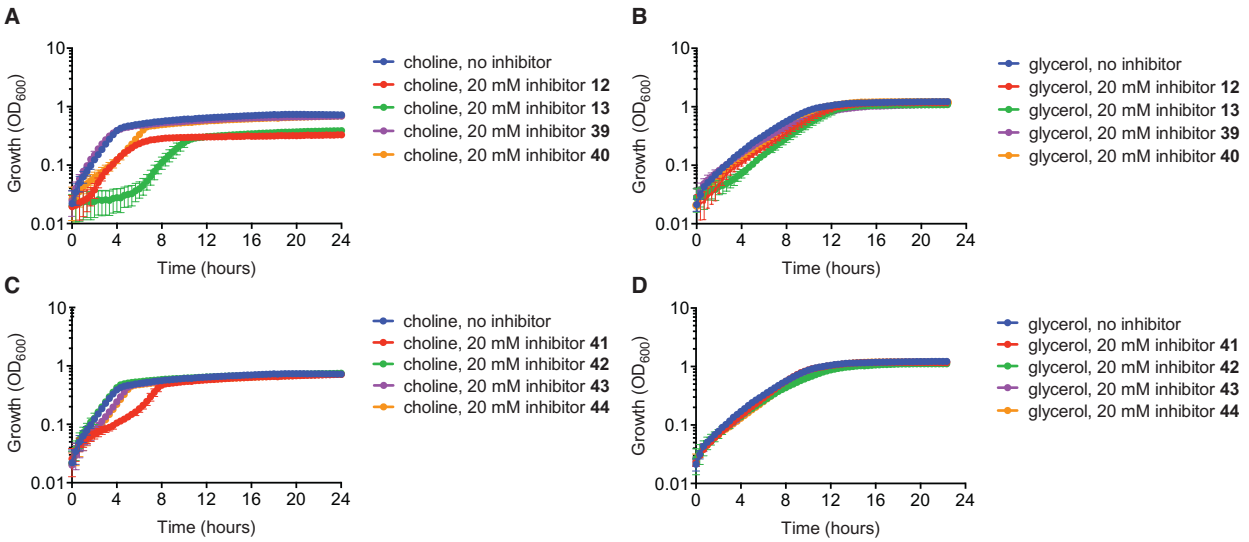

Figure 3.15. Effects of compounds 12, 13, and 39-44 on anaerobic growth of *E. coli* on minimal media. *E. coli* MS 69-1 was grown in an MBraun glovebox, under an N_2 atmosphere, in (A, C) 30 mM choline or (B, D) 30 mM glycerol minimal media. Cultures were supplemented with either phosphate buffer or inhibitor and incubated for 24 hours at 37 °C. Error bars represent the mean ± SD of three replicates (or, in the case of inhibitors **12** and **13**, four replicates).

We then examined an additional panel of compounds that were structurally related to **12** (Table 3.8). As anticipated, substitution of the *tert*-butyl group with a trimethylsilane group (**45**) did not improve potency nor did it impact growth on choline minimal medium (Figure 3.16C). Although the corresponding azide (**46**) was not tested in the *E. coli* whole cell assay, its delay of exponential growth on minimal media was more pronounced on glycerol than on choline, suggesting that it behaves as a bacteriostatic compound (Figure 3.16A,B), which is not surprising given that azides tend to be nucleophilic and react non-specifically with various targets in the cell.

Although the nitro group is considered to be a versatile functional group in medicinal chemistry and is found in a number of clinically approved anticancer, antitubercular, and antiparasitic drugs, it has also been well known to induce severe toxicity.[18] Furthermore, reduction of nitro groups by FMN-dependent nitroreductases produces amines via nitroso and

hydroxylamine intermediates, which are also associated with mutagenicity.[18] Unsurprisingly, the nitro analog (**47**) resulted in complete inhibition of growth on both choline and glycerol minimal media (Figure 3.16A,B), supporting the hypothesis that it functions as a bacteriostatic agent and does not specifically target CutC in cells.

Table 3.8. EC_{50} values and minimal media growth results for compounds 12, 45-50

Compound	Structure	EC_{50} (mM)	Max OD_{600} / Time of ½ max(OD_{600})	
			Choline	Glycerol
—	No inhibitor	—	0.7 / 4.0 h	1.2 / 8.3 h
12	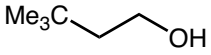	>10	0.3 / 4.7 h	1.1 / 9.7 h
45	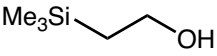	No inhibition	—	—
46	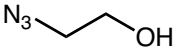	—	0.8 / 5.3 h	1.2 / 9.3 h
47	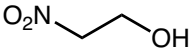	—	0.03 / 0.3 h	0.03 / 0.3 h
48	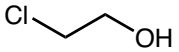	>10	—	—
49	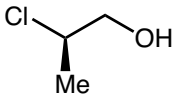	0.92	—	—
50	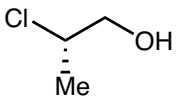	0.45	—	—

E. coli MS 200-1 was incubated in BHI medium containing 1 mM d_9-choline and buffer or inhibitor (tested at ≥3 concentrations) at 37 °C in an anaerobic chamber. [d_9-TMA] was measured by LC-MS/MS after 3.5 hours. Dose-response curves were fit using nonlinear regression to determine the EC_{50}. OD_{600} values were obtained by incubating *E. coli* MS 69-1 with buffer or 20 mM of inhibitor on 30 mM choline or 30 mM glycerol minimal media. Cultures were grown anaerobically for 24 hours at 37 °C.

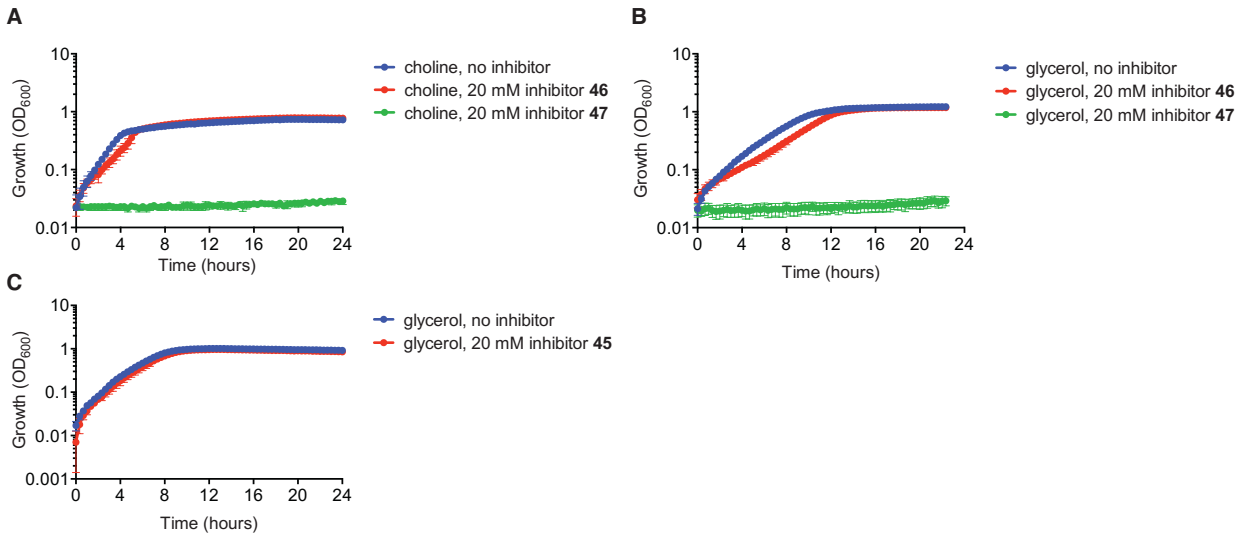

Figure 3.16. Effects of compounds 45-46 on anaerobic growth of *E. coli* on minimal media. *E. coli* MS 69-1 was grown in an MBraun glovebox, under N_2, in minimal media with (A) 30 mM choline or (B) 30 mM glycerol or in a vinyl chamber, under 95% N_2 / 5% H_2, in (C) 30 mM glycerol minimal medium. Cultures were supplemented with buffer or inhibitor and incubated for 24 hours at 37 °C. Error bars represent the mean ± SD of three replicates.

Replacement of the *tert*-butyl moiety of **12** with a chlorine atom yielded the compound **48**, which was completely inactive. However, further modification of **48** with a methyl group on C2 yielded the (*R*)- (**49**) and (*S*)-enantiomers (**50**), which had EC_{50} values of 0.92 and 0.45 mM, respectively. This was our first indication that choline metabolism could be more susceptible to inhibition by one enantiomer of a chiral inhibitor than the other. However, given the small difference in potencies between the two enantiomers, it is impossible to make any definitive conclusions. Nevertheless, we wondered whether this trend would hold true for other chiral molecules.

3.2.2. Development of allylic alcohol compounds as CutC inhibitors

We next began developing a series of allylic alcohols that could potentially function as mechanism-based inhibitors (Table 3.9). If these molecules were to bind in the CutC active site

in an analogous manner to choline, it follows that the Cys489 thiyl radical would abstract the hydrogen atom α- to the allylic alcohol. Unlike with choline, however, the resulting α-hydroxyalkyl radical intermediate would be resonance stabilized by the adjacent alkene, potentially derailing catalysis. We first tested the simple allylic alcohol **51**, which showed modest inhibition with an EC_{50} of 2.3 mM and slightly delayed exponential phase growth on glycerol minimal medium (Figure 3.17B).

Non-stereospecific addition of a methyl group on C1 of compound **51** resulted in a racemic mixture of 3-buten-2-ol (**52**), which was not active (EC_{50} >10 mM). However, moving the methyl group onto C2 of **51** (i.e. β- to the OH) formed the β-methallyl alcohol **53**, which had an EC_{50} of 0.18 mM and slowed the rate of exponential growth on choline minimal medium (Figure 3.17A). Compound **53** has not been investigated for its effect on growth in glycerol minimal medium but, when tested *in vitro* assay recombinant CutC, it exhibited a relatively high IC_{50} of 642 μM compared to betaine aldehyde (**9**, IC_{50} = 23 μM) (Figure 3.18). 2-Chloroallyl alcohol (**54)** was 10 times more potent in *E. coli* than **53**, displaying an EC_{50} of 14 μM and inhibiting growth on choline minimal medium without impacting growth on glycerol (Figure 3.17) or rich medium (Figure 3.19). Its bromine analog (**55**) had a similar potency of 29 μM.

Table 3.9. EC_{50} values and minimal media growth results for compounds 51-60

Compound	Structure	EC_{50} (mM)	Max OD_{600} / Time of ½ max(OD_{600})	
			Choline	Glycerol
—	No inhibitor	—	1.0 / 4.0 h	1.0 / 6.3 h
51	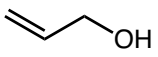	2.3	—	1.0 / 9.0 h
52	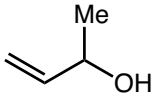	>10	—	1.0 / 6.7 h
53	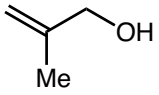	0.18	1.0 / 9.3 h	—
54	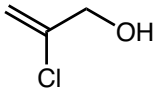	1.4×10^{-2}	0.2 / 1.7 h	1.1 / 7.0 h
55	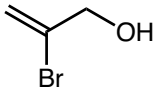	2.9×10^{-2}	—	—
56	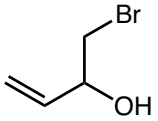	1.0	—	—
57	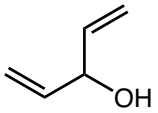	0.58	—	—
58	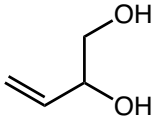	0.1 mM: 15%	—	—
59	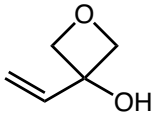	0.1 mM: 35%	—	—
60	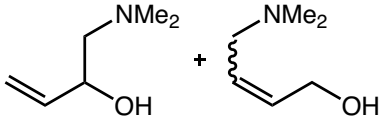 **a** + **b**	4.1×10^{-2}	0.7 / 11.7 h	—

Table 3.9. (continued) *E. coli* MS 200-1 was incubated in BHI containing 1 mM d_9-choline and either buffer or inhibitor (tested at ≥3 concentrations, except for compounds **58** and **59**) at 37 °C in an anaerobic chamber. [d_9-TMA] was measured by LC-MS/MS after 3.5 hours. Dose-response curves were fit using nonlinear regression to determine the EC_{50}. OD_{600} values were obtained by incubating *E. coli* MS 69-1 with buffer or 20 mM inhibitor in 30 mM choline or 30 mM glycerol minimal media. Cultures were grown anaerobically for 24 hours at 37 °C.

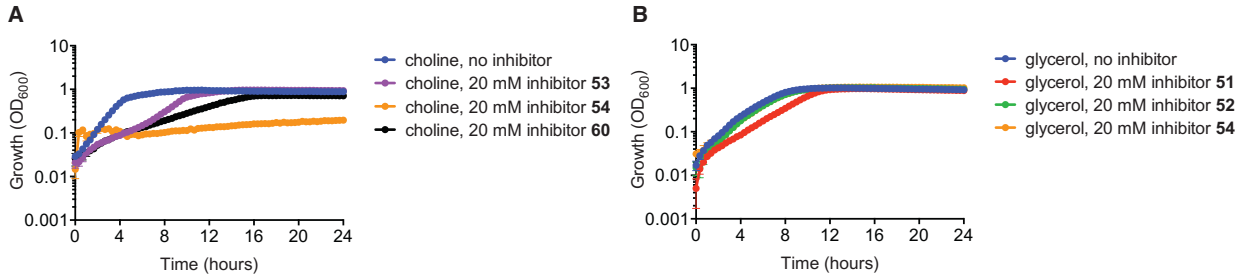

Figure 3.17. Effects of compounds 51-54 and 60 on anaerobic growth of *E. coli* on minimal media. *E. coli* MS 69-1 was grown in a vinyl glovebox, under 95% N_2 / 5% H_2, in minimal media with either (A) 30 mM choline or 30 mM glycerol. Cultures were supplemented with either phosphate buffer or inhibitor and incubated for 24 hours at 37 °C. Error bars represent the mean ± SD of three replicates.

Non-specific methylbromine substitution on C1 of the allylic alcohol scaffold (compound **51**) furnished the racemic mixture **56**, which showed modest inhibition of TMA production (EC_{50} = 1.0 mM). Placing two vinyl groups α- to the alcohol (compound **57**) increased potency by only ~4-fold relative to the parent compound, **51**. Non-stereospecific attachment of methanol on C1 of the allylic alcohol framework resulted in the racemic mixture **58**. At, 100 μM of 3-butene-1,2-diol (**58**) reduced TMA production in *E. coli* by 15% relative to the negative control (no inhibitor). In the same assay, 100 μM of betaine aldehyde (**9**) reduced TMA levels by 28%. Thus, on the basis of potency, diol **58** was not found suitable for further development.

Replacement of the methanol group of **58** with an oxetane ring proved to be a more promising strategy for increasing activity (Table 3.9). At 100 μM, 3-vinyloxetan-3-ol (**59**) reduced TMA production in *E. coli* by 35%. The oxetane functional group is present in several biologically active molecules and is an attractive element for medicinal chemistry.[19,20] The best-

known example of an oxetane-containing drug is probably the natural product paclitaxel, marketed under the brand name Taxol, which is utilized as a chemotherapeutic agent that binds to and stabilizes microtubules. Although lower activity was observed for synthetic paclitaxel analogs that lacked the oxetane ring, studies have shown that this moiety is not essential for biological activity. Instead, the small, polar heterocycle improves the pharmacokinetic properties of Taxol and other drugs, functioning as a surrogate for *gem*-dimethyl and carbonyl groups and increasing the solubility and rigidity of drug scaffolds.

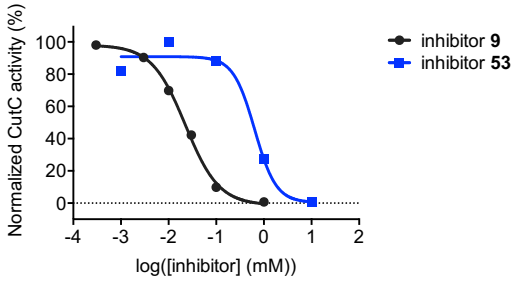

Figure 3.18. Effect of compounds 9 and 53 on CutC-mediated TMA production *in vitro*. The activity of CutC was coupled to that of yeast alcohol dehydrogenase. Inhibitors (0.30 μM to 1 mM) were added prior to the addition of choline. The absorbance of NADH at 340 nm was recorded over time to calculate initial rates and kinetic parameters. Initial rates were normalized to a control assay without inhibitor, and data were fit using nonlinear regression in Graphpad Prism to obtain IC_{50} values of 23 and 642 μM for compounds **9** and **53**, respectively. Error bars represent the mean ± SD of three replicates.

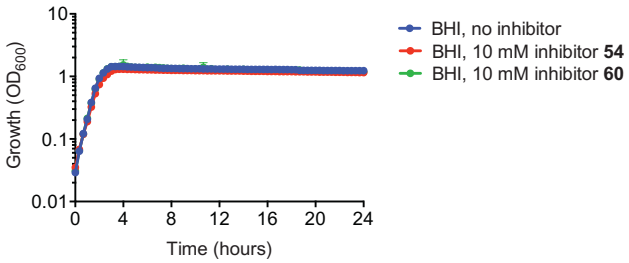

Figure 3.19. Effect of compounds 54 and 60 on anaerobic growth of *E. coli* on rich medium. *E. coli* MS 200-1 was grown on BHI medium containing 11 mM glucose in a vinyl chamber, under 95% N_2 / 5% H_2. Cultures were supplemented with phosphate buffer or inhibitor and incubated for 24 hours at 37 °C. Error bars represent the mean ± SD of three replicates.

A mixture of stereoisomers containing the allylic alcohol functionality and the methylamine moiety of choline (in this case, a dimethylamine) was synthesized by the contract research organization WuXi. The isomers were not further purified but tested as one mixture (**60**), which displayed an EC_{50} of 41 μM and drastically slowed growth on choline minimal medium (Table 3.9, Figure 3.17A). Mixture **60** has not been investigated on glycerol medium.

Next, analogs of β-methallyl alcohol (**53**, EC_{50} = 0.18 mM) were tested (Table 3.10). Replacing the OH moiety with a thiol (**61**, no inhibition), an amine (**62**, EC_{50} = 1.2 mM), or a carbonyl (**63**, EC_{50} = 1.2 mM) did not provide any major improvements in cellular potency. For this reason, these compounds were not tested on choline minimal media, although they were incubated on glycerol and did not cause any discernable growth defects (Figure 3.20). Exchanging the alkene substituent with a carbonyl (**64**) proved unsuccessful for lowering the EC_{50}, despite that a carbonyl group could stabilize the radical formed on the adjacent carbon.

Table 3.10. EC_{50} values and minimal media growth results for compounds 53, 61-64

Compound	Structure	EC_{50} (mM)	Max OD_{600} / Time of ½ max(OD_{600})	
			Choline	Glycerol
—	No inhibitor	—	1.0 / 4.0 h	1.1 / 6.0 h
53	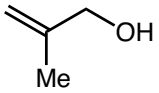	0.18	1.0 / 9.3 h	—
61	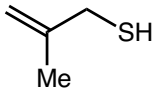	No inhibition	—	1.0 / 5.7 h
62	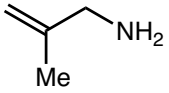	1.2	—	1.0 / 6.3 h
63	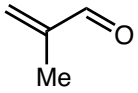	1.2	—	1.0 / 6.3 h
64	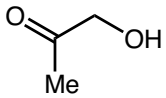	>10	—	—

E. coli MS 200-1 was incubated in BHI containing 1 mM d_9-choline and either buffer or inhibitor (tested at ≥3 concentrations) at 37 °C in an anaerobic chamber. [d_9-TMA] was measured by LC-MS/MS after 3.5 hours. Dose-response curves were fit using nonlinear regression to determine the EC_{50}. OD_{600} values were obtained by incubating *E. coli* MS 69-1 with either buffer or 20 mM of inhibitor (or 10 mM of compounds **62** and **63**) in 30 mM choline or 30 mM glycerol minimal media. Cultures were grown anaerobically for 24 hours at 37 °C.

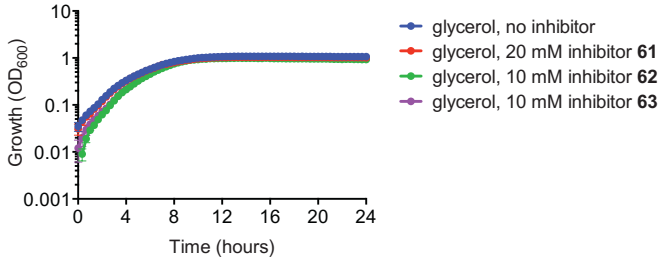

Figure 3.20. Effects of compounds 61-63 on anaerobic growth of *E. coli* on minimal media. *E. coli* MS 69-1 was grown in a vinyl chamber, under 95% N_2 / 5% H_2, in minimal medium with 30 mM glycerol. Cultures were incubated with either buffer or inhibitor for 24 hours at 37 °C. Error bars represent the mean ± SD of three replicates (or, for inhibitor **61**, two replicates).

As noted above, the stereoisomers tested together as mixture **60** (EC_{50} = 41 μM) were a promising starting point (Table 3.9) for further analog design. Although we have not isolated or synthesized pure enantiomers of 1-(dimethylamino)but-3-en-2-ol (referred to as **60a**), we began testing a series of analogs based on this scaffold (Table 3.11). The allylic alcohol with a methylamine substitution on C2 (**65**) proved to be more potent (EC_{50} = 0.32 mM) than its analog, 3-amino-2-methyl-1-propanol (**66,** EC_{50} > 10 mM), which lacks the vinyl group and therefore cannot stabilize the radical generated on C1. When tested for inhibition of CutC *in vitro*, alcohol **65** (IC_{50} = 39 μM) performed similarly to betaine aldehyde (**9**, IC_{50} = 23 μM) (Figure 3.21).

Exchange of the primary amine of **65** for a hydroxyl generated the methylene-propanediol **67**, which had a similar EC_{50} (0.53 mM) to **65** in whole cells and slowed exponential growth on choline without affecting growth on glycerol (Figure 3.22A,B). Diol **67** was not potent *in vitro,* however (Figure 3.21). Removal of a vinyl group from diol **67** resulted in loss of cellular potency for compound **68**, again highlighting that the alkene might be crucial for inhibition. Changing the position of the methanol substituent in compound **67** to afford (*Z*)-but-2-ene-1,4-diol (**69**) did not considerable change cellular potency, but replacement of the methanol with a propyl group rendered the resulting (*Z*)-alkene (**70**) ineffective at lowering TMA levels in whole cells. Although the (*E*)-isomer (**71**) showed modest activity, possessing an EC_{50} of 1.2 mM, it inhibited growth on glycerol minimal medium (Figure 3.22C).

Table 3.11. EC_{50} values and minimal media growth results for compounds 60a, 65-71

Compound	Structure	EC_{50} (mM)	Max OD_{600} / Time of ½ max(OD_{600})	
			Choline	Glycerol
—	No inhibitor	—	1.0 / 4.0 h	1.0 / 6.0 h
60a	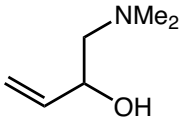	—	—	—
65	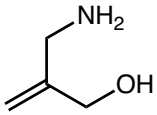	0.32	—	1.0 / 6.0 h
66	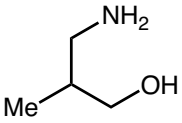	>10	—	—
67	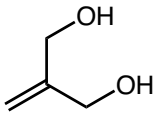	0.53	0.8 / 8.7 h	0.9 / 6.0 h
68	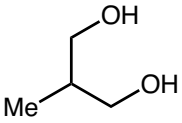	>10	—	—
69	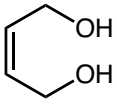	0.36	—	1.0 / 6.0 h
70	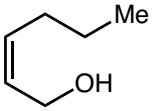	No inhibition	—	0.9 / 6.0 h
71	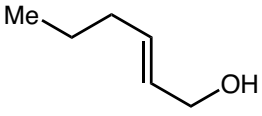	1.2	—	0.04 / 0.3 h

E. coli MS 200-1 was incubated in BHI containing 1 mM d_9-choline and either buffer or inhibitor (tested at ≥3 concentrations) at 37 °C in an anaerobic chamber. [d_9-TMA] was measured by LC-MS/MS after 3.5 hours. Dose-response curves were fit using nonlinear regression to determine the EC_{50}. OD_{600} values were obtained by incubating *E. coli* MS 69-1 with either buffer or 20 mM of inhibitor in 30 mM choline or 30 mM glycerol minimal media. Cultures were grown anaerobically for 24 hours at 37 °C.

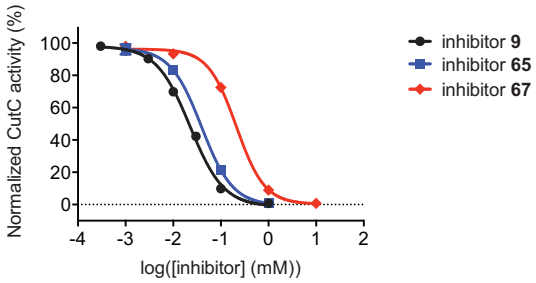

Figure 3.21. Effects of compounds 9, 65, and 67 on CutC-mediated TMA production *in vitro*. Activity of CutC was coupled to that of YADH. Inhibitors were added prior to choline. Absorbance of NADH at 340 nm was recorded over time to calculate initial rates and kinetic parameters. Initial rates were normalized to a control without inhibitor, and data were fit using nonlinear regression in Graphpad Prism to obtain IC_{50} values of 23, 39, and 212 μM for compounds **9**, **65**, and **67**, respectively. Error bars represent the mean ± SD of three replicates.

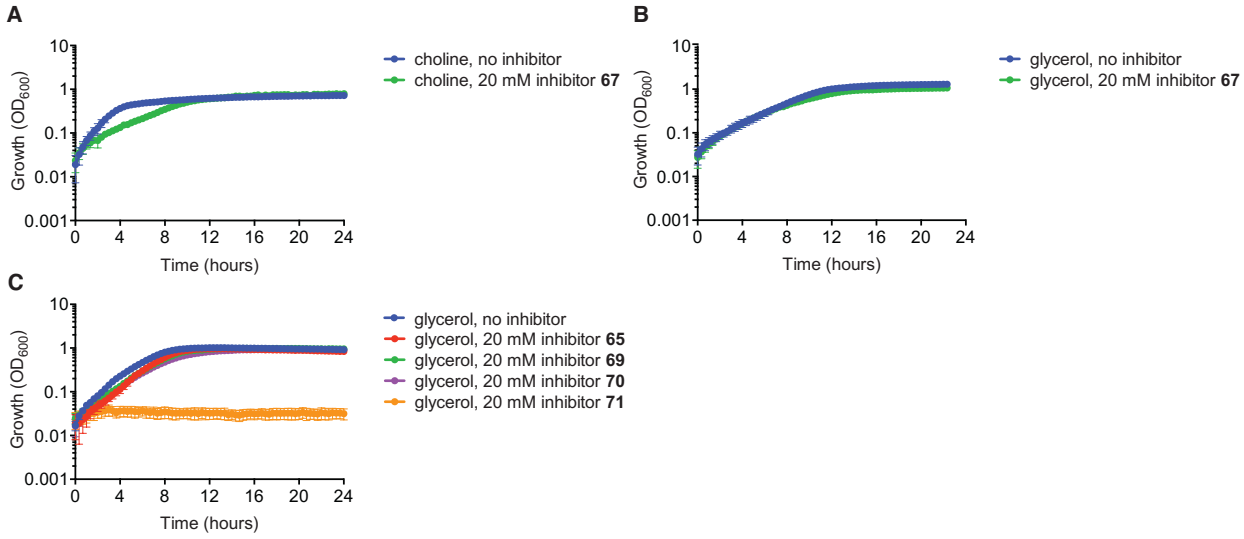

Figure 3.22. Effects of compounds 65, 67, and 69-71 on anaerobic growth of *E. coli* on minimal media. *E. coli* MS 69-1 was grown in an MBraun glovebox, under an N_2 atmosphere, in minimal media with either (A) 30 mM choline or 30 mM glycerol or in a vinyl chamber, under 95% N_2 and 5% H_2, in (C) 30 mM glycerol minimal media. Cultures were supplemented with phosphate buffer or inhibitor and incubated for 24 hours at 37 °C. Error bars represent the mean ± SD of three replicates.

As was the case for the mixture of enantiomers referred to as **60a**, we have not isolated or synthesized the various stereoisomers of 4-(dimethylamino)-2-buten-1-ol (together referred to as mixture **60b**). Nevertheless, we continued to develop the scaffold of **60b**, substituting the

dimethylamino moiety of the (*E*)-isomer with a chlorine atom (**72**) or the hydroxyl group with a carboxylic acid (**73**) (Table 3.12). While the racemic mixture **72** was not tested at a range of concentrations, adding 100 μM of this compound to *E. coli* growing in choline-containing rich medium resulted in an 18% decrease of TMA relative to the negative control (no inhibitor). In this same assay, 100 μM of betaine aldehyde (**9**, EC_{50} = 0.40 mM) and of racemic mixture **73** (EC_{50} = 1.5 mM) lowered TMA levels by 28% and 10%, respectively. Thus, neither **72** nor **73** appeared to be potential CutC inhibitors.

Table 3.12. EC_{50} values and minimal media growth results for compounds 60b, 72, 73

Compound	Structure	EC_{50} (mM)	Max OD_{600} / Time of ½ max(OD_{600})	
			Choline	Glycerol
—	No inhibitor	—	1.0 / 4.0 h	1.0 / 6.0 h
60b	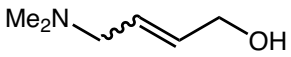	—	—	—
72	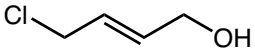	0.1 mM: 18%	—	—
73	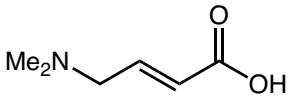	1.5	—	—

E. coli MS 200-1 was incubated in BHI medium containing 1 mM d_9-choline and either phosphate buffer or inhibitor (tested at ≥3 concentrations, except for compound **72**) at 37 °C in an anaerobic chamber. [d_9-TMA] was measured by LC-MS/MS after 3.5 hours. Dose-response curves were fit using nonlinear regression to determine the EC_{50}. OD_{600} values were obtained by incubating *E. coli* MS 69-1 with either buffer or 20 mM of inhibitor on 30 mM choline or 30 mM glycerol minimal media. Cultures were grown anaerobically for 24 hours at 37 °C.

3.2.3. Development of cyclic compounds as CutC inhibitors

Our next strategy relied on reducing the number of rotatable bonds in our inhibitor scaffolds. We first connected the C2 and nitrogen atoms of choline within a pyrrolidine ring (Table 3.13), resulting in the racemic mixture **74**, whose potency (EC_{50} = 0.30 mM) was on par with betaine aldehyde. Unlike betaine aldehyde, mixture **74** did not impact growth on choline (Figure 3.23A). It did not appear to act as a bacteriostatic agent given its lack of impact on glycerol (Figure 3.23B), nor did it affect growth on rich medium (Figure 3.24). The (*S*)-enantiomer (**75**) of this compound possessed a similar EC_{50} as the racemic mixture, while the (*R*)-enantiomer (**76**) was 10-fold less potent, suggesting that the active site of CutC, if indeed it is the target of these inhibitors, might preferentially bind one stereoisomer over the other.

Table 3.13. EC_{50} values and minimal media growth results for compounds 74-78

Compound	Structure	EC_{50} (mM)	Max OD_{600} / Time of ½ max(OD_{600})	
			Choline	Glycerol
—	No inhibitor	—	0.9 / 4.3 h	1.0 / 6.0 h
74	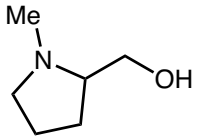	0.30	1.1 / 4.7 h	1.0 / 5.7 h
75	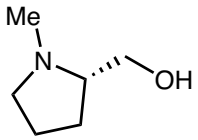	0.29	—	—
76	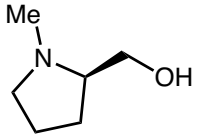	2.0	—	—
77	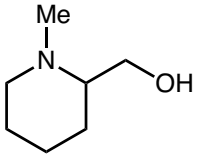	0.12	1.0 / 4.7 h	1.0 / 5.7 h
78	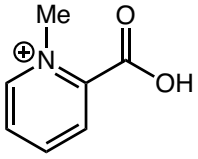	3.4	—	—

E. coli MS 200-1 was incubate in BHI medium containing 1 mM d_9-choline and either phosphate buffer or inhibitor (tested at ≥3 concentrations) at 37 °C in an anaerobic chamber. [d_9-TMA] was measured by LC-MS/MS after 3.5 hours. Dose-response curves were fit using nonlinear regression to determine the EC_{50}. OD_{600} values were obtained by incubating *E. coli* MS 69-1 with either buffer or 10 mM of inhibitor in 30 mM choline or 30 mM glycerol minimal media. Cultures were grown anaerobically for 24 hours at 37 °C.

Increasing the size of the heterocycle from a pyrrolidine to a piperidine (mixture **77**) improved the EC_{50} slightly (by ~2-fold). Although this mixture did not affect growth on glycerol or on rich medium, it also did not noticeably impact growth on choline minimal media (Figures 3.23 and 3.24). As mentioned previously, a molecule's effect on choline-dependent growth may not necessarily correlate with its potency. Pure enantiomers of mixture **77** have not been isolated.

Exchanging the piperidine for a pyridine and the primary alcohol for a carboxylic acid resulted in the compound referred to as trigonelline (**78**),[21] which showed a modest potency of 3.8 mM.

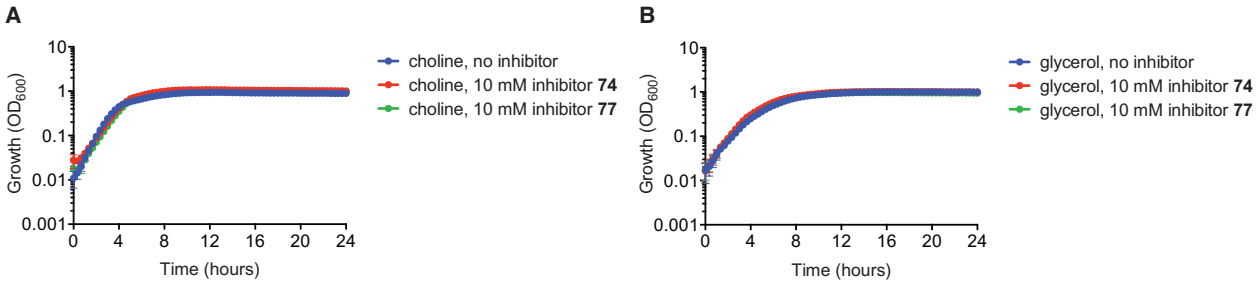

Figure 3.23. Effects of compounds 74-77 on anaerobic growth of *E. coli* on minimal media. *E. coli* MS 69-1 was grown in a vinyl chamber, under an atmosphere of 95% N_2 / 5% H_2, in minimal media with either (A) 30 mM choline or (B) 30 mM glycerol. Cultures were supplemented with phosphate buffer or inhibitor and incubated for 24 hours at 37 °C. Error bars represent the mean ± SD of two replicates.

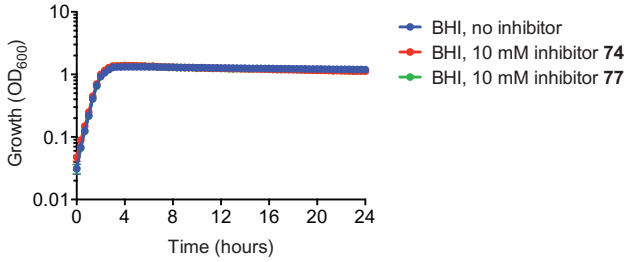

Figure 3.24. Effects of compounds 74 and 77 on anaerobic growth of *E. coli* on rich medium. *E. coli* MS 200-1 was grown in BHI medium containing 11 mM glucose in a vinyl chamber, under 95% N_2 / 5% H_2. Cultures were supplemented with either buffer or inhibitor and incubated for 24 hours at 37 °C. Error bars represent the mean ± SD of three replicates.

Incorporating C1, C2, and the nitrogen atoms of choline into a pyrrolidine ring resulted in the racemic mixture **79** (Table 3.14), which was 10-fold less potent than the previously tested choline-based pyrrolidine (**74**). However, unlike **74**, it delayed growth on choline minimal media without impacting growth on glycerol (Figure 3.25). Compound **80**, the ketone analog of **79**, proved to be a poor inhibitor. The *N*-dimethylated analog of **79** was tested as a pure (*R*)-enantiomer (**81**), which exhibited modest inhibition with an EC_{50} of 2.1 mM and delayed growth on both choline and glycerol minimal media (Figure 3.25). Exchanging the hydroxyl group of **79** for a thiol resulted in the racemic mixture **82**, which, when tested in the *in vitro* assay with recombinant CutC, was unable to inhibit TMA production from choline, even at the highest concentration tested (1 mM) (Figure 3.26).

Table 3.14. EC_{50} values and minimal media growth results for compounds 79-82

Compound	Structure	EC_{50} (mM)	Max OD_{600} / Time of ½ max(OD_{600})	
			Choline	Glycerol
—	No inhibitor	—	0.7 / 3.3 h	1.3 / 7.3 h
74	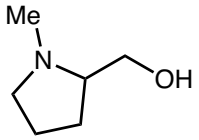	0.30	1.1 / 4.7 h	1.0 / 5.7 h
79	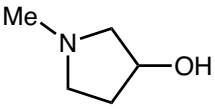	6.3	0.9 / 5.0 h	1.3 / 7.3 h
80	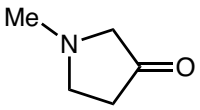	>10	—	—
81	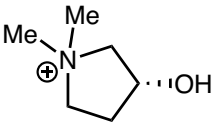	2.1	0.8 / 8.7 h	1.3 / 11.0 h
82	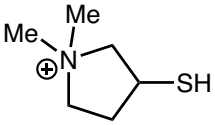	—	—	—

E. coli MS 200-1 was incubated in BHI containing 1 mM d_9-choline and either phosphate buffer or inhibitor (tested at ≥3 concentrations) at 37 °C in an anaerobic chamber. [d_9-TMA] was measured by LC-MS/MS after 3.5 hours. Dose-response curves were fit using nonlinear regression to determine the EC_{50}. OD_{600} values were obtained by incubating *E. coli* MS 69-1 with either buffer or 20 mM of inhibitor in 30 mM choline or 30 mM glycerol minimal media. Cultures were grown anaerobically for 24 hours at 37 °C.

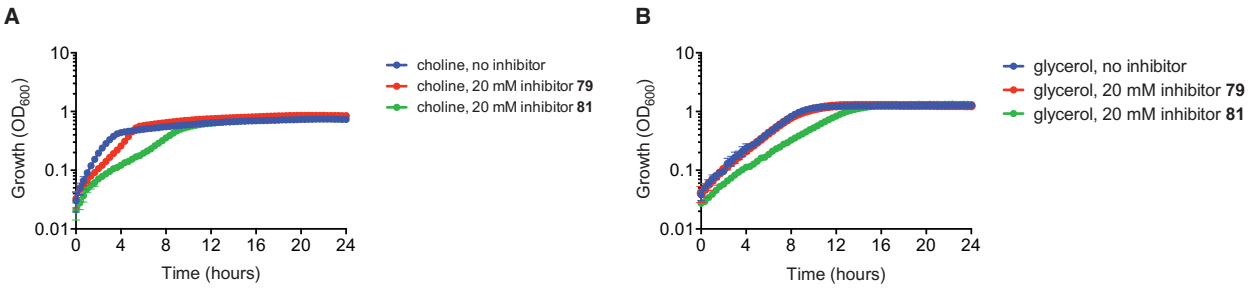

Figure 3.25. Effects of compounds 79 and 81 on anaerobic growth of *E. coli* on minimal media. *E. coli* MS 69-1 was grown in an MBraun glovebox, under N_2, in minimal media with either (A) 30 mM choline or (B) 30 mM glycerol. Cultures were incubated with buffer or inhibitor for 24 hours at 37 °C. Error bars represent the mean ± SD of three replicates.

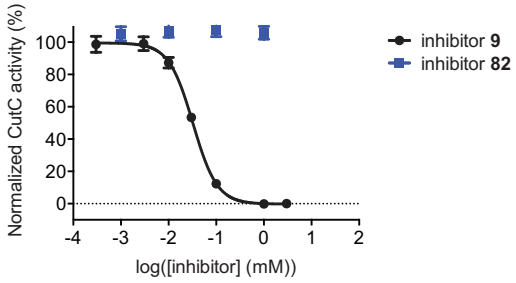

Figure 3.26. Effects of compounds 9 and 82 on CutC-mediated TMA production *in vitro*. Activity of CutC was coupled to that of YADH. Inhibitors were added prior to choline. A_{340} of NADH was recorded over time to calculate initial rates and kinetic parameters. Initial rates were normalized to a control without inhibitor, and data were fit using nonlinear regression in Graphpad Prism to obtain an IC_{50} = 33 μM for compound **9**, whereas no IC_{50} could be computed for compound **82**. Error bars represent the mean ± SD of three replicates.

Increasing the size of the heterocycle from a pyrrolidine to a piperidine produced a racemic mixture of 1-methylpiperidin-3-ol (**83**) and resulted in a 10-fold increase in potency in *E. coli* whole cells compared to pyrrolidine **79** (Table 3.15). This compound slowed growth on choline without affecting growth on glycerol (Figure 3.27). As was seen for inhibitors **79** and **80**, exchanging the hydroxyl of **83** for a carbonyl (**84**) was detrimental to activity. We had observed that the *N*-dimethylated pyrrolidine (**81**) was ~4-fold more potent than its mono-methylated analog (**79**). However, this same principle did not hold true for piperidinine **83** and its N-dimethylated version (**85**). Compound **86**, in which the *meta*-positioned hydroxyl was moved

para to the nitrogen in the piperidine, exhibited modest potency (EC_{50} = 4.5 mM), as did the methylmorpholine analog (**87**). Increasing the size of the heterocycle from piperidine to azapane gave the racemic mixture 1-methylazepan-4-ol (**88**), which was well tolerated (EC_{50} = 0.76 mM).

Table 3.15. EC_{50} values and minimal media growth results for compounds 79, 83-88

Compound	Structure	EC_{50} (mM)	Max OD_{600} / Time of ½ max(OD_{600})	
			Choline	Glycerol
—	No inhibitor	—	0.7 / 3.3 h	1.3 / 7.3 h
79	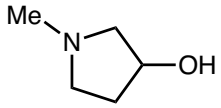	6.3	0.9 / 5.0 h	1.3 / 7.3 h
83	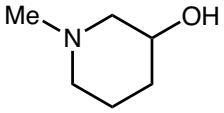	0.95	0.8 / 4.7 h	1.3 / 7.7 h
84	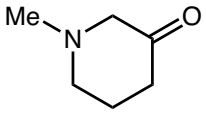	9.5	—	—
85	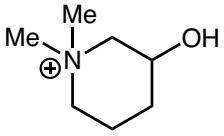	>10	—	—
86	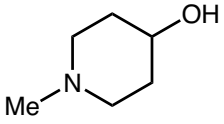	4.5	—	—
87	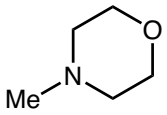	4.5	—	—
88	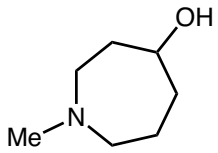	0.76	—	

Table 3.15 (continued) *E. coli* MS 200-1 was incubated in BHI containing 1 mM d_9-choline and either buffer or inhibitor (tested at ≥3 concentrations) at 37 °C in an anaerobic chamber. [d_9-TMA] was measured by LC-MS/MS after 3.5 hours. Dose-response curves were fit using nonlinear regression to determine the EC_{50}. OD_{600} values were obtained by incubating *E. coli* MS 69-1 with buffer or 20 mM of inhibitor on 30 mM choline or 30 mM glycerol minimal media. Cultures were grown anaerobically for 24 hours at 37 °C.

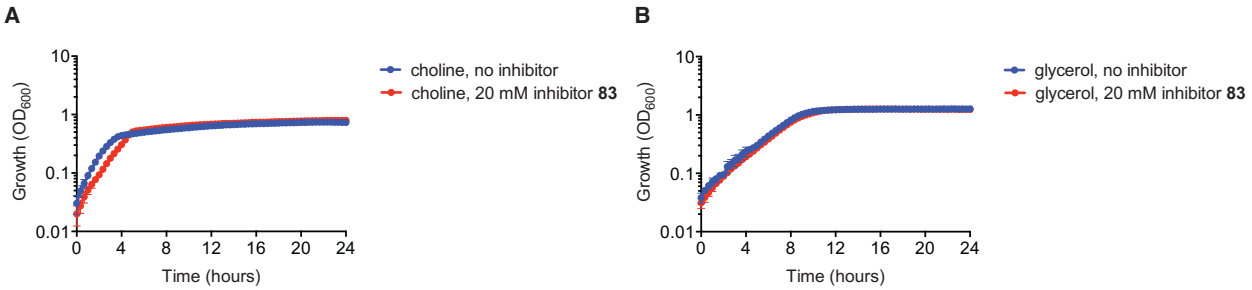

Figure 3.27. Effects of compound 83 on anaerobic growth of *E. coli* on minimal media. *E. coli* MS 69-1 was grown in an MBraun glovebox, under an N_2, on minimal media with either (A) 30 mM choline or (B) 30 mM glycerol. Cultures were supplemented with buffer or inhibitor and incubated for 24 hours at 37 °C. Error bars represent the mean ± SD of three replicates.

3.2.4. Combining the allylic alcohol and cyclic compound scaffolds to identify novel CutC inhibitors

The next compounds developed (Table 3.16) were based on combining structural features found in the cyclic series of inhibitors, such as 1-methylpiperidin-3-ol (**83**, EC_{50} = 0.95 mM) and the putative mechanism-based allylic alcohol inhibitors, such as the stereoisomers of **60** (EC_{50} = 41 μM). We first tested a racemic mixture of 2-cyclohexen-1-ol (**89**), which had an EC_{50} of 0.33 mM and delayed growth on glycerol minimal medium (Figure 3.28B). The pure (*S*)- and (*R*)-enantiomers, compounds **90** and **91**, respectively, did not lead to noticeable changes in potency. These stereoisomers were not tested on minimal media.

Exchanging C5 of compound **89** for an oxygen atom resulted in a racemic mixture of the unsaturated heterocycle **92**, which showed strong inhibitory activity, with an EC_{50} of 26 μM and did not affect growth on rich medium (Figure 3.29). However, the pyranol **92** inhibited growth

on both choline and glycerol minimal media (Figure 3.28). The (*R*)- and (*S*)-enantiomers of **92**, compounds **93** and **94**, respectively, were also tested, and showed EC_{50} values of 85 and 16 μM, respectively. Adding a methyl group onto C2 of the cyclohexenol scaffold resulted in racemic mixture **95**, which displayed poor potency and inhibited growth on glycerol (Figure 3.28B). Moving the methyl group to C3 resulted in modest inhibition by the racemic mixture **96** (EC_{50} = 3.8 mM).

Table 3.16. EC_{50} values and minimal media growth results for compounds 89-96

Compound	Structure	EC_{50} (mM)	Max OD_{600} / Time of ½ max(OD_{600})	
			Choline	Glycerol
—	No inhibitor	—	0.9 / 4.3 h	1.1 / 6.0 h
89	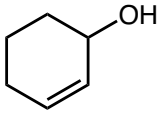	0.33	—	0.9 / 9.3 h
90	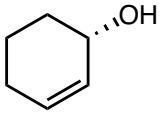	0.35	—	—
91	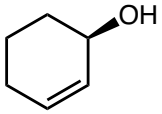	0.48	—	—
92	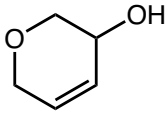	2.6×10^{-2}	0.02 / 0.3 h	0.04 / 0.3 h
93	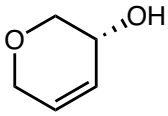	8.5×10^{-2}	—	—
94	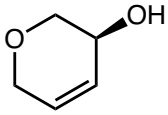	1.6×10^{-2}	—	—
95	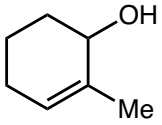	>10	—	0.5 / 13.3 h
96	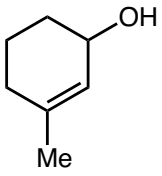	3.8	—	—

Table 3.16 (continued) *E. coli* MS 200-1 was incubated in BHI medium containing 1 mM d_9-choline and phosphate buffer or inhibitor (tested at ≥3 concentrations) at 37 °C in an anaerobic chamber. [d_9-TMA] was measured by LC-MS/MS after 3.5 hours. Dose-response curves were fit using nonlinear regression to determine the EC_{50}. OD_{600} values were obtained by incubating *E. coli* MS 69-1 with phosphate buffer or 20 mM of inhibitor on 30 mM choline or 30 mM glycerol minimal media. Cultures were grown anaerobically for 24 hours at 37 °C.

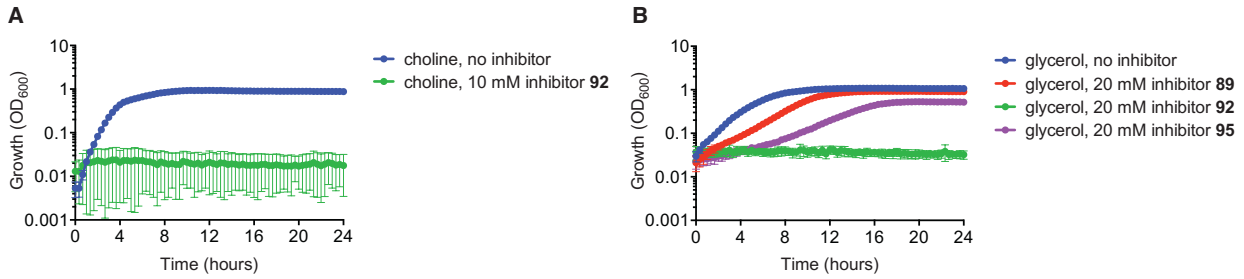

Figure 3.28. Effects of compounds 89, 92, and 95 on anaerobic growth of *E. coli* on minimal media. *E. coli* MS 69-1 was grown in a vinyl chamber, under an atmosphere of 95% N_2 / 5% H_2, in minimal media with either (A) 30 mM choline or (B) 30 mM glycerol. Cultures were supplemented with either buffer or inhibitor and incubated for 24 hours at 37 °C. Error bars represent the mean ± SD of three replicates (or, in the case of inhibitor **92**, two replicates).

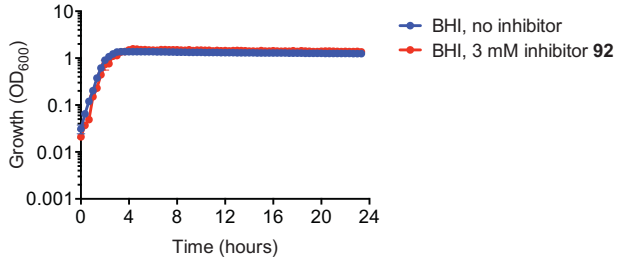

Figure 3.29. Effect of compound 92 on anaerobic growth of *E. coli* on rich medium. *E. coli* MS 200-1 was grown on BHI medium containing 11 mM glucose in a vinyl chamber, under 95% N_2 / 5% H_2. Cultures were supplemented with phosphate buffer or inhibitor and incubated for 24 hours at 37 °C. Error bars represent the mean ± SD of three replicates.

Simply by increasing the size of the saturated heterocycle, from pyrrolidine **79** (EC_{50} = 6.3 mM) to piperidine **83** (EC_{50} = 0.95 mM), we were able to obtain a 10-fold increase in potency. We had also seen promising results with the putative mechanism-based allylic alcohols, particularly mixture **60** (41 μM). Encouraged by this result, we combined the two scaffolds to

generate a series of unsaturated heterocyclic alcohols (Table 3.17). The racemic mixture of 1-methyl-1,2,3,6-tetrahydropyridin-3-ol (**97**) was highly potent in whole cells (EC_{50} = 10 μM) and significantly delayed the rate of growth on choline minimal media without affecting growth on glycerol (Figure 3.30A,B) or on rich medium (Figure 3.31). The (*R*)- and (*S*)-enantiomers of **97**, compounds **98** and **99**, respectively, were tested and found to exhibit a similar potency as the racemic mixture, with the (*S*)-isomer (**99**) slightly more active (EC_{50} values of 16 and 10 μM, respectively). This same stereochemical preference, albeit to a stronger degree, was seen with the racemic mixture **92** and its enantiomers **93** and **94**. In addition, compounds **98** and **99** severely impacted growth on choline without affecting growth on glycerol (Figure 3.30A,B), suggesting that they may selectively target choline metabolism.

To assess whether reduction of TMA formation by (*R*)-**98** and (*S*)-**99** arose from inhibition of CutC, we performed *in vitro* experiments with recombinant CutC and CutD, obtaining IC_{50} values of 6.7 and 1.4 μM, respectively (Figure 3.32). This suggests that the ability of these molecules to reduce TMA levels in *E. coli* may indeed arise from their direct targeting of CutC inside cells. The *in vitro* data also confirmed the stereochemical preference for the (*S*)-enantiomer (**99**), which is consistent with the EC_{50} results obtained with whole cells.

Table 3.17. EC_{50} values and minimal media growth results for compounds 97-104

Compound	Structure	EC_{50} (mM)	Max OD_{600} / Time of ½ max(OD_{600})	
			Choline	Glycerol
—	No inhibitor	—	1.0 / 4.7 h	1.1 / 5.7 h
97	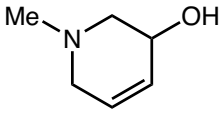	1.0×10^{-2}	0.6 / 16.0 h	1.1 / 6.0 h
98	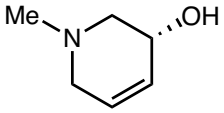	1.6×10^{-2}	0.2 / 10.7 h	1.1 / 6.0 h
99	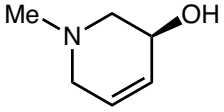	1.0×10^{-2}	0.7 / 15.0 h	1.0 / 6.3 h
100	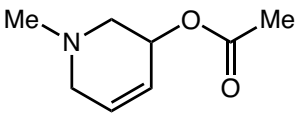	1.8	—	—
101	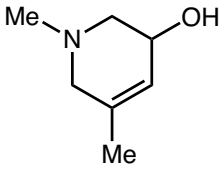	0.92	—	—
102	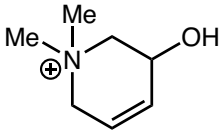	9.9×10^{-3}	0.5 / 13.7 h	1.1 / 7.3 h
103	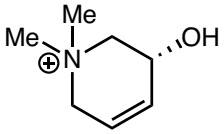	2.3×10^{-2}	0.7 / 13.3 h	1.1 / 7.0 h
104	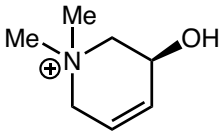	9.1×10^{-3}	0.7 / 15.0 h	1.1 / 6.0 h

E. coli MS 200-1 was incubated in BHI medium containing 1 mM d_9-choline and either phosphate buffer or inhibitor (tested at ≥3 concentrations) at 37 °C in an anaerobic chamber. [d_9-

TMA] was measured by LC-MS/MS after 3.5 hours. Dose-response curves were fit using nonlinear regression to determine the EC_{50}. OD_{600} values were obtained by incubating *E. coli* MS 69-1 with either buffer or 20 mM of inhibitor on 30 mM choline or 30 mM glycerol minimal media. Cultures were grown anaerobically for 24 hours at 37 °C.

Substitution of the hydroxyl group of 1-methyl-1,2,3,6-tetrahydropyridin-3-ol (**97**) with an acetate (**100**) resulted in a 100-fold decrease in potency in *E. coli*, which was surprising given that the ester group would likely be hydrolyzed in cells to release the potent alcohol **97**. In fact, ester pro-drug moieties have been exploited to shift polarity, increase bioavailability, decrease toxicity, and disrupt unfavorable interactions of common antibiotics, including the β-lactams.[22] The core structure of most β-lactam drugs includes a carboxylate group that participates in binding to active site residues of their target enzymes, transpeptidases, which are responsible for bacterial cell wall synthesis. One strategy for improving the poor bioavailability of some β-lactams is to mask their carboxylate moieties with lipophilic esters, which can then be cleaved by human or bacterial esterases.

Appending a methyl group onto C3 of hydropyridine **97** afforded the racemic mixture **101**, which was ~100-fold less potent than the parent compound. On the other hand, mixture **102,** the *N*-dimethyl analogs of **97**, displayed similar activity (EC_{50} = 9.9 μM) as the parent compound. While the *N*-dimethyl mixture did not noticeably impact growth on glycerol minimal medium or on rich medium, its delay of growth on choline was striking (Figures 3.30C,D and 3.31). In the *in vitro* assay with recombinant CutC, mixture **102** proved to be highly potent, with an IC_{50} of 0.82 μM (Figure 3.32). Encouraged by these results, the (*R*)- and (*S*)-enantiomers of **102**, compounds **103** and **104**, respectively, were tested in *E. coli*. Once again, the (*S*)-isomer (**104**) proved to be more potent, with an EC_{50} of 9.1 μM (versus 23 μM for **103**). Both stereoisomers did not affect growth on glycerol but delayed growth on choline (Figure 3.30C,D).

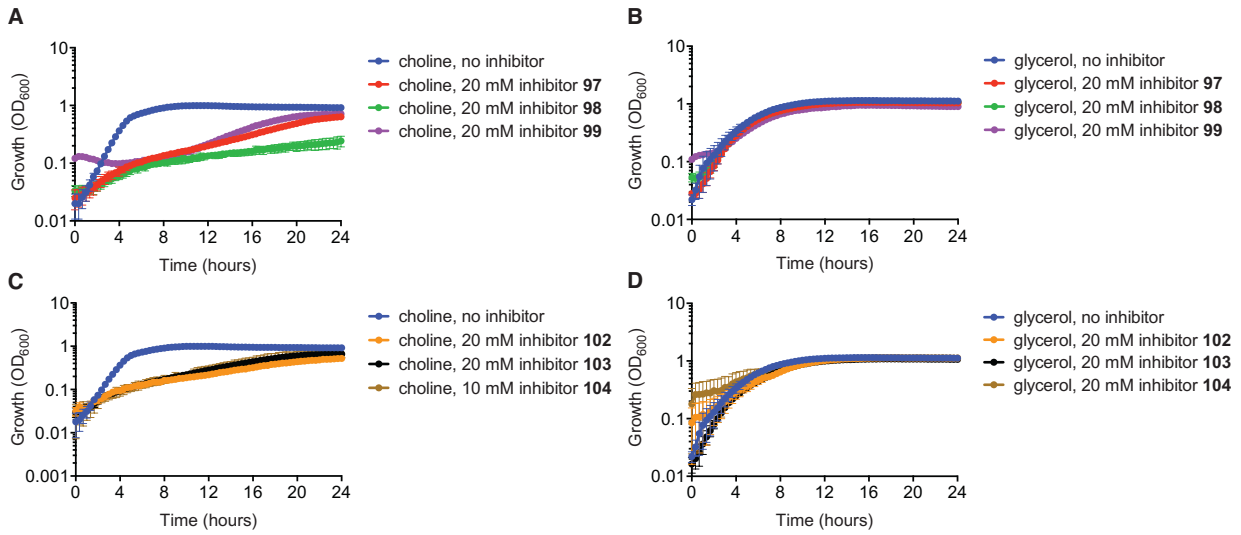

Figure 3.30. Effects of compounds 97-35 on anaerobic growth of *E. coli* on minimal media. *E. coli* MS 69-1 was grown in a vinyl chamber, under an atmosphere of 95% N_2 / 5 % H_2, in (A, C) 30 mM choline or (B, D) 30 mM glycerol minimal media. Cultures were supplemented with either phosphate buffer or inhibitor and incubated for 24 hours at 37 °C. Error bars represent the mean ± SD of three replicates (or, in the case of inhibitors **98**, **102**, and **104**, two replicates).

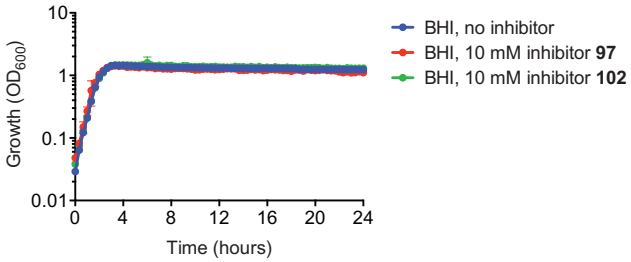

Figure 3.31. Effects of compounds 97 and 102 on anaerobic growth of *E. coli* on rich medium. *E. coli* MS 200-1 was grown in BHI medium containing 11 mM glucose in a vinyl chamber, under 95% N_2 / 5% H_2. Cultures were supplemented with either phosphate buffer or inhibitor and incubated for 24 hours at 37 °C. Error bars represent the mean ± SD of three replicates.

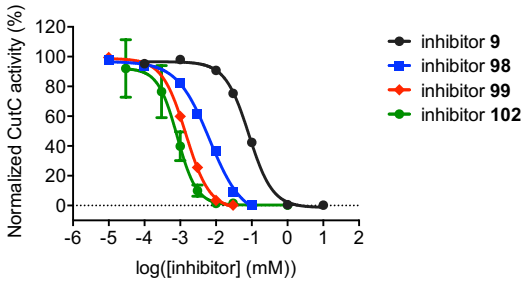

Figure 3.32. Effects of compounds 9, 98, 99, and 102 on CutC-mediated TMA production *in vitro*. Activity of CutC was coupled to that of yeast alcohol dehydrogenase. Inhibitors were added prior to choline. A_{340} of NADH was recorded over time to calculate initial rates and kinetic parameters. Initial rates were normalized to a control without inhibitor, and data were fit using nonlinear regression in Graphpad Prism to obtain IC_{50} values of 83, 6.7, 1.4, and 0.82 μM for **9**, **98**, **99**, and **102**, respectively. Error bars represent the mean ± SD of three replicates.

We wanted to see if expanding the steric bulk on the nitrogen of the hydropyridine **97** (EC_{50} = 10 μM) could further improve its potency (Table 3.18). Adding a cyclobutyl group, resulting in the racemic mixture **105**, decreased activity by 10-fold in the *E. coli* whole cell assay and inhibited growth on both choline and glycerol minimal media (Figure 3.33). Exchanging the cyclobutyl for a cyclopentyl ring resulted in **106**, whose potency was similar to compound **97**. While racemic mixture **106** delayed growth on glycerol minimal medium, it completely inhibited growth on choline medium (Figure 3.33), suggesting that it may be possible to find a range of concentrations at which this compound will selectively inhibit choline metabolism without exerting cytotoxic effects. Furthermore, mixture **106** did not impact growth on rich medium (Figure 3.34).

Table 3.18. EC_{50} values and minimal media growth results for compounds 97, 105-111

Compound	Structure	EC_{50} (mM)	Max OD_{600} / Time of ½ max(OD_{600})	
			Choline	Glycerol
—	No inhibitor	—	1.0 / 4.7 h	1.0 / 5.7 h
97	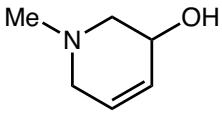	1.0×10^{-2}	0.6 / 16.0 h	1.1 / 6.0 h
105	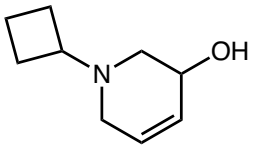	0.15	0.8 / 15.7 h	0.8 / 11.3 h
106	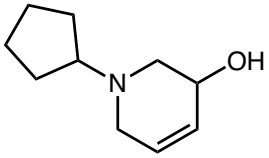	3.6×10^{-2}	0.05 / 0.3 h	0.9 / 15.0 h
107	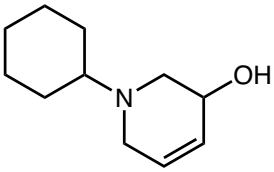	2.9×10^{-2}	0.09 / 20.7 h	0.1 / 15.0 h
108	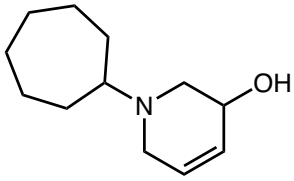	2.4×10^{-2}	—	—
109	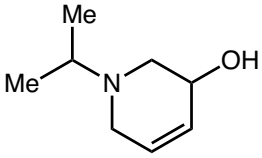	3 mM: 4%	—	—
110	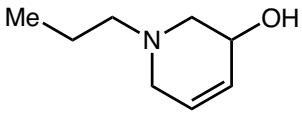	0.14	—	0.8 / 6.0 h
111	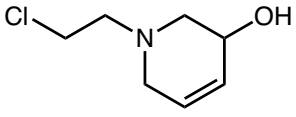	3 mM: 32%	—	—

Table 3.18 (continued) *E. coli* MS 200-1 was incubated containing BHI with 1 mM d_9-choline and either buffer or inhibitor (tested at ≥3 concentrations, except for compounds **109** and **111**) at 37 °C in an anaerobic chamber. [d_9-TMA] was measured by LC-MS/MS after 3.5 hours. Dose-response curves were fit using nonlinear regression to determine the EC_{50}. OD_{600} values were obtained by incubating *E. coli* MS 69-1 with either buffer or 10 mM of inhibitor on 30 mM choline or glycerol minimal media. Cultures were grown anaerobically for 24 hours at 37 °C.

Further increasing the steric bulk of the unsaturated heterocycle **97** by appending an *N*-cyclohexane (**107**) or *N*-cycloheptane (**108**) moiety did not affect potency. However, the racemic mixture **107** completely inhibited growth on both choline and glycerol minimal media (Figure 3.33), although it did not effect growth on BHI medium (Figure 3.34). Mixture **108** was not tested on minimal media.

Replacing the cyclic ring with a more flexible alkyl chain, such as isobutane (**109**), led to a substantial loss of potency. In the whole cell assay, 3 mM of **109** caused a mere 4% reduction of TMA levels in *E. coli* relative to the negative control (no inhibitor), whereas 1 mM of betaine aldehyde (**9**) caused an 86% reduction. Swapping the isobutane for a propyl chain resulted in racemic mixture **110**, which demonstrated an EC_{50} similar to that of the cyclobutyl-containing analog **105**, but, unlike **105**, did not lead to inhibition of growth on glycerol minimal medium (Figure 3.33B). Exchanging the propyl group for a dimethylchlorine (**111**) produced a compound that, when tested at 3 mM, inhibited TMA levels in *E. coli* whole cells by only 32% relative to the negative control (no inhibitor).

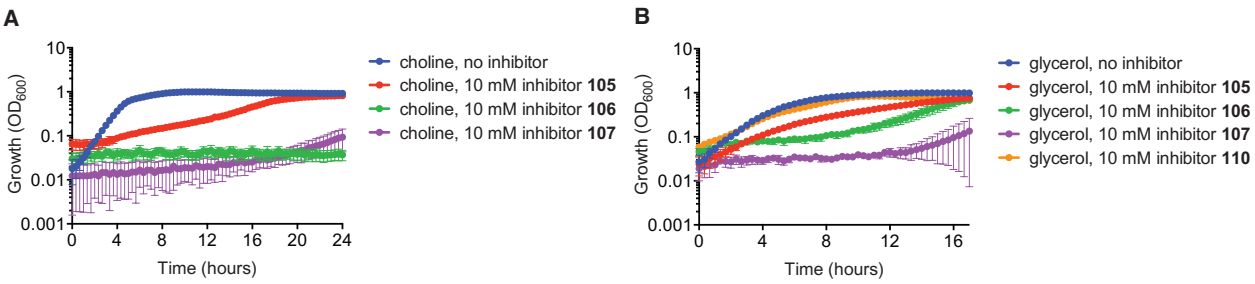

Figure 3.33. Effects of compounds 105-107 on anaerobic growth of *E. coli* on minimal media. *E. coli* MS 69-1 was grown in a vinyl chamber, under an atmosphere of 95% N_2 / 5% H_2, in minimal media with either (A) 30 mM choline or (B) 30 mM glycerol. Cultures were supplemented with buffer or inhibitor and incubated for 24 hours at 37 °C. Error bars represent the mean ± SD of three replicates (or, in the case of inhibitors **105**, **107**, and **110**, two replicates).

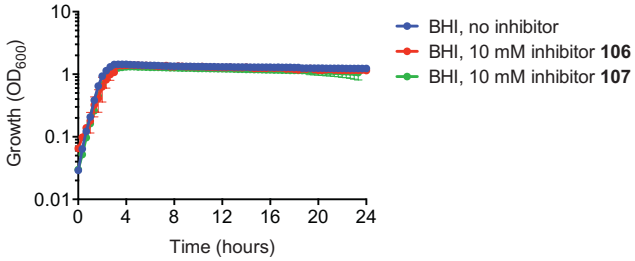

Figure 3.34. Effects of compounds 106 and 107 on anaerobic growth of *E. coli* on rich medium. *E. coli* MS 200-1 was grown in BHI medium containing 11 mM glucose in a vinyl chamber, under 95% N_2 / 5% H_2. Cultures were supplemented with either phosphate buffer or inhibitor and incubated for 24 hours at 37 °C. Error bars represent the mean ± SD of three replicates (or two replicates for inhibitor **106**).

The (*R*)- and (*S*)-enantiomers of the *N*-cyclobutyl-substituted unsaturated heterocycle **105**, compounds **112** and **113**, respectively, displayed similar activity to the racemic mixture (Table 3.19). They also delayed growth on glycerol and choline minimal media (Figure 3.35).

Table 3.19. EC_{50} values and minimal media growth results for compounds 105, 112, 113

Compound	Structure	EC_{50} (mM)	Max OD_{600} / Time of ½ max(OD_{600})	
			Choline	Glycerol
–	No inhibitor	–	1.0 / 4.7 h	0.9 / 8.0 h
105	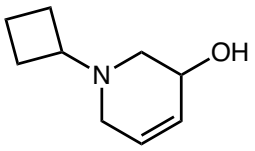	0.15	1.0 / 4.7 h	0.9 / 11.0 h
112	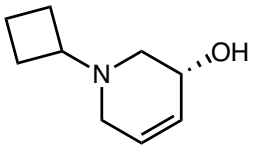	0.19	0.8 / 17.3 h	0.9 / 12.3 h
113	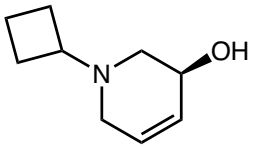	0.12	0.8 / 16.7 h	0.9 / 10.0 h

E. coli MS 200-1 was incubated in BHI containing 1 mM d_9-choline and buffer or inhibitor (teat ≥3 concentrations) at 37 °C in an anaerobic chamber. [d_9-TMA] was measured after 3.5 hours. Dose-response curves were fit using nonlinear regression to determine the EC_{50}. OD_{600} values were obtained by incubating *E. coli* MS 69-1 with buffer or 10 mM inhibitor in 30 mM choline or glycerol minimal media. Cultures were grown anaerobically for 24 hours at 37 °C.

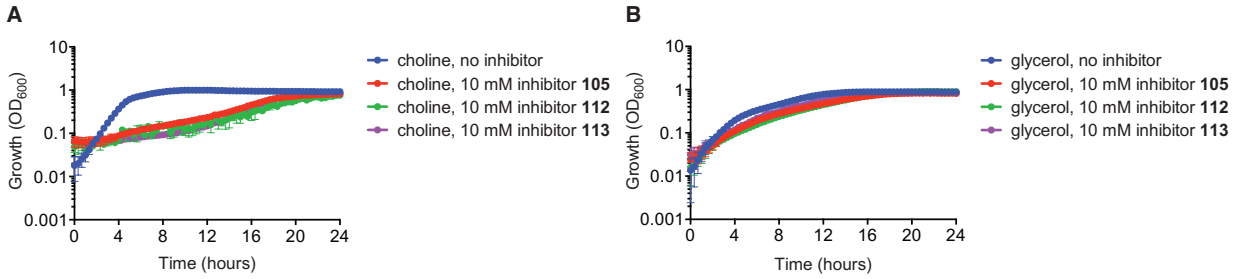

Figure 3.35. Effects of compounds 105, 112, and 113 on anaerobic growth of *E. coli* on minimal media. *E. coli* MS 69-1 was grown in a vinyl chamber, under 95% N_2 / 5% H_2, in minimal media with either (A) 30 mM choline or (B) 30 mM glycerol. Cultures were supplemented with buffer or inhibitor and incubated for 24 hours at 37 °C. Error bars represent the mean ± SD of three replicates (or, in the case of inhibitors **105** and **113**, two replicates).

Similarly, there was no obvious difference between the *N*-cyclopentane (*R*)- and (*S*)-enantiomers, compounds **114** and **115**, respectively, in terms of potency (Table 3.20). However, while the racemic mixture (**106**) and the (*R*)-enantiomer (**114**) inhibited growth on choline minimal medium, they also increased the length of lag phase growth on glycerol (Figure 3.36). The (*S*)-enantiomer (**115**) slowed the rate of exponential growth on choline minimal media without affecting growth on glycerol (Figure 3.36), suggesting that there may be a preference for this particular stereoisomer in the CutC active site. None of the *N*-cyclopentane compounds (**106**, **114**, and **115**) affected growth on BHI medium (Figure 3.37).

This stereochemical preference for the OH on the unsaturated ring was seen in the case of **92** and its enantiomers, **93** and **94**, as well as **97**, **98**, and **99** and **102**, **103**, and **104**. However, it should be noted that the (*S*)-enantiomer (**115**) was tested on minimal media at a lower concentration (5 mM) than the mixture **106** or the (*R*)-enantiomer (**114**), both of which were tested at 10 mM. It is possible that, at 10 mM, compound **115** will also cause a delay in growth on glycerol minimal media.

Table 3.20. EC_{50} values and minimal media growth results for compounds 106, 114-118

Compound	Structure	EC_{50} (mM)	Max OD_{600} / Time of ½ max(OD_{600})	
			Choline	Glycerol
—	No inhibitor	—	1.0 / 4.7 h	1.0 / 5.7 h
106	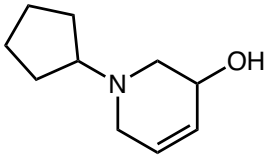	5.4×10^{-2}	0.05 / 0.3 h	0.9 / 15.0 h
114	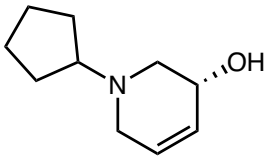	6.2×10^{-2}	0.6 / 20.0 h	1.1 / 10.7 h
115	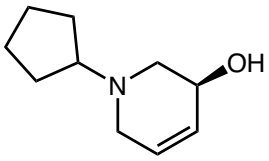	4.1×10^{-2}	1.0 / 8.3 h*	1.0 / 7.0 h*
116	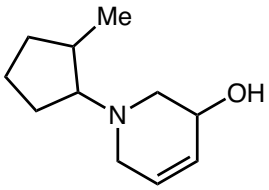	1.4×10^{-2}	0.9 / 17.0 h	0.9 / 8.7 h
117	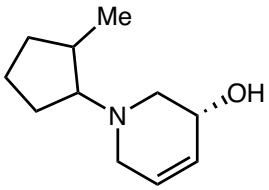	0.16 0.17	—	—
118	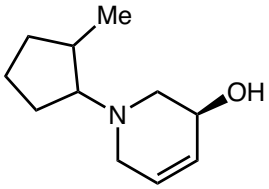	8.8×10^{-3} 9.4×10^{-3}	—	—

E. coli MS 200-1 was grown anaerobically at 37 °C in BHI containing 1 mM d_9-choline and buffer or inhibitor (≥3 concentrations). [d_9-TMA] was measured after 3.5 hours. Dose-response curves were fit using nonlinear regression to determine EC_{50}. **116** is a mixture of 4 diastereomers. The two EC_{50} values for **116** and **117** correspond to the two diastereomers of each compound. OD_{600} values were obtained by incubating *E. coli* MS 69-1 with buffer or 10 mM

inhibitor (*5 mM for inhibitor **115**) on 30 mM choline or glycerol minimal media. Cultures were grown anaerobically for 24 hours at 37 °C.

Non-stereospecific addition of a methyl group at C2 of the cyclopentyl-containing enantiomers (**106)** resulted in a mixture of four *N*-substituted methylcyclopentyl diastereomers (**116**), which showed a small (~4-fold) increase in potency (EC_{50} = 14 μM) relative to the parent compound. Although this mixture (**116)** slightly delayed growth on glycerol minimal media, it severely impacted growth on choline (Figure 3.36) without affecting growth on BHI (Figure 3.37). While these results seemed promising, in the *in vitro* assay with recombinant, activated CutC, treatment with **116** resulted in little to no change in TMA production from the negative control (Figure 3.38). At the highest concentration of **116** tested (10 μM), CutC activity remained at 92% relative to the control, whereas the same concentration of betaine aldehyde (**9**), which has a ~30-fold higher EC_{50} in *E. coli* (0.40 mM), reduced CutC activity to 83%.

The 4 diastereomers of **116** were separated into two groups: mixture **117**, containing two diastereomers with the OH in the (*R*)-configuration, and mixture **118**, containing two diasteromers with the OH in the (*S*)-configuration. Both mixtures were further purified into their diastereomeric components, generating **117a**, **117b**, **118a**, and **118b**. The position of the methyl group (*R* versus *S*) on the *N*-cyclopentane moiety of these compounds has not been assigned. Diastereomers **118a** and **118b** displayed similar activities (EC_{50} = 8.8 and 9.4 μM, respectively) in *E. coli* and were ~100 times more potent than both **117a** and **117b** (EC_{50} = 0.16 and 0.17 mM, respectively), again supporting the preference for the (*S*)-stereochemistry of the OH at C3 of the unsaturated ring.

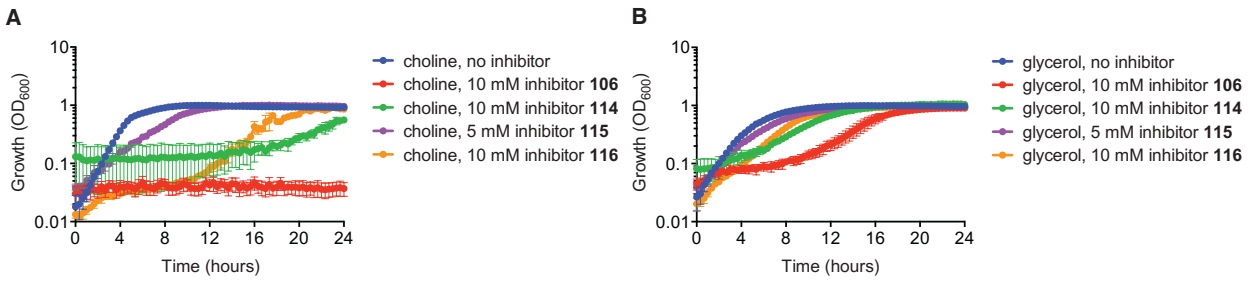

Figure 3.36. Effects of compounds 106 and 114-116 on anaerobic growth of *E. coli* on minimal media. *E. coli* MS 69-1 was grown in a vinyl chamber, under an atmosphere of 95% N_2 / 5% H_2, in minimal media with either (A) 30 mM choline or (B) 30 mM glycerol. Cultures were supplemented with buffer or inhibitor and incubated for 24 hours at 37 °C. Error bars represent the mean ± SD of three replicates (or two replicates in the case of inhibitor **116**).

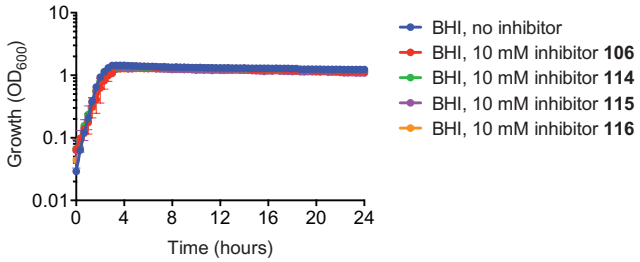

Figure 3.37. Effects of compounds 106 and 114-116 on anaerobic growth of *E. coli* on rich medium. *E. coli* MS 200-1 was grown in BHI medium containing 11 mM glucose in a vinyl chamber, under 95% N_2 / 5% H_2. Cultures were supplemented with either phosphate buffer or inhibitor and incubated for 24 hours at 37 °C. Error bars represent the mean ± SD of three replicates (or two replicates for inhibitor **106**).

The individual diastereomers **117a**, **117b**, **118a**, and **118b** performed similarly to the mixture (**116**) in the *in vitro* assay with recombinant enzyme (Figure 3.38), exhibiting little inhibition of CutC activity even at 10 μM. While higher concentrations can be tested, it is worthwhile to note that inhibitors **98** and **99**, which bear an *N*-methyl in place of the N-methylcyclopentyl moiety of **116-118** and possess similar EC_{50} values of 10-16 μM, showed strong inhibitory activity *in vitro*, with IC_{50} values of 1.4-6.7 μM (Figure 3.23). Thus, this suggests that the ability of molecules **116-118** to reduce TMA levels in *E. coli* does not arise from their direct targeting of CutC inside cells but from an alternative mechanism that is

currently unknown. This non-selectivity for CutC may explain the delay of growth on glycerol minimal medium caused by mixture **116** (Figure 3.36).

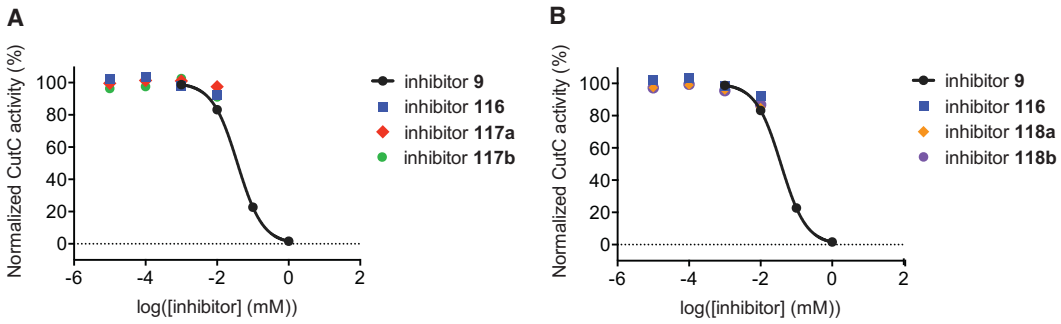

Figure 3.38. Effects of compounds 9, 116, 117a, 117b, 118a, and 118b on CutC-mediated TMA production *in vitro*. Activity of CutC was coupled to that of YADH. Inhibitors were added prior to choline. A_{340} of NADH was recorded over time to calculate initial rates and kinetic parameters. Initial rates were normalized to a control without inhibitor, and data were fit using nonlinear regression in Graphpad Prism to obtain IC_{50} values of 37 μM for **9**. IC_{50} values could not be calculated for **116**, **117a**, **117b**, **118a**, and **118b**. Error bars represent the mean ± SD of three replicates.

Exchange of the methyl group of compound **116** for a chlorine atom afforded a mixture of stereoisomers (**119**) that showed decreased potency (by ~4-fold) in *E. coli* relative to the parent compound (Table 3.21). Changing the position of the methyl from C2 to C3 of the cylcopentyl ring generated stereoisomers, which were tested as one mixture (**120**), whose potency was similar to that of **116**. Like mixture **116**, **120** delayed growth on glycerol and inhibited growth on choline minimal medium (Figure 3.39), suggesting that it is also non-selective for CutC. Mixture **116** did not affect growth on BHI medium (Figure 3.40). Replacement of the cyclopentane moiety with a tetrahydrothiophene furnished a set of compounds with only modest activity (**121**).

Table 3.21. EC_{50} values and minimal media growth results for compounds 106, 114-118

Compound	Structure	EC_{50} (mM)	Max OD_{600} / Time of ½ max(OD_{600})	
			Choline	Glycerol
—	No inhibitor	—	1.0 / 4.7 h	1.0 / 5.7 h
116	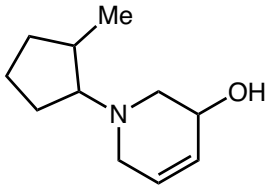	1.4×10^{-2}	0.9 / 17.0 h	0.9 / 8.7 h
119	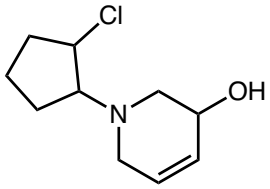	5.2×10^{-2}	—	—
120	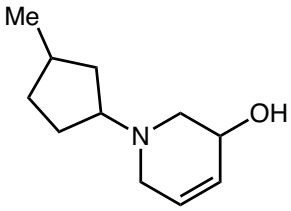	5.0×10^{-2}	0.2 / 13.7 h	0.9 / 13.0 h
121	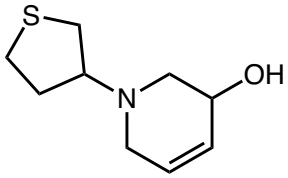	0.17	—	—
122	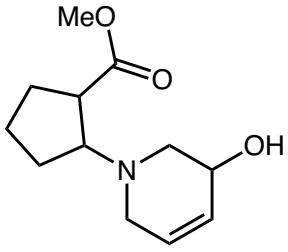	1 mM: 62%	—	—

E. coli MS 200-1 was incubated in BHI medium containing 1 mM d_9-choline and buffer or inhibitor (tested at ≥3 concentrations, except for compound **122**) at 37 °C in an anaerobic chamber. [d_9-TMA] was measured by LC-MS/MS after 3.5 hours. Dose-response curves were fit using nonlinear regression to determine the EC_{50}. OD_{600} values were obtained by incubating *E. coli* MS 69-1 with either buffer or 10 mM of inhibitor on 30 mM choline or 30 mM glycerol minimal media. Cultures were grown anaerobically on 96-well plates for 24 hours at 37 °C.

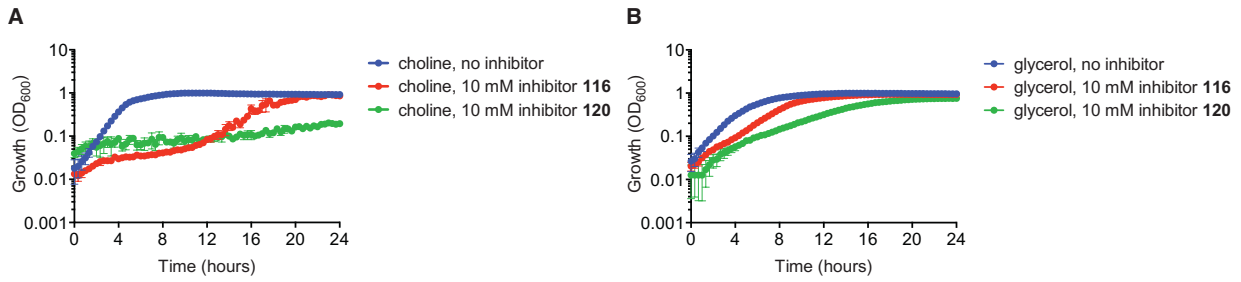

Figure 3.39. Effects of compounds 116 and 120 on anaerobic growth of *E. coli* on minimal media. *E. coli* MS 69-1 was grown in a vinyl chamber, under an atmosphere of 95% N_2 / 5% H_2, in minimal media with either (A) 30 mM choline or (B) 30 mM glycerol. Cultures were supplemented with buffer or inhibitor and incubated for 24 hours at 37 °C. Error bars represent the mean ± SD of three replicates (or two replicates in the case of inhibitor **116**).

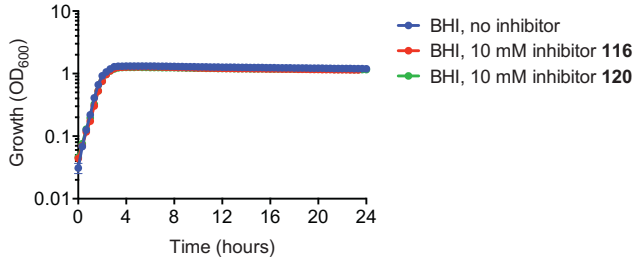

Figure 3.40. Effects of compounds 106 and 120 on anaerobic growth of *E. coli* on rich medium. *E. coli* MS 200-1 was grown in BHI medium containing 11 mM glucose in a vinyl chamber, under 95% N_2 / 5% H_2. Cultures were supplemented with either buffer or inhibitor and incubated for 24 hours at 37 °C. Error bars represent the mean ± SD of three replicates.

Exchange of the methyl group of compound **116** for a methyl acetate afforded a mixture of enantiomers (**122**) that, at 1 mM, decreased TMA levels by 62% relative to the negative control. In this same assay, 1 mM of betaine aldehyde (**9**) decreased TMA by 100%, indicating the comparatively low potency of the methyl acetate analog (**122**).

In the case of the racemic mixture of cyclohexyl-substituted tetrahydropyridin-3-ol (**107,** EC_{50} = 29 μM), the (*S*)-enantiomer (**124**) proved to be more potent than its (*R*)-isomer (**123**) by a factor of 10 (Table 3.22). However, both enantiomers inhibited growth on glycerol and choline minimal media (Figure 3.41), suggesting that they are not specific for choline metabolism in bacterial cells.

Table 3.22. EC_{50} values and minimal media growth results for compounds 107, 123-127

Compound	Structure	EC_{50} (mM)	Max OD_{600} / Time of ½ max(OD_{600})	
			Choline	Glycerol
—	No inhibitor	—	1.0 / 4.7 h	1.0 / 5.7 h
107	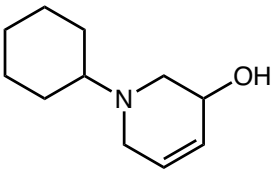	2.9×10^{-2}	0.09 / 20.7 h	0.1 / 15.0 h
123	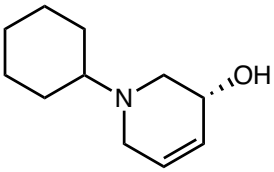	0.11	0.02 / 0.3 h	0.01 / 17.7 h
124	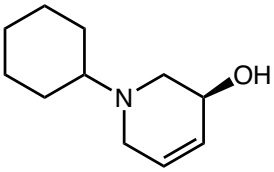	1.4×10^{-2}	0.02 / 0.3 h	0.02 / 1.0 h
125	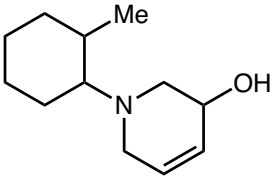	1.4×10^{-3}	0.06 / 11.7 h	0.03 / 0.3 h
126	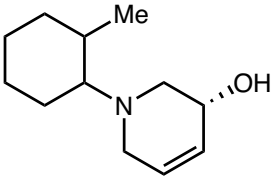	6.8×10^{-2}	—	—
127	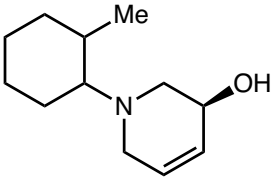	1.2×10^{-3}	—	—

E. coli MS 200-1 was incubated in BHI medium containing 1 mM d_9-choline and phosphate buffer or inhibitor (tested at ≥3 concentrations) at 37 °C in an anaerobic chamber. [d_9-TMA] was

measured by LC-MS/MS after 3.5 hours. Dose-response curves were fit using nonlinear regression to determine the EC_{50}. OD_{600} values were obtained by incubating *E. coli* MS 69-1 with phosphate buffer or 10 mM of inhibitor on 30 mM choline or 30 mM glycerol minimal media. Cultures were grown anaerobically on 96-well plates for 24 hours at 37 °C.

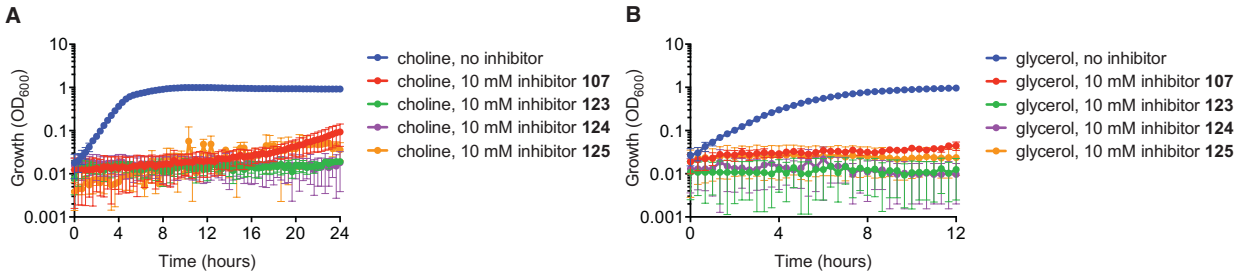

Figure 3.41. Effects of compounds 107, 123-125 on anaerobic growth of *E. coli* on minimal media. *E. coli* MS 69-1 was grown in a vinyl chamber, under an atmosphere of 95% N_2 / 5% H_2, in minimal media with either (A) 30 mM choline or (B) 30 mM glycerol. Cultures were supplemented with buffer or inhibitor and incubated for 24 hours at 37 °C. Error bars represent the mean ± SD of three replicates (or two replicates in the case of inhibitors **107**, **123**, and **125**).

Non-stereospecific addition of a methyl to the cyclohexyl ring of **107** furnished a mixture of stereoisomers (**125)**, which were not further purified but, when tested as one mixture, increased potency by ~10-fold (EC_{50} = 1.4 μM) relative to the parent compound. However, as with **107**, growth on both choline and glycerol minimal media was inhibited (Figure 3.41). Non-stereospecific methylation of the cyclohexane of (*R*)-cyclohexyl-tetrahydropyridin-3-ol (**123**) resulted in a mixture diastereomers **126**, while methylation of the cyclohexane of the (*S*)-isomer (**124**) resulted in diastereomers **127**. Once again, the stereoisomers with the OH in the (*S*)-configuration (**127**) were more potent for inhibition of TMA production by over 10-fold.

Table 3.23. EC_{50} values and minimal media growth results for compounds 125, 128-131

Compound	Structure	EC_{50} (mM)	Max OD_{600} / Time of ½ max(OD_{600})	
			Choline	Glycerol
—	No inhibitor	—	1.0 / 4.7 h	1.0 / 5.7 h
125	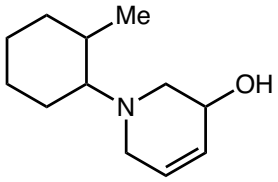	1.4×10^{-3}	0.06 / 11.7 h	0.03 / 0.3 h
128	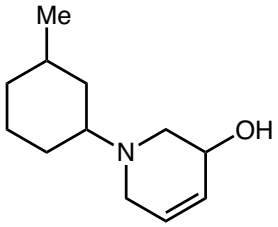	1.8×10^{-2}	0.1 / 20.0 h	0.6 / 16.3 h
129	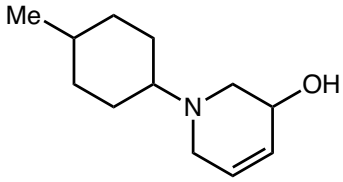	4.2×10^{-2}	—	—
130	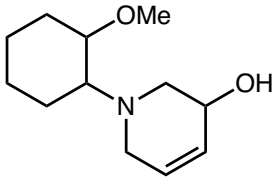	0.1 mM: 26%	—	—
131	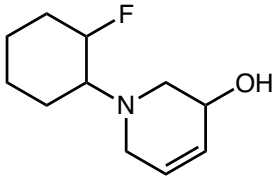	01.2×10^{-2}	—	—

E. coli MS 200-1 was incubated in BHI containing 1 mM d_9-choline and either buffer or inhibitor (tested at ≥3 concentrations, except for compound **130**) at 37 °C in an anaerobic chamber. [d_9-TMA] was measured by LC-MS/MS after 3.5 hours. Dose-response curves were fit using nonlinear regression to determine the EC_{50}. OD_{600} values were obtained by incubating *E. coli* MS 69-1 with phosphate buffer or 10 mM of inhibitor in 30 mM choline or 30 mM glycerol minimal media. Cultures were grown anaerobically on 96-well plates for 24 hours at 37 °C.

Performing a brief SAR analysis on the methyl-substituted cyclohexane of **125** (EC_{50} = 14 μM), we first moved the methyl from C2 to C3 of the cyclohexane (**128**), thereby impairing activity by ~10-fold (Table 3.23). The resulting mixture (**128**) also delayed growth on glycerol and inhibited growth on choline minimal medium (Figure 3.42). Moving the methyl onto C4 of the cyclohexyl ring again furnished a mixture (**129**) that was less potent than the parent compound **125**. This *para*-methyl-substituted cyclohexyl analog (**129**) also delayed growth on glycerol and inhibited growth on choline minimal medium (Figure 3.42).

Finally, we exchanged the methyl substituent of **125** for a methoxy group (**130**) and a fluorine atom (**131**). When testing the mixture of stereoisomers **125** at 100 μM in the *E. coli* whole cell assay, TMA levels were reduced by 26% relative to the negative control. The same concentration of betaine aldehyde (**9**, EC_{50} = 0.40 mM) lowered TMA by 33%. The mixture of fluorine analogs (**131**) was separated into two components, one of which exhibited an EC_{50} of 12 μM.

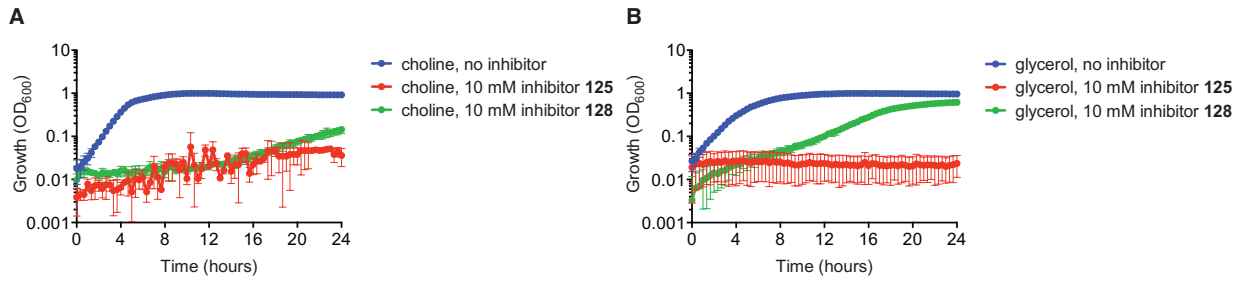

Figure 3.42. Effects of compounds 125 and 128 on anaerobic growth of *E. coli* on minimal media. *E. coli* MS 69-1 was grown in a vinyl chamber, under an atmosphere of 95% N_2 / 5% H_2, in minimal media with either (A) 30 mM choline or (B) 30 mM glycerol. Cultures were supplemented with buffer or inhibitor and incubated for 24 hours at 37 °C. Error bars represent the mean ± SD of three replicates (or two replicates in the case of inhibitor **125**).

We returned to 1-methyl-1,2,3,6-tetrahydropyridin-3-ol (**97**), which was highly potent in whole cells (Table 3.17, EC_{50} = 10 μM) and significantly delayed the rate of growth on choline

minimal medium without affecting growth on glycerol (Figure 3.31). Efforts to optimize this compound proved challenging. Attachment of a cyclobutane (**105**, **112**, and **113**), cyclopentane (**106**, **114**, and **115**), or cyclohexane (**107**, **123**, and **124**) resulted in delay or even inhibition of growth on glycerol minimal media (Figures 3.35, 3.36 and 3.41), suggesting that selectivity for choline metabolism was lost. Attachment of a methyl-substituted cyclopentane (**116** and **120**) was tolerated in terms of potency (Tables 3.20 and 3.21) but had unpromising results on minimal media, slightly delaying growth on glycerol (Figures 3.36 and 3.39). Attachment of a methyl-substituted cyclohexane (**125, 126, 127, 128,** and **129**) did not affect potency (Tables 3.22 and 3.23) but, at least for the 2 analogs tested (**125** and **128**), growth on glycerol minimal medium was inhibited (Figures 3.41 and 3.42), implying that these inhibitors exert off-target effects in *E. coli* cells.

Continuing to elaborate on the scaffold of 1-methyl-1,2,3,6-tetrahydropyridin-3-ol (**97**, EC_{50} = 10 μM), we replaced the methyl group on the nitrogen with a cyclopropylmethyl (**132**), which reduced potency by 100-fold (Table 3.24). The *N*-cyclopropylmethyl mixture of enantiomers (**132**) also delayed growth on glycerol medium and inhibited growth on choline, as did the individual (*R*)- and (*S*)-enantiomers (compounds **133** and **134**, respectively), albeit to lesser degrees ((Figure 3.43).

Alternatively, swapping the N-substituent of 1-methyl-1,2,3,6-tetrahydropyridin-3-ol (**97**) for a cyclohexylmethyl group (**135**), toluene (**136**), *para*-methylanisole (**137**), or ethylbenzene (**138**) resulted in EC_{50} values of 91 μM, 0.37 mM, 0.26 mM, and 0.29 mM, respectively. It would be interesting to see whether these compounds impact growth on glycerol minimal media or inhibit recombinant CutC *in vitro*.

Table 3.24. EC_{50} values and minimal media growth results for compounds 97, 132-138

Compound	Structure	EC_{50} (mM)	Max OD_{600} / Time of ½ max(OD_{600})	
			Choline	Glycerol
—	No inhibitor	—	1.0 / 5.0 h	0.9 / 8.0 h
97	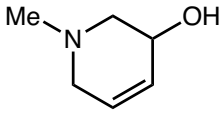	1.0×10^{-2}	0.6 / 16.0 h	1.1 / 6.0 h
132	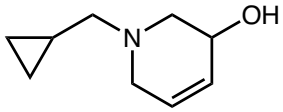	0.25	0.07 / 0.3 h	0.9 / 14.0 h
133	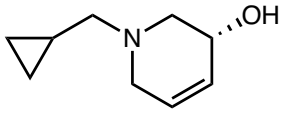	—	0.5 / 19.7 h	0.9 / 10.7 h
134	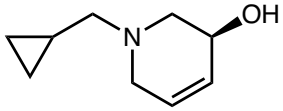	—	0.9 / 15.3 h	0.8 / 9.7 h
135	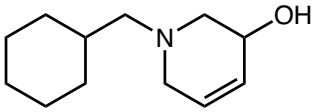	9.1×10^{-2}	—	—
136	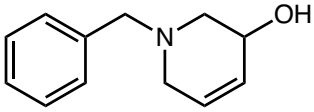	0.37	—	—
137	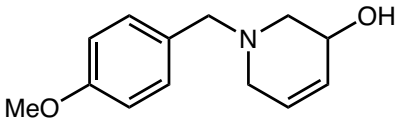	0.26	—	—
138	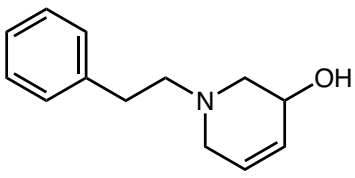	0.29	—	—

E. coli MS 200-1 was incubated in BHI containing with 1 mM d_9-choline and either phosphate buffer or inhibitor (tested at ≥3 concentrations) at 37 °C in an anaerobic chamber. [d_9-TMA] was

measured by LC-MS/MS after 3.5 hours. Dose-response curves were fit using nonlinear regression to determine the EC_{50}. OD_{600} values were obtained by incubating *E. coli* MS 69-1 with phosphate buffer or 10 mM of inhibitor (or 20 mM of inhibitor **132**) in 30 mM choline or 30 mM glycerol minimal media. Cultures were grown anaerobically on 96-well plates for 24 hours at 37 °C.

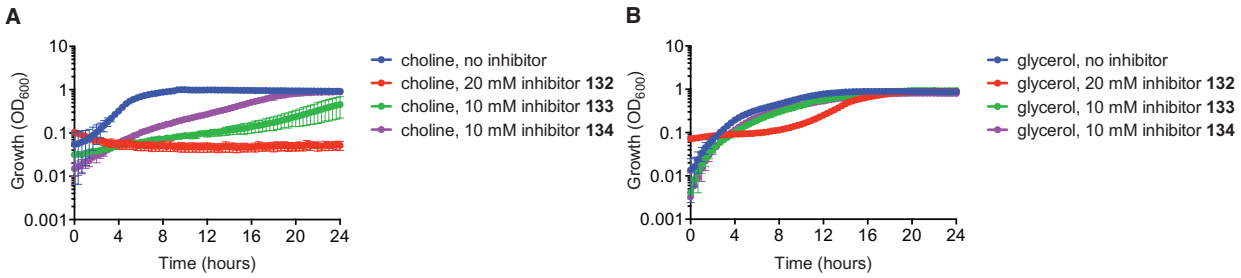

Figure 3.43. Effects of compounds 132-134 on anaerobic growth of *E. coli* on minimal media. *E. coli* MS 69-1 was grown in a vinyl chamber, under an atmosphere of 95% N_2 / 5% H_2, in minimal media with either (A) 30 mM choline or (B) 30 mM glycerol. Cultures were supplemented with buffer or inhibitor and incubated for 24 hours at 37 °C. Error bars represent the mean ± SD of three replicates (or two replicates in the case of inhibitor **133**).

Our last SAR series was focused around 1-benzyl-1,2,3,6-tetrahydropyridin-3-ol (**136**), which had an EC_{50} of 0.37 mM in *E. coli*. Exchanging the benzene for a pyridine (**139**), a thiophene (**140** and **141**), or a furan (**142** and **142**) made little impact on potency (Table 3.25). None of these compounds have been investigated on minimal media or i*n vitro*.

Table 3.25. EC_{50} values and minimal media growth results for compounds 136-143

Compound	Structure	EC_{50} (mM)	Max OD_{600} / Time of ½ max(OD_{600})	
			Choline	Glycerol
—	No inhibitor	—	1.0 / 5.0 h	0.9 / 8.0 h
136	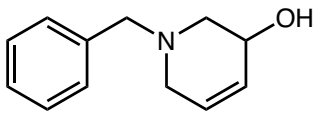	0.37	—	—
139	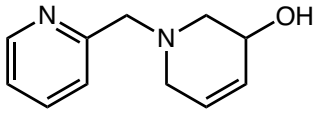	3 mM: 12%	—	—
140	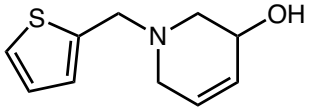	0.32	—	—
141	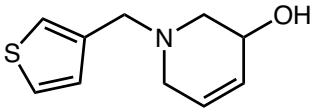	0.26	—	—
142	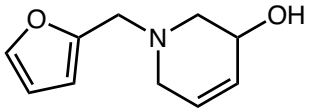	0.20	—	—
143	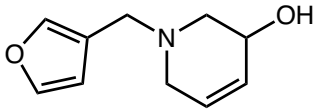	0.26	—	—

E. coli MS 200-1 was incubated in BHI medium containing 1 mM d_9-choline and either phosphate buffer or inhibitor (tested at ≥3 concentrations, except for compound **139***) at 37 °C in an anaerobic chamber. [d_9-TMA] was measured by LC-MS/MS after 3.5 hours. Dose-response curves were fit using nonlinear regression to determine the EC_{50}.

3.3. Material and methods

3.3.1. General materials and methods

Unless stated otherwise, all chemicals were purchased from Sigma-Aldrich. Trimethylamine-d_9 hydrochloride was purchased from CDN Isotopes, choline chloride-(trimethyl-d_9) was purchased from Cambridge Isotope Laboratories, and β-nicotinamide adenine dinucleotide reduced disodium salt hydrate (NADH) was purchased from EMD Millipore. Lennox Luria-Bertani (LB) medium and Lennox LB agar were purchased from EMD Millipore, BBL Brain Heart Infusion (BHI) broth and BBL BHI agar were purchased from BD Biosciences, Reinforced Clostridial Medium (RCM) was purchased from BD Biosciences, and Dulbecco's Phosphate Buffered Saline (PBS) was purchased from ThermoFisher Scientific. Acetonitrile used for liquid chromatography-mass spectrometry (LC-MS) was a B&J Brand high-purity solvent (Honeywell Burdick & Jackson). NMR solvents were purchased from Cambridge Isotope Laboratories.

LC-MS/MS was performed on an Agilent 6410 Triple Quadrupole LC-MS instrument (Agilent Technologies) using electrospray ionization. The mass spectrometer was operated in multiple reaction monitoring (MRM) mode with positive ionization monitoring. The precursor-product ion pairs used in MRM mode were: m/z 69.1 → 49.1 (d_9-TMA), m/z 113.2 → 69.1 (d_9-choline), m/z 111.1 → 66.1 (d_9-betaine aldehyde), m/z 60.1 → 40.1 (TMA), and m/z 109.1 → 60.1 (choline). The capillary voltage was set to 4.0 kV and the fragmentor voltage to 110 V. The drying gas temperature was maintained at 200 °C, with a flow rate of 10 L/min and a nebulizer pressure of 25 psi. The collision energy for the precursor-product ion pairs was set to 21 V. MS^1 resolution was set to wide and MS^2 resolution to unit. The time filter width used was 0.07 min, and the ΔEMV (Electron Multiplier Voltage) was 400 V. The injection volume of all samples

was 5 μL. Samples were injected onto a Kinetex (Phenomenex) HILIC column (2.6 μm, 30×2.1 mm, 100 Å). The LC conditions were: 0% B for 1 min, a gradient increasing to 100% B over 2 min, 100% B for 1.5 min, a gradient decreasing to 0% B over 1.5 min, and, finally, 0% B for 2 min (solvent A = 95% acetonitrile / 5% of 100 mM ammonium formate in water, with 0.02% formic acid; solvent B = 50% acetonitrile / 45% water / 5% of 100 mM ammonium formate in water, with 0.02% formic acid). The flow rate was maintained at 0.6 mL/min for each run. Data analysis was performed with Mass Hunter Workstation Data Acquisition software (Agilent Technologies).

Optical densities of bacterial cultures (for plasmid overexpression) were determined with a DU 730 Life Sciences UV/Vis spectrophotometer (Beckman Coulter) by measuring absorbance at 600 nm. *E. coli* BL21 (DE3) cells overexpressing CutC were lysed with a cell disruptor (Avestin EmulsiFlex-C3). Sonication for disrupting *E. coli* BL21 (DE3) cells overexpressing CutD was performed with a Branson Sonifier S-450D equipped with a 1⁄2 inch horn in a glove box (Coy Laboratory Products) under an atmosphere of 98% N_2 and 2% H_2 at 4 °C. Sonication for disrupting *Proteus mirabilis* cells was performed with a Branson Sonifier S-450D equipped with a 1⁄4 inch horn in the same glove box at 4 °C. Nickel-nitrilotriacetic acid agarose (Ni-NTA) resin was purchased from Qiagen. SDS-PAGE gels were purchased from BioRad.

All *in vitro* experiments with CutC-52aa and CutD were conducted anaerobically in an MBraun glovebox (MBraun) under an N_2 atmosphere with less than 5 ppm of O_2. Activity assays were set up in 96-well plates (Corning) and performed at 20 °C. The absorbance at 340 nm was monitored using a PowerWave HT Microplate Spectrophotometer (BioTek).

Other than cultures for protein overexpression, all bacteria were grown anaerobically, either in a vinyl glovebox (Coy Laboratory Products) under an atmosphere of 95% N_2 and 5% H_2

or an MBraun glovebox (described above). For measuring optical densities of bacteria grown on 96-well plates, plates were brought into an anaerobic glovebox and the absorbance of each well was monitored at 600 nm using a PowerWave HT Microplate Spectrophotometer (BioTek). Absorbance values were corrected for a path length of 1 cm. A Genesys^{TM} 20 Visible spectrophotometer was used for measuring optical densities of bacteria grown in Hungate tubes (16×125 mm, Chemglass Life Sciences).

Samples were made anaerobic as follows. Solids were brought into anaerobic chambers (MBraun and Coy Laboratory) in perforated 1.5 mL microcentrifuge tubes. CutC protein solutions were made anaerobic by flushing the headspace of the solution with argon for 30 min. Buffers and other solutions were made anaerobic by bubbling argon through the liquid for 30 min. Media solutions of 200 to 500 mL in volume were first autoclaved and then sparged with argon for 30 min.

Proton nuclear magnetic resonance (^{1}H NMR) spectra and carbon nuclear magnetic resonance (^{13}C NMR) spectra were recorded in the Magnetic Resonance Laboratory in the Harvard University Department of Chemistry and Chemical Biology on a Varian Inova-500 (500 MHz, 125 MHz) or Varian Mercury-400 (400 MHz, 100 MHz) NMR spectrometer. Chemical shifts are reported in parts per million downfield from tetramethylsilane using the solvent resonance as an internal standard for ^{1}H (CD_3OD, δ_H = 3.31, 4.87 ppm or D_2O, δ_H = 4.79 ppm) and ^{13}C (CD_3OD, δ_C = 49.00 ppm). Data are reported as follows: chemical shift, integration multiplicity (s = singlet, d = doublet, t = triplet, m = multiplet), coupling constant, integration, and assignment. NMR spectra were visualized using MestReNova Version 11.0.2-18153 (Mestrelab Research).

High-resolution mass spectral (HRMS) data for the synthetic compounds were obtained in the Magnetic Resonance Laboratory in the Harvard University Department of Chemistry and Chemical Biology on a Bruker Micro QTOF-QII fitted with a dual-spray electrospray ionization (ESI) source. The capillary voltage was set to 4.5 kV and the end plate offset to -500 V, the drying gas temperature was maintained at 190 °C with a flow rate of 8 L/min and a nebulizer pressure of 21.8 psi. The liquid chromatography (LC) was performed using an Agilent Technologies 1100 series LC with 50% H_2O and 50% acetonitrile as solvent.

3.3.2. LC-MS/MS assay for determining choline TMA-lyase activity in *E. coli* MS 200-1

A frozen stock of *E. coli* MS 200-1 was streaked out onto a BHI agar plate inside an anaerobic chamber (Coy Laboratory) and incubated at 37 °C overnight. A single colony was inoculated into 5 mL of BHI supplemented with 1 mM choline chloride (to induce expression of the *cut* genes) and grown anaerobically at 37 °C. The starter culture was inoculated (2%) into fresh BHI containing 1 mM of choline chloride-(trimethyl-d_9). The bacterial culture was distributed among the wells of a 96-well plate (Corning). Inhibitors were dissolved in 50 mM potassium phosphate buffer, pH 7.4, and aliquoted to the wells so that the final volume of each well was 200 µL. Plates were covered with aluminum seals (VWR) and incubated at 37 °C for 3.5 hours inside an anaerobic chamber (Coy Laboratory). An aliquot of each culture was diluted (up to 3750-fold) in a mixture composed of 95% acetonitrile and 5% of 100 mM ammonium formate buffer (final formic acid concentration of 0.02%) and analyzed by LC-MS/MS for d_9-TMA and d_9-choline.

Concentrations of d_9-TMA and d_9-choline in each sample were determined by comparing the peak integrations to that of a standard curve of d_9-TMA and d_9-choline (0.1 to 2.0 mM). The

calculated [d_9-TMA] values were plotted against the logarithm of inhibitor concentration in each sample and fit to a nonlinear regression model in Graphpad Prism to obtain EC_{50} values.

3.3.3. Overexpression and purification of CutC and CutD

Plasmids containing the wild-type *D. desulfuricans* G20 *cutC* gene with an 18- or 52-residue, N-terminal truncation of the resulting protein sequence were constructed previously.[19,20] The N-terminal truncations remove a putative microcompartment localization sequence. Both truncation constructs incorporate an N-terminal hexahistidine tag and thrombin cleavage site. Truncated constructs were found to have similar activity to wild-type protein, but the truncated variants are more soluble and less prone to aggregation.[19,20]

CutC was purified in 50 mM potassium phosphate, pH 8.0, 50 mM KCl, and 10% glycerol according to the protocol previously described,[19,20] but was not concentrated after dialysis since the process of concentration contributed to aggregation. The 18-residue truncated construct was used for crystallization. The 52-residue construct was rendered anoxic by sparging with argon prior to its use in EPR and kinetics assays. A NanoDrop 2000 UV-Vis Spectrophotometer (Thermo Scientific) was used to measure the absorbance at 280 nm of CutC variants (ε = 128 870 $M^{-1}cm^{-1}$). The extinction coefficients were obtained using the ExPASy protparam tool (http://www.expasy.org/tools/protparam.html).

CutD was also purified as previously described except for two modifications to the protocol. Upon induction with 500 μM IPTG (Teknova), cells expressing CutD were brought inside the MBraun anaerobic chamber and incubated at 15 °C for 16 to 18 hours without shaking. As previously described, cells were subsequently harvested by centrifugation, brought inside a Coy anaerobic chamber (containing an atmosphere of 98% N_2/2% H_2 and kept at 4 °C), and re-

suspended in 45-50 mL of anoxic lysis buffer. However, instead of removing the re-suspension from the anaerobic chamber and lysing cells with a cell disruptor, the cells were disrupted using a sonicator inside the oxygen-free Coy chamber. Purification with Ni-NTA resin, reconstitution of iron-sulfur clusters, and dialysis were performed as previously described.[19,20] CutD was used for *in vitro* EPR and kinetics assays. The concentration of CutD was determined according to the method of Bradford,[28] using bovine serum albumin (New England Biolabs) as a standard and dye reagent concentrate from BioRad. All proteins were judged to be of high purity by denaturing polyacrylamide gel electrophoresis.

3.3.4. Glycyl radical quantification by EPR spectroscopy

CutC-52aa was prepared for EPR spectroscopy as follows. Assays were set up in an anaerobic chamber (MBraun) kept at 20 °C in 1.5 mL polypropylene Eppendorf tubes. All assay concentrations are final concentrations. CutD (40 μM) and sodium dithionite (150 μM) were incubated together in buffer (50 mM potassium phosphate, pH 8.0, 50 mM KCl) for 20 min. CutC was rendered anoxic by sparging the headspace of the solution with argon for 30 min. Anoxic CutC (20 μM total monomer concentration) and SAM (200 μM) were added to the activating enzyme mixture and incubated for 1 h. The entire volume of 220 μL for each sample was used for analysis. EPR assays were performed in triplicate.

Perpendicular mode X-band EPR spectra were recorded on a Bruker ElexSysE500 EPR instrument fitted with a quartz dewar (Wilmad Lab-Glass) for measurements at 77 K. All samples were loaded into EPR tubes with 4 mm outer diameter and 8” length (Wilmad Lab-Glass, 734-LPV-7), sealed, and frozen in liquid N_2. Data acquisition was performed with Xepr software (Bruker). The magnetic field was calibrated with a standard sample of α,γ-

bisdiphenylene-β-phenylallyl (BDPA), g = 2.0026 (Bruker). The experimental spectra for the glycyl radical were modeled with EasySpin (Version 5.0.22)[29] or Matlab (MathWorks) to obtain g values, hyperfine coupling constants, and line widths. Spin concentration measurements were performed by numerically calculating the double integral of the simulated spectra and comparing the area with that of a $K_2(SO_3)_2NO$ standard. This standard was freshly prepared before each set of EPR measurements by dissolving solid $K_2(SO_3)_2NO$ under anaerobic conditions in anoxic 0.5 M $KHCO_3$ and diluting to a final concentration of 0.3–0.5 mM. To account for any decomposition during dissolution, the concentration was measured at 248 nm (ε = 1690 $M^{-1}cm^{-1}$) using a NanoDrop 2000 UV-Vis Spectrophotometer. For glycyl radical-containing samples and the $K_2(SO_3)_2NO$ standard, EPR spectra represent the average of 3 scans and were recorded under the following conditions: temperature, 77 K; center field, 3370 Gauss; sweep width, 200 Gauss; microwave power, 20 μW; microwave frequency, 9.45 MHz; modulation amplitude, 0.4 mT; modulation frequency, 100 kHz; time constant, 20.48 ms; conversion time, 20.48 ms; scan time, 20.97 s; receiver gain, 60 dB (for enzymatic assays) or 30 dB (for standards). Normalization for the difference in receiver gain was performed by the spectrometer. EPR experiments showed that CutD activated 18 ± 1% of CutC monomers, consistent with the results of previous studies.[19]

3.3.5. *In vitro* assay for measuring CutC activity in the presence of inhibitors

The activity of CutC was coupled to the reduction of acetaldehyde by NADH-dependent yeast alcohol dehydrogenase (YADH). Assays were conducted in a buffer of 50 mM potassium phosphate, pH 8.0, 50 mM KCl and were set up in an anaerobic chamber (MBraun) kept at 20 °C in 1.5 mL polypropylene Eppendorf tubes. CutD (40 μM) and sodium dithionite (150 μM) were incubated for 20 min prior to the addition of 200 μM of *S*-(5'-adenosyl)-L-methionine (SAM,

purchased from Sigma-Aldrich as a *p*-toluenesulfonate salt) and 20 μM of CutC monomer in a total reaction mixture of 50 μL. Glycyl radical formation was carried out for 1 hour, after which the activated CutC mixture was immediately diluted 20-fold into phosphate buffer. An aliquot of the diluted mixture was added to a master mix containing NADH (200 μM) and YADH (0.4 μM) such that the final concentration of CutC monomer was 5 nM (after addition of inhibitor/buffer and choline). The master mix was distributed to the wells of a 96-well plate (180 μL per well), to which was added either inhibitor or buffer (10 μL per well), followed by choline (10 μL per well). The final concentration of choline was 200 μM (~K_M value).

Following the addition of choline, the absorbance of NADH at 340 nm was immediately recorded, with measurements taken every 20 s for 10 min. Initial rates were calculated from absorbance measurements that decreased linearly. Path lengths were corrected to 1 cm and absorbance values were converted to concentrations assuming ε_{340} = 6,220 $M^{-1}cm^{-1}$ for NADH. The rate from assays containing no substrate was subtracted from assays containing substrate to account for background activity. Assays were performed in triplicate. All of the data were fit to the Michaelis–Menten equation simultaneously using nonlinear regression in Graphpad Prism. Initial rates at each inhibitor concentration were normalized to control samples without inhibitor. Normalized activity values were plotted against the logarithm of inhibitor concentration and fit to a nonlinear regression model in Graphpad Prism to obtain IC_{50} values.

3.3.6. Growth studies of *E. coli* strains in minimal and rich media

A frozen stock of *E. coli* MS 200-1 was streaked out onto a BHI agar plate inside an anaerobic chamber (Coy Laboratory) and incubated at 37 °C overnight. A single colony was inoculated into 5 mL of BHI supplemented with 1 mM choline chloride, which was grown

anaerobically at 37 °C. The starter culture was inoculated (2%) into fresh BHI containing 1 mM of choline chloride. Aliquots of the culture were transferred to a 96-well plate (Corning). Inhibitors, dissolved in 50 mM potassium phosphate buffer, pH 7.4, or phosphate buffer alone were added to the samples so that the final volume in each well was 200 μL. Plates were incubated at 37 °C for 16-24 hours either in an Mbraun glove box or a Coy vinyl glovebox and OD_{600} values were measured using a BioTek spectrophotometer.

A minimal medium for *E. coli* MS 69-1 was developed based on the "no carbon E" medium utilized for ethanolamine-dependent growth of *Salmonella enterica*.[24,34] The optimized media for *E. coli* MS 69-1 contained 29 mM potassium phosphate monobasic, 29 mM potassium phosphate dibasic, 17 mM ammonium sodium phosphate dibasic, 40 mM sodium fumarate dibasic, 0.4% (wt/v) casamino acids (Becton Dickinson), and either 30 mM choline chloride or 30 mM glycerol. This mixture was supplemented with 1 mM magnesium sulfate, 1% ATCC vitamin supplement, and 1% ATCC trace mineral supplement.

A frozen stock of *E. coli* MS 69-1 was streaked out onto a BHI agar plate inside an anaerobic chamber (Coy Laboratory) and incubated at 37 °C overnight. A single colony was inoculated into 5 mL of BHI supplemented with 1 mM choline chloride (to induce expression of the *cut* genes), which was grown anaerobically at 37 °C. Minimal media were inoculated with 1% of the saturated *E. coli* MS 69-1 starter culture. Aliquots of the minimal media culture were transferred to a 96-well plate (Corning). Inhibitors, dissolved in 50 mM potassium phosphate buffer, pH 7.4, or phosphate buffer alone were added to the samples so that the final volume in each well was 200 μL. Plates were incubated at 37 °C for 16-24 hours either in an Mbraun glove box or a Coy vinyl glovebox under a nitrogen atmosphere and OD_{600} values were measured using a BioTek spectrophotometer.

3.4. References

(1) Arrowsmith, C. H.; Audia, J. E.; Austin, C.; Baell, J.; Bennett, J.; Blagg, J.; Bountra, C.; Brennan, P. E.; Brown, P. J.; Bunnage, M. E.; Buser-Doepner, C.; Campbell, R. M.; Carter, A. J.; Cohen, P.; Copeland, R. A.; Cravatt, B.; Dahlin, J. L.; Dhanak, D.; Edwards, A. M.; Frederiksen, M.; Frye, S. V.; Gray, N.; Grimshaw, C. E.; Hepworth, D.; Howe, T.; Huber, K. V. M.; Jin, J.; Knapp, S.; Kotz, J. D.; Kruger, R. G.; Lowe, D.; Mader, M. M.; Marsden, B.; Mueller-Fahrnow, A.; Müller, S.; O'Hagan, R. C.; Overington, J. P.; Owen, D. R.; Rosenberg, S. H.; Ross, R.; Roth, B.; Schapira, M.; Schreiber, S. L.; Shoichet, B.; Sundström, M.; Superti-Furga, G.; Taunton, J.; Toledo-Sherman, L.; Walpole, C.; Walters, M. A.; Willson, T. M.; Workman, P.; Young, R. N.; Zuercher, W. J. The Promise and Peril of Chemical Probes. *Nat. Chem. Biol.* **2015**, *11* (8), 536–541.

(2) Dougherty, D.; Stauffer, D. Acetylcholine Binding by a Synthetic Receptor: Implications for Biological Recognition. *Science* **1990**, *250* (4987), 1558–1560.

(3) Gu, Y.; Kar, T.; Scheiner, S. Fundamental Properties of the CH···O Interaction: Is It a True Hydrogen Bond? *J. Am. Chem. Soc.* **1999**, *121* (40), 9411–9422.

(4) Raymo, F. M.; Bartberger, M. D.; Houk, K. N.; Stoddart, J. F. The Magnitude of [C−H···O] Hydrogen Bonding in Molecular and Supramolecular Assemblies. *J. Am. Chem. Soc.* **2001**, *123* (38), 9264–9267.

(5) Horowitz, S.; Trievel, R. C. Carbon-Oxygen Hydrogen Bonding in Biological Structure and Function. *J. Biol. Chem.* **2012**, *287* (50), 41576–41582.

(6) Horowitz, S.; Dirk, L. M. A.; Yesselman, J. D.; Nimtz, J. S.; Adhikari, U.; Mehl, R. A.; Scheiner, S.; Houtz, R. L.; Al-Hashimi, H. M.; Trievel, R. C. Conservation and Functional Importance of Carbon–Oxygen Hydrogen Bonding in AdoMet-Dependent Methyltransferases. *J. Am. Chem. Soc.* **2013**, *135* (41), 15536–15548.

(7) Craciun, S.; Marks, J. A.; Balskus, E. P. Characterization of Choline Trimethylamine-Lyase Expands the Chemistry of Glycyl Radical Enzymes. *ACS Chem. Biol.* **2014**, *9* (7), 1408–1413.

(8) Bodea, S.; Funk, M. A.; Balskus, E. P.; Drennan, C. L. Molecular Basis of C-N Bond Cleavage by the Glycyl Radical Enzyme Choline Trimethylamine-Lyase. *Cell Chem. Biol.* **2016**, *23* (10), 1206–1216.

(9) Gehringer, M.; Laufer, S. A. Emerging and Re-Emerging Warheads for Targeted Covalent Inhibitors: Applications in Medicinal Chemistry and Chemical Biology. *J. Med. Chem.* **2019**, acs.jmedchem.8b01153–52.

(10) Garcia-Garcia, J. C.; Hazen, S. L.; Wos, J. A. Compound and Methods for Inhibiting Production of Trimethylamine. May 27, 2017.

(11) De Cesco, S.; Kurian, J.; Dufresne, C.; Mittermaier, A. K.; Moitessier, N. Covalent Inhibitors Design and Discovery. *European Journal of Medicinal Chemistry* **2017**, *138*, 96–114.

(12) Romano, K. A.; Martínez-del Campo, A.; Kasahara, K.; Chittim, C. L.; Vivas, E. I.; Amador-Noguez, D.; Balskus, E. P.; Rey, F. E. Metabolic, Epigenetic, and Transgenerational Effects of Gut Bacterial Choline Consumption. *Cell Host Microbe* **2017**, *22* (3), 279–290.

(13) Massi, A.; Nanni, D. Thiol–Yne Coupling: Revisiting Old Concepts as a Breakthrough for Up-to-Date Applications. *Org. Biomol. Chem.* **2012**, *10* (19), 3791–17.

(14) Dondoni, A. The Emergence of Thiol-Ene Coupling as a Click Process for Materials and Bioorganic Chemistry. *Angew. Chem. Int. Ed.* **2008**, *47* (47), 8995–8997.

(15) Ritchie, T. J.; Macdonald, S. J. F.; Young, R. J.; Pickett, S. D. The Impact of Aromatic Ring Count on Compound Developability: Further Insights by Examining Carbo- and Hetero-Aromatic and -Aliphatic Ring Types. *Drug Discovery Today* **2011**, *16* (3-4), 164–171.

(16) Bauer, R. A. Covalent Inhibitors in Drug Discovery: From Accidental Discoveries to Avoided Liabilities and Designed Therapies. *Drug Discovery Today* **2015**, *20* (9), 1061–1073.

(17) Wang, Z.; Roberts, A. B.; Buffa, J. A.; Levison, B. S.; Zhu, W.; Org, E.; Gu, X.; Huang, Y.; Zamanian-Daryoush, M.; Culley, M. K.; DiDonato, A. J.; Fu, X.; Hazen, J. E.; Krajcik, D.; DiDonato, J. A.; Lusis, A. J.; Hazen, S. L. Non-Lethal Inhibition of Gut Microbial Trimethylamine Production for the Treatment of Atherosclerosis. *Cell* **2015**, *163* (7), 1585–1595.

(18) Nepali, K.; Lee, H.-Y.; ORCID: 0000-0002-3775-6405, J.-P. L. Nitro-Group-Containing Drugs. *J. Med. Chem.* **2018**, 1–43.

(19) Wuitschik, G.; Carreira, E. M.; Wagner, B.; Fischer, H.; Parrilla, I.; Schuler, F.; Rogers-Evans, M.; Müller, K. Oxetanes in Drug Discovery: Structural and Synthetic Insights. *J. Med. Chem.* **2010**, *53* (8), 3227–3246.

(20) Bull, J. A.; Croft, R. A.; Davis, O. A.; Doran, R.; Morgan, K. F. Oxetanes: Recent Advances in Synthesis, Reactivity, and Medicinal Chemistry. *Chem. Rev.* **2016**, *116* (19), 12150–12233.

(21) Anwar, S.; Bhandari, U.; Panda, B. P.; Dubey, K.; Khan, W.; Ahmad, S. Trigonelline Inhibits Intestinal Microbial Metabolism of Choline and Its Associated Cardiovascular Risk. *Journal of Pharmaceutical and Biomedical Analysis* **2018**, *159*, 100–112.

(22) Larsen, E. M.; Johnson, R. J. Microbial Esterases and Ester Prodrugs: an Unlikely

Marriage for Combating Antibiotic Resistance. *Drug Dev Res* **2018**, *80* (1), 33–47.